GRAVITY AND OTHER GEOPHYSICAL STUDIES OF THE CRUST OF SOUTHERN BRITAIN

by

Halit Tuğrul Genç

B.Sc., Istanbul Technical University

Thesis presented for the degree of

Doctor of Philosophy

of the University of Edinburgh in the

Faculty of Science

SEPTEMBER 1988

DECLARATION

I hereby declare the work presented in this thesis is my own unless otherwise stated in the text, and that the thesis has been composed myself.

Halit Tuğrul Genç

Our understanding of our planet is as little as our understanding of ourselves. Like every individual person, she has her own character. We are determined to know her more and more, because we love her as we love each other.

ACKNOWLEDGMENT

I would like to thank to Professor K M Creer, Head of Geophysics Department, for allowing me to use the departmental facilities in my research.

I am deeply grateful to Dr Roger Hipkin not only for supervising me, but also encouraging me throughout my study in Edinburgh.

I would like to express my thanks to G Day and J Edwards (British Geological Survey) for their help in recompiling data, and their valuable comments.

I am grateful to D Kerridge (British Geological Survey) for allowing me use of his program for spherical harmonic analysis.

I would like to acknowledge the authorities of Ministry of Education, Republic of Turkey who supported me financially

ABSTRACT

Gravitational attraction of sediments younger than Carboniferous was computed on a 2 km grid in a region of southern Britain between 100 km and 700 km easting and between −50 km and 556 km northing of the British National Grid. This was based on comprehensive study of hand sample, neutron-log and topographic regression of rock densities. The effect was stripped from a Bouguer anomaly map. Stripping revealed a step of about 40 mgal between the eastern and western parts of the map. The step has a linear NW trend from the Bray Fault in the English Channel to Swansea, then a NE trend from Swansea to Charnwood Forest. Gravity modelling of the step showed that the southern part can be explained by a contact of two deep crustal bodies under the Variscan front. The spectral analysis of the stripped Bouguer anomaly showed sources at two depths, 11±2 km and 30±3 km. A digital data set of aeromagnetic and marine magnetic anomalies for a 540 km by 390 km region of southern Britain was prepared and reduced to a common height of 550 m. Spectral analysis also showed deep sources at 14±1 km but gave no indication of the Curie depth. Trend analysis of both gravity and magnetic anomalies based on second derivatives clearly identified the major deformation events. A two-dimensional isostatic response function was calculated and revealed that there was no compensation of the topographic and sedimentary load at Moho depths, but that the compensation was at a depth of 11–12 km. The midcrustal source identified by spectral and isostatic analysis is explained by a brittle to ductile transition at about 11 km depth. Ductile flow in the lower crust has allowed the Moho to distort independently of the present surface load. The present topography on the Moho may reflect forces acting in the sub-Moho Lithosphere.

CONTENTS

Chapter 4

Magnetic Anomaly Analysis

Chapter 5

Isostasy

Chapter 6

Conclusions and Discussion

CHAPTER 1

INTRODUCTION

1.1 Geological Review

Caledonian and Variscan deformation phases are the dominant events of the crustal structure of southern Britain. The Caledonian trend shows a NE-SW direction and series of faults along this direction over Scotland, northern England and north Wales. The Variscan trend has an E-W direction with thrust nappes in southern England. The phases are not local to Britain, but their evidence can be seen throughout Europe and north America.

1.1.1 Caledonian Phase

Pre-Cambrian age water-lain tuff and conglomerate sedimentation in Leicestershire indicates the spreading of an ocean which is called Iapetus (Dewey and Kidd, 1974). The Iapetus Ocean continued to expand until early Ordovician. From Pre-Cambrian to Ordovician the main activities were deep water sedimentation, although an ophiolitic complex along Highland Boundary Fault suggests local subduction during the Dalradian (Henderson and Robertson, 1982).

During the Ordovician, the Iapetus Ocean started to close. On its northern margin an ophiolite complex around Ballantrae (Scotland) is the evidence of the closure. The movement of the plate on the northern side of the ocean generated the deformation and metamorphism of the Highlands about 450 Ma (Pankhurst, 1974).

At the same time on the southern margin of the ocean, there were two subduction zones, one in north Wales and the other in the Lake District. This generated the

volcanic activity around these places, but the grade of metamorphism was not as high as on the northern side.

The sedimentation in mid-Ordovician suggests that uplift and erosion was taking place, although on the southern margin it was not as extensive as on the northern margin (Windley, 1986).

In the Silurian, the lack of volcanic activity suggests that subduction of oceanic crust was complete. When the northern and southern plate collided in the late Silurian, it generated further deformation and volcanism, although the collision took place at a later time in the south west (Phillips et al, 1976). The suture is thought to be underneath the Solway Firth-Northumberland Basin (Anderton et al 1979).

The northern deformation front is well identified in northwest Scotland and Greenland, but the southern deformation front is not clear because the evidence was destroyed by Variscan deformation. Figure 1.1 illustrates the closure of the ocean.

1.1.2 Variscan Phase

The Variscan phase is problematic because of younger sedimentation cover and the evidence being destroyed by new orogenic belts eg the Alpine. This is why there are several tectonic models which may even disagree on the fundamental questions. They may be classified into two main groups: subduction orogeny, and strike-slip orogeny.

1.1.2.1 Subduction Orogeny

This theory assumes an ocean closure, but there is again a disagreement on which ocean closed, mid-European or Tethys.

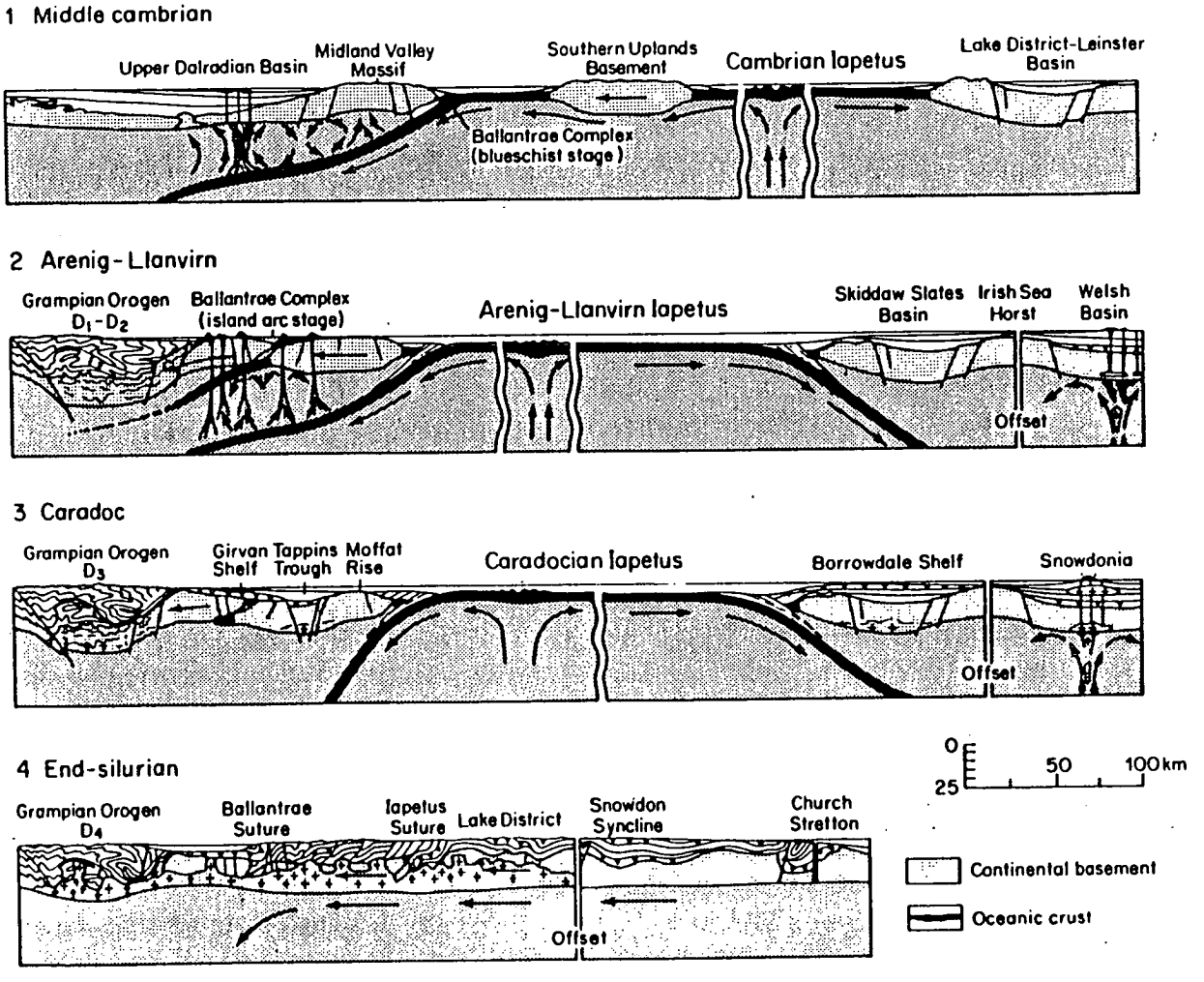

Figure 1.1 A plate tectonic model for British Caledonides (from Windley, 1986)

Nicolas (1972) suggested that the closure of the Tethys Ocean was the cause for the Variscan deformation. This generated a north dipping subduction zone. The continental margin lies underneath the Alpine fold belt which was the result of the collision between Africa and Eurasia after the closure of the ocean. In this model, all the Variscan zone lying north of the Alps was formed on a continental basement. Before the continental collision, fragments of the ocean floor drifted against the continental margin, and were obducted. Figure 1.2 shows the position of the plates before the closure.

This model was immediately challenged by Burrett (1972). He argued that Africa did not collide with north America until the Carboniferous, but there is evidence for the closure of a mid-European ocean during the Devonian and Carboniferous. The evidence is Devonian deep water sedimentation in Devon and Cornwall, and southern Europe. The volcanic activity in these places suggests that subduction zones were operating on both sides of the ocean. Figure 1.3 shows the closure of the ocean in time.

Riding (1974) pointed out that the correlation between the deformation zones of Texas and Russia indicates that the orogen resulted from the collision between Africa and Laurasia. The Variscan deformation of south east Europe was generated by the closure of the Tethys ocean but further west the continental microplate of north Spain was caught between the two continental plates. This generated an extra subduction zone and as a result of this volcanic activity and metamorphism took place. Figure 1.4 shows the dynamics of the process.

1.1.2.2 Strike Slip Orogeny

Badham and Halls (1975) suggested that the deformation of the Variscan orogeny was strike-slip motion of microplates, generated by the closure of the Tethys ocean. They argued that in order to generate the Variscan features by major plate

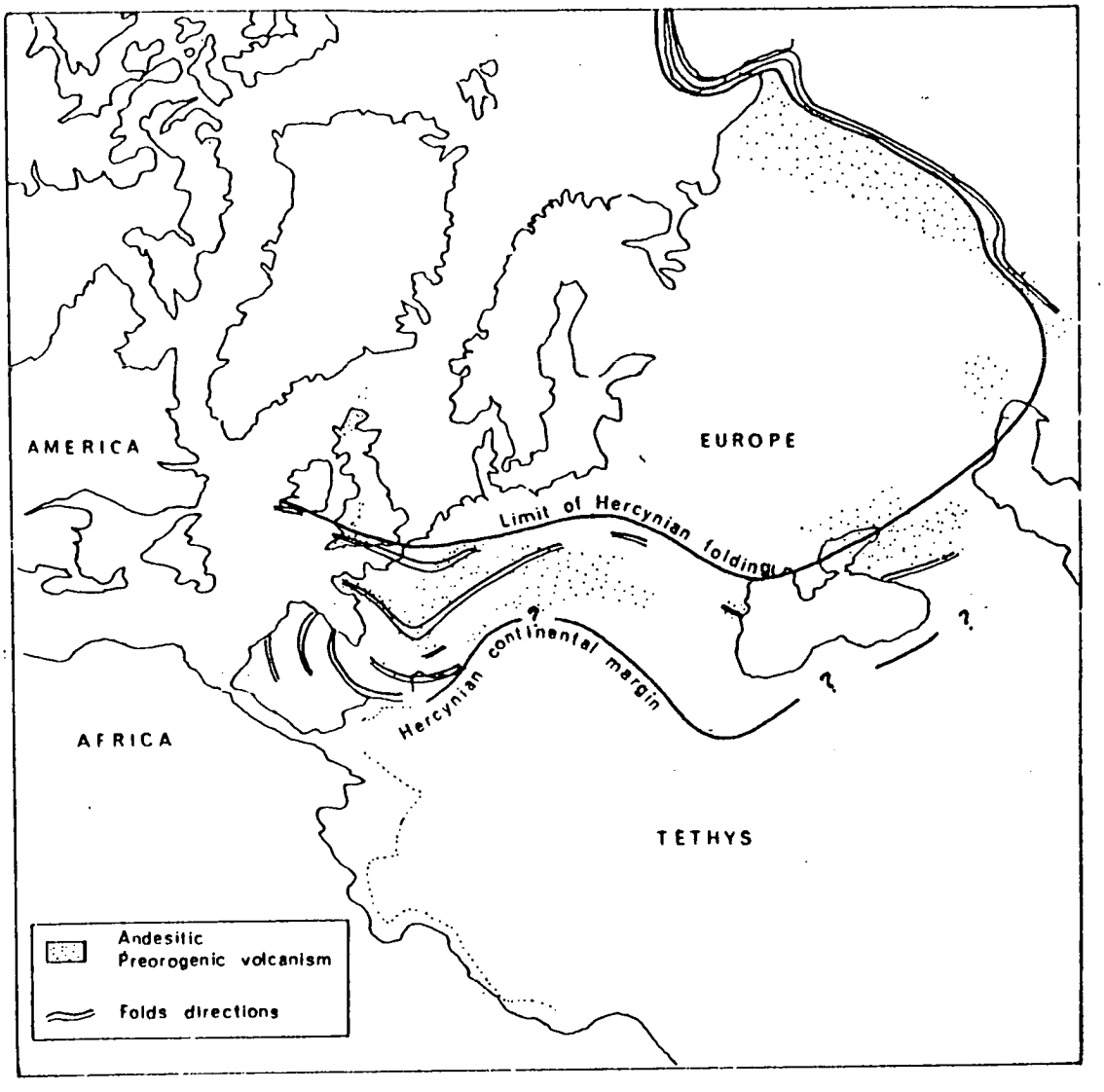

Figure 1.2 Possible positions of plates which generated the Variscan deformation (from Nicolas 1972)

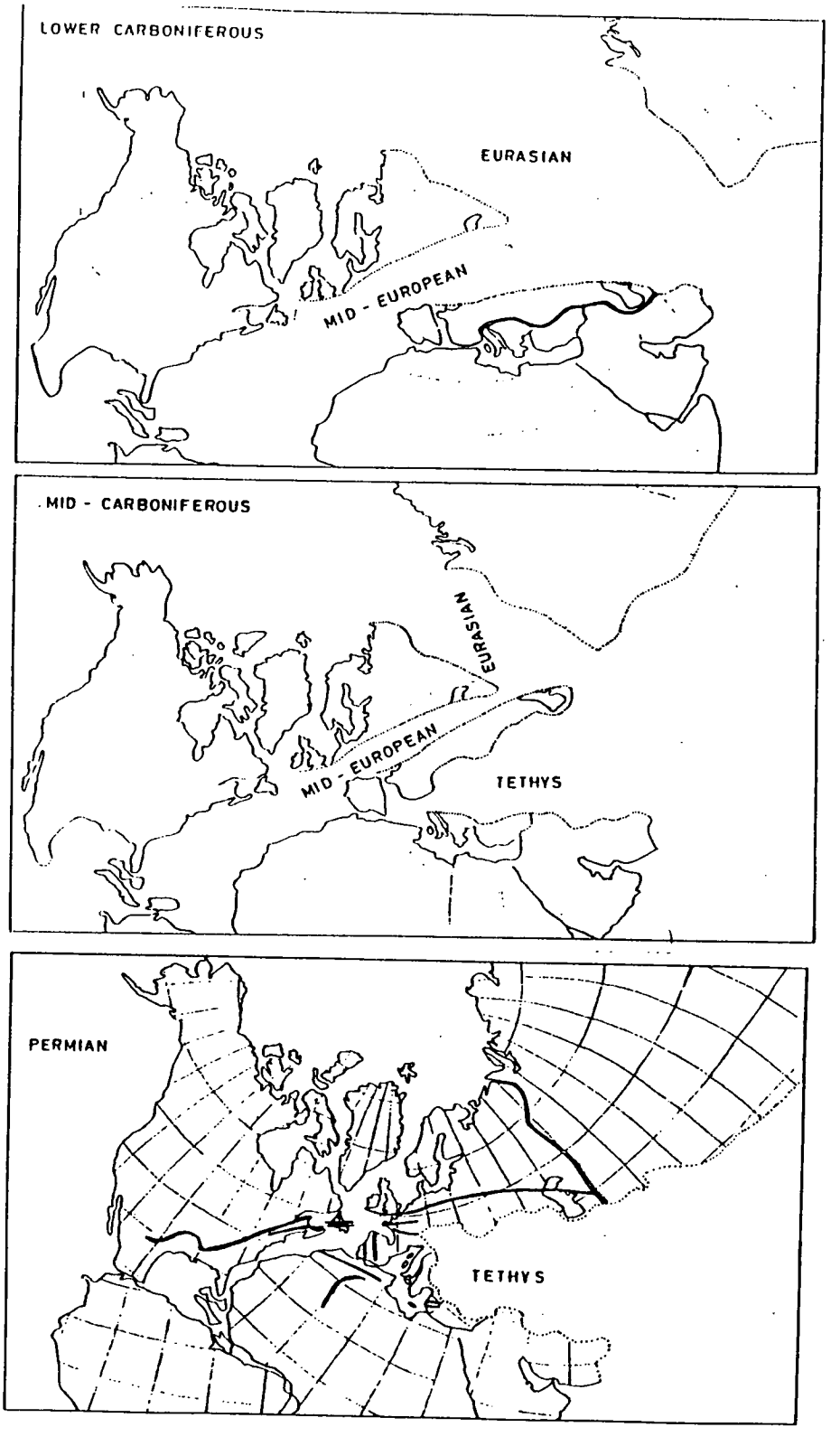

Figure 1.3 Closure of the mid-European Ocean in time sequences (from Johnson 1973)

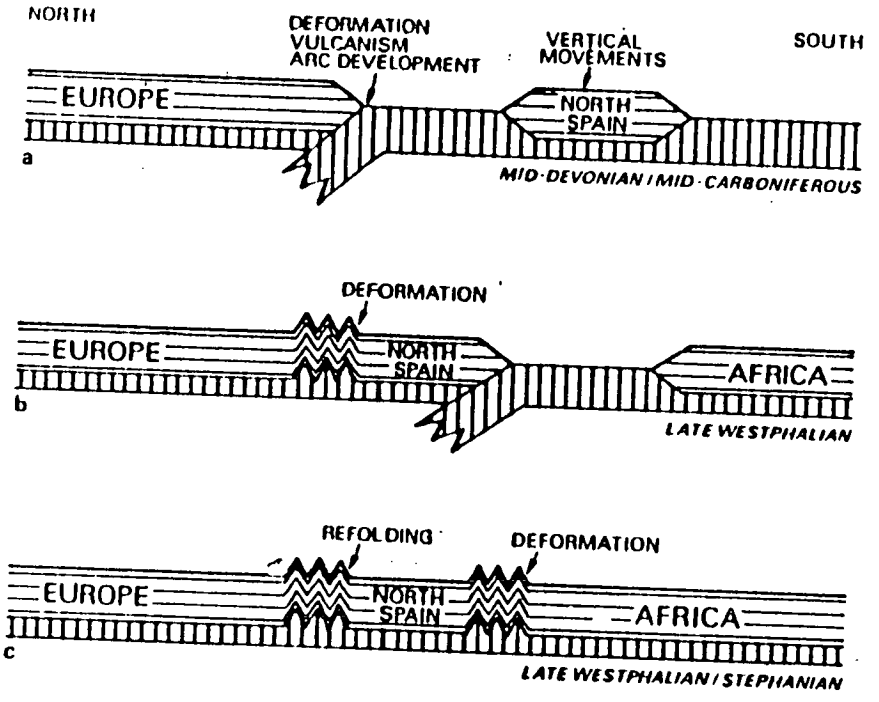

Figure 1.4 Possible plate tectonic model for Variscides (from Riding 1974)

movements, the plates would have had to move fast in Silurian and Devonian times, then change direction and slow down in Carboniferous time. Simple global models of the movements of Laurasia against Gondwana would result in France, Morocco and Iberia being overridden.

An alternative approach is to separate microplates with large strike-slip faults in the late Silurian and early Devonian. Along these strike-slip faults, the microplates moved westwards until the actual collision of the continental plates. During this migration the microplates suffered erosion, uplift and reactivation. They also obducted oceanic crust, for example the Lizard Complex.

The correlation of Variscan features in western Europe suggests that the formations were displaced by long dextral strike-slip faults (Holder and Leveridge, 1986). The Bristol Channel-Bray Fault is one of them, and a displacement in the order of 400 km is proposed (figure 1.5). From a seismic reflection profile in the ECORS program, Day (1986) reports that the Bray fault appears to displace the Moho in the Paris Basin, with thicker crust to the east.

1.2 Gravity

Over the past 10 years, a gravity data bank has been created in the Department of Geophysics, Edinburgh University by combining gravity observations from various organizations. The gravity data bank contains observations over most of the British Isles, Ireland and France and over waters surrounding the British Isles.

Hipkin et al (1986) produced the Bouguer anomaly map of southern Britain with contours drawn from a representation of the data on a regular 2 km grid. The main work in this research involves this data set, so that introduction to the preparation of the data set is necessary.

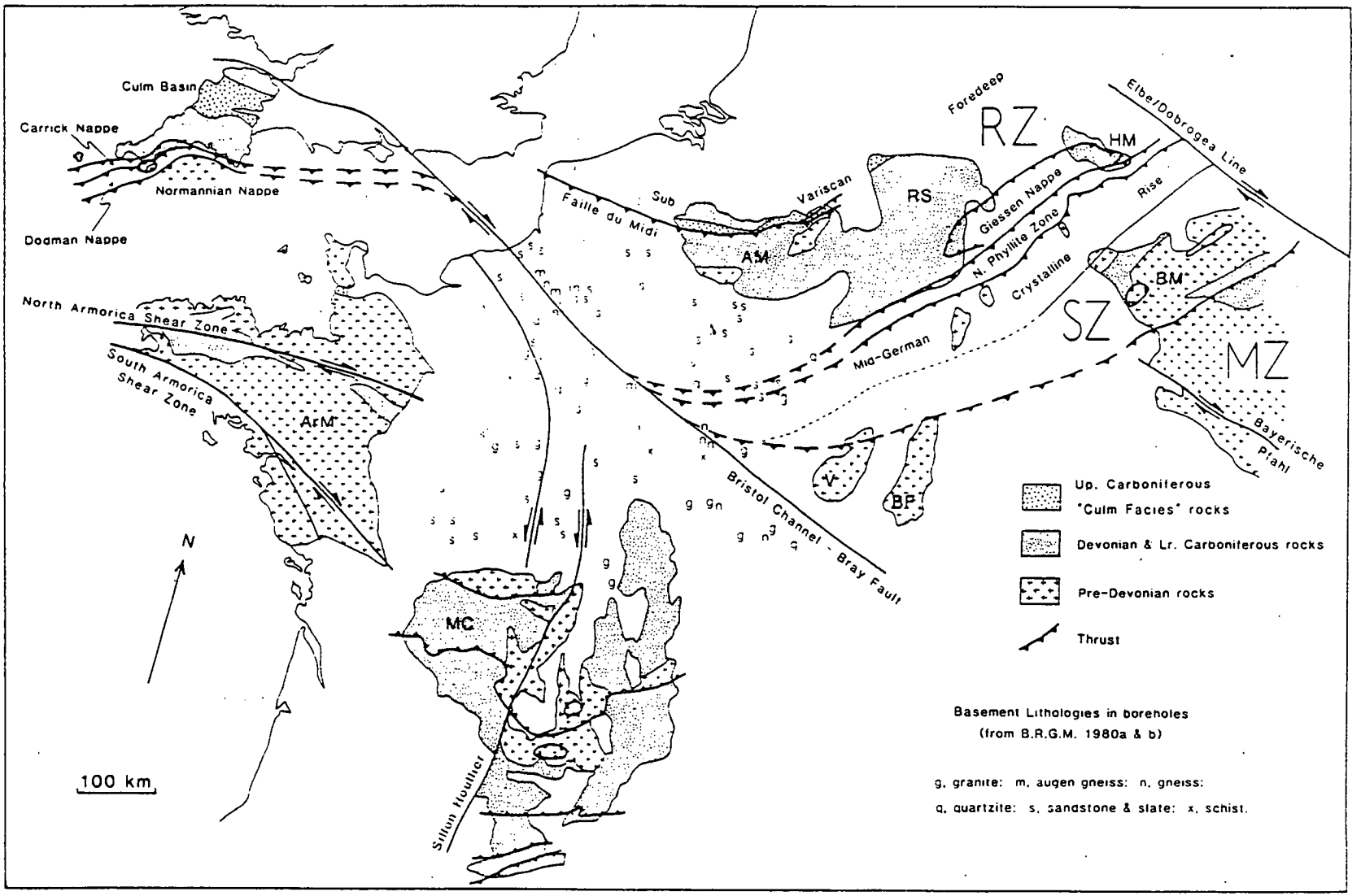

Figure 1.5 Variscan strike-slip faults of western Europe (from Holder and Leveridge 1986)

1.2.1 Gravity Data

There are more than 160000 data points over the region of 100 km to 700 km easting and -50 km to 55600 km northing of the British National Grid. Figure 1.6 shows the data coverage of the region. Note that the observation points are thinned for display purpose so that spacing between stations would not be closer than 2 km. Over the blank areas, the interpolation was done by digitizing contour maps based on commercial surveys where the original point data were not publicly available (see key on map, Hipkin et al, 1986).

1.2.2 Production of the Gravity Anomaly Map

The Calcomp GPCP (Calcomp 1972) computer program was used to interpolate the irregular gravity observations on to a regular grid. The way the program interpolates is explained in appendix 1.

The interpolation was made in blocks 100 km square. For each block, contoured, posted-value maps were drawn at a scale of 1:250000 to verify the data and the interpolation routine. Data from beyond the border were included so that no discontinuity occurred when joining arrays of gridded values from those blocks.

Over the land areas there was at least 1 observation per 2 km^2. Such close spacing of measurements was good enough to interpolate the data set on to a 2 km grid. However, over sea areas, although the observations were very close along ship tracks, the spacing between the ship tracks could be as large as 15 km. This was inadequate to interpolate the data every 2 km. The reason is that the interpolation routine uses only a limited number of nearby data points. If the spacing between ship tracks was too large, then only data points on the same ship track would be used for interpretation. For this reason the data set was thinned and grid spacing was increased to 4 km.

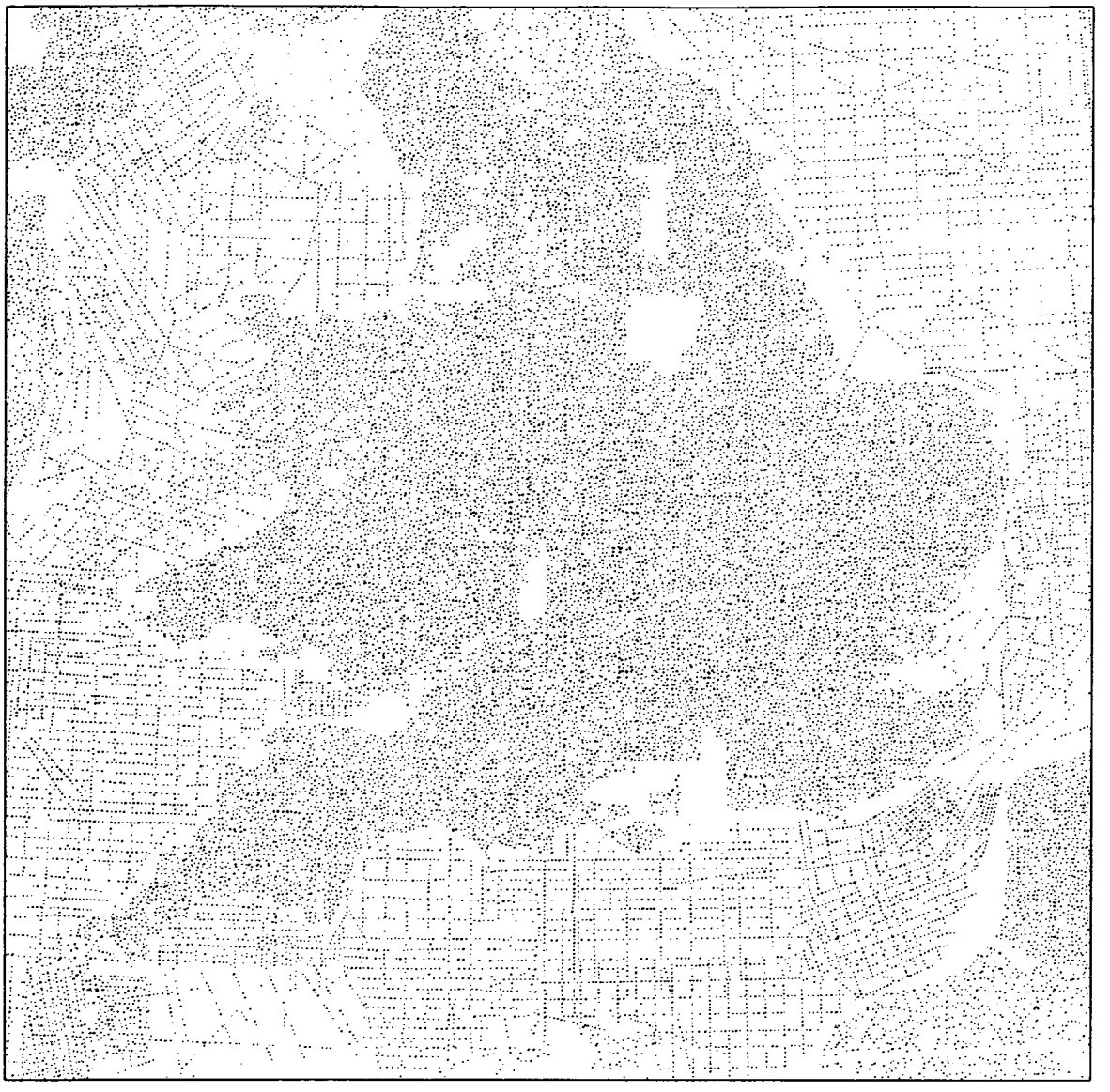

Figure 1.6 Data point distribution of the gravity observations. The points were thinned to 2 km.

After computing gridded gravity values with a 2 or 4 km grid spacing, 4 km blocks are then smoothly evaluated on to a 2 km grid using a cubic interpolation formula. The Bouguer gravity anomaly map is given in figure 1.7 and at back of the thesis.

1.2.3 The Bouguer Gravity Anomaly Map

The Bouguer gravity anomaly map shows a gravity high over the western half and a gravity low to the east with a step between. This step has only become apparent by putting together data for a very large region. Several local studies of gravity anomaly data (eg Bott et al, 1958; Bacon, 1975) have misinterpreted it as a linear regional gradient.

Between Cherbourg and Swansea, the step trends about NNW. This is surprising because none of the Variscan events in this region have this direction. From Swansea to Charnwood Forest, the trend of the step is approximately NE; from Charnwood Forest to Carlisle the trend is again NNW. The N-S trend over the Malvern hills is due to shallow volcanic basement of Pre-Cambrian age. In the North Sea, a NW trend of the gravity anomaly follows the Sole Pit - Dowsing Fault line marking the edge of a gravity low associated with the North Sea Basin.

Much of the remainder of the map is dominated by gravity lows caused by sedimentary basins. A broad gravity low over south and central England marks the London basin. Several more local, fault-bounded basins stand out prominently. The anomalies due to the Cardigan Bay and Cheshire Basins clearly follow Caledonian trend. Running E-W in the centre of the English Channel, there is a narrow linear gravity low, called the Central Channel Anomaly related to Variscan deformation. Continuing west from the Central Channel Anomaly there is a strong E-W lineament running into the Southern margin of the Cornubian granites. Other, nearly E-W lineaments show up clearly in the Bristol Channel.

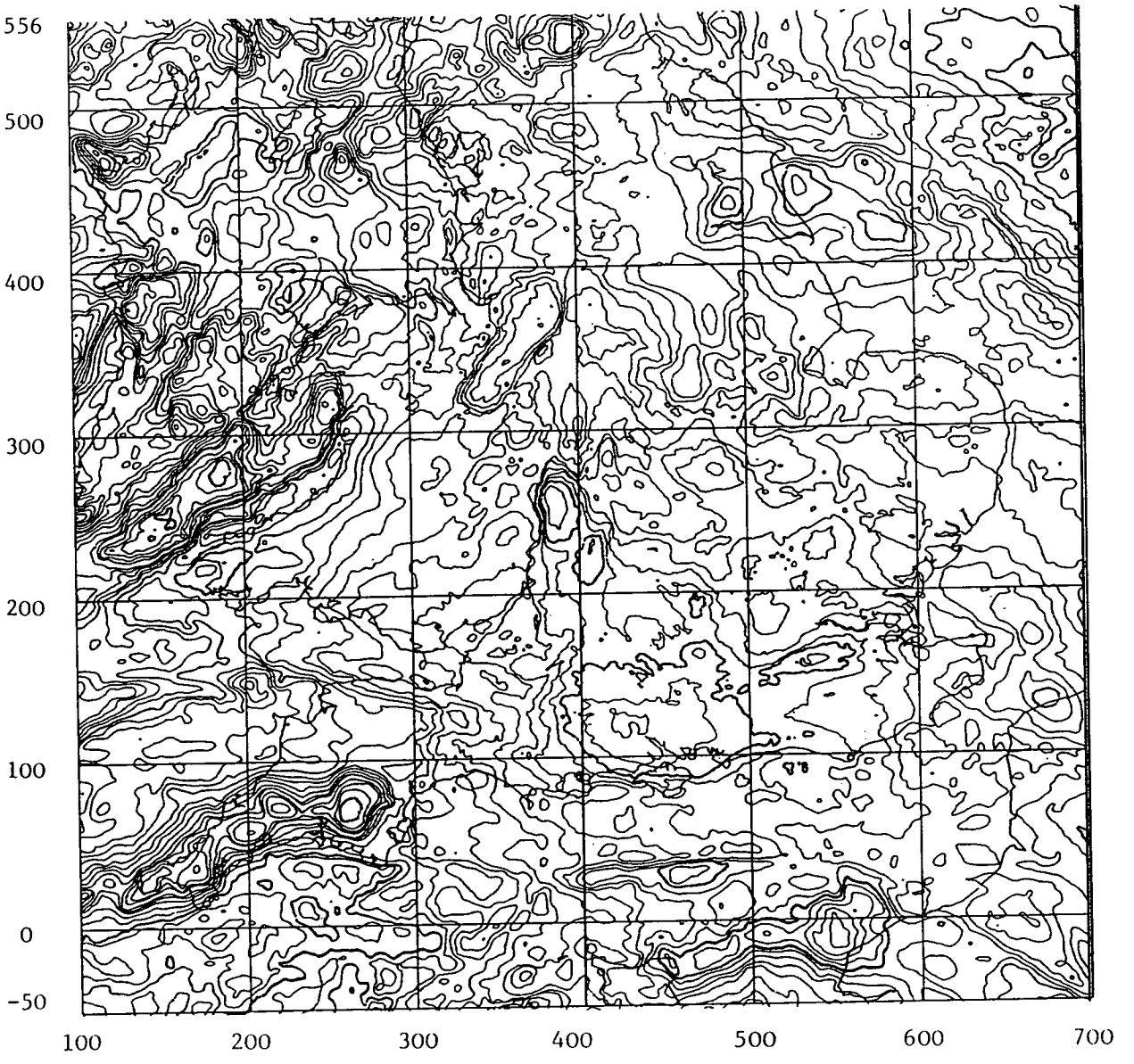

Figure 1.7 Bouguer anomaly map of southern Britain. The contour interval is 5 mgal. (Plate 1 at the back of the thesis is a larger version at a scale of 1:1000000.)

Apart from sedimentary basins, the other major source of negative gravity anomalies is granite. The largest amplitude anomaly is due to Cornubian granites, reaching -26 mGal compared with an approximately regional field between +35 to 40 mGal. The gradients average about 2 mGal per km over a distance of 30 km. Other clear anomalies associated with granites are the Weardale [395,540], Lake District [310,495], Askrigg [393,495], Market Weighton [490,437] and Leicester [465,330]. (The numbers in brackets refer to British National Grid easting and northing.) The elongated ENE trending anomaly running from Barfleur in the Cotentin Peninsula towards the Normandy coast has also been interpreted as a series of major granite batholiths similar to those in Cornwall (Day, 1986).

These two granite batholiths seem to be offset by the NNW trending gravity step. One of the original purposes of this project was to investigate this feature.

A broad view of the gravity anomaly of western Europe is produced by Karner at (1987). al. They used the British gravity data alongside land gravity measurements in France, the Netherlands, Belgium, Ireland, Luxembourg and West Germany and gravity data derived from SEASAT altimetry measurements. The data was interpolated onto a 5° grid. The gravity anomaly clearly identified the gravity anomaly trends related to Caledonian and Variscan deformation phases.

CHAPTER 2

STRIPPING OF THE GRAVITATIONAL ATTRACTION OF THE SEDIMENTS FROM THE BOUGUER ANOMALY

2.1 Introduction

Gravity anomaly sources may be separated into deep and shallow features. Deep features will generate long wavelength anomalies, but shallow features may contribute to long wavelength anomalies as well as short wavelength anomalies. This occurs when the near surface materials are deposited on a large scale. If this is the case, then the separation of the anomalies by filtering the data is impossible. However the problem may be resolved by minimizing the gravitational effect of near surface materials by computing their gravitational attraction and stripping off their effect from the Bouguer anomaly.

One of the biggest density contrasts within the crust is the density contrast between sediments and basement. If the sediment depth is modelled adequately, then the gravitational attraction of the materials can be stripped off from the gravity anomaly, providing the density of the materials is known. The sediment depth model, the density analysis and the computation of the gravitational attraction of the sediments are discussed in this chapter.

Another big density contrast within the crust is the density contrast of granites within the basement. Unfortunately granite models for southern Britain are not well defined, so the effect of these features could not be reduced with the available data.

2.2 Sediment Cover

The reference model for the sediment cover is the map of Contours on the Top to the Pre-Permian Surface of the United Kingdom (South) published by the British Geological Survey (Brown, 1985) (figure 2.1). It is compiled on the basis of boreholes and seismic reflection data. The contour interval on the original map is 100 m on land areas and 500 m over sea. Unfortunately this map does not cover Irish and French waters or the land areas of France.

The Atlas of Sedimentary Basins in England and Wales (Whittaker 1985) includes more information about the sediment cover for southern Britain. It has 9 different interfaces ranging from young chalks to Pre-Permian basement. This information about the sediment cover was not used in computing the gravity attraction of the sediments for two reasons. First of all when this atlas was published, the gravity attraction of the sediments had already been computed, taking about 6 days cpu computing time using an ICL 2988 machine. Introducing more complex structure with 9 different interfaces meant another 54 days of cpu time corresponding to more than a year in real time. Secondly it only covers the land areas.

Two forms of model of the sediment depth were compiled; one by digitizing the depth contours of the Pre-Permian basement map (section 2.4.3), and the other by interpolating these digitized depth contours on to a regular grid (section 2.4.5.2).

2.3 Densities

One of the most important parameters in the stripping process is density. If the density of the sediment is known everywhere, and the sediment geometry is also determined, then the stripping process will be completely successful. However, determining every detail of the density everywhere is impossible.

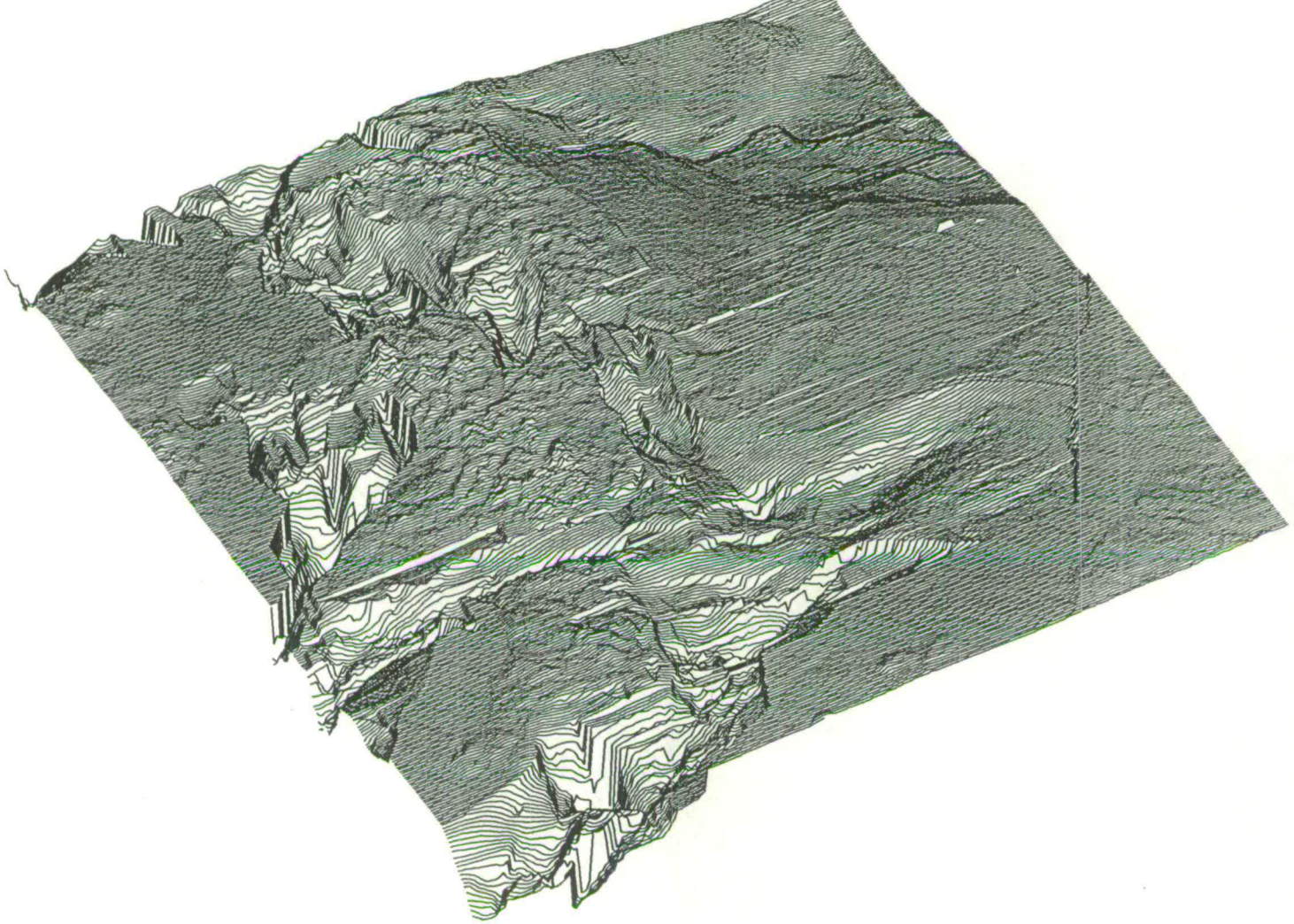

Figure 2.1 A 3-dimensional view of Pre-Permian basement, looking from the south.

If the large scale variation of the density is determined then local fluctuations in density generate only the short wavelength anomalies on the resulting stripped gravity anomaly map.

A density data bank was created including hand samples and neutron log densities from boreholes. It was used to analyse which parameters were most important in controlling rock densities, so that a simple one parameter model of density could be generated. This model was used to strip the deeper part of sedimentation.

However, the near surface materials have to be excluded in this regional model because even a small fluctuation of the density may produce a large gravity anomaly. If they are on a relatively large scale, then features will be present in the long wavelength anomalies. So there is also a need for a model of surface densities, for the shallow part of the stripping process. Surface densities may be obtained by regression analysis of the Bouguer anomaly.

2.3.1 Regression Density Analysis

If we formulate the Bouguer anomaly as

$$ba=fa-2\pi\mathcal{G}h\rho_0+T\rho_0, \qquad 2.1$$

where fa is the free air anomaly, h is the elevation of the gravity station, ρ_0 is the terrain density, T is the terrain coefficient and $\mathcal{G}$ is the gravitational constant, provided that the topography does not represent lithological changes, the true terrain density value may be computed by regressing ba against $2\pi\mathcal{G}h-T$.

The regression can be achieved by representing the Bouguer anomaly with a polynomial trend surface and searching for a terrain density value which makes the Bouguer anomaly fit the surface best. It is clear from equation 2.1 that over the

flat areas the solutions become ambiguous.

Estimating the terrain density was carried out for every land 10 km square of the British National Grid. This was done by representing the Bouguer anomaly by a quadratic surface. The same process was repeated for a cubic representation of the Bouguer anomaly but the solutions were mainly unsuccessful.

After statistical analysis of each fit, some solutions were rejected. Acceptance criteria were that the standard error on the density should be less than 0.05 g/cm^3, the standard error in fitting data to the surface should be less than 0.5 mGal and the surface should be represented by at least 10 observations. Unacceptable solutions like negative densities were eliminated from the data set even if their statistical analysis showed that it was a good fit. Successful solutions are given in appendix 2 table 1 for different periods and average densities are given here in table 2.1.

The Calcomp GPCP program was used to interpolate successful solutions on a 25 km grid. The model of outcrop density was then obtained by smoothly interpolating this on to a 2 km grid. Figure 2.2 shows this model for southern Britain.

2.3.2 Well Densities

2.3.2.1 Hand Samples

In a joint project called BIRDS, between the British Geological Survey and the University of Edinburgh, Geophysics Department, an attempt was made to catalogue the rock densities around Britain. Unfortunately the project has never been completed. The existing data were laboratory measurements of rocks from boreholes and surface outcrop.

Figure 2.2 Density contour map for southern Britain. Contour interval is 0.1 g/cm^3.

In an extension to the data set, the literature was searched for published density data. The additional data, like the BIRDS data, are mainly hand sampled. The recording starts as early as 1952. The compilation of the two data sets is given in appendix 2 table 2.

The contribution of these data sets in determining the density relation to the different parameters is tiny, because the depth of the specimens is too shallow.

2.3.2.2 Neutron Logs

J. E. Armstrong (personal communication) digitized FDC neutron density logs from North Sea well logs held by the Hydrocarbons Unit of the British Geological survey. The main intention in this work was to determine the average densities of different lithologies belonging to different periods. Nevertheless this work has contributed enormously to analysing density variations.

With permission from the British Geological Survey, 20 additional FDC well logs were digitized. The location of these wells is displayed in figure 2.3.

The density curve was averaged over successive intervals of 100 feet and the uncertainty estimated. The corresponding lithology and age were also recorded. The averaging was done by eye rather than using sophisticated electronic devices. That was the only option because the logs are kept in a location where there are no such devices available, and for security reasons the logs could not be borrowed. The results are given in appendix 2 table 3.

2.3.3 Density Relation with Different Parameters

The conventional approach to computing the gravitational attraction of sediments is to have interfaces between different age units each of which has a constant

Table 2.1

Average densities of the different lithologies. The number in the parentheses refers to the lithological indexes in the Geological map of the British Isles. Parameter N defines number of data.

Density	N	Structure
2.756+/-0.04 2	11	Wenlock-Silurian (73)
2.720+/-0.025	16	Lu dlow-Silurian (74)
2.611+/-0.079	28	Lower Old Red Sandstone-Devonian (75)
2.576+/-0.083	26	Limestone-Carboniferous (80)
2.569+/-0.084	58	Namurian-Carboniferous (81)
2.561+/-0.094	40	Lower Westphalian-Carboniferous (82)
2.580+/-0.075	8	Upper Westphalian-Carboniferous (83)
2.321+/-0.270	9	Sandstone-Permian&Triassic (89)
2.324+/-0.178	21	Mudstone-Triassic (90)
2.296+/-0.131	24	Lower Lias-Jurassic (91)
2.369+/-0.110	19	Inferior Oolite-Jurassic (94)
2.289+/-0.076	16	Great Oolite-Jurassic (95)
2.298+/-0.160	12	Oxford Clay-Jurassic (97)
2.269+/-0.127	13	Corallian-Jurassic (98)
2.136+/-0.196	55	Chalk-Cretaceous (106)
2.085+/-0.124	18	London Clay-Tertiary (108)

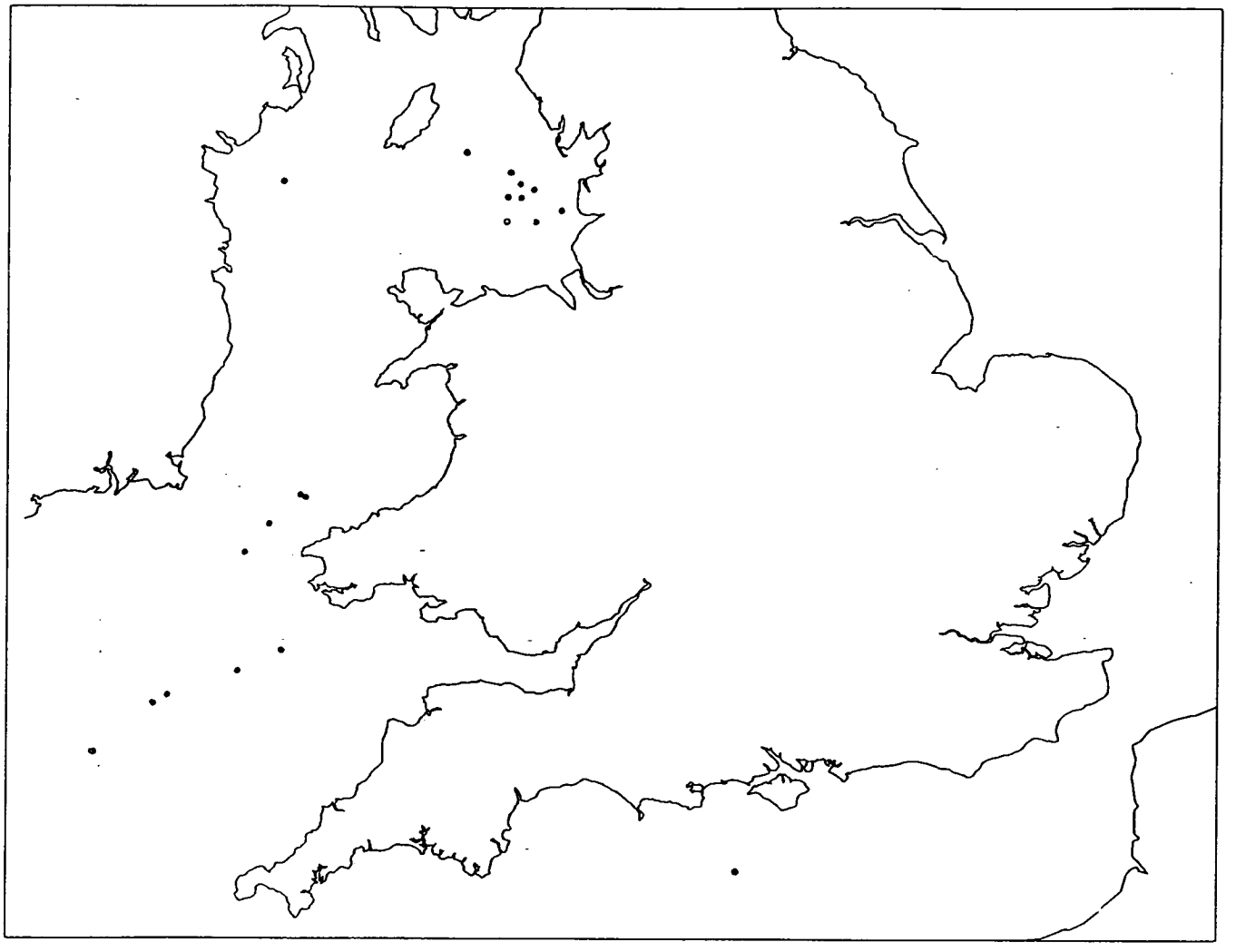

Figure 2.3 Location of the boreholes.

density. Figure 2.4 and figure 2.5 show the density changes with depth for the Triassic and Jurassic periods. It is clear that the density changes with depth. Any model based on age units needs also to vary density with depth. This approach will give a satisfactory result when the computation is carried out for local regions, which could be added together to form a larger region but this would require a tremendous amount of computing time.

The other approach to the computation is to have interfaces between different lithologies. When densities of different lithologies are plotted against depth, the data are again scattered about a clear trend of increasing density with depth. (sandstones in figure 2.6 and clay in figure 2.7).

It has been shown that there is a common trend for density to increase with depth for all age units and lithologies. The scatter about one common curve (figure 2.8) is not significantly greater than the scatter about individual curves for one lithology or one age unit.

The only exception of this generalization is salt. It is well known that the density of salt hardly changes even under very high pressure, because of its plastic behaviour. Figure 2.9 shows density changes of salt with depth. For this reason salt was excluded from figure 2.8. The remaining data were used to find a simple exponential curve to model the density depth relation. Similar findings were obtained from the North Sea data shown in figure 2.10. The only difference between these two data sets is that the density values in the North Sea are slightly lower than the ones in Celtic Sea and Irish Sea. This may be because the North Sea wells were in the Central Basin where the present day sedimentation rate is much greater than in the Celtic and Irish Sea. The Central Basin of North Sea covers only a small area in the north east of the map, so this density variation may be taken as a local effect.

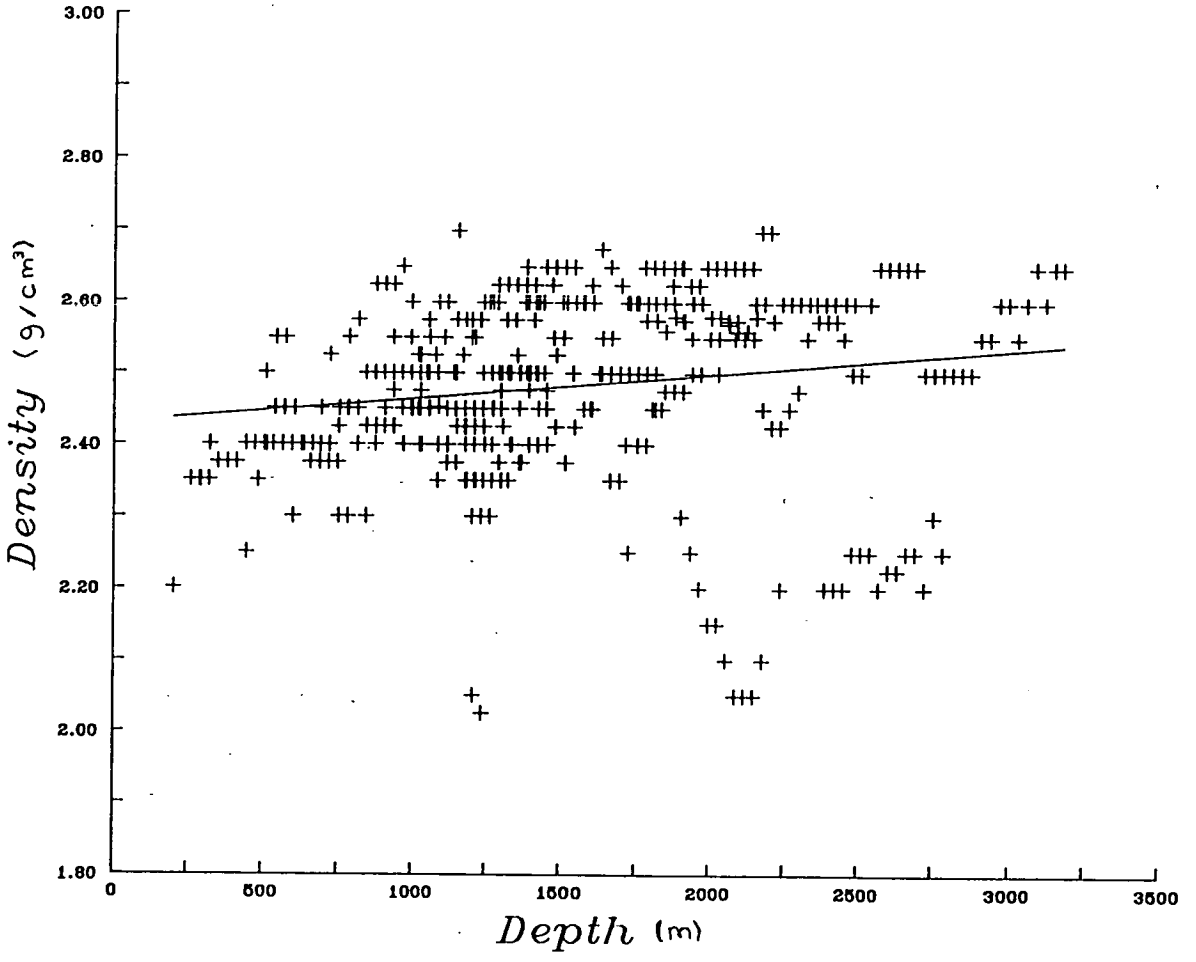

Figure 2.4 Density changes with depth for the Triassic.

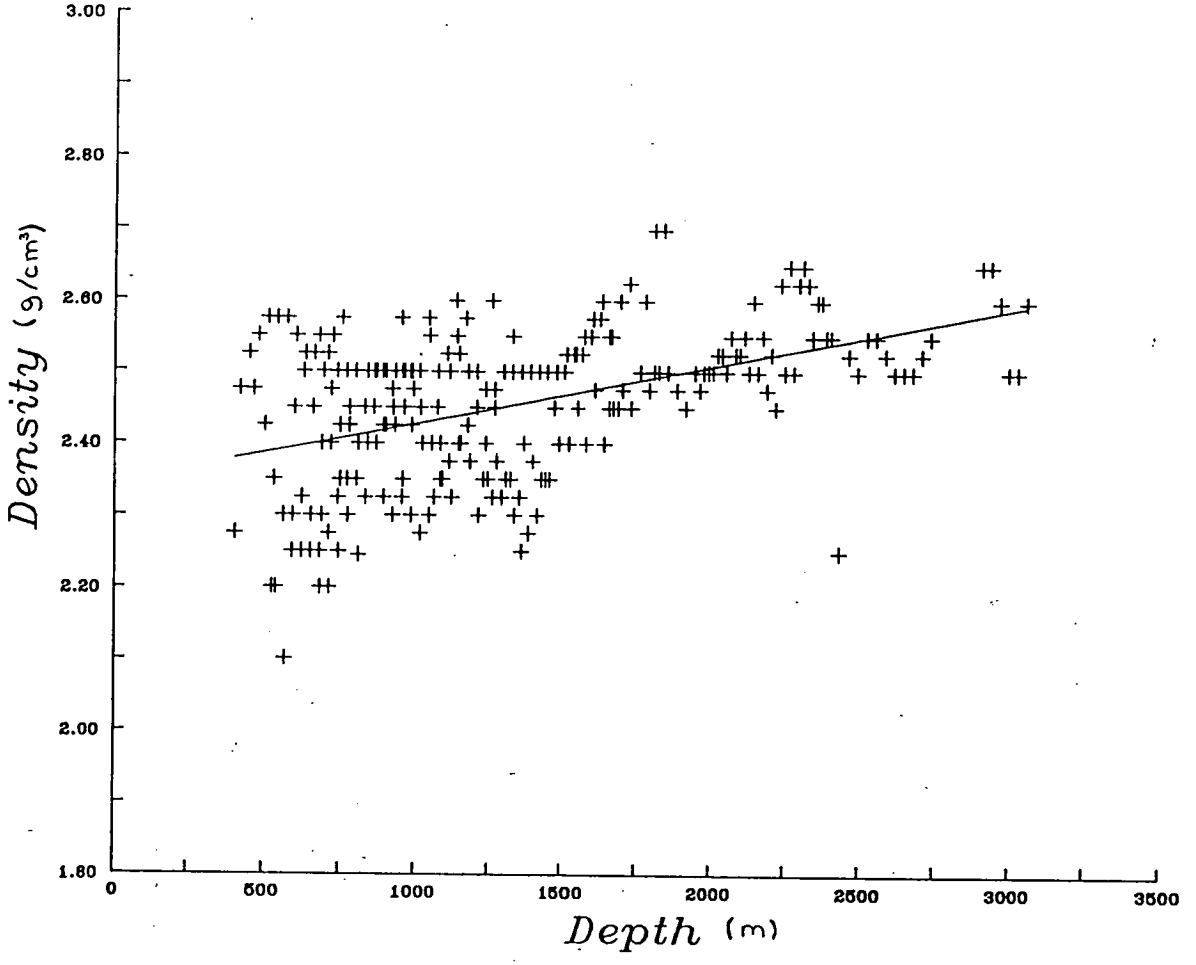

Figure 2.5 Density changes with depth for the Jurassic.

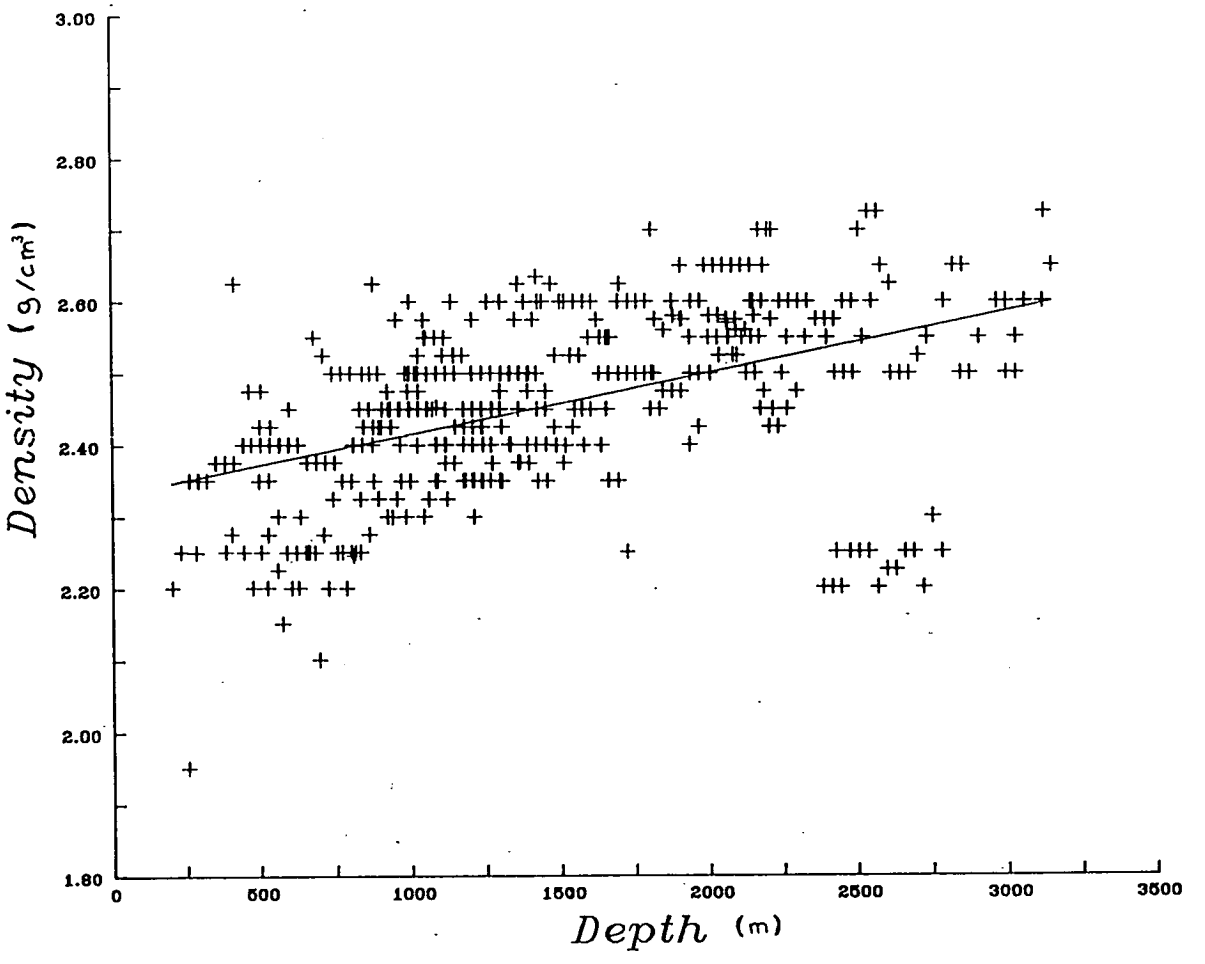

Figure 2.6 Density changes with depth for sandstones.

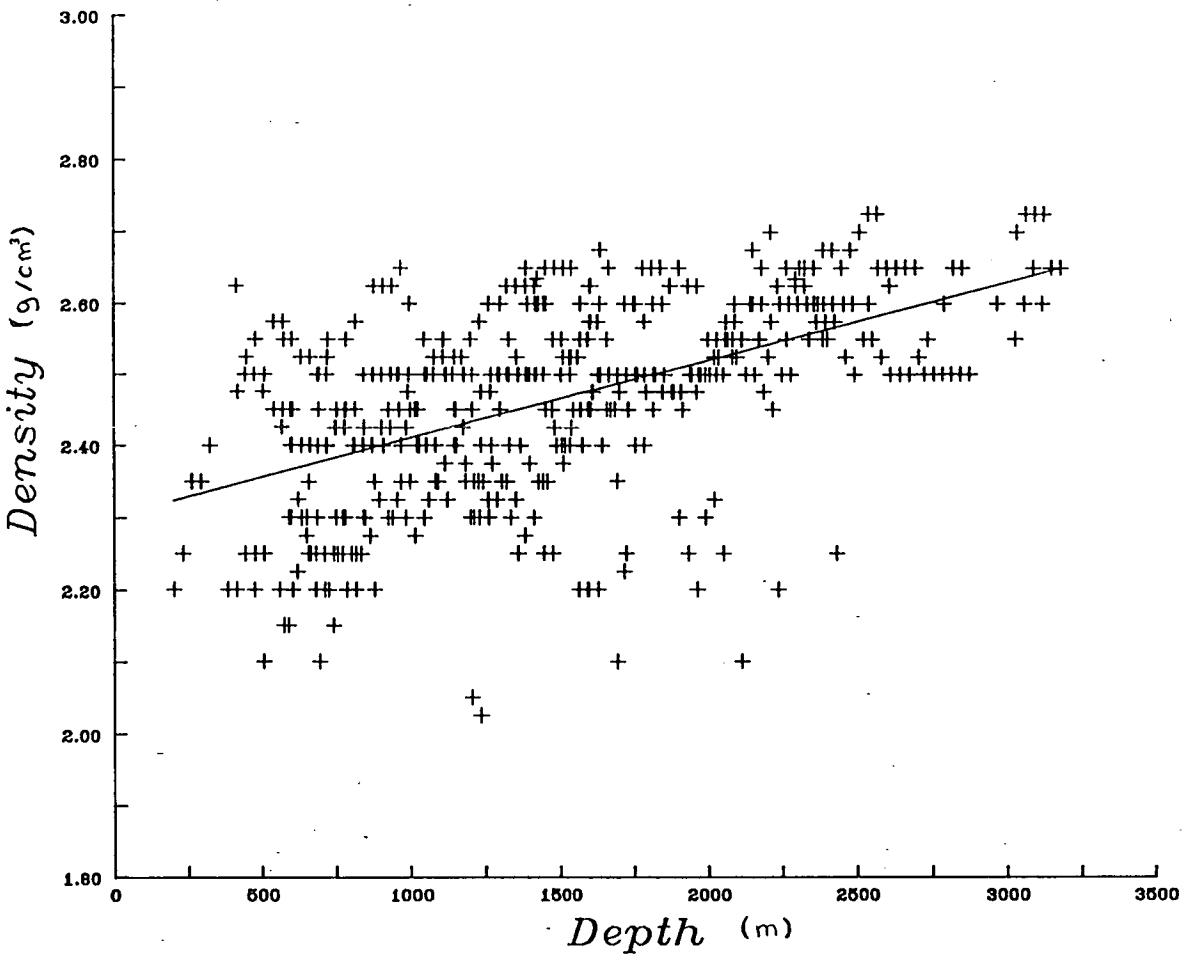

Figure 2.7 Density changes with depth for clay.

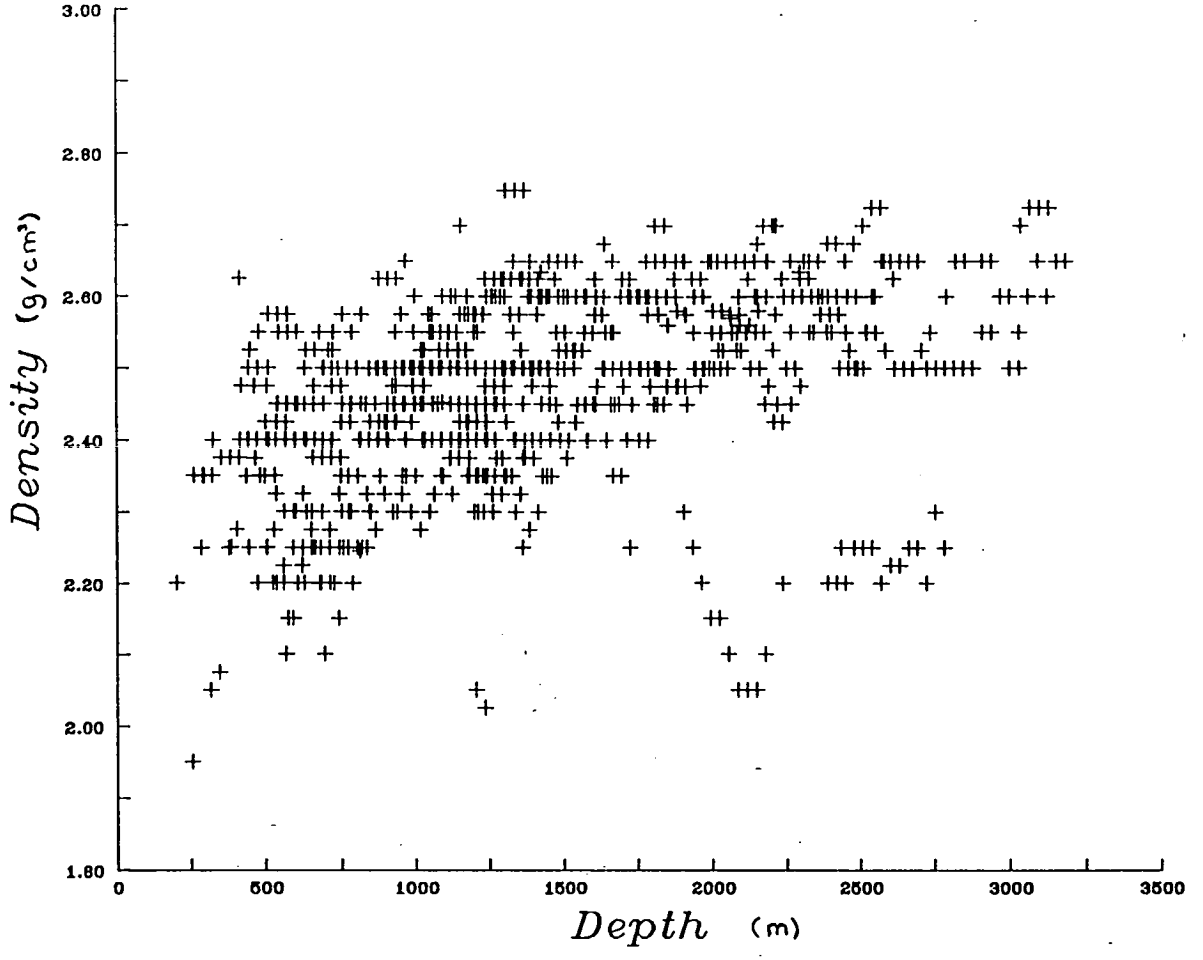

Figure 2.8 Density changes with depth for all samples except salt

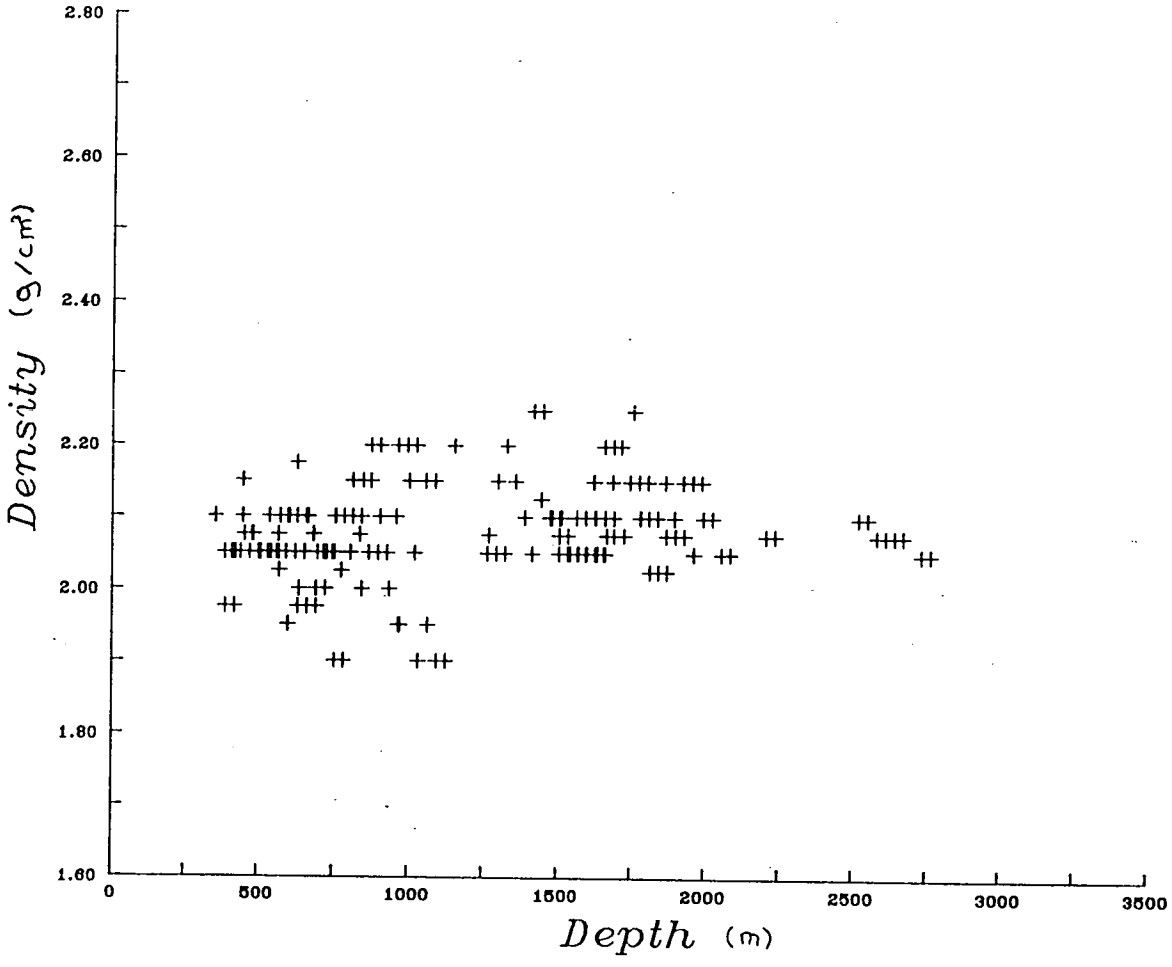

Figure 2.9 Density changes with depth for salt.

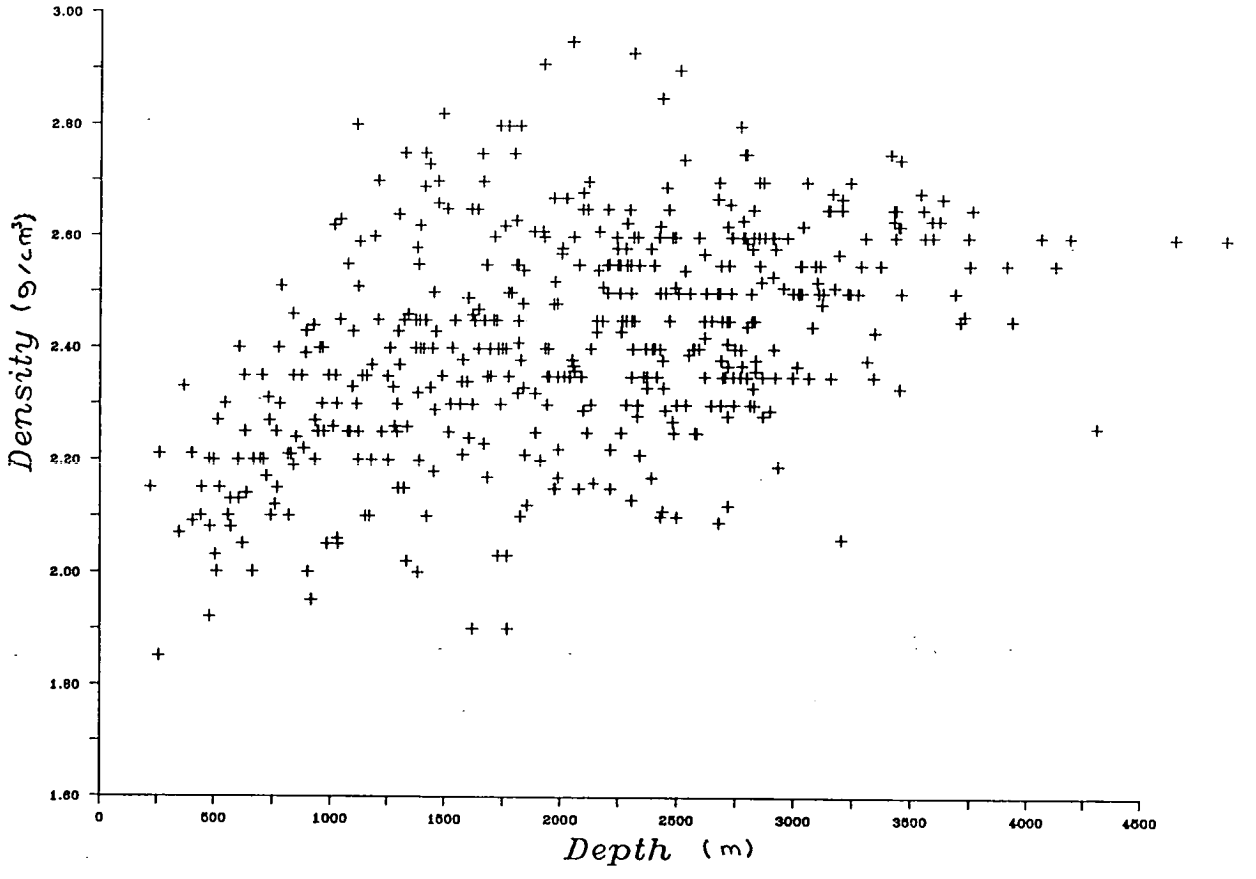

Figure 2.10 Density changes with depth for the North Sea.

The density function is made to approach a density value of 2.7 g/cm^3 at a depth of 12 km, which is the deepest point in the Pre-Permian basement. (2.7 g/cm^3 approximates the density of crystalline basement, and so was used for the Bouguer density on the original map). Figure 2.11 shows the density function, finally used for stripping.

It is obvious that over a few regions the density depth function may not represent the density values properly. If this is the case, then the gravitational attraction of the materials can be corrected locally after computing the regional effect.

2.3.4 Low Density Layer in Celtic Sea

Lovelock (1977) pointed out that Permo-Triassic sandstones over the United Kingdom have a very low density, going as low as 2.04 g/cm^3, around Yorkshire and Durham. This low density value of the Permo-Triassic sandstones may not act as an important parameter in computing the gravitational attraction of the sediments when they are near to the surface. Lateral density change on the surface has already been dealt with and the density function shows a low density value for shallow structures. However the problem arises if this type of rock is deep and its sedimentation is on a large scale.

The lithological well logs of 106/24-1, 106/24-2b, 106/28-01 and 103/2-1, plotted in figure 2.12, show these Triassic sandstone sediments in Cardigan Bay. Their average density over the area is 2.22 g/cm^3 and some sort of local correction is necessary. The shape of the layer was obtained by using a simple relation between its depth and the depth of Pre-Permian basement. This relationship was found from the four boreholes and then extrapolated elsewhere using the Pre-Permian basement. Figure 2.13 shows the relation between the basement and the low density layer depth.

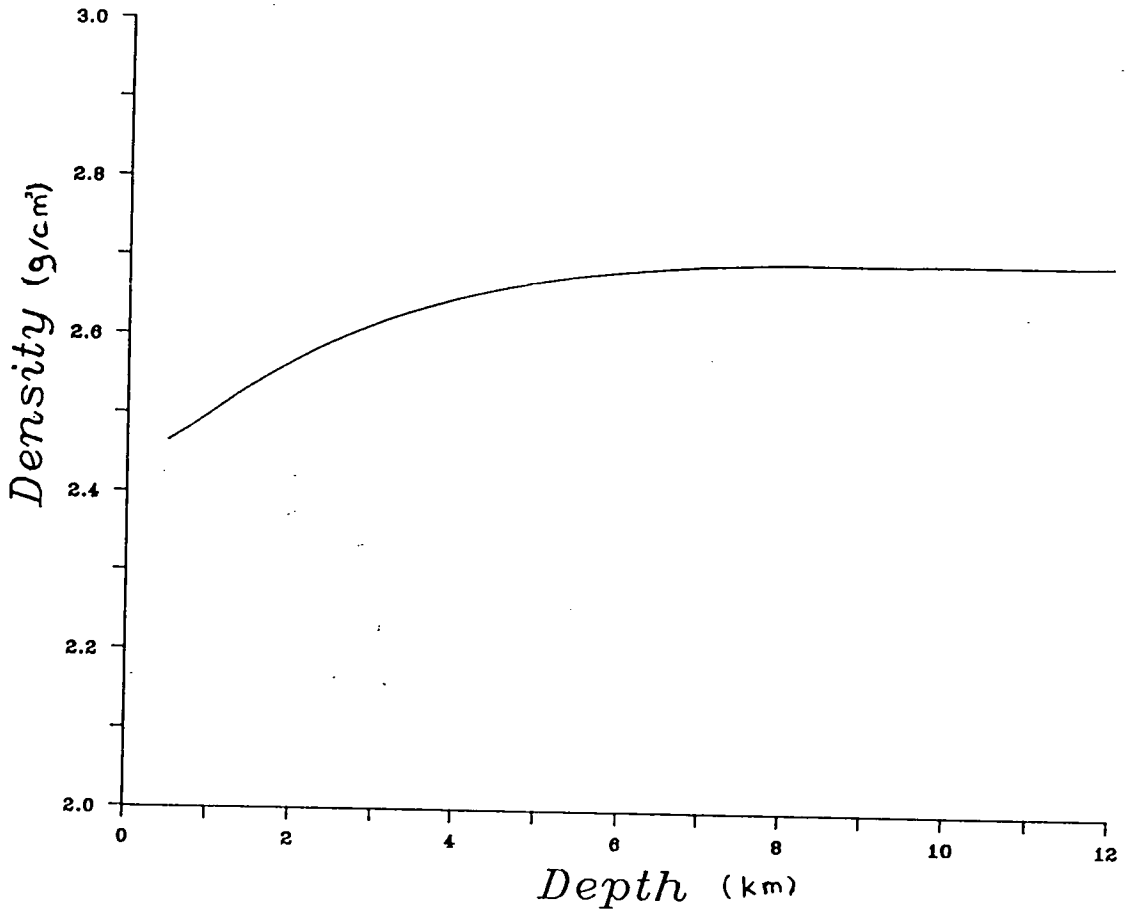

Figure 2.11 Density depth function used for stripping.

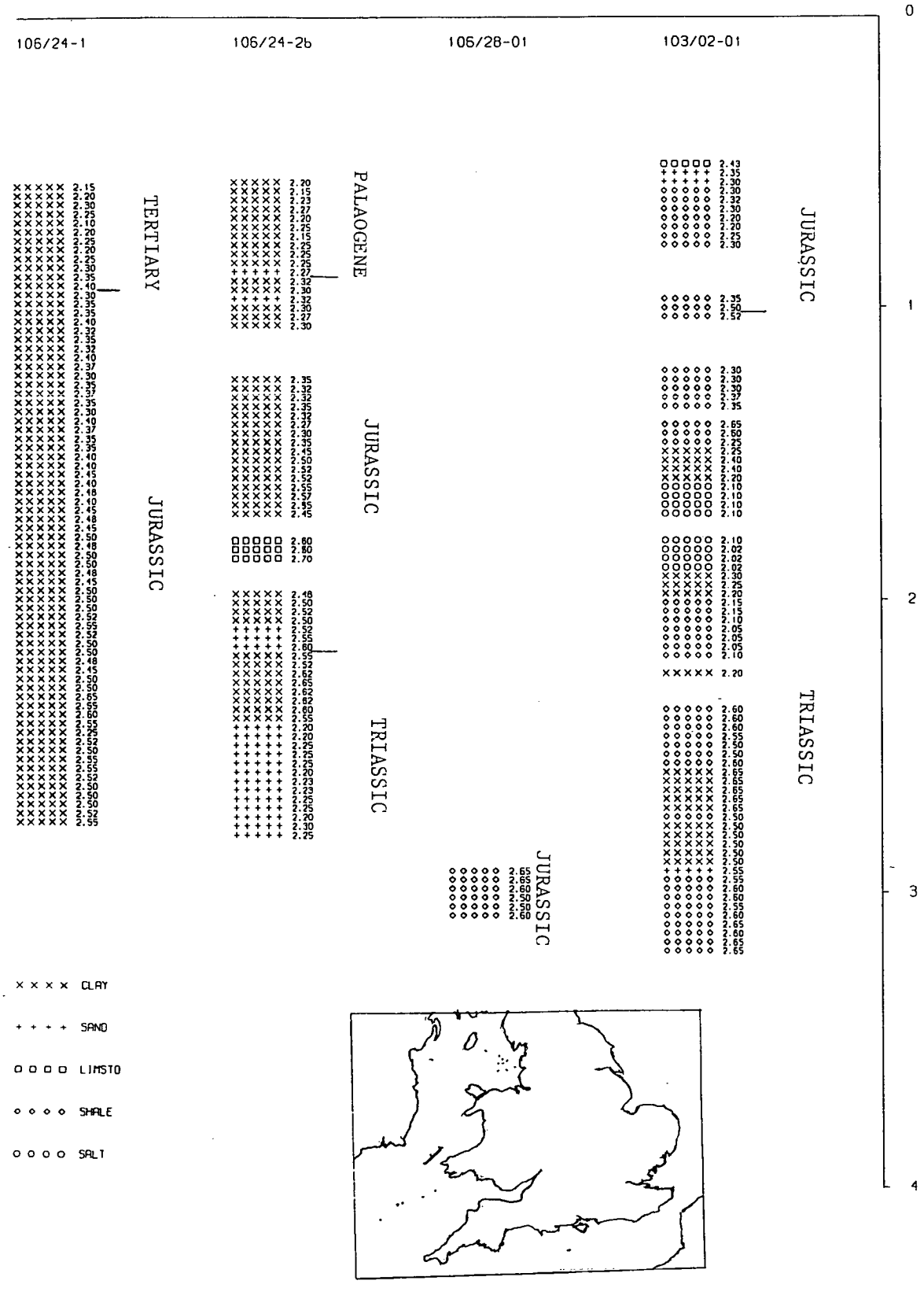

Figure 2.12 Lithological log of 4 boreholes. Inset is the location of the logs.

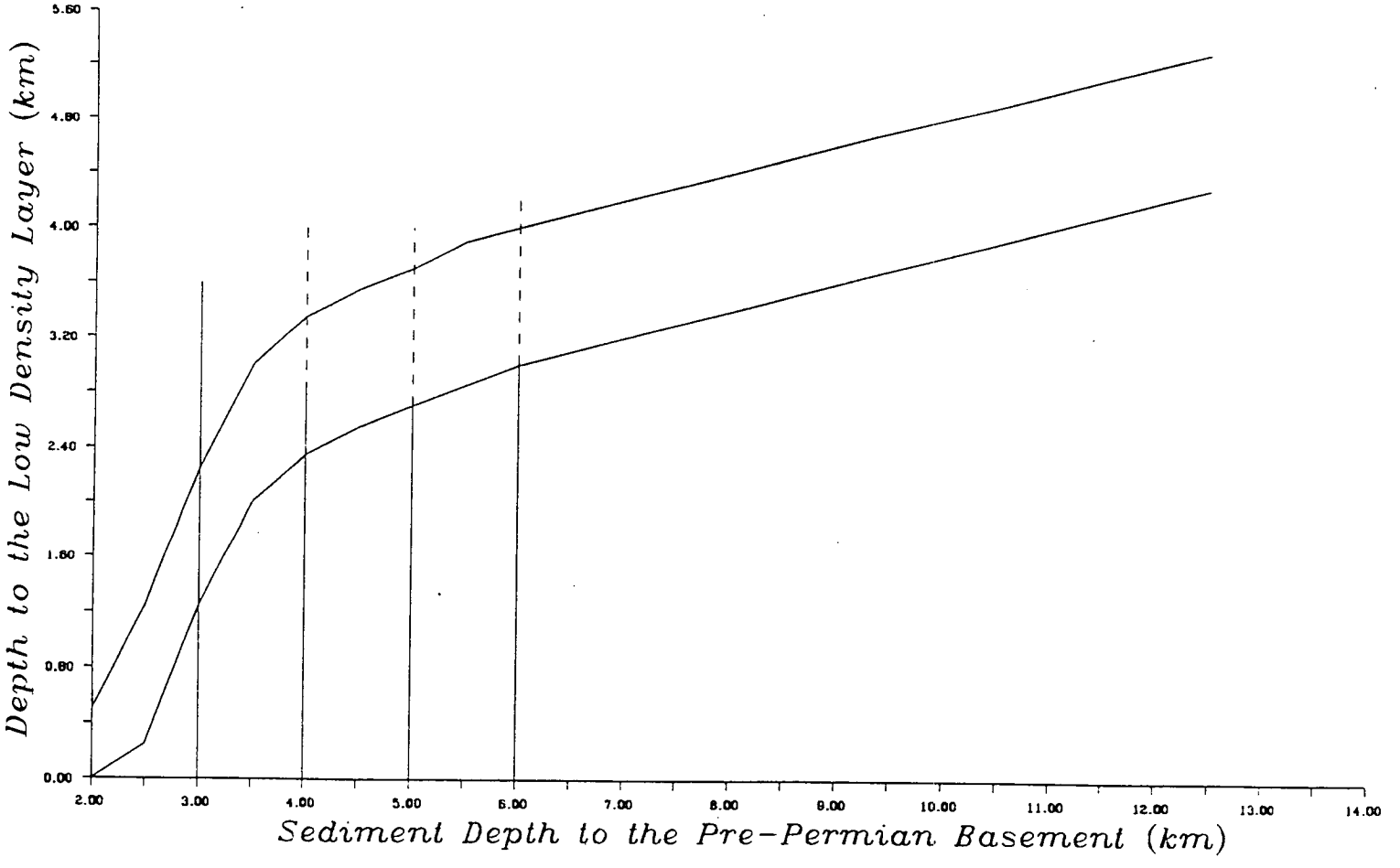

Figure 2.13 Relation between the depth and the thickness of the low density layer and depth of the Pre-Permian basement. Vertical lines show the extent of the boreholes control.

2.4 Computation

2.4.1 Sediment Model

The Pre-Permian basement map of southern Britain was digitized at a spacing of 1.3 km along every contour. The direction of the digitizing was chosen so that the deep part of the basement was always on the left hand side of the contour. (This is required for use with the contour integration routine described in section 2.4.4).

The digitized representation of the Pre-Permian basement map has around 50000 coordinate pairs over 600x700 km^2 area. If the gravitational attraction of the sediments was to be computed using all the data points, the predicted computing time would have been approximately 90 days cpu time which may be managed inside two years of real time. To overcome the problem, a representation of the sediments in 100 km square blocks was introduced.

2.4.2 100 km Square Sediment Models

When a gravity source is far away from the field point, then its gravitational attraction is negligible provided that the linear dimensions of the mass are small compared with the distance. The biggest sediment depth in the region is in Cardigan Bay and it is about 12 km with horizontal dimensions of 60x30 km^2. The gravitational attraction of this source is in the order of 0.1 mGal at a distance of 100 km, when a density contrast is chosen as 0.2 g/cm^3. This gives us the confidence not to calculate its gravity attraction beyond this distance.

Systematically the digitized representation of the sediment cover was divided into 100 km squares blocks of the British National Grid. This was done by using a FORTRAN program called SEPDEPTH, written for this purpose (appendix 3).

The program takes the digitized points and finds which square they belong to. If the contours go out of the 100 km square, then the program finds their intercept with the border of the square, and adds these points to the contours for both squares. Extra essential data points are also added at the corners to form closed contours around each 100 km square.

When a block was further than 100 km away from the field point, its gravity attraction was taken as 0; thus no more than 9 blocks of sediment model were used. This simple arrangement of the sedimentary cover cut down the computation time from 80 to 1-5 cpu seconds of computing time for a single field point. In total, it was reduced to around 6 days of cpu computing time.

2.4.3 Algorithms for Computing the Gravity Attraction of the Sediments

There are several algorithms for computing the gravitational attraction of an irregular body. Probably the commonest one is the one developed by Talwani and Ewing (1960), which involves the contour integration of horizontal polygonal laminae. This algorithm was chosen for two reasons. First, the data were already in the form needed for input to the algorithm. Preparing the data for other different algorithms means extra work on the sediment model. Secondly, the contour integration method is more convenient for representing complex shapes than for example a prism model.

2.4.4 Contour Integration Method

If the irregular body is represented by polygonal laminae, defined by the digital contours of the body, then the gravity anomaly caused by unit thickness is obtained by surface integration around the lamina. At a depth of $z=z_n$, the surface integration defined by

$$V(z)=\mathcal{G}\Delta\rho\left(\int d\psi-\int z/(r^2+z^2)^{-1/2}\, d\psi\right), \qquad 2.2$$

where $\mathcal{G}$ is the gravitational constant, ψ is the azimuthal angle, V is the gravity anomaly per unit thickness, $\Delta\rho$ is the density contrast of the body, z is the vertical distance and r is the horizontal distance. The line integrals are evaluated around the contour line. The gravity anomaly on the surface of the Earth may be written as

$$\Delta g=\int_z V(z)dz. \qquad 2.3$$

The limits of the integration are from the top to the bottom of the body. If we know V then we can evaluate 2.3 by using a suitable approximation. If the density varies with depth, the equation 2.2 may be modified as

$$V(z)=\mathcal{G}\Delta\rho(z)\left(\int d\psi-\int z/(r^2+z^2)^{-1/2}\, d\psi\right). \qquad 2.4$$

Using the corners of the lamina these two line integrals can be represented by summations as

$$V(z)=\mathcal{G}\Delta\rho\,\Sigma_i\left(\psi_{i+1}-\psi_i-\arcsin(z\cos\theta_i/(p_i^2+z^2)^{1/2})\right.$$
$$\left.+\arcsin(z\cos\phi_i/(p_i^2+z^2)^{1/2})\right). \qquad 2.5$$

The parameters in this equation are given in figure 2.14. It is clear from figure 2.14 that the sign of the result depends upon the direction of integration around the polygonal lamina. This was the reason for digitizing the sediment depth contours in the systematic way as described in section 2.4.1.

It is obvious that when the projection of the field point is inside the contour line $\Sigma_i(\psi_{i+1}-\psi_i)=2\pi$ and when it is outside $\Sigma_i(\psi_{i+1}-\psi_i)=0$; therefore the gradient of V will change suddenly as the field point goes in and out of the contour line. The

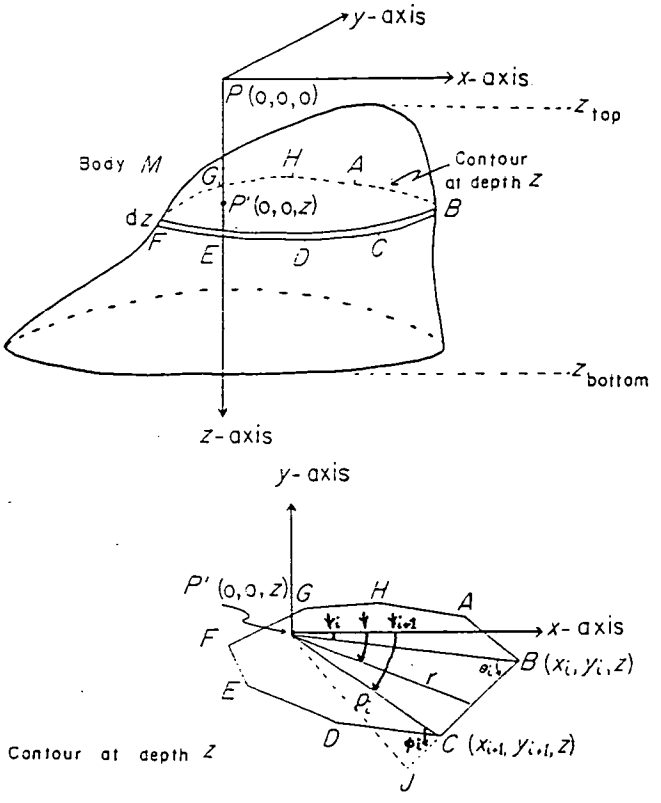

Figure 2.14 Geometrical elements involved in the computation of the gravity anomaly for contour integration method (from Talwani and Ewing 1960).

sudden change in V makes the integration in equation 2.4 unstable especially for the near surface materials.

The sudden change in V is plotted in figure 2.15 for a prism and in figure 2.16 for a cylinder. In order to represent V with a good approximation, more dense contouring of the body is necessary for shallow structures, otherwise the vertical integration in equation 2.4 may result in big numerical errors.

Comparing figure 2.17 and 2.18 shows that the most of the error occurs when the vertical distance to the top of the body is small compared with the contour interval of the body. It suggests that when the two parameters are equal, the error is insignificant.

In figure 2.17 and 2.18, the curves represent two different integration techniques. One is the quadratic routine used by Talwani and Ewing, the other is the NAG routine D01GAF. In addition, higher order polynomial routines were written and tested. The results showed that as the degree of the polynomial increased, the solutions became better. However none of them was better than the NAG routine D01GAF.

With these findings, the method was restricted to the lower part of the sedimentary model, where the NAG routine was used for numerical integration. The first 100 m of the sediments on land and the first 500 m of the sediments at sea were computed using another method.

2.4.5 Gravity Attraction of the Top Part of the Sediments

2.4.5.1 Prism Model

Error in evaluating equation 2.4 was not the only reason not to compute the top

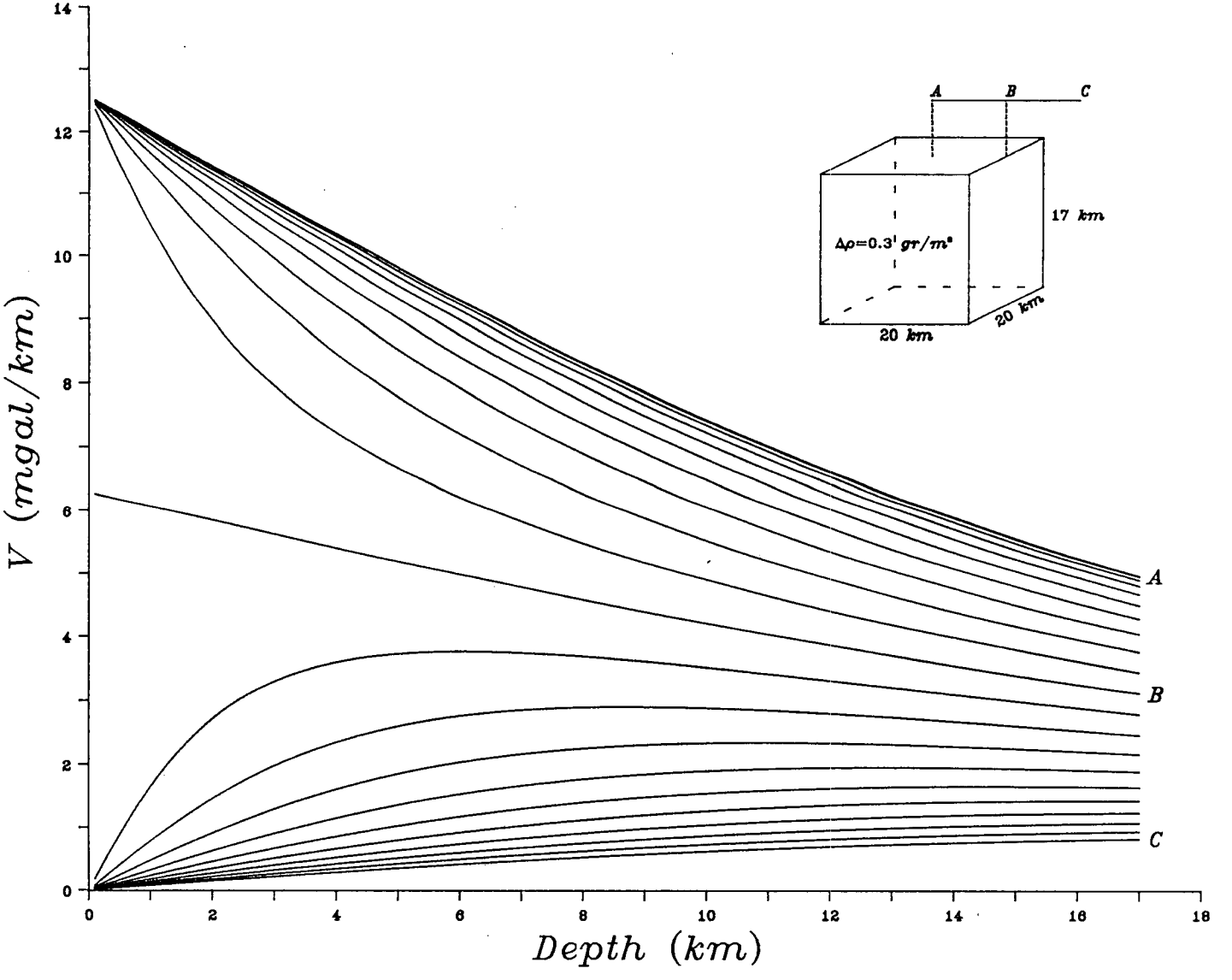

Figure 2.15 Sudden changes on V near the edges of a prism. Each curve plots V against the depth of the contour.

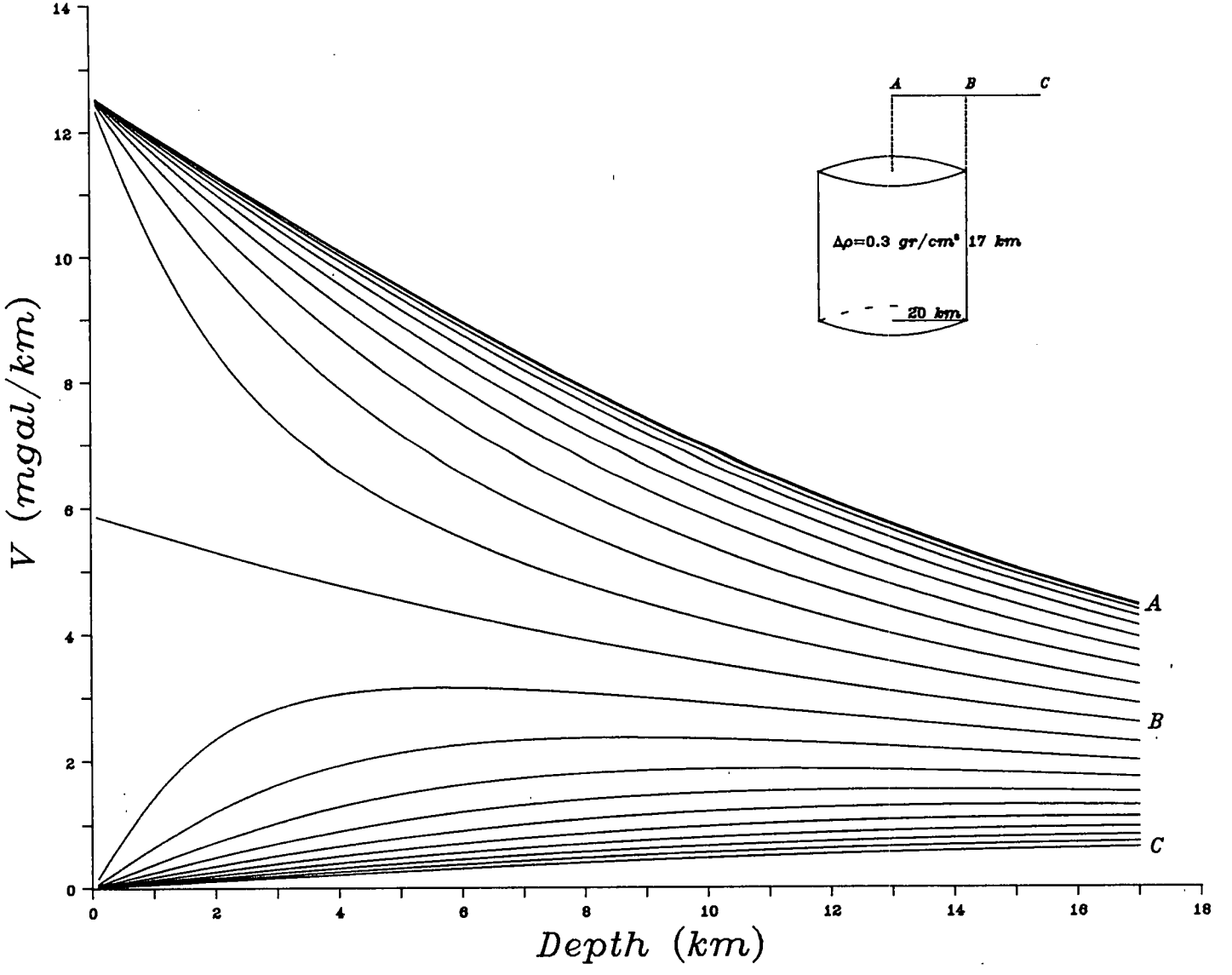

Figure 2.16 Sudden changes on V near the edges of a cylinder. Each curve plots V against the depth of the contour.

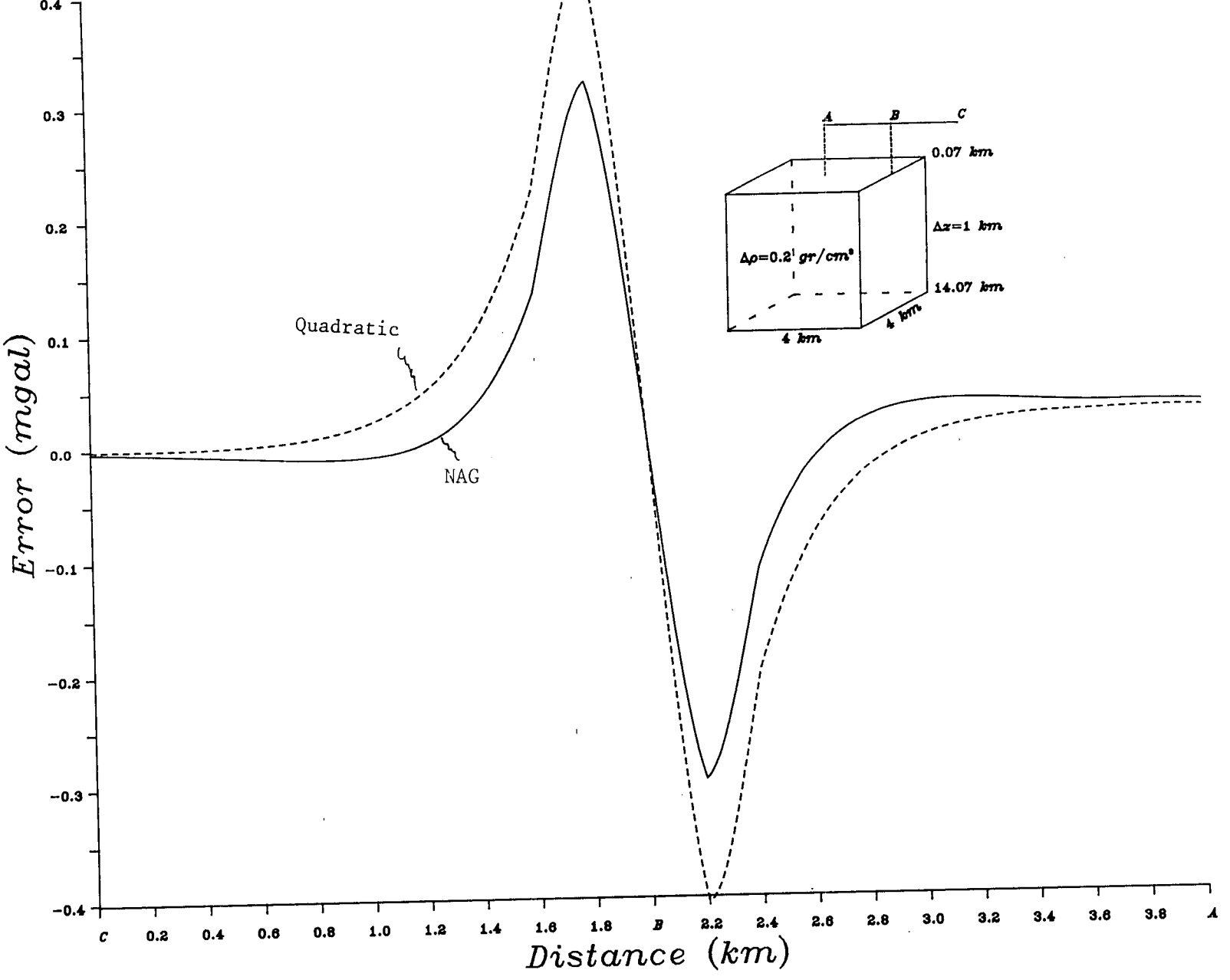

Figure 2.17 Errors in numerical integration for a shallow prism.

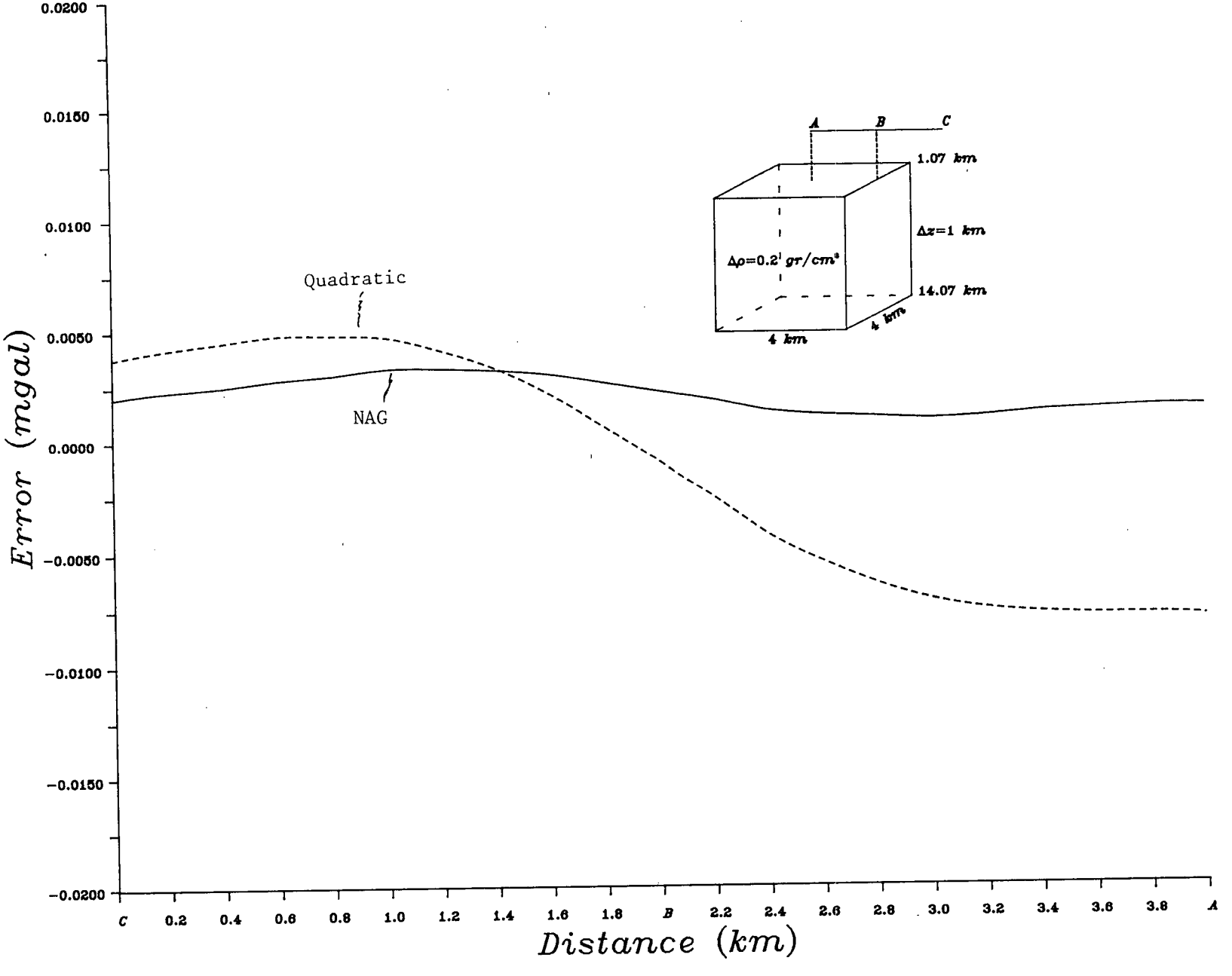

Figure 2.18 Errors in numerical numerical integration for a deep prism.

part of the sediments by using the contour integration method. That algorithm cannot cope with lateral density changes, and lateral density changes are more likely to give rise to errors for near surface materials.

If the top part of the sediments are represented by rectangular prisms, then using the formula for gravitational attraction of a prism, their gravitational attraction can be computed. Thus

$$\Delta g(x',y',0)=-\mathcal{G}\Delta\rho[[[\{(x-x')\log(y-y')+R+(y-y')\log(x-x')+R\} + z\tan^{-1}\{zR/(x-x')(y-y')\}]^{x_2}_{x_1}]^{y_2}_{y_1}]^{z_2}_{z_1}, \quad 2.6$$

where x' and y' are the field coordinates, x, y, and z to be replaced by x_1, x_2, y_1, y_2, z_1, and z_2, and $R=[(x-x')^2+(y-y')^2+z^2]^{1/2}$.

2.4.5.2 Gridded Depth Contours

The sediment model has to be interpolated on to a regular grid if the prism model is to be used. The interpolation routine has to account for a vertical displacement of the sediment depth. The GPCP interpolation routine which is based on a weighted local average, cannot account for this type of feature.

For this purpose, a FORTRAN program called LININT was developed (appendix 3). The input data are closed contours and only the grid points inside the outermost contour line are interpolated. The program finds the points where contours intercept grid lines. After ordering the intercept points in an array, it evaluates the grid values by fitting a straight line between successive intercept points. The process is done for both E-W and N-S directions, and the averaged value is taken as the grid value.

Using the program, the sediment depth contours were interpolated on to a 2 km

regular grid. In the computation, the sediment depth to top was averaged using the four corners of the prism. The same averaging was applied to the bottom of the sediments when the depth to the Pre-Permian basement was shallower than 100m on land and 500m at sea.

2.4.5.3 Densities of the Prisms

The density of the prism was taken from a combination of the density depth function and the surface density model. (These have been discussed in sections 2.3.1 and 2.3.3.) Density was varied linearly with depth between the surface density value and the density value obtained from the density function at a depth of 100 m. For computational purposes, the linear gradient of density was replaced by its mean value.

Unfortunately there is no way of estimating the lateral density changes at the sea bed from the available data set. The density value of the sea bed was chosen as the density of the wet mud (1.9 g/cm^3), and the density of the prism was an average of the wet mud density and the density function at a depth of 100 m. The remaining part (100 m. 500 m.) was computed with a second prism, whose density was the average of the density-depth function over this range.

2.5 Stripped Bouguer Gravity Anomaly Map

Computation of the attraction of the sediments was carried out every 2 km of the British National Grid. The gravitational attraction of the sediments is shown in figure 2.19 excluding the shallow part. Figure 2.20 shows the gravitational attraction of all the sediments. After accounting for the low density of Triassic sandstones, the final sediment effect is shown in figure 2.21.

Since the sediments have low density value compared with the basement, their

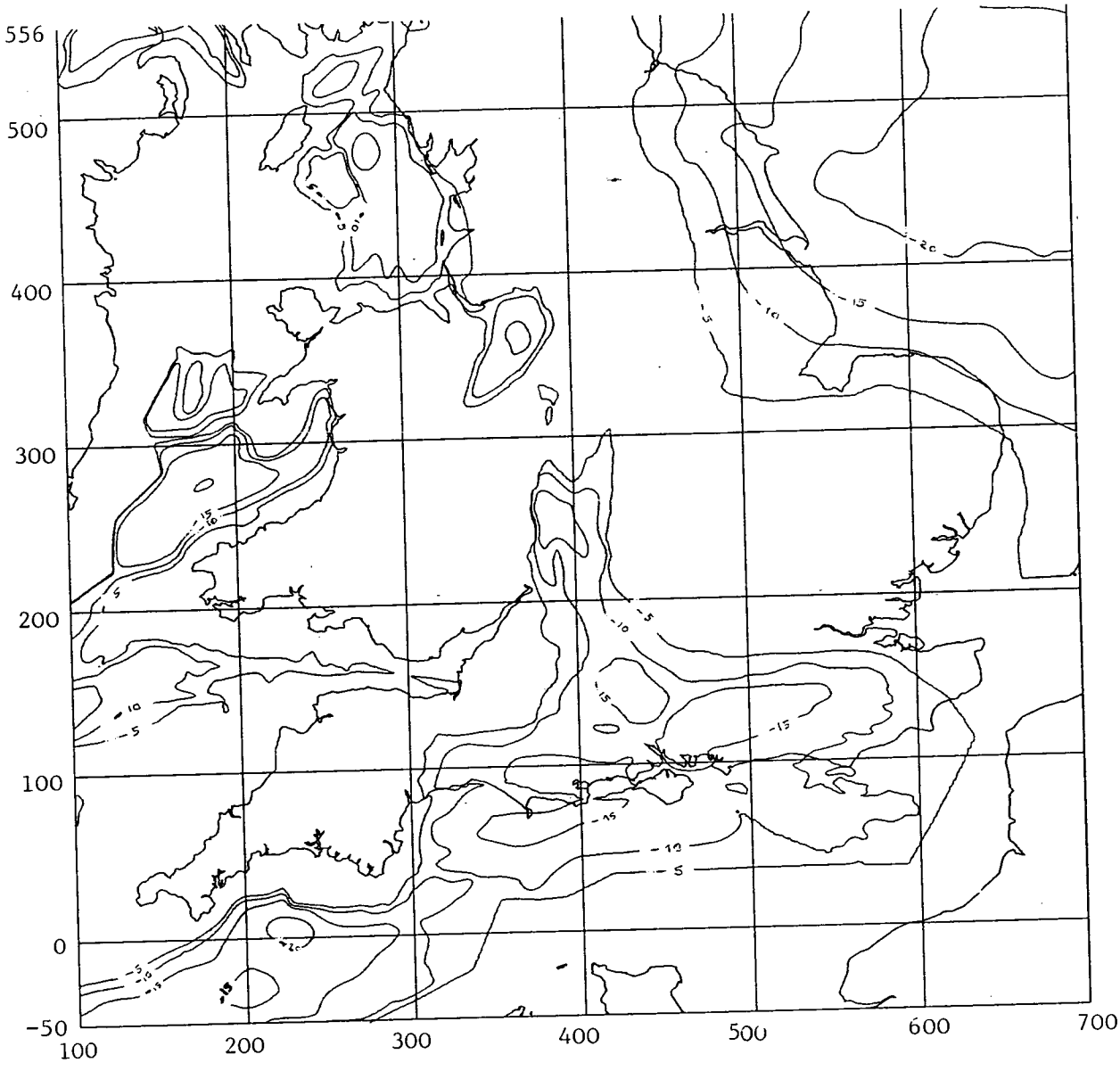

Figure 2.19 Gravitational attraction of the sediments excluding first 100 m on land and first 500 m at sea (Contour interval 5 mgal).

Edge effects in the western Irish Sea and in the southern English Channel are due to the discontinuity in the data

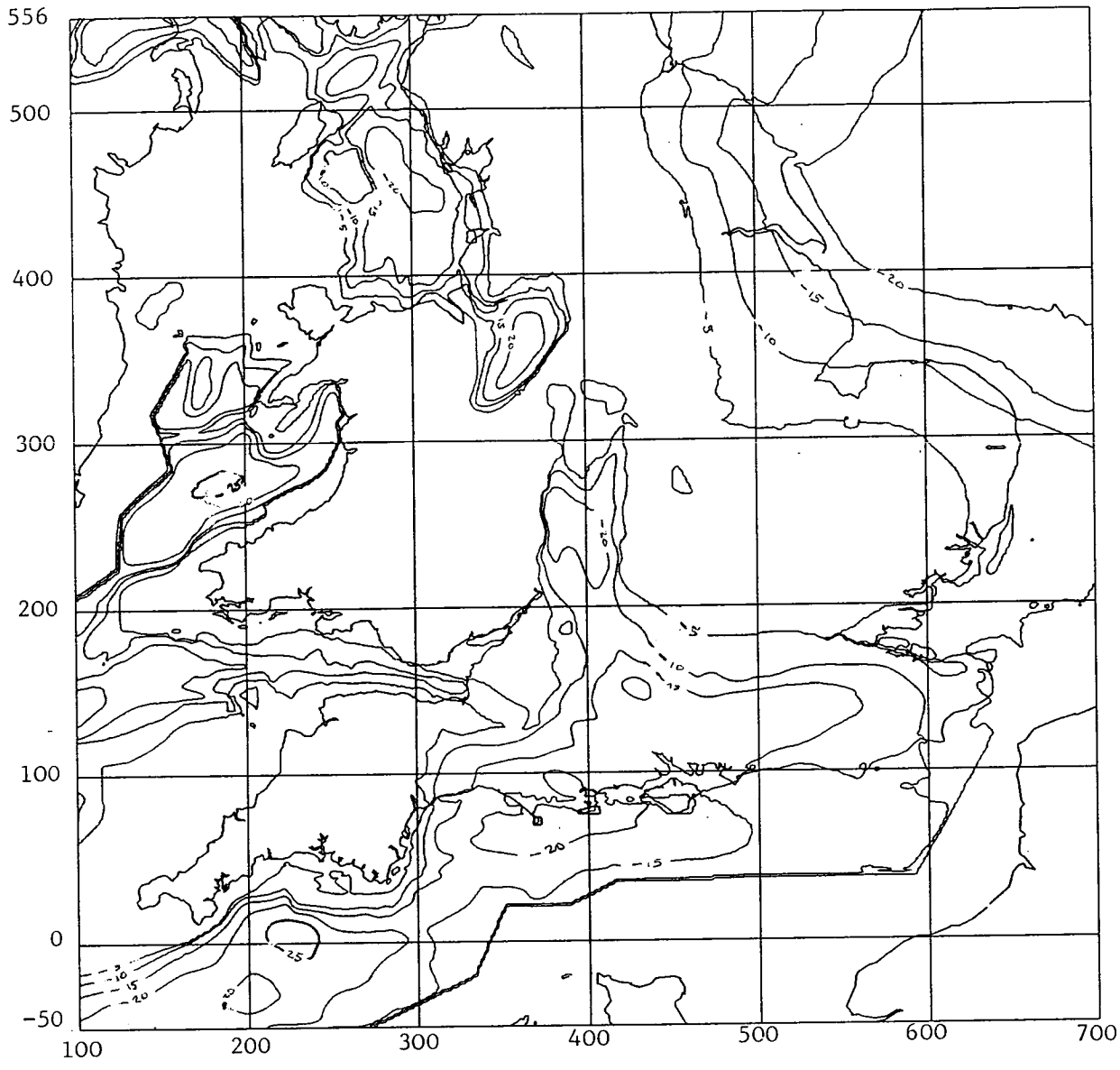

Figure 2.20 Gravitational attraction of the sediments including first 100 m on land and first 500 m at sea (Contour interval 5 mgal).

Edge effects in the western Irish Sea and in the southern English Channel are due to the discontinuity in the data

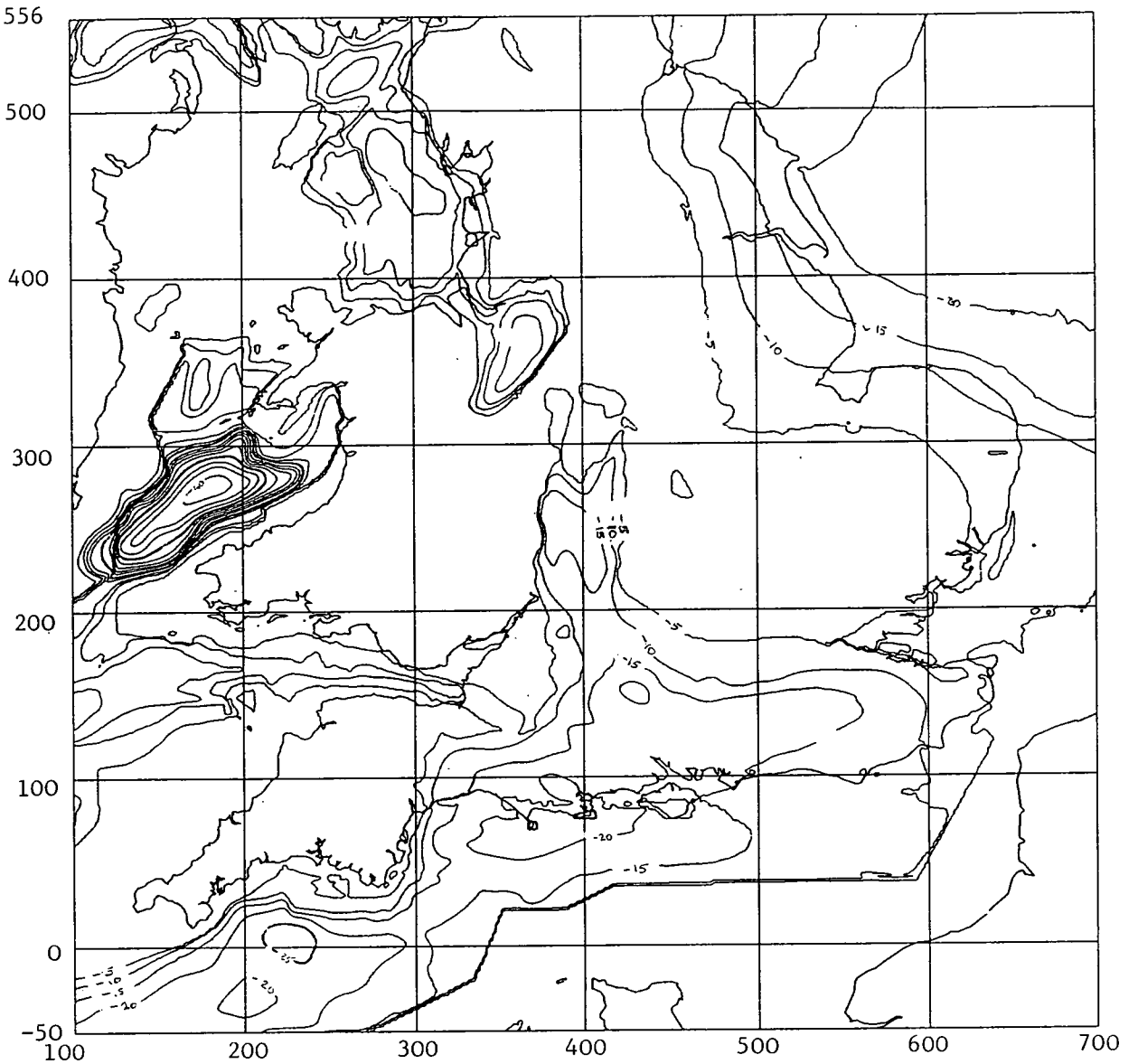

Figure 2.21 Gravitational attraction of the sediments after computing the effect of the low density layer in Cardigan Bay (Contour interval 5 mgal).

Edge effects in the western Irish Sea and in the southern English Channel are due to the discontinuity in the data

gravitational attraction must be added to the Bouguer anomaly to get the stripped Bouguer anomaly. The stripped Bouguer anomaly map is shown in figure 2.22, and also at the back of the thesis.

Most of the sedimentary basins are disappeared in the stripped Bouguer gravity anomaly map, but the Worcester basin is still visible. Analysis of the seismic reflection profiles over the basin showed that the basement is Pre-Cambrian (Chadwick 1985b, and Chadwick and Smith 1988). This suggests that there is a local density change in this region, probably in the Permo-Triassic sandstone sedimentation. Unfortunately borehole coverage in the region is poor, so no local correction could be applied.

The stripped Bouguer anomaly map is by no means smooth, but this behaviour is expected because no attempt was made to deal with geological features older than Permian. This is likely to arise a question that low density materials (especially Carboniferous sedimentation) could contaminate the long wavelength anomalies. Lee (1988) showed that the thickness of Carboniferous sedimentation in the Midlands is approximately 4 km. This suggests that the contamination will not have big effect. However, for modelling Carboniferous sedimentation should be accounted for.

The Sole Pit - Dowsing Fault Line (from [500,556] to [700,350]) which marks the boundary of the main North Sea Basin has become clearer after the stripping. It shows as a prominent, linear gravity high. The NW-SE direction of the anomaly trend has not changed, but the gravity anomaly over the feature is extended. This suggests that the feature is a more significant tectonic lineament than suggested by the original Bouguer anomaly map.

The low gravity anomaly closure over the London Basin is enlarged, perhaps showing the extent of Pre-Cambrian basement. North of the London Basin, there

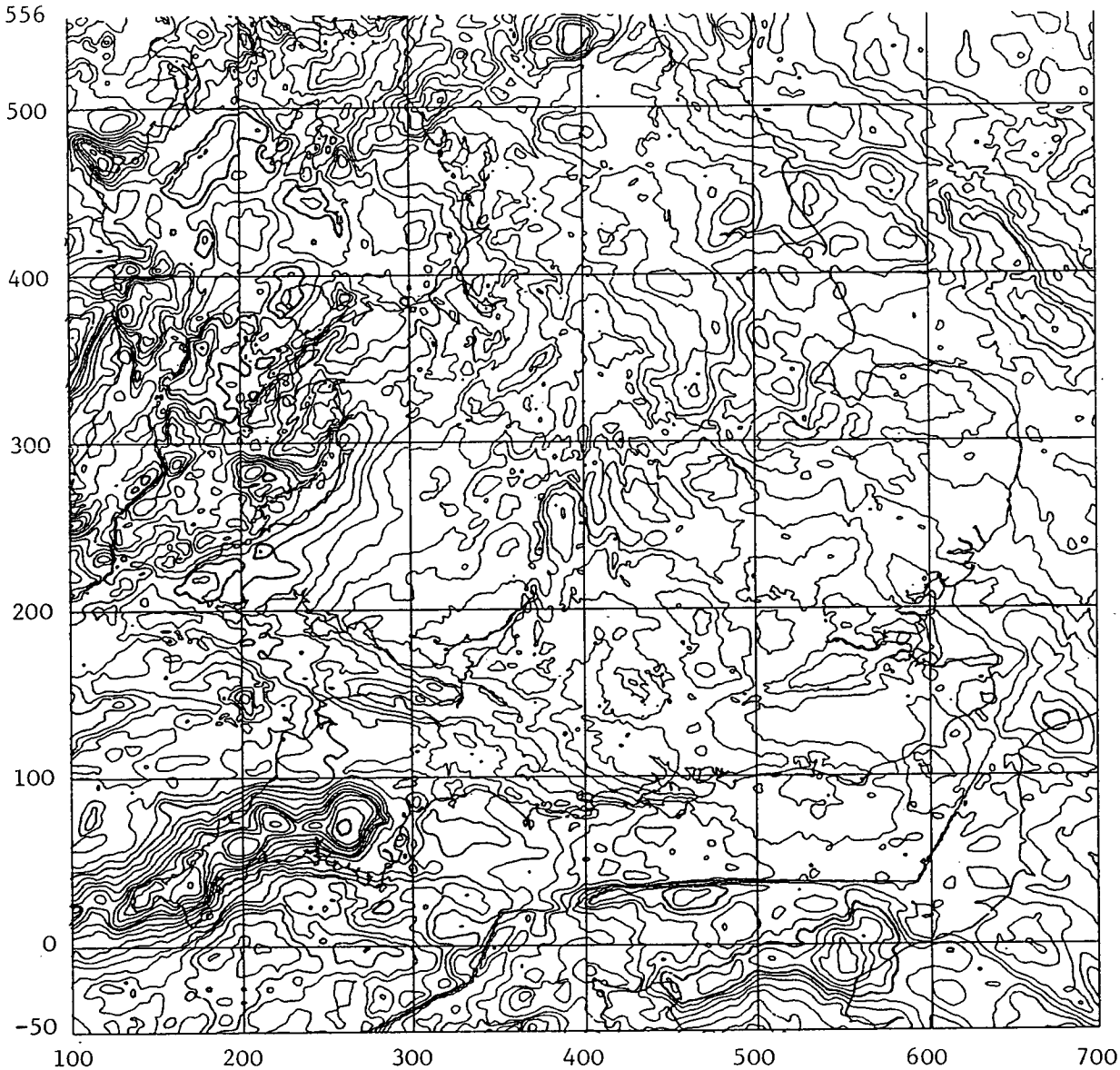

Figure 2.22 Stripped Bouguer anomaly map of southern Britain (Contour interval 5 mgal). (Plate 2 at the back of the thesis is a large version at a scale of 1:1000000.)

Edge effects in western Irish Sea and in southern English Channel are due to the discontinuity in the data.

lies another gravity low closure.

Probably the most remarkable feature on the stripped Bouguer anomaly map is that the step on the original Bouguer anomaly map which separates the gravity high on the west from the gravity low on the east, has first turned into a NW-SE and then a NE-SW trend. The NW-SE trend location coincides with the Variscan front zone, and the NE-SW trend is the Caledonian deformation trend over the area.

The stripped Bouguer anomaly map is the final shape of the stripped Bouguer anomaly map as far as this work is concerned, but it is by no means definitive. It is a pity that at the moment there are no data available for the sediment cover in Irish and French waters and in France. The artificial effects due to discontinuity in the stripping are clearly visible on the stripped Bouguer anomaly map.

CHAPTER 3

ANALYSIS OF THE GRAVITY ANOMALY

3.1 Spectral Analysis

3.1.1 The Theory

The gravity anomaly due to an interface within the Earth can be written as (Parker 1972)

$$\mathcal{F}[\Delta g(x,y)]=2\pi\mathcal{G}\Delta\rho e^{-kz}\left(\sum k^{n-1}/n!\ \ \mathcal{F}[h_z{}^n(x,y)]\right) \qquad 3.1$$

where $\mathcal{F}$ denotes the Fourier transform, $\mathcal{G}$ is the gravitational constant, k is the wavenumber, ($k=(k_x{}^2+k_y{}^2)^{\frac{1}{2}}$, k_x and k_y are the wavenumbers in the x and y directions), z is the depth to the interface, h is the topography of the interface, and $\Delta\rho$ is the density contrast between underlying and overlaying materials. When the topographic changes are small compared with the depth, the effect of the summation in equation 3.1 becomes small as n becomes large, so an approximation may be made as

$$\Delta G(k_x,k_y)=2\pi\mathcal{G}\Delta\rho e^{-kz}H(k_x,k_y) \qquad 3.2$$

where upper case letters represent the Fourier transform eg $\mathcal{F}[h]=H$. If the topography of the interface is taken as a random distribution then the Fourier transform of the topography will be a constant, a characteristic of white noise. Azimuthal averaging equation 3.2 simplifies the analysing, and taking the natural logarithm of the averaged Bouguer anomaly gives

$$\log\langle G(k)\rangle = -kz + \text{constant}. \qquad 3.3$$

Using this relation, z may be obtained from the gravity spectrum over a given waveband. For two layered media, the logarithm of the averaged spectrum will be

$$\log\langle G(k)\rangle = \log(2\pi\vartheta) + \log(\Delta\rho_1 e^{-kz}H_1 + \Delta\rho_2 e^{-kz}H_1) \qquad 3.4$$

Assuming that $z_1 > z_2$, the average spectrum is dominated by z_1 for long wavelength, and by z_2 for short wavelength provided that $H_2\Delta\rho_2 > H_1\Delta\rho_1$. If $\log\langle G(k)\rangle$ shows any kind of linearity, then the lines may be analysed in terms of different layering.

3.1.2 Results

The Fourier transform of the Bouguer gravity anomaly map was taken, and the spectrum was averaged. The averaging was done by dividing the wavenumber into 1000 wavebands between zero and the Nyquist frequency and by averaging the square modulus of the transform around annuli in the wavenumber domain.

There are two different wavenumber intervals on the averaged gravity anomaly spectrum which are approximately linear (figure 3.1). The first line is represented by features which have 90 km wavelength or more and the other line is represented by the features which have less than 90 km wavelength. Least square linear regression analysis of the two lines shows the corresponding depths at 12±1 km and 25±3 km. 25±3 km depth is smaller than the expected value of the Moho around Britain which is around 30–35 km (Edwards, and Blundell 1984)

A similar spectral analysis of the stripped Bouguer anomalies was carried out. The stripped Bouguer anomalies show sources at a depth of 30±3 km (figure 3.2). This shows how much the long wavelength end of the spectrum could be contaminated

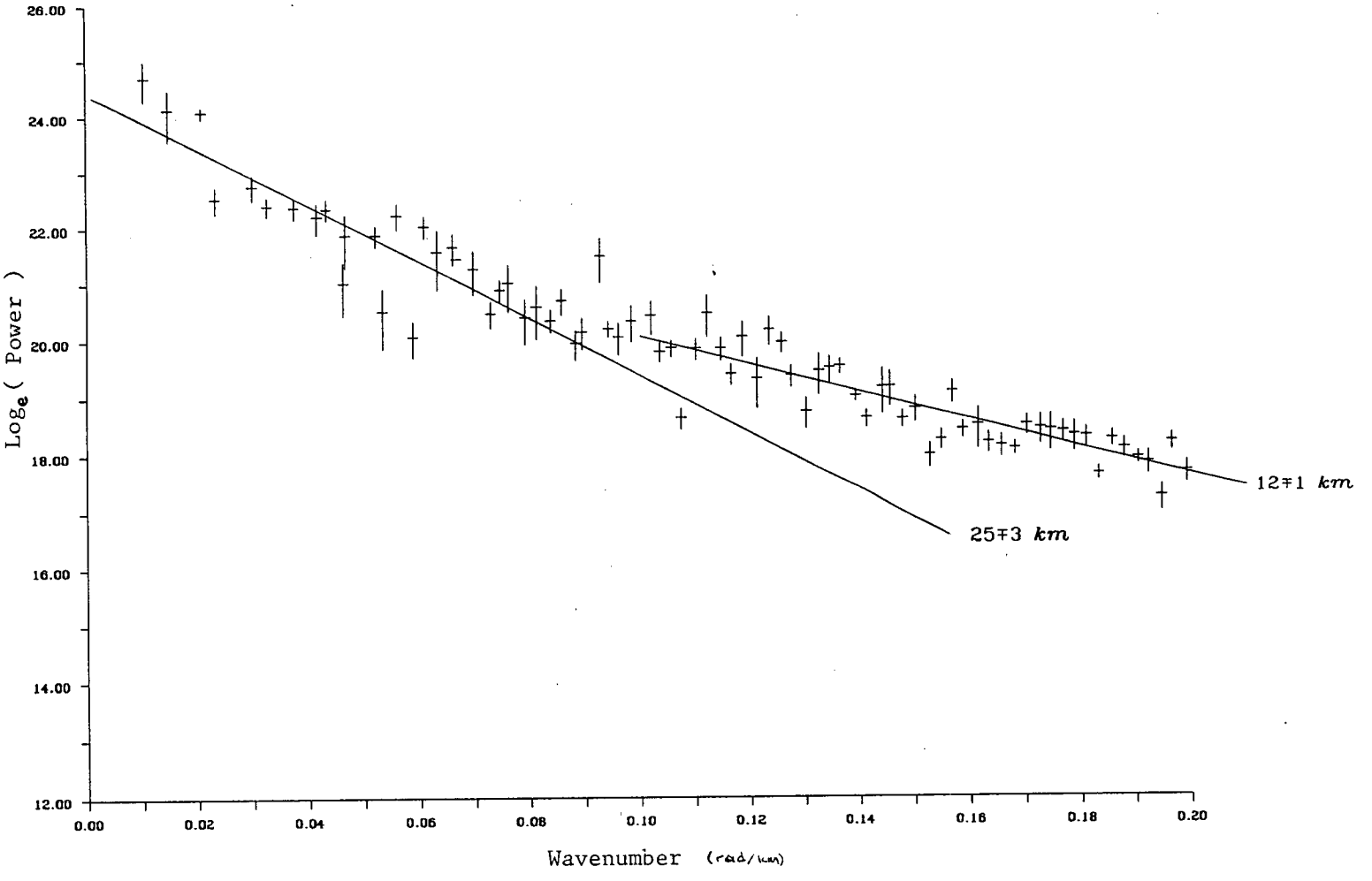

Figure 3.1(a) Bouguer anomaly spectrum

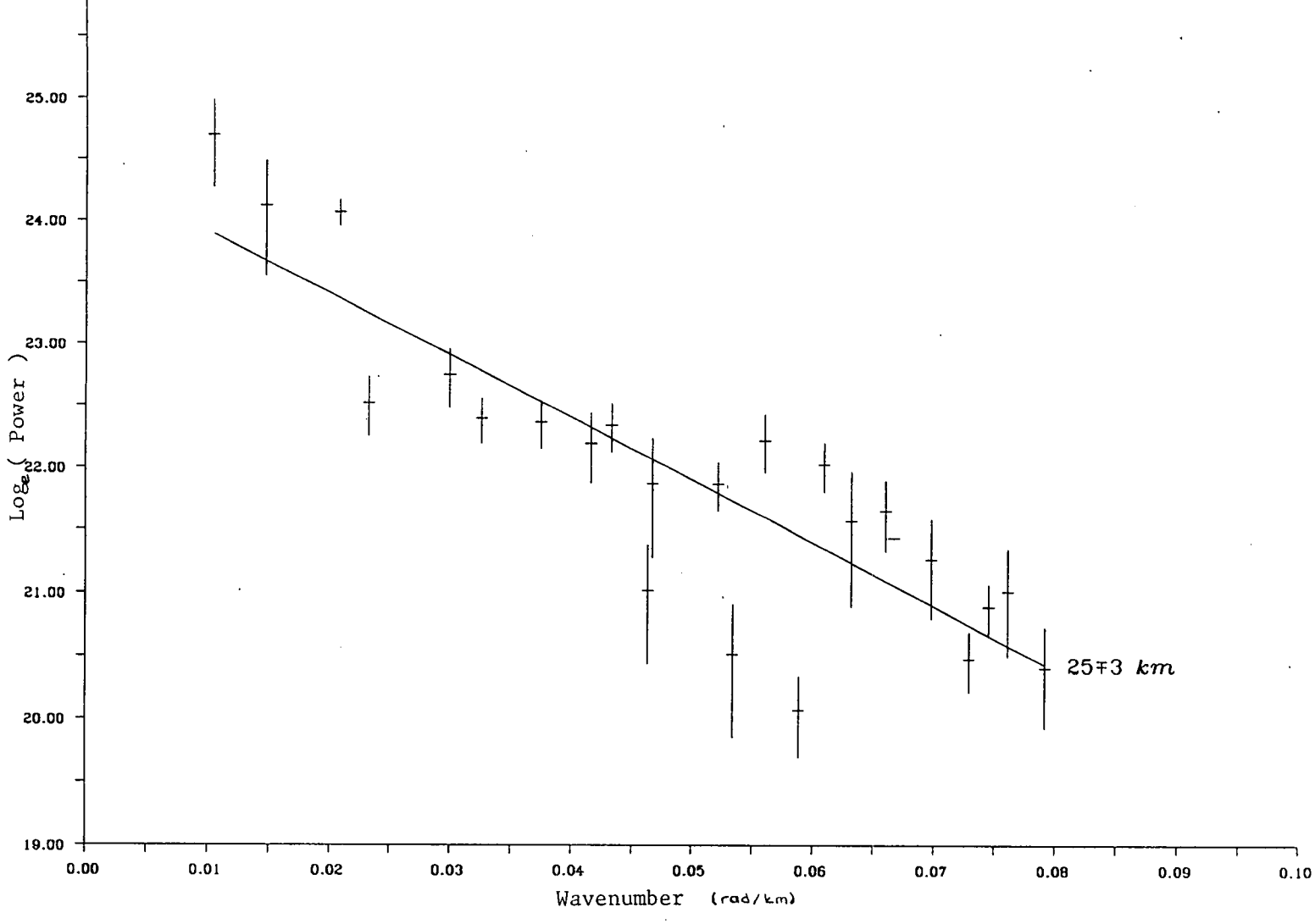

Figure 3.1(b) Bouguer anomaly spectrum: enlarged at the long wavelength

by near surface structures. Although this is slightly smaller than the seismic refraction lines suggest, it is reasonably close. If the signal is from the Moho then there are two explanations of the difference of depth. One is that the seismic findings of the depth of the Moho around Britain were not correct, the other is that the topography of the Moho is not randomly distributed. The latter would imply that the the spectrum of the topography on the Moho is a 'blue' spectrum, thus the energy of the short wavelength features of the topography on the Moho is more than the energy of the long wavelength features. The alternative case where the signal does not originate from the Moho is discussed in section 6.5.

It may be argued that the 12 km depth is reflecting the sediment depth, although the average depth of the sediments is around 3-4 km. This argument requires that the spectrum of the sediment depth is 'red', so the averaged gravity spectrum is overestimating the averaged sediment depth. The argument would be valid only if the spectrum of the stripped Bouguer anomaly showed different solutions to the equation 3.2. Figure 3.2 shows the depth of the layer at 11±2 km. This rules out any such a argument.

Seismic profiles over the southern Britain suggest that the depth to the lower crust is in the order of 11-22 km (Chadwick 1985a), so 11-12 km depth may originate at the bottom of the upper crust.

3.1.3 Filtered Gravity Anomaly Maps

As observed above, the spectrum of the Bouguer anomaly showed two linear lines reflecting different gravity anomaly sources. The actual gravity anomaly due to those features may be obtained by applying a high, or low, or band pass filter. The cut off wavenumber for the filters will be at a point where the line no longer represents the spectral data points. The cut off wavelength of the deep features corresponds to the 90 km wavelength as shown above, so the filter should pass

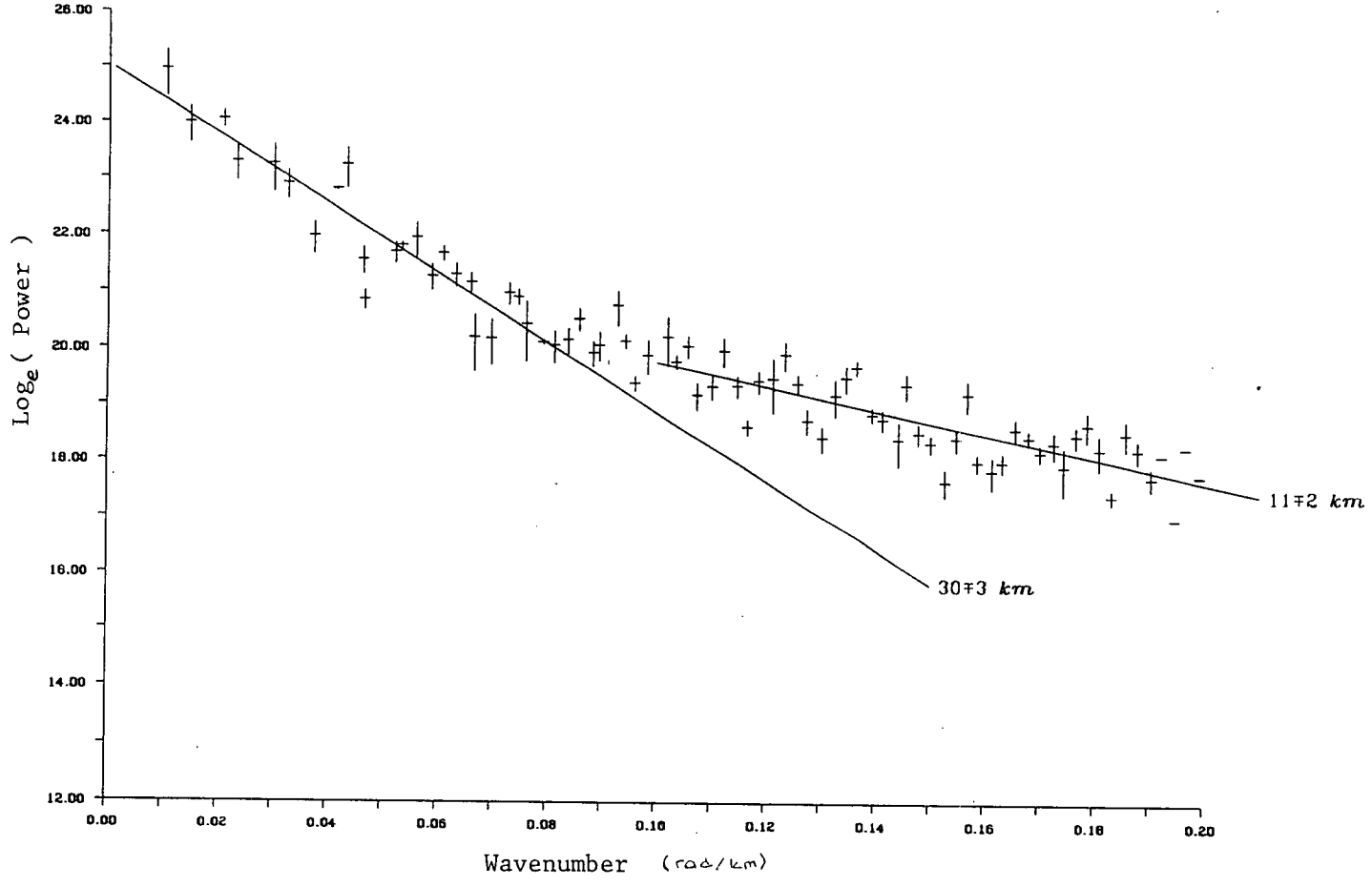

Figure 3.2(a) Stripped Bouguer anomaly spectrum

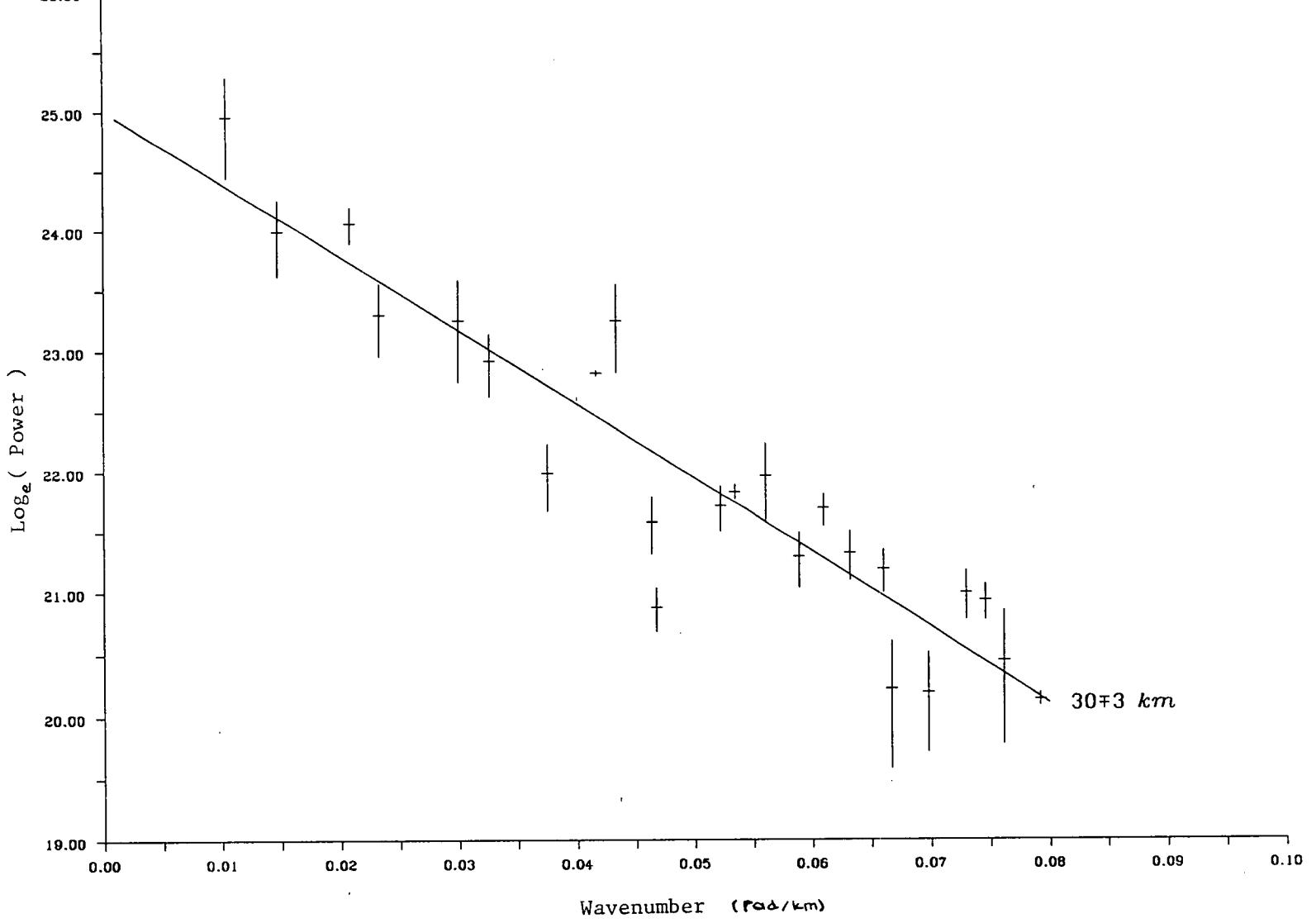

Figure 3.2(b) Stripped Bouguer anomaly spectrum: enlarged at the long wavelength

the anomalies which have a wavelength bigger than 90 km. The filter is smoothed between the wavelengths 80 and 100 km by a cosine taper so the discontinuity is avoided.

The filtered Bouguer anomaly map still shows the effect of the major sedimentary basins such as the Cardigan Bay (figure 3.3). This clearly indicates the contamination of the long wavelength anomalies by the near surface materials.

On the other hand, the filtered stripped Bouguer anomaly map does not show the effect of these features. All the main features on the stripped Bouguer anomaly map remain after the low pass filter, showing that they are predominantly of deep origin (figure 3.4).

3.1.4 Second Derivative of the Bouguer Anomaly

One useful way of identifying the tectonic events from the Bouguer anomaly map is to compute the second horizontal derivative of the Bouguer anomaly map. The second horizontal derivative of the Bouguer anomaly emphasizes short wavelength features near geological boundaries. It changes sign at the points of maximum slope, which are usually near these boundaries. The geological boundaries are related to the tectonic of the region, so the events can be seen more clearly on the second derivative map.

The second derivative of the gravity anomaly can be obtained by using potential theory. The Laplacian of the potential will be zero, providing that the field point is outside the body, so the second horizontal derivative of the potential is the second vertical derivative of the potential. Thus

$$\partial^2 U/\partial z^2 = -\partial^2 U/\partial x^2 - \partial^2 U/\partial y^2. \qquad 2.5$$

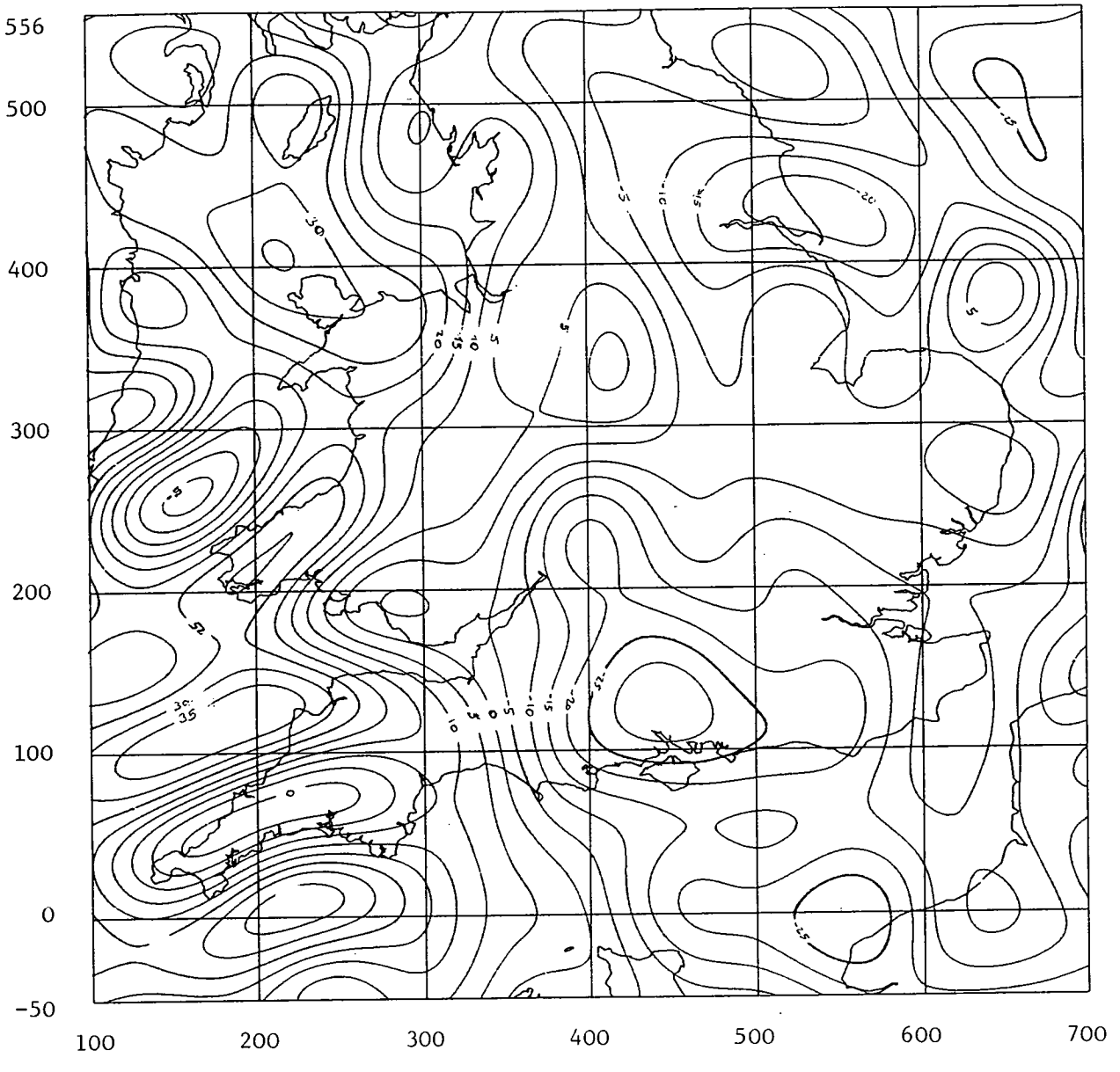

Figure 3.3 Filtered Bouguer anomaly map.

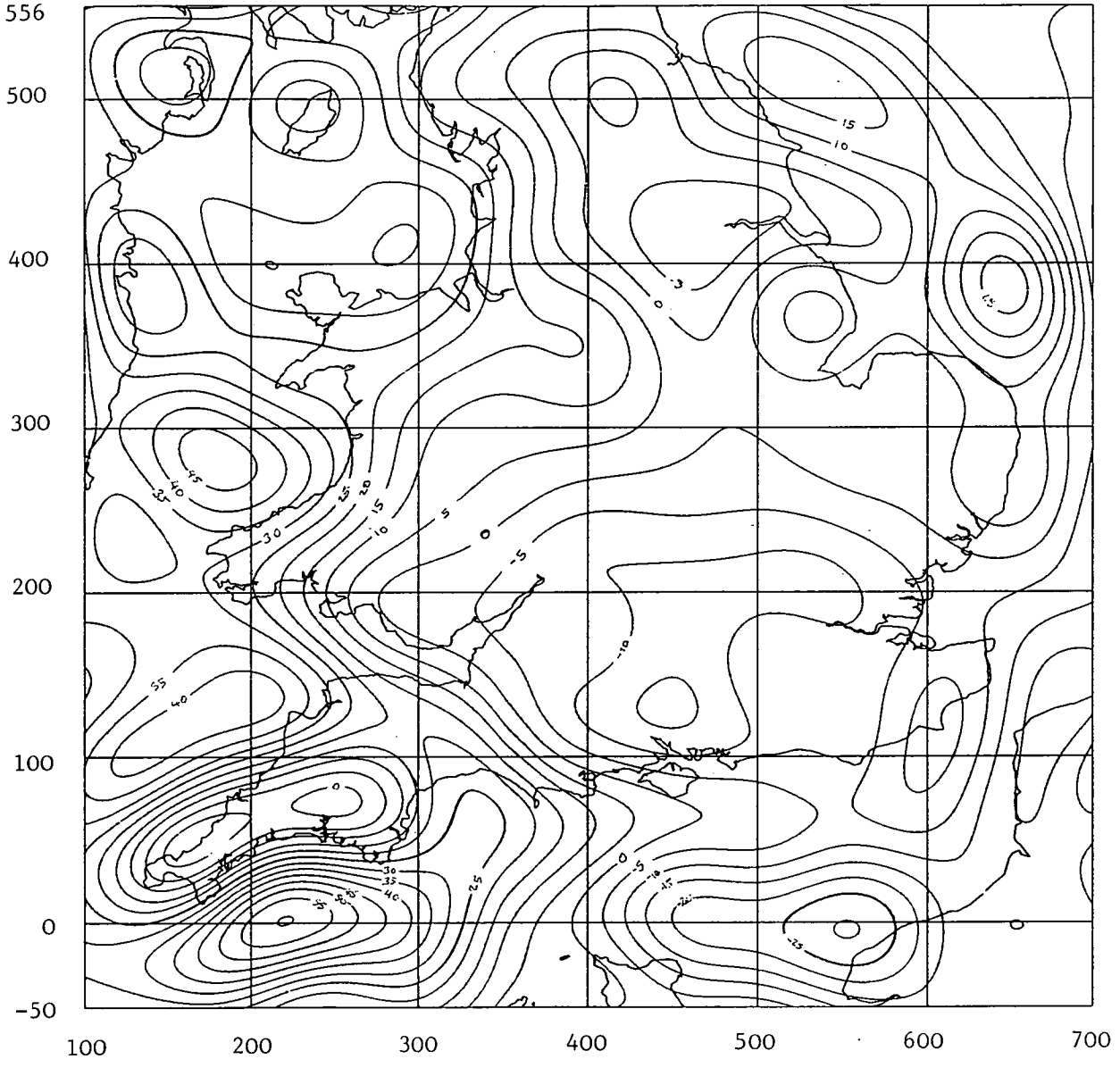

Figure 3.4 Filtered stripped Bouguer anomaly map.

From the definition of the Fourier transform, the equation 2.5 can written as

$$\mathcal{F}[\partial^2 U/\partial z^2]=\mathcal{F}[U](k_x^2+k_y^2)=\mathcal{F}[U]k^2. \qquad 2.6$$

Using this equation. the second derivative of the gravity Bouguer anomaly is computed (figure 3.5).

The different pattern of the data on land and sea areas is caused by the preparation of the data (section 1.2.2). As it is mentioned in chapter 1, the gravity anomaly is interpolated onto 2 km grid spacing on land, and 4 km grid spacing at sea. After this process the sea data are interpolated onto 2 km grid spacing by fitting a smooth cubic surface to the data, so the resolution on land areas is much higher than the sea areas. The difference between the two patterns is mainly reflected in the short wavelength anomalies, which are less than 6 km.

The other problem is the lineaments along the boundaries of 100 km squares of the British National Grid. The problem arises on the edges of the squares on which the original interpolation was on 4 km grid spacing. This is because the interpolation near the edges only used data points in the same square as the grid point. These features will have a dimension of 4x100 km^2, so the features are represented in the Fourier domain by the anomalies which have a wavelength of 8 km or less.

These two known features on the second derivative map can be eliminated by filtering. The biggest wavelength due to errors in the preparation of the data set, is 8 km, so not much information will be lost by filtering the second derivative map for the features which have less than 8 km wavelength (figure 3.6).

A more serious problem arises at sea over the ship tracks, some of which can be seen over the Strait of Dover. This is mainly the errors in the gravity reduction

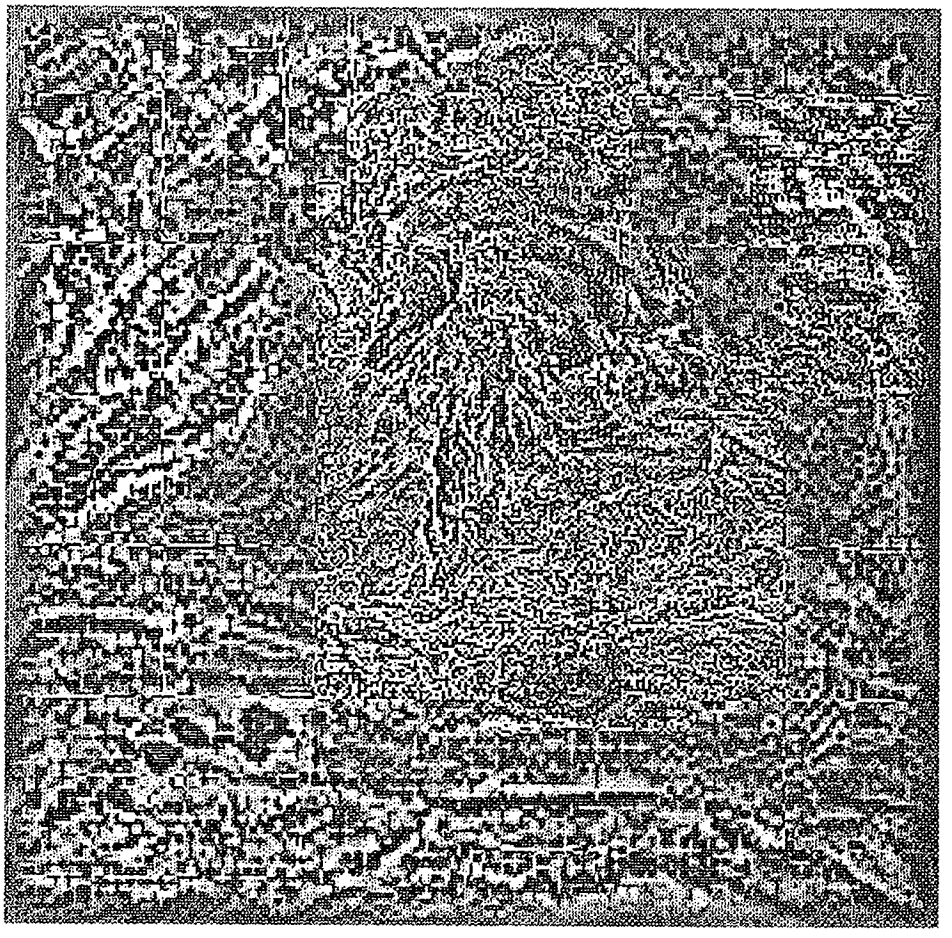

Figure 3.5 Map of second derivative of the Bouguer anomaly.

Figure 3.6 Map of filtered second derivative of the Bouguer anomaly.

over these ship tracks. Although the gravity anomaly map does not show such an effect, the error appeared because by taking the second derivative of the gravity anomaly, the errors are magnified. Nothing could be done about these features without reprocessing the gravity anomaly data.

3.1.5 The Patterns of the Second derivative Map

In the north west, the second derivative map shows a series of NE-SW lineaments. This direction is the direction of the Caledonian deformation. The lineaments disappear on the eastern side of the Malvern axis over which the direction of the lineaments is N-S.

On the eastern side of the Malvern axis, the general trend is NW-SE. The region covers the areas of the North Sea Margin and Carboniferous basins in the Midlands as well as north east England.

The ESE-WNW direction of lineaments, running from southern Ireland to west Europe, coincides with the Variscan deformation front. Although the lineament in the west appears to be a single one, it seems to separate into branches on the eastern side west of London, one going towards Holland, and the other towards France. On the southern side of the lineaments, the trend is generally E-W, which is the Variscan deformation direction. Between the branches, the E-W directional features suggest that the Variscan features are defined by the northern lineament. The southern lineament marks the location of the Bristol Channel-Bray fault.

Over mid Wales, between the NE-SW directional lineaments in the north and the NW-SE lineaments over the Variscan front, there is a quiet zone, suggesting that the deformation was not as high as in the surrounding region. This zone may mark the southern edge of the Caledonian front.

3.2 Gravity Modelling of the Variscan Front

The gravity anomaly over the Variscan front is the most exciting and the most promising feature on the stripped Bouguer anomaly map, as mentioned in chapter 2. The gravity anomaly changes sharply over the front, typically at 6 mGal per km, generating a step of 35-40 mGal. Four gravity profiles across the trend were chosen for modelling (figure 3.7). They were restricted to the area west of Hampshire because the trend is less clear in the eastern Channel, where there is a discontinuity in the sediment model.

Using a density depth function will leave short wavelength anomalies due to local density variations. To model these features, density variations should be determined independently from the density depth function. For this reason the gravity profiles were taken from the Bouguer anomaly map and the sediments included in the model.

3.2.1 Gravity Modelling Routine

Computing the gravitational attraction of the models was done by the two dimensional algorithm introduced by Talwani et al (1959).

An improvement in modelling procedure was made by applying EDWIN interactive graphical routines (Hughes, 1981). The new program allows the user to adjust the model more effectively by altering the position of the corners of the model and displaying its gravitational attraction on the terminal immediately. The documentation of the program is given in appendix 4.

3.2.2 Modelling the Regional Gravity Anomaly

It is important that the regional anomaly should be identified correctly in the

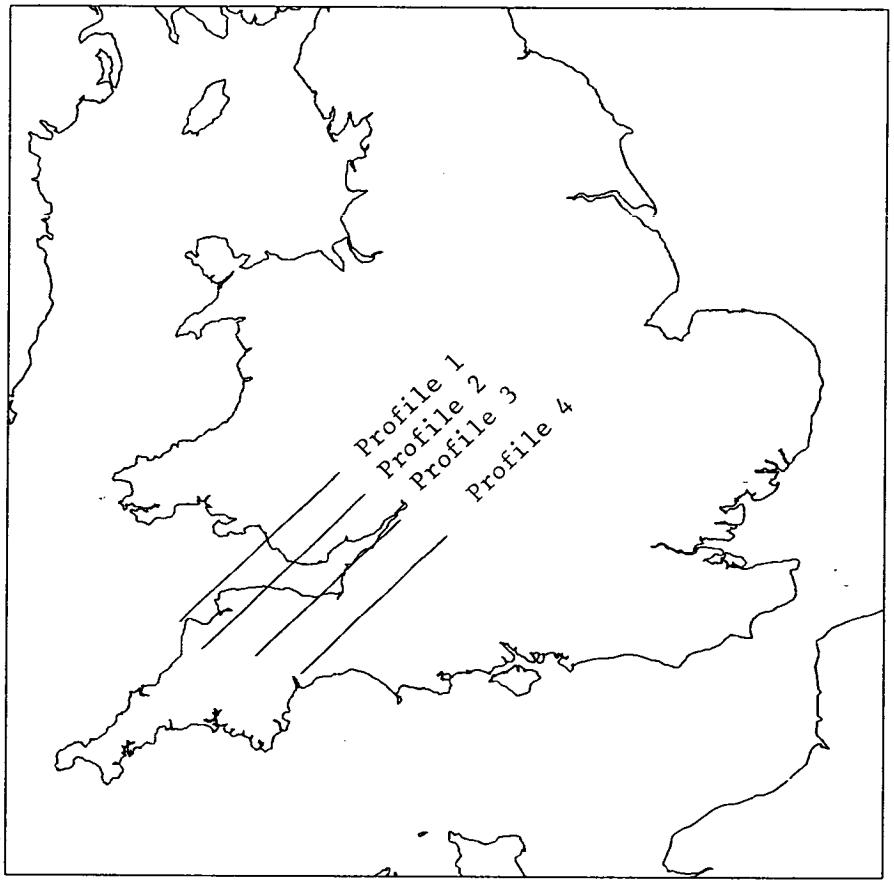

Figure 3.7 Location of the gravity profiles for modelling.

modelling procedure. Probably the best way of determining it is to filter the stripped anomaly map.

Before attempting a detailed model of the unstripped Bouguer anomalies, profiles from the filtered stripped map were modelled. The purpose of the process was only to determine the location of the features which generate the regional anomaly An example is given in figure 3.8.

3.2.3 Modelling the Shallow Materials

Contours on the top of the Pre-Permian Surface of the United Kingdom (South) (Brown 1985) supplied the sedimentary thickness for modelling the subsurface materials, but it was found that the the short wavelength features could not be modelled by this information alone. Over the areas where there is no indication of young sedimentation, the gravity anomaly still showed that some features related to shallow structures. This was the main reason to introduce a 'Carboniferous' layer. The reason for calling the layer 'Carboniferous' is that the boundaries of its outcrop were taken as those of Carboniferous sedimentation on the Pre-Permian Geology of the United Kingdom (South) (Brown, 1985). This layer is only to model the short wavelength anomalies and may include non-Carboniferous sources, so that its geological interpretation needs caution.

Even introducing Carboniferous sedimentation could not solve the problem over the areas where there are no Carboniferous sediments. These features were not modelled by introducing another layer, and the misfit of the models is related to these features. They are likely to be due to lateral density variations in either the sub-Carboniferous or the shallow crystalline basement, for which there was not enough information to model.

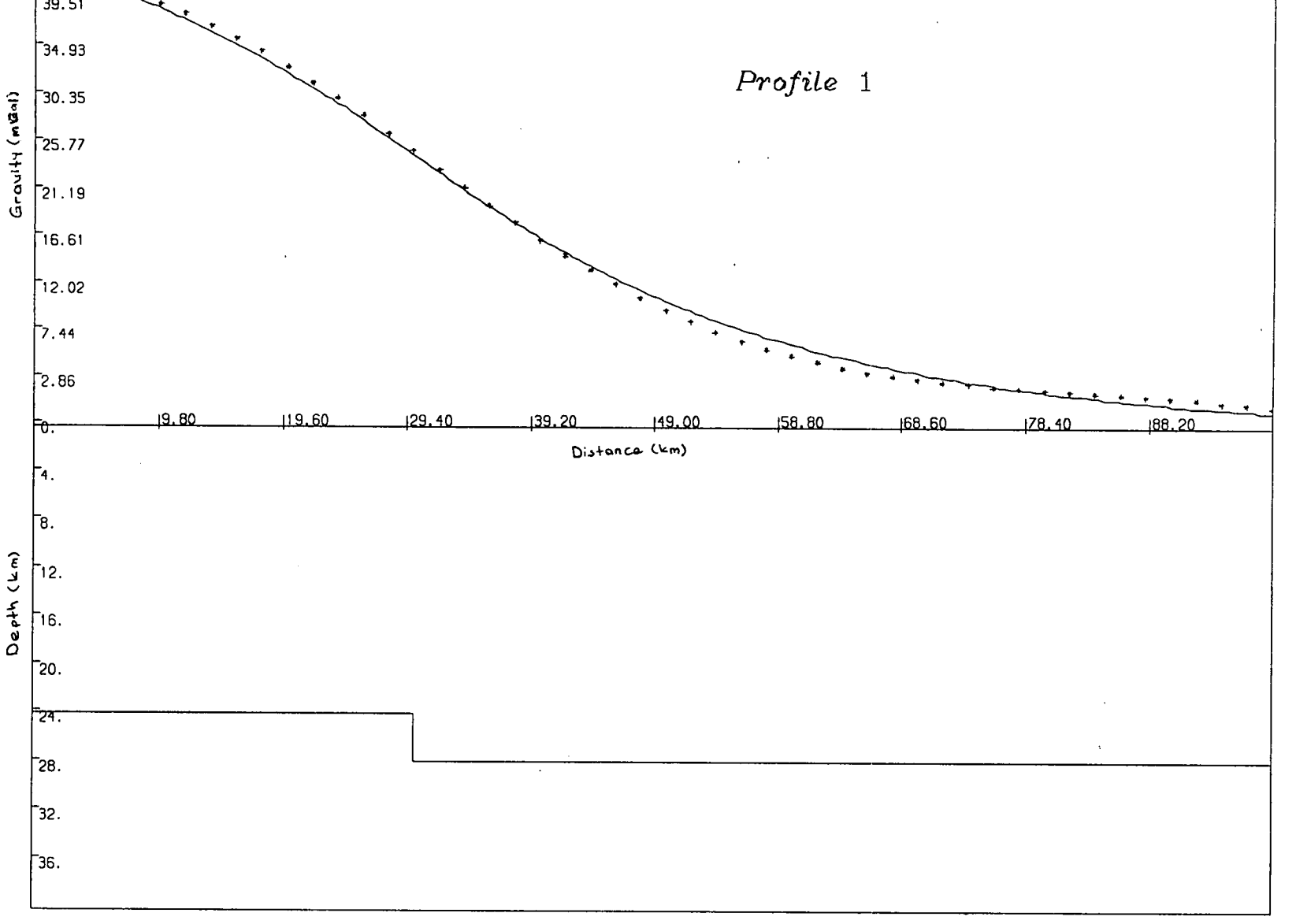

Figure 3.8 An example of modelling the long wavelength gravity anomaly.

3.2.4 The Models

In section 3.1.2 it was found that the gravity anomaly spectrum could be separated into two lines referring to gravity anomaly sources at depths of 25-30 km and 11-12 km. That information is applied to the modelling to investigate cases where the average depth of the deep structures is either 11-12 km or 25-30 km.

In all models the density of the layers was chosen as

Sediments younger than Carboniferous : 2.4 g/cm^3

'Carboniferous' layer : 2.6 g/cm^3

Upper crust : 2.7 g/cm^3

Lower crust : 2.8 g/cm^3

Mantle : 3.3 g/cm^3

In the modelling process, it is assumed that the regional gravity anomaly is generated by a vertical step. If the step is too shallow, it generates a steeper gradient, and if it is too deep, it cannot generate a steep enough gradient, so there is a limit on the depth of the step. The smaller limit was found to be close to 12 km. 30 km was less than the larger limit.

Firstly the average depth of 11-12 km obtained from gravity spectrum, is applied to the modelling program. This is achieved by assuming a step on the boundary between the upper and lower crust. The model suggests that this assumption results in an 8 km displacement in the crust (figure 3.9). If instead the average depth of the gravity anomaly source is at a depth 25-30 km, the modelling yields a 3 km displacement (figure 3.10).

The models may be made more complex by accounting for displacements at a

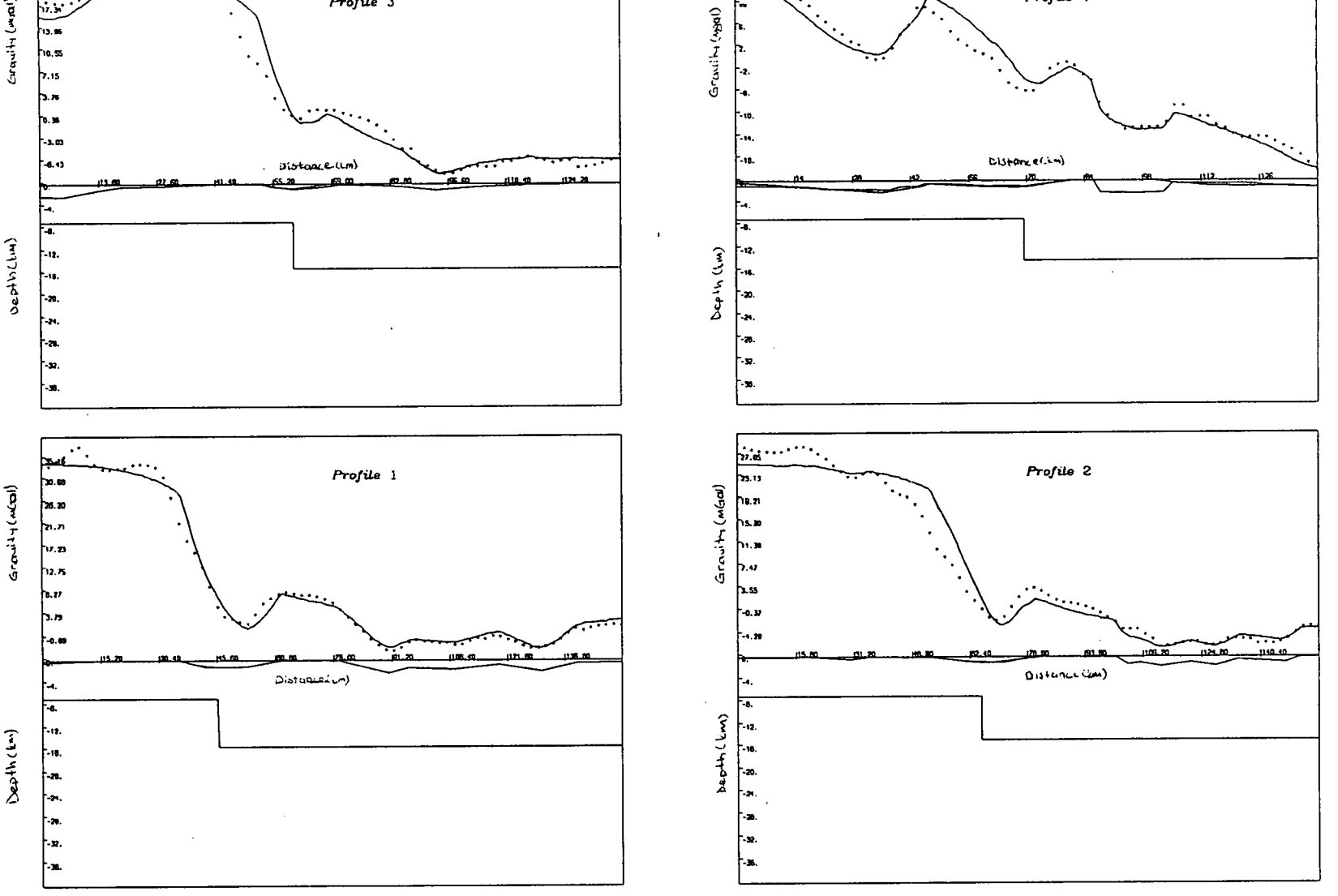

Figure 3.9 Gravity modelling of the four profiles with a step on the boundary of the lower and upper Crust.

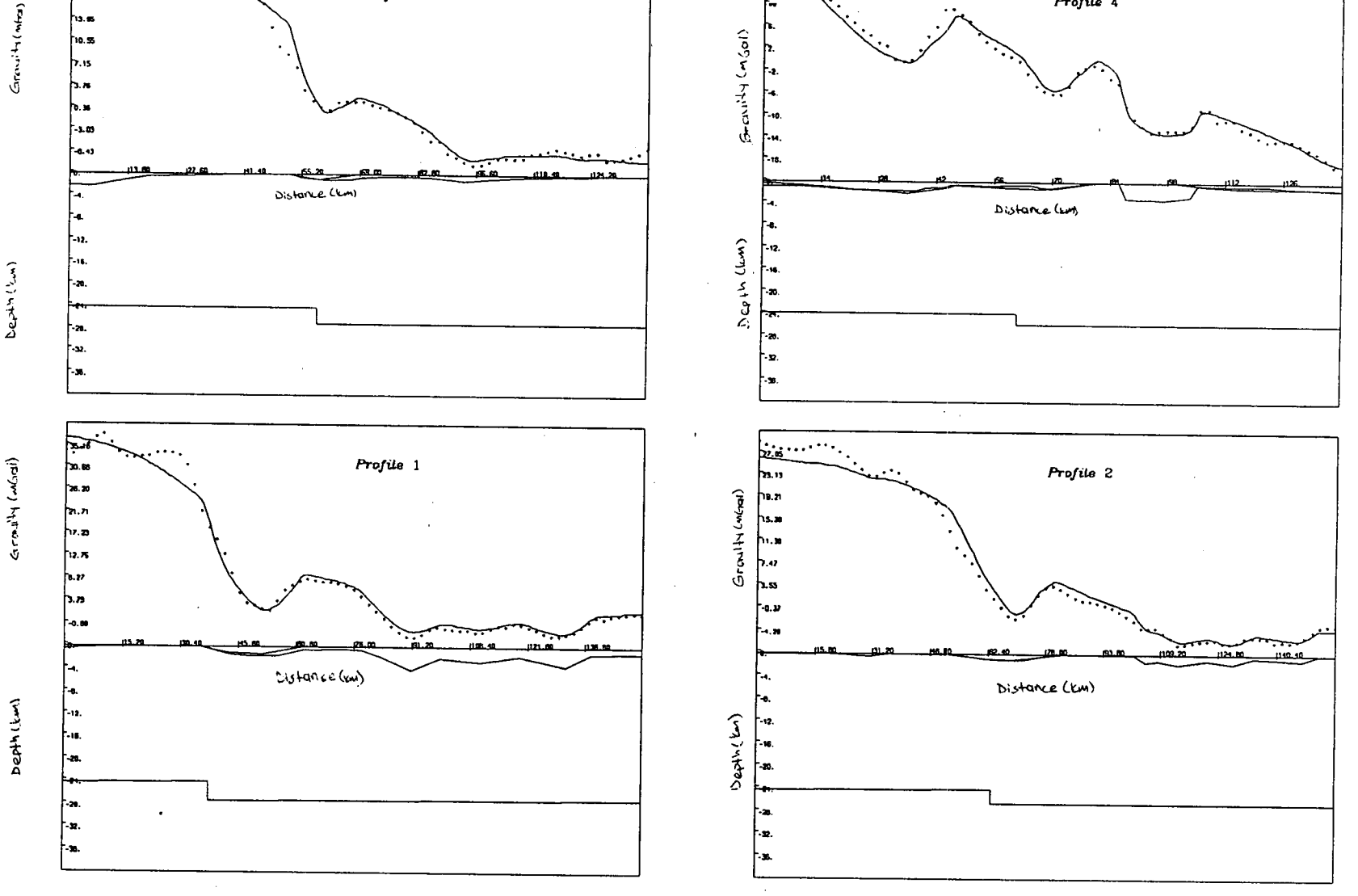

Figure 3.10 Gravity modelling of the four profiles with a step on the Moho.

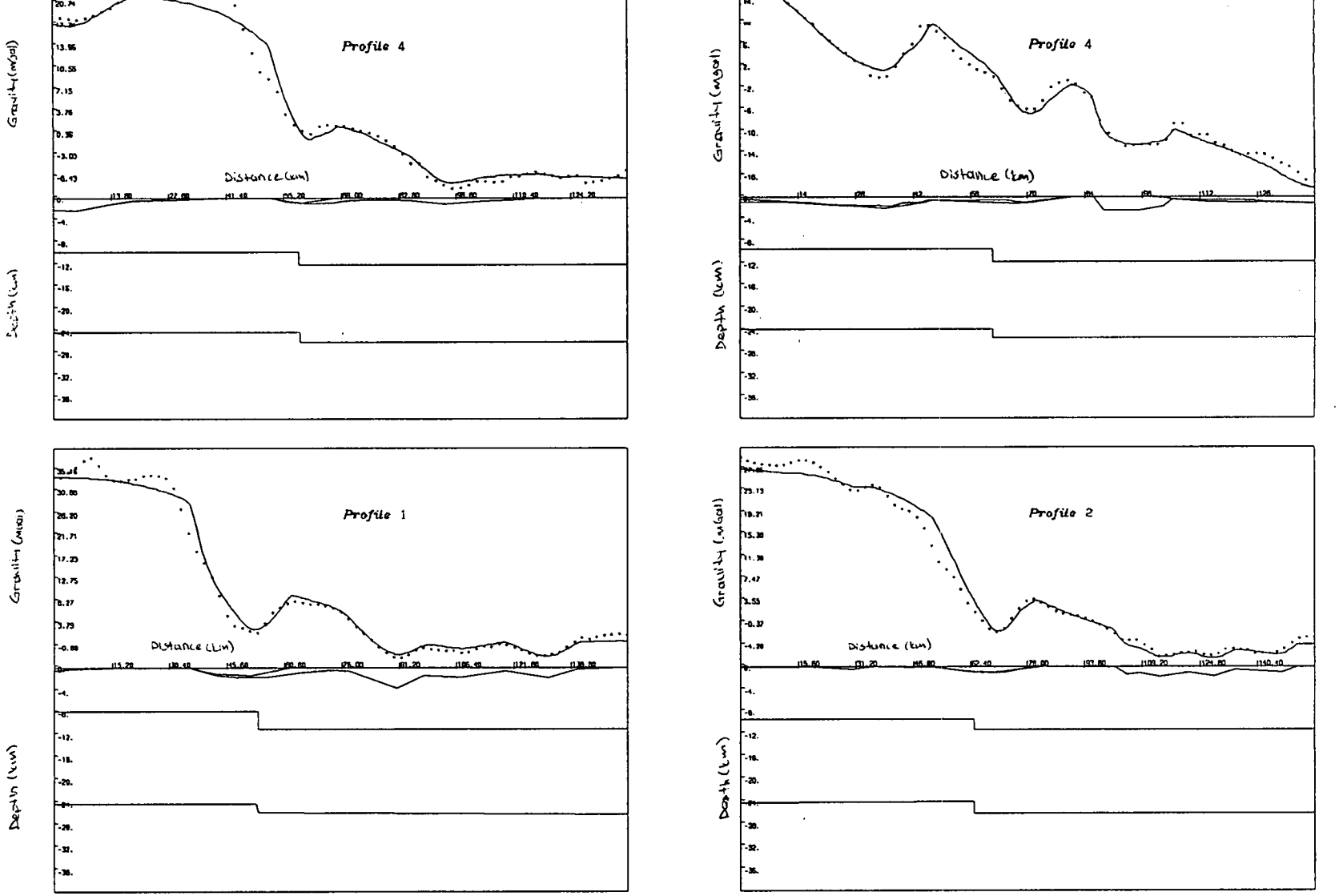

Figure 3.11 Gravity modelling of the four profiles with steps on the boundary of the lower and upper Crust and on the Moho.

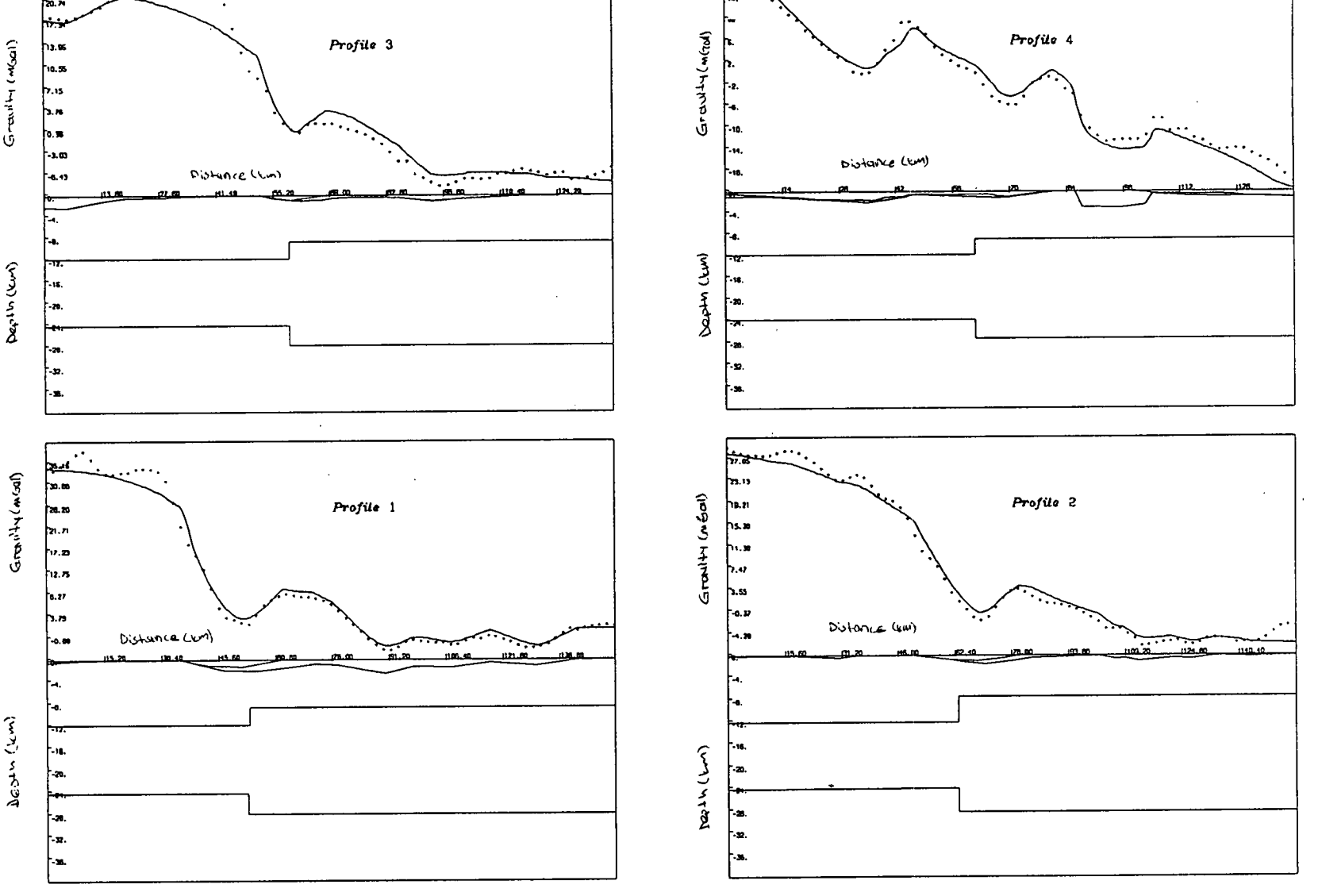

Figure 3.12 Same as figure 3.11, but with the displacement of the lower and upper crust boundary reversed.

depth of 11-12 km and 25-30 at the same time. The results show how non-unique gravity modelling is. All 4 models are able to generate the required gravity anomalies (figure 3.11, 3.12). However it clearly indicates that the gravity anomaly source has a deep origin.

3.3 Discussion

The non-uniqueness of the gravity modelling showed that there are several possible solutions to gravity modelling of the gravity trend over Variscan front. On the other hand it showed that the features are deep in the crust, and the gravity anomaly may be explained by a vertical contact of two different bodies. Note that the models are consistent with strike-slip faulting, but not with normal faulting. Major strike-slip faults may displace the whole crust, so on a cross section it may give an impression that it is normal faulting.

The features deduced from the Bouguer anomalies may be sketched in a single map by superimposing the line drawings from the second derivative and the filtered stripped Bouguer anomaly maps (figure 3.13). It shows that the gravity lows and highs have similar boundaries as consistent gravity trends. This may be an indication of the existence of areas whose tectonic histories are different.

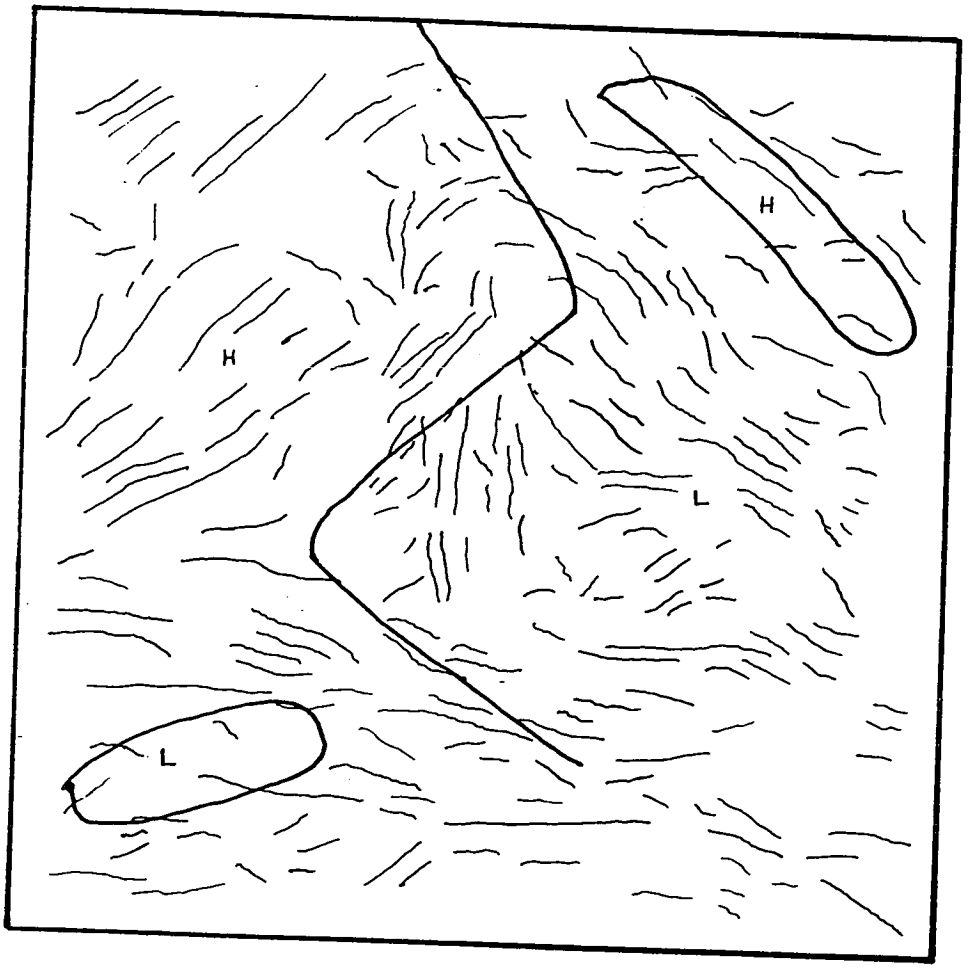

Figure 3.13 Line drawing of second derivative map superimposed on the filtered stripped Bouguer anomaly map features.

CHAPTER 4

MAGNETIC ANOMALY ANALYSIS

4.1 Introduction

The aeromagnetic map of southern Britain (Stubblefield 1965) shows a crescent shape anomaly in the English channel marking an important Variscan thrust feature. The magnetic anomaly is near the south east border of the map and the immediately surrounding areas are magnetically quiet.

Although the aeromagnetic measurements stop over the feature, there are some marine measurements in the region. In this chapter the aeromagnetic anomaly map reproduction, the marine magnetic anomaly map production and the analysis of the magnetic anomalies are discussed.

4.2 Aeromagnetic Anomaly

4.2.1 Aeromagnetic Data

The British Geological Survey publications of 1:250000 scale aeromagnetic maps each covering 2° of longitude and 1° of latitude, are the main reference for the data set. The contours on 9 map sheets (Lundy, Portland, Wight, Chilterns, Land's End, Mid-Wales and Marches, Midland, Bristol Channel, and Cardigan Bay) were digitized with 1 km spacing along the contour lines.

4.2.2 The Aeromagnetic Map Reproduction

The digitized points were then put into the GPCP contouring program to generate gridded aeromagnetic anomalies, and to draw contours. The spacing of the grids were chosen as 1 km which is the flight line spacing over most of the region. However, for analysing the data set it was reduced to 2 km gridding, because some programs could not handle the amount of information.

Unfortunately the heights of the flight lines were not all the same. Figure 4.1. shows the mean terrain clearance of the flights which is in the range of 152 m to 550 m.

The problem of different flight altitudes may be solved by applying analytical continuation of the anomaly. Using the Fourier transform, the magnetic anomaly continuation can be written as

$$M_z(k_x,k_y)=M_0(k_x,k_y)\ e^{-zk} \qquad 4.1$$

where z is the altitude, k_x and k_y are the wavenumbers on x and y directions, and k is the two dimensional wavenumber ($k=(k_x^2+k_y^2)^{1/2}$).

The upward continuation process was chosen, because downward continuation can become unstable in the presence of noise and the short wavelength errors generated by the contouring package. Over the areas where the flight heights were not 550 m, the magnetic anomalies were upward continued to 550 m. The outcome is displayed in figure 4.2.

Complex anomalies in North Wales are associated with the igneous intrusions. The London Basin is associated with a broad nearly circular magnetic high. North of this basin is another more complex magnetic anomaly region, which reflects a further series of igneous intrusions. The south western part of the map indicates a quiet zone of magnetic anomalies over which the Variscan deformation took

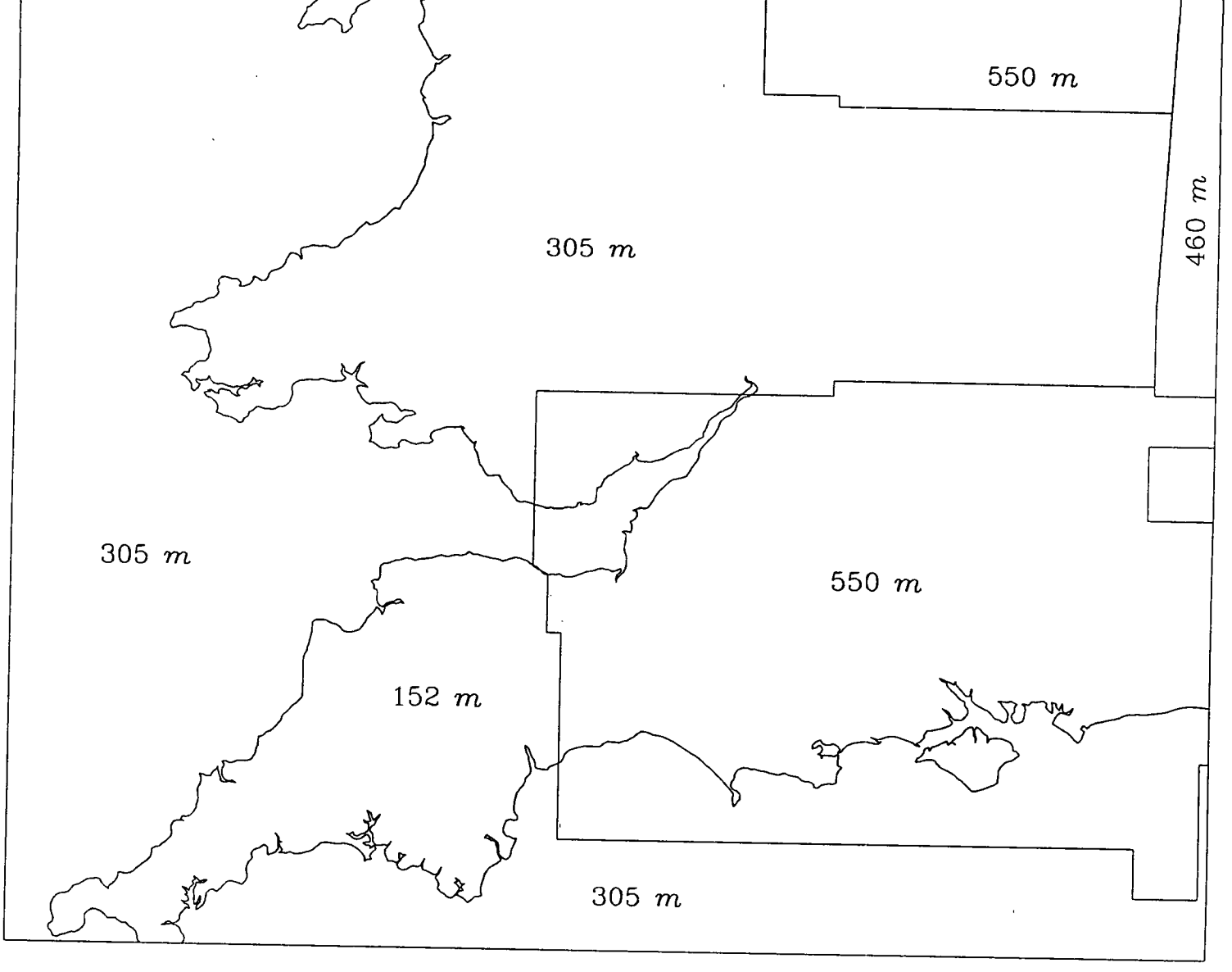

Figure 4.1 Mean terrain clearance of aeromagnetic surveys.

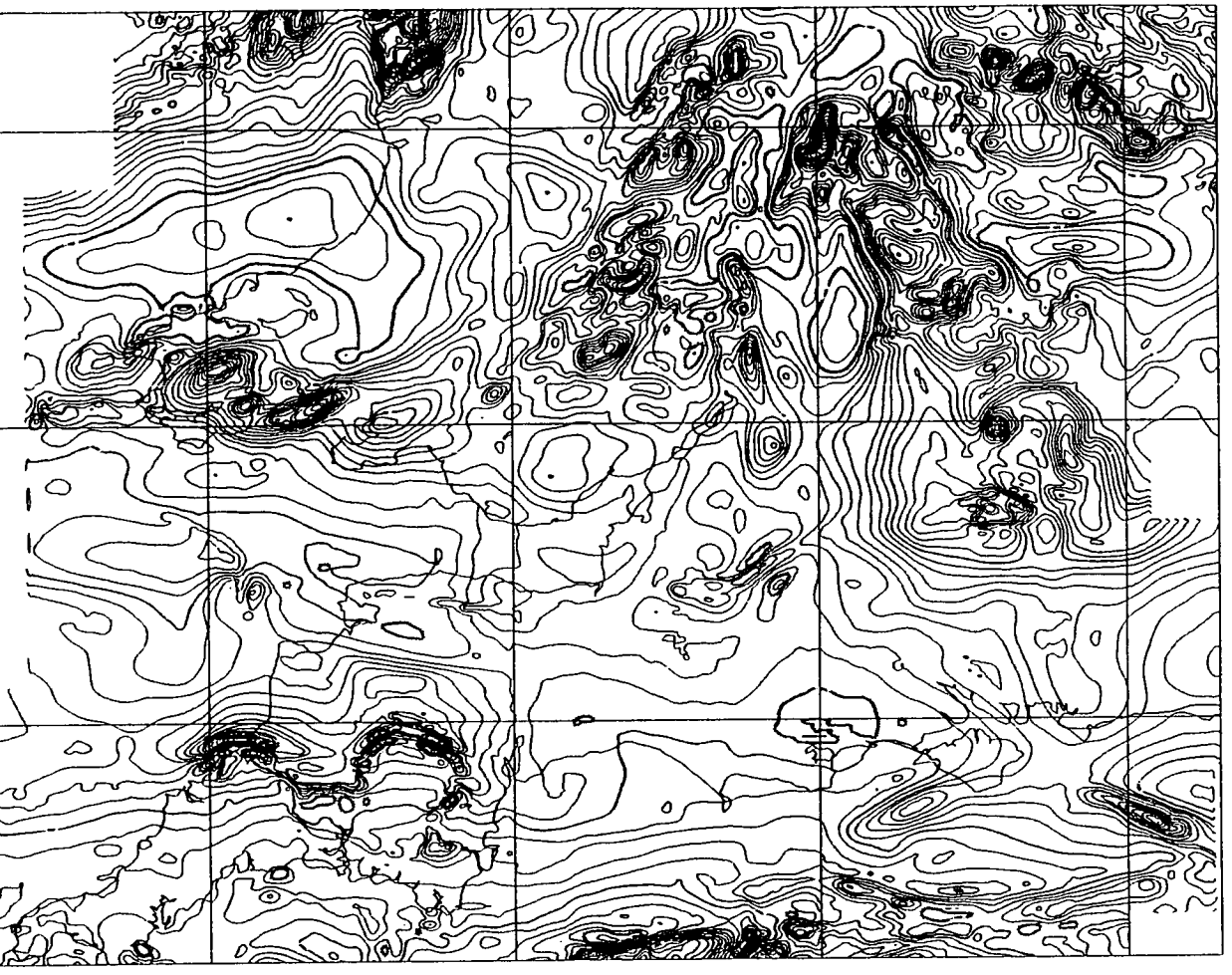

Figure 4.2 Aeromagnetic anomaly map after reduction to a common terrain clearance of 550 m (Contour interval 20 nT).

place. The region is disturbed only by anomalies associated with the Cornubian granites. The crescent shaped anomaly on the south eastern corner of the map is surrounded by these quiet regions although the southern margin of the map generally starts to show more complex magnetic anomalies, associated with the Central Channel Anomaly.

4.2.3 Spectral Analysis of the Aeromagnetic Anomaly

Using the same approach as the spectral analysis of the gravity anomalies, here assuming that the magnetic anomaly at the depth of its sources is a random function, the logarithm of the averaged magnetic anomaly can be written as

$$\log(M(k))=-kz+\text{constant} \qquad 4.2$$

from which the average depth to the layer can be obtained.

The spectrum appears to show two straight lines (figure 4.3). A linear least squares approximation to the lines yields the depth of the layers as 13±1 km, 4±0.5 km.

4.3 Marine Magnetic Anomaly

4.3.1 The Marine Magnetic Data

In 1976, 1980 and 1981 the British Geological Survey conducted shipborne total magnetic anomaly measurements in the English Channel. The spacing between the ship tracks was around 10 km in the western part of the area and 5 km in the eastern part (figure 4.4). The measurements were taken at equal time intervals along the ship tracks.

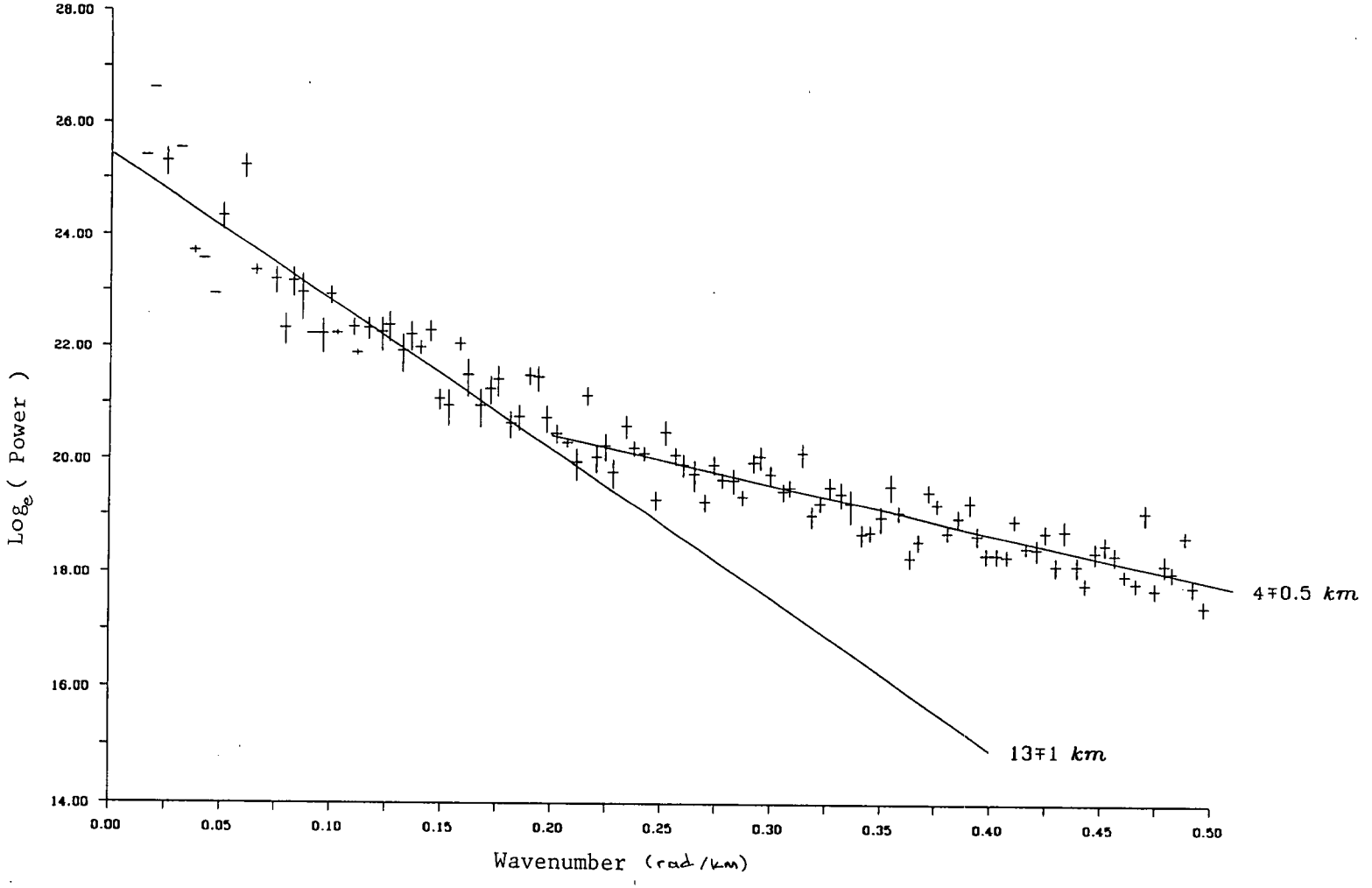

Figure 4.3(a) Aeromagnetic anomaly spectrum.

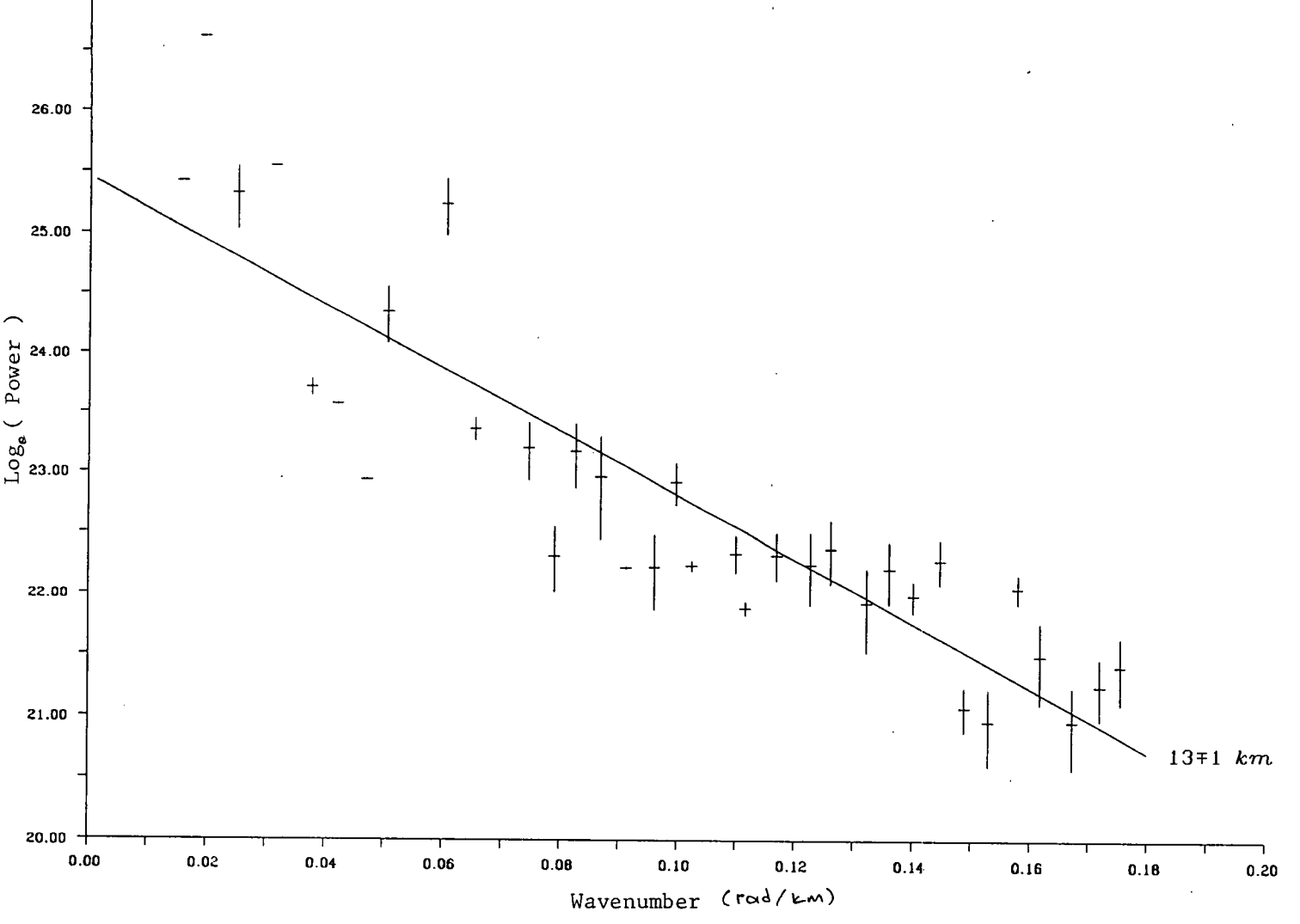

Figure 4.3(b) Aeromagnetic anomaly spectrum: enlargement at the long wavelength.

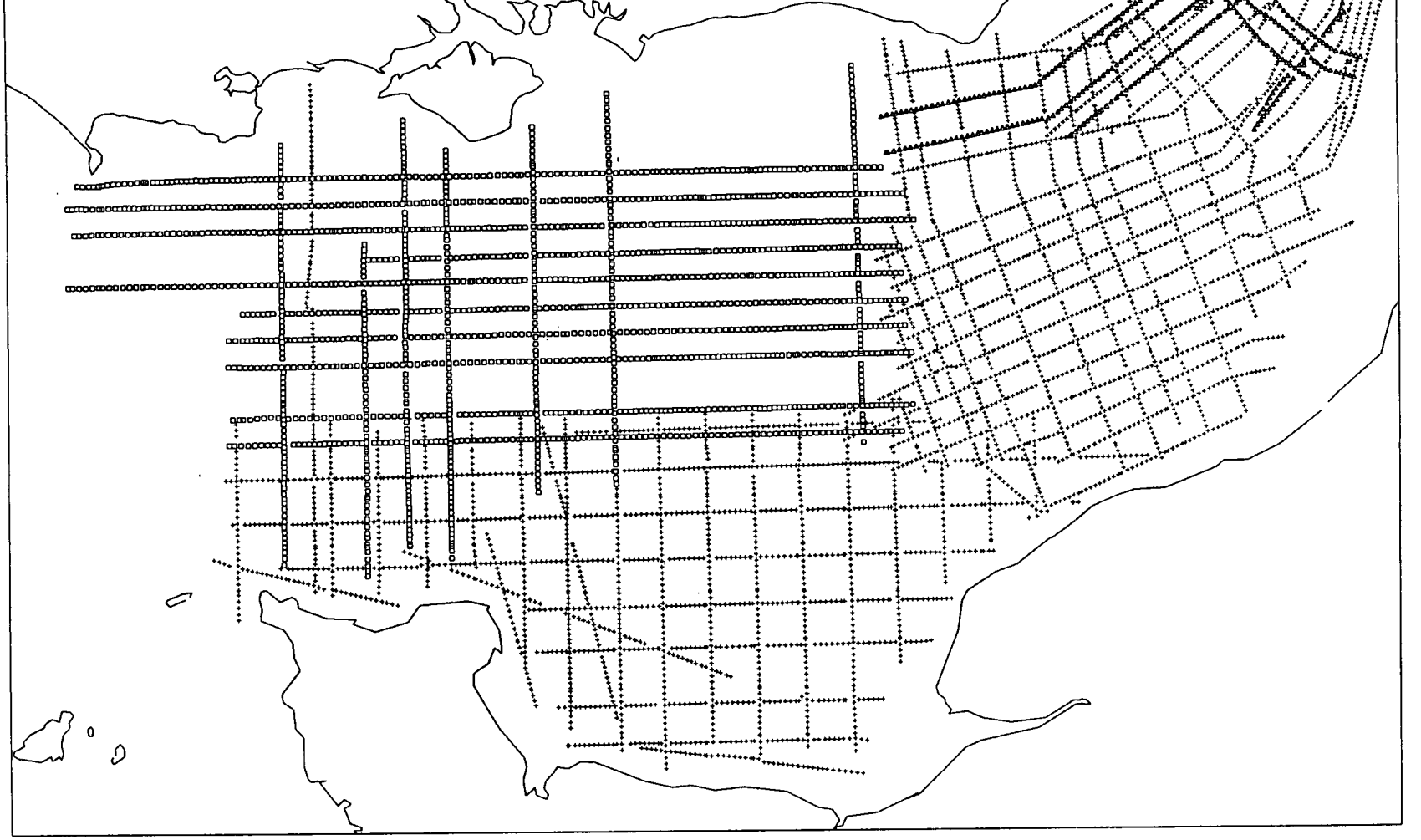

Figure 4.4 Map of data points from marine magnetic surveys. (Triangles for 1981, crosses for 1980 and squares for 1976)

4.3.2 The Marine Magnetic Anomaly Map Production

The measurements were originally reduced by using the coefficients of the International Geomagnetic Reference Field of 1975 (IGRF75) for the 1976 data set and IGRF80 coefficients for 1980 and 1981 data sets. The differences between the two generations of the coefficients are approximately 120 nT in the region, so before doing anything to the data, the data set had to be reduced to a common epoch of the reference field, IGRF80. The computations were carried out by using a FORTRAN program kindly supplied to the author by D. Kerridge (British Geological Survey) in 1985.

Contours of the data were generated using the Calcomp GPCP (1973) program described in appendix 1. The input to the program was thinned so that the spacing between the consecutive measurements was not less than 300 m. The contouring routine takes 8-24 neighbouring data points nearest to the grid point. Some data points are only 80 m apart so it would be possible that all the nearest points would be taken from only one ship track. The thinning process provides the opportunity to evaluate the grid value from measurements along several ship tracks. The grid spacing was chosen as 2 km, and the contouring of the data is shown in figure 4.5.

The N-S trending features on the map near [440,0] coincide with the overlapping of two different data sets. This indicates that the data reduction was not a complete success. The other overlapping regions do not show a similar pattern. It indicates that the main cause is only two of the 1980 ship tracks which may therefore have been faulty. These features ought not to affect the analysis of the data, because they are short wavelength features.

The crescent shape anomaly on the aeromagnetic map is just inside the marine data set and it is clearly visible. The anomaly trend becomes more complex to the

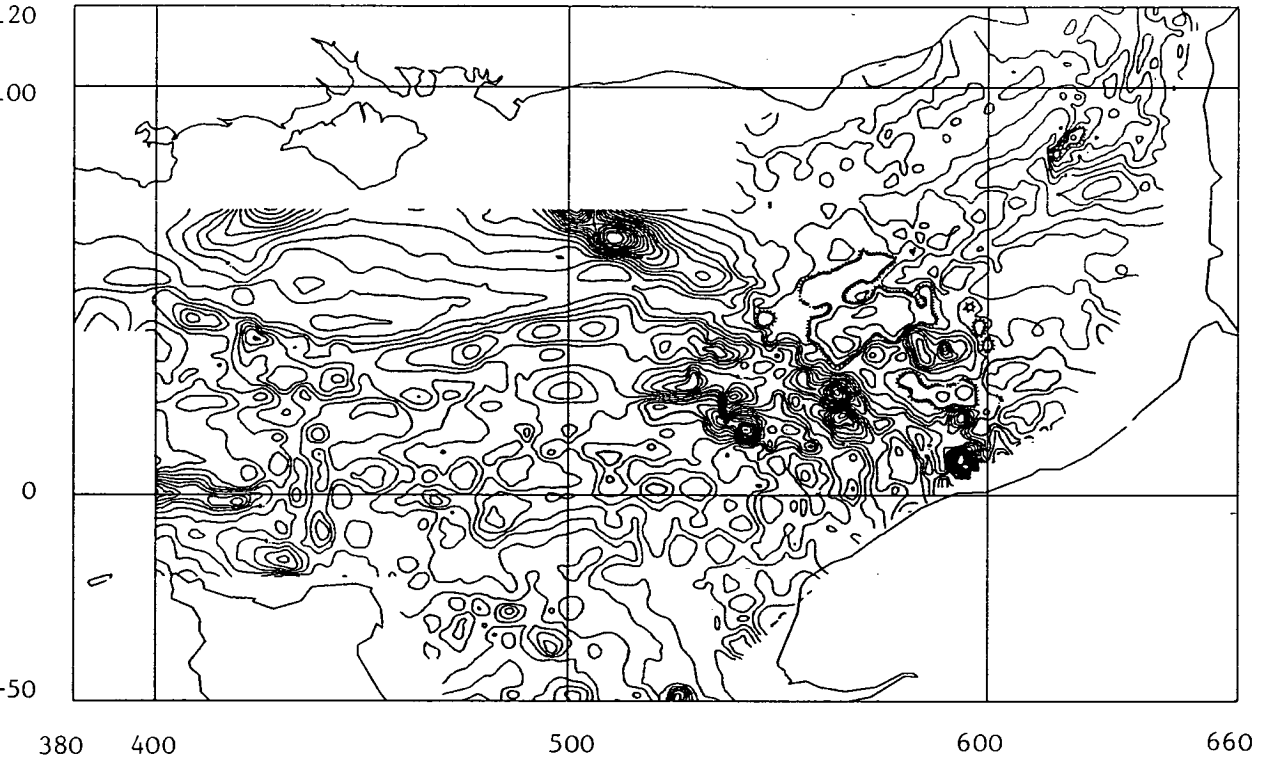

Figure 4.5 Marine magnetic anomaly map. (Contour interval 20 nT)

south eastern side of the feature. The magnetic anomaly trend over the supposed Bristol Channel - Bray Fault location, coincides with the gravity anomaly trend over the same area, and the magnetic anomaly trend continues towards France. The western side of the anomaly trend shows complex magnetic anomalies, whereas on the eastern side there is a relatively quiet region. This may imply that the main deformation was on the western side.

There is a well defined linear magnetic low in the central Channel called the Central Channel Anomaly which trends east west. There are magnetic anomaly trends to the west, again mainly in an east west direction which is the direction of the Variscan deformation.

4.3.3 Spectral Analysis of the Marine Magnetic Anomalies

Using the same approach as the spectral analysis of the aeromagnetic anomaly, the average depth of sources may be obtained from the spectrum of the marine magnetic anomaly.

The spectrum of the marine magnetic anomaly shows only one straight line (figure 4.6). The analysis of the line yields the depth of the source as 6±0.5 km.

4.4 Composite Contouring of the Magnetic Anomaly

The two maps may be joined together to obtain a complete picture of the magnetic anomaly.

Upward continuing the marine data to 550 m solves the problem of a common altitude for both data sets. However the data sets do not have a common reference field. As it is mentioned in section 4.3.2, the marine data set was reduced by using IGRF80 coefficients. Unfortunately the aeromagnetic data were

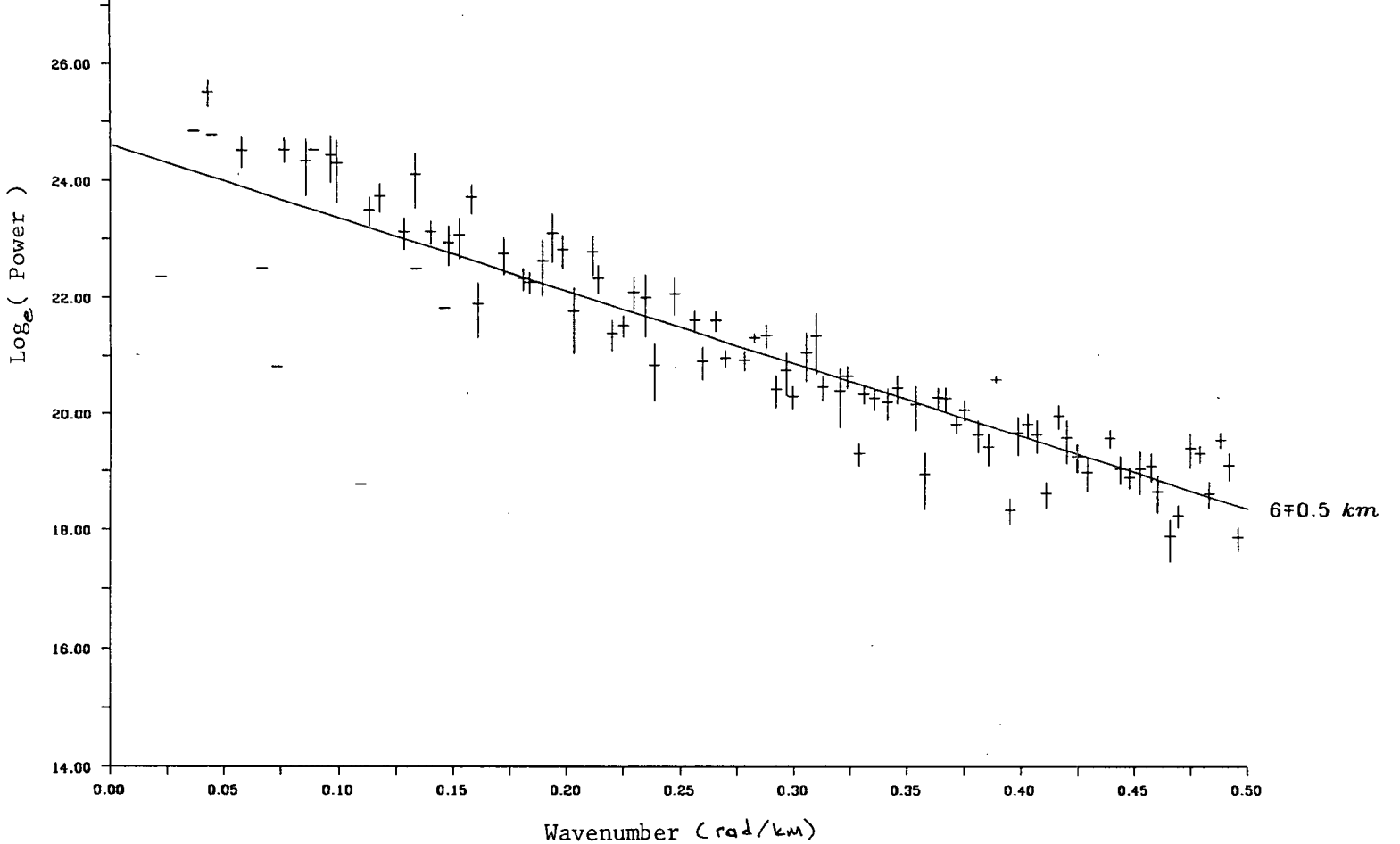

Figure 4.6 Spectrum of the marine magnetic anomaly

reduced using a local linear approximation to the 1955.5 main magnetic field. The publishers of the maps give a way to compute the reduction of the anomalies by a linear interpolation of corrections given for the corners of each map sheet. This should reduce the data to the IRGF65 magnetic field with an uncertainty of 4 nT. Interpolating the aeromagnetic data as described, and reducing the marine data set to IGRF65 should give the solutions for joining the two maps. However a different approach was made here.

The differences between the two data sets should be more or less constant. Statistical analysis of the overlapping region shows that the average difference between the two data sets is 106 nT. In producing the magnetic anomaly map, the marine data set was updated with this average value.

In producing the composite magnetic map, over the overlapping region, priority was given to the aeromagnetic map, because the aeromagnetic maps were prepared with a denser spacing of the observations, so the contouring should be more reliable. The outcome is displayed in figure 4.7 and at the back of the thesis.

4.5 Spectral Analysis of the Magnetic Anomaly

The blank regions were filled with zeros and the magnetic anomaly spectrum was computed. The results were similar to those obtained for section 4.2.3. The approximately linear section of the spectrum gave the depth to the layers as 14±1 and 4±0.5 (figure 4.8).

Considering the extent of the area, the expectation was that the Curie depth would show in the spectrum. The Curie depth is the bottom of the magnetization, so cumulative pole strength from all sources above it should be zero. Thus the cumulative spectrum should go to zero at its long wavelength end where all the upward continuity operators tend to unity. If the Curie depth is in the order of 25

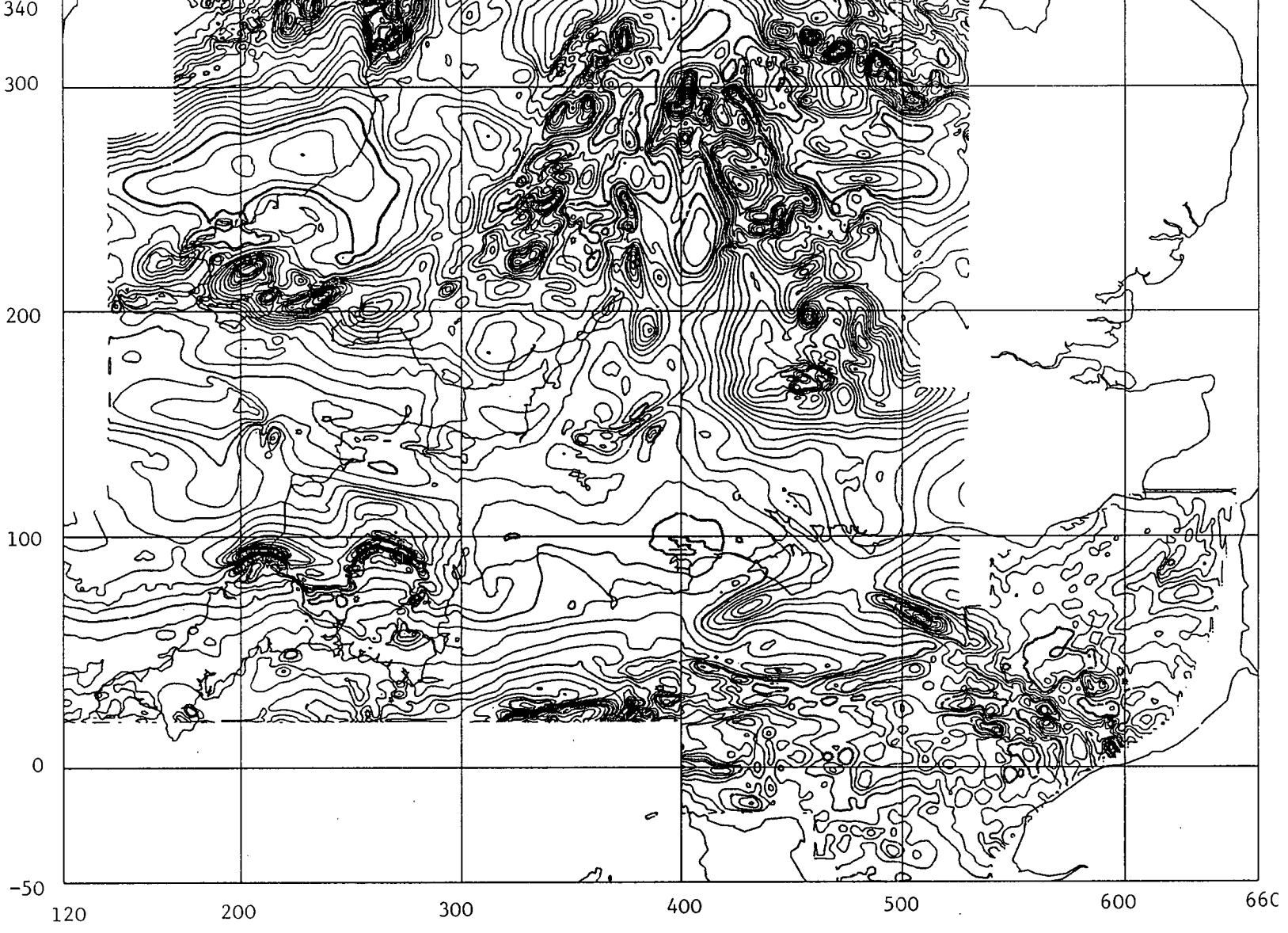

Figure 4.7 Composite contour map of magnetic anomalies. (Contour interval 20 nT)

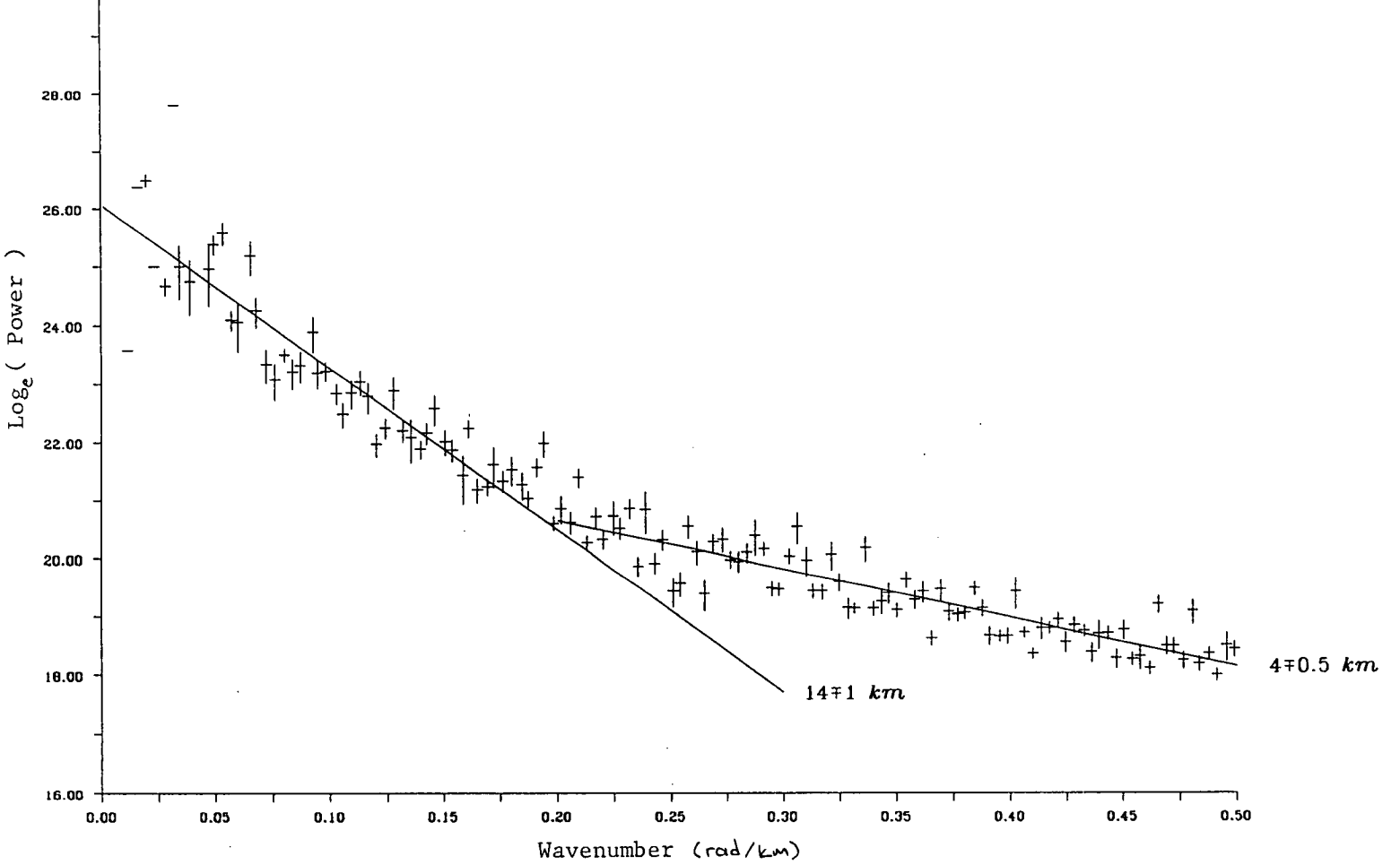

Figure 4.8(a) Spectrum of the composite magnetic anomaly

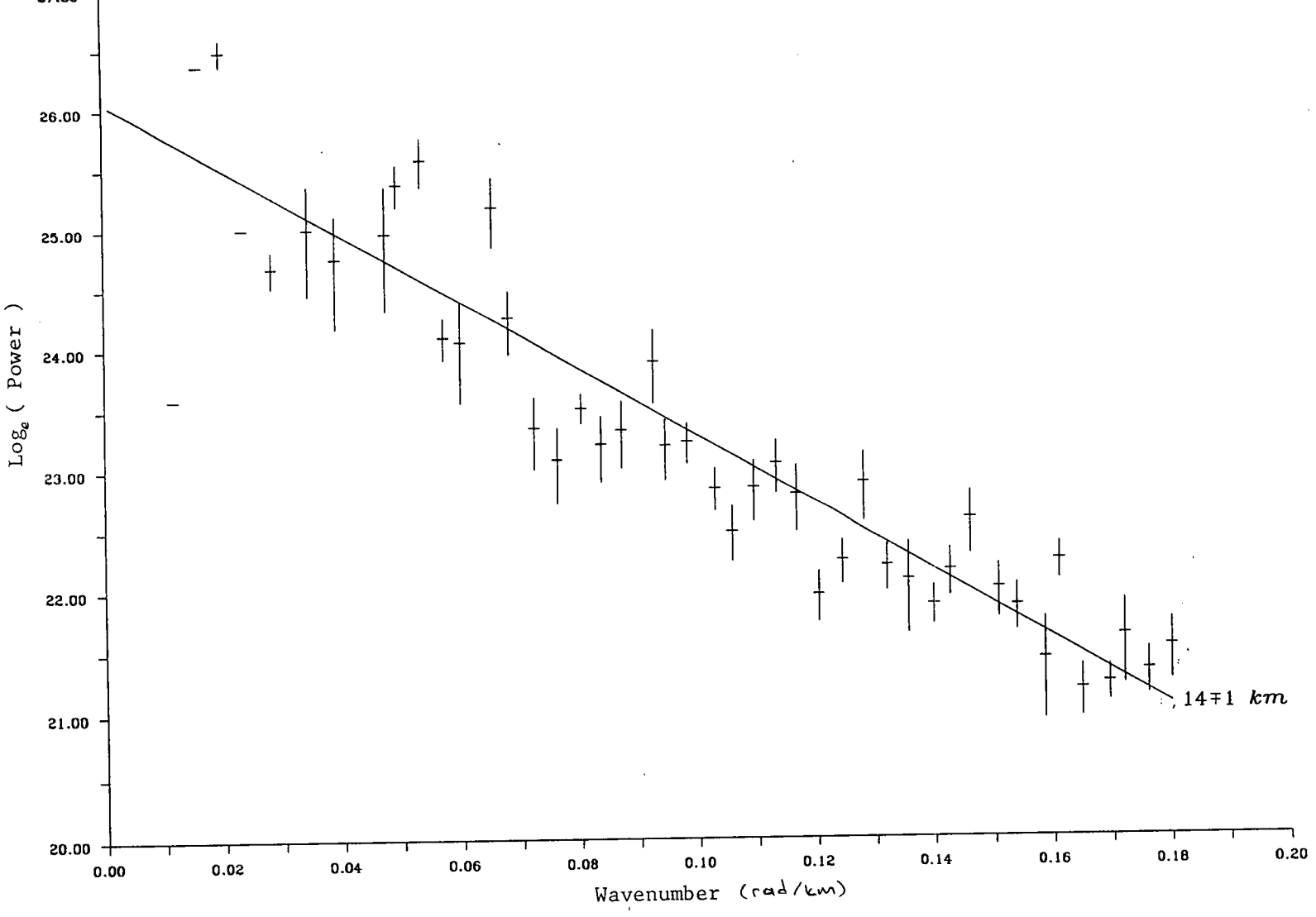

Figure 4.8(b) Spectrum of the composite magnetic anomaly: enlargement at the long wavelength.

km, then the area required for finding a signal from it is about 200x200 km^2 (Spector and Grant, 1970). The dimension of the area is 540x390 km^2, so the signal from Curie depth should be within reach. This may imply that the area required for determining the Curie depth is larger than reported by Spector and Grant or the Curie depth is much deeper than 25 km.

4.6 Separation of the Anomalies

The magnetic anomaly due to deep sources (figure 4.9) may be obtained by filtering the anomaly map. Spectral analysis has shown that 60 km is the cut-off wavelength for features deeper than 14 km.

Most of the features on the magnetic anomaly map have disappeared after filtering. The complex anomalies over the Midlands and Cornwall have greatly diminished, suggesting that these features are shallow. The disappearance of the anomalies over the Cornubian granites contrasts with the results from the gravity anomaly data where the feature is seen as a deep one. This suggests that the magnetic anomalies over the Cornubian granites are not generated by themselves but by a shallow marginal structure, interpreted as dykes in the region (Edmonds at al 1968).

4.7 Second Vertical Derivative of the Magnetic Anomaly

The usefulness of the second derivative map is demonstrated in 3.1.5 for the gravity anomalies. The same method can be applied to the magnetic anomaly map to look at the relation between the magnetic anomaly and the tectonic events.

The second derivative of the magnetic anomaly is computed using the equation 3.6 (figure 4.10). It shows that the marine magnetic anomaly map mainly reflects the ship tracks. The reason could have been that the 2 km grid spacing was too small,

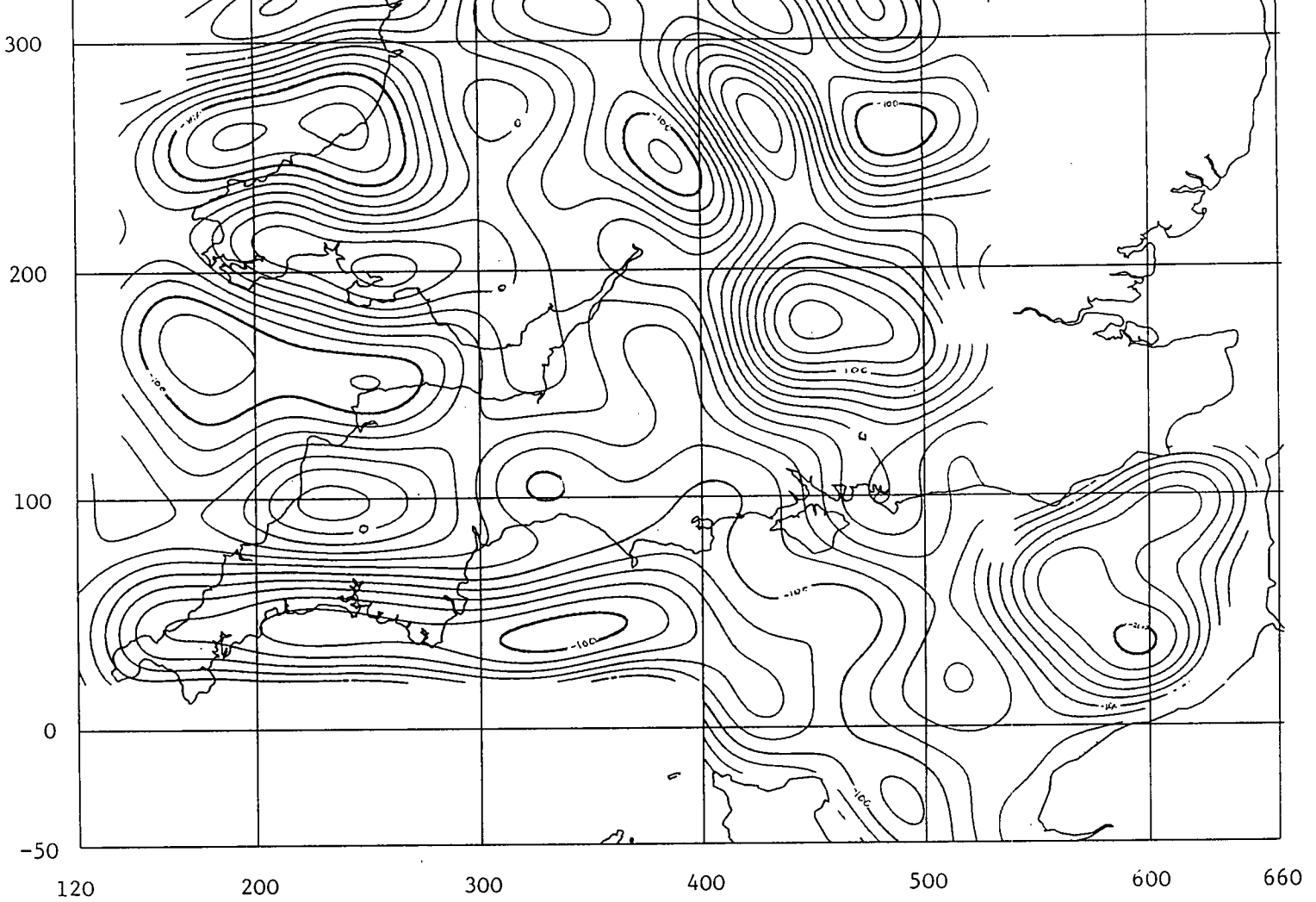

Figure 4.9 Filtered magnetic anomaly map.

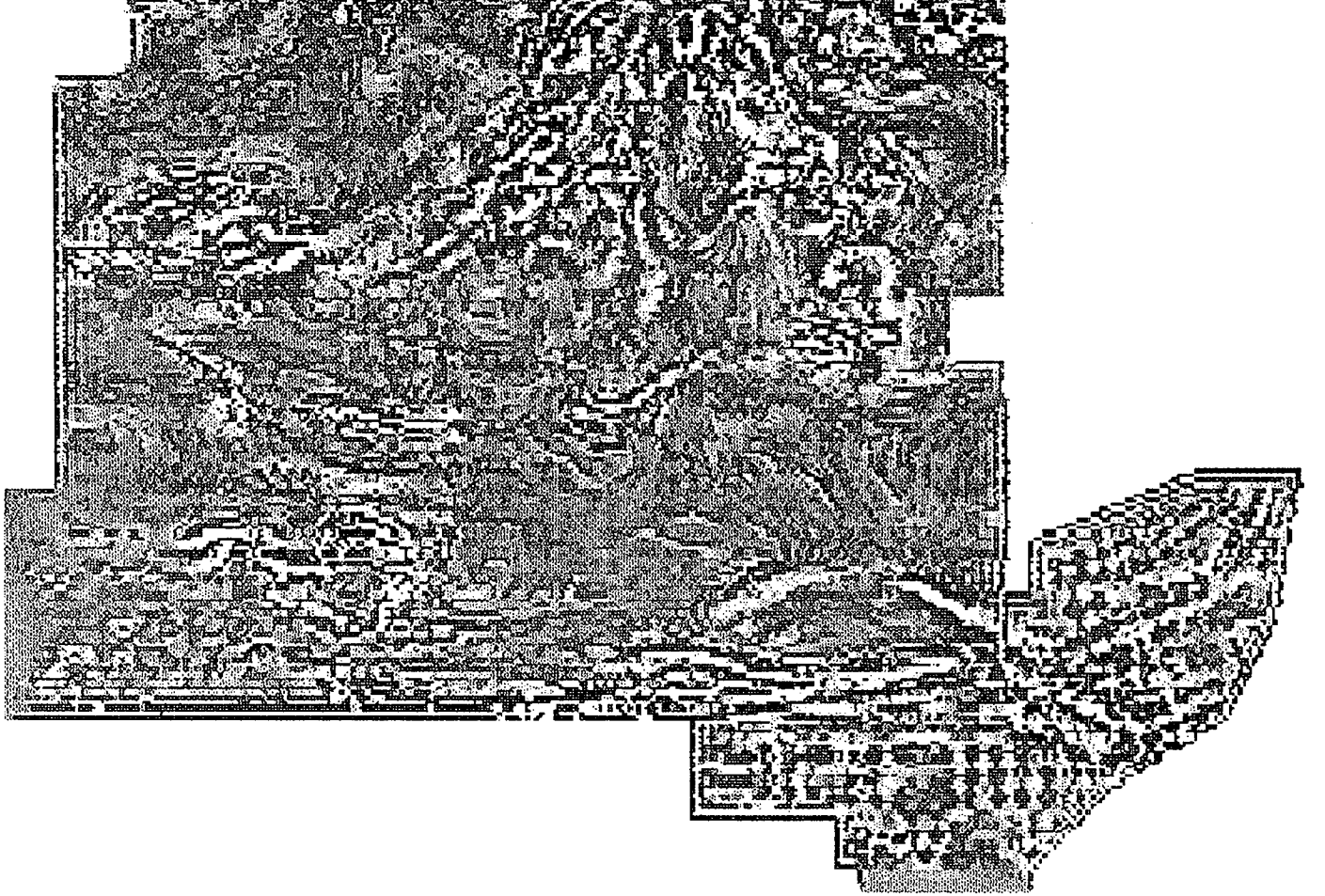

Figure 4.10 Second derivative of the magnetic anomaly

or that the thinning distance should have been bigger than 300 m. However, it was most likely to have been due to the misfit between the different data sets, as on two occasions, it was detected directly on the contour map of the marine magnetic anomaly.

The only lineament in the marine data area, which is not related to the ship tracks is the NW-SE directional line over the Bristol Channel - Bray fault zone. This demonstrates the magnitude of the feature by overcoming the effect of the noise.

Over north Wales, The aeromagnetic data area shows the same NE-SW directional features as on the second derivative of the gravity anomaly map. Again the lines stop as they reach the Malvern axis, over which lies N-S directional trends. It is not clear what happens on the eastern side of the axes due the lack of data.

While the pattern of the magnetic second derivative is similar to that of the gravity anomaly on the northern side of the Variscan front zone, on the southern side the picture is completely different. The area is unexpectedly quiet. The only strong feature is due to the Cornubian granites. This may be due to magnetic basement having a different nature in the south and being too deep to be seen on the second derivative map.

4.8 Conclusions

The spectral analysis of the magnetic anomaly showed an interface at a depth of about 14 km similar to the result obtained from the gravity anomaly spectrum.

The anomaly due to deep features showed that the most of the magnetic anomalies are generated by near surface materials. Probably the most important result is the contrast in the magnetic anomaly pattern between regions north and south of the Variscan front.

CHAPTER 5

ISOSTASY

5.1 Introduction

Isostatic compensation of the topography of southern Britain is investigated in this chapter. Different methods are used to estimate the isostatic response function relating the gravity anomaly and the topography.

5.2 Plate Bending Under a Load

When an elastic plate is loaded, the plate responds to this load and deforms. The vertical displacement is determined by the equation (Love 1944)

$$D\nabla_L^4 w = p \qquad 5.1$$

where ∇_L is the surface Laplacian, w is the vertical displacement, p is the load per unit area and D is the flexural rigidity. The flexural rigidity can be expressed in terms of the elastic plate thickness T

$$D = ET^3/12(1-\sigma^2) \qquad 5.2$$

where E is the Young's modulus and σ is the Poisson's ratio. For a floating plate, there will be an additional load-like force due to buoyancy acting on to the plate (figure 5.1) and equation becomes

$$p = D\nabla^4_L w + g\Delta\rho w \qquad 5.3$$

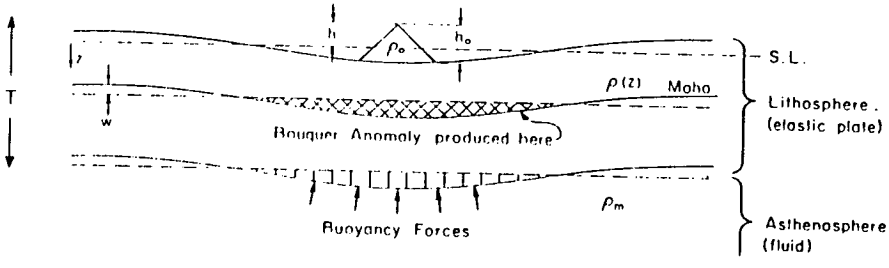

ure 5.1 The elastic plate model for isostatic compensation (from
ks et al).

where g is the gravitational acceleration and $\Delta\rho$ is the density contrast between the overlying and underlying material.

If the load is due to the Earth's topography, we can write down the equation 5.3 as

$$-g\rho_t h = D\nabla_L^4 w + \Delta\rho w g \qquad 5.4$$

where ρ_t is the density of the topography and h is the topography. Note that the minus sign comes because the topography is measured positive upwards. From the definition of a Fourier transform $\mathcal{F}[\nabla_L^4 w] = k^4 W(k)$, so that working in the frequency domain makes equation 5.4 easier to solve

$$-g\rho_t H(k) = D\nabla_L^4 W(k) + \Delta\rho W(k) g \qquad 5.5$$

and

$$W(k) = -\rho_t/\Delta\rho \; (1 + k^4 D/g\Delta\rho)^{-1} \; H(k) \qquad 5.6$$

where upper case letters are used for Fourier transforms.

For Airy type isostasy the displacement is

$$W(k) = -(\rho_t/\Delta\rho) \; H(k) \qquad 5.7$$

corresponding to the limit when the flexural rigidity, D, tends to zero.

5.3 Gravity Anomaly Caused by Vertical Displacement

If the elastic plate thickness is greater than the depth of the Moho, the surface displacement of the plate will be the same as that on the Moho. This vertical

displacement of the elastic plate will be reflected in the surface Bouguer anomaly variations. Thus, if G(k) is the Fourier transform of the Bouguer anomaly (Parker 1972)

$$G(k)=2\pi\mathcal{G}\Delta\rho e^{-kz}\sum k^{n-1}/n!\ \mathcal{F}[w^n(x)] \qquad 5.8$$

where z_c is the depth to Moho or (compensation depth), $\mathcal{G}$ is the gravitational constant. If the topography on the Moho is small compared with the compensation depth, then a linear approximation may be made as

$$G(k)=2\pi\mathcal{G}\Delta\rho e^{-kz}W(k) \qquad 5.9$$

Combining this equation with 5.6, the relation between the Bouguer anomaly and the topography is established as

$$G(k)=2\pi\mathcal{G}\rho_t\ (1 + k^4D/g\Delta\rho\ )^{-1}\ e^{-kz}\ H(k) \qquad 5.10$$

and, for the Airy type of isostasy

$$G(k)=2\pi\mathcal{G}\rho_t\ e^{-kz}\ H(k) \qquad 5.11$$

If we define a new function R(k), called the isostatic response function, where

$$R(k)=2\pi\mathcal{G}\rho_t\ (1 + k^4D/g\Delta\rho\ )^{-1}\ e^{-kz} \qquad 5.12$$

and, for the Airy type isostasy,

$$R(k)=2\pi\mathcal{G}\rho_t\ e^{-kz}, \qquad 5.13$$

then

$$G(k)=R(k)H(k). \qquad 5.14$$

So far we have assumed that the only density contrast within the lithosphere is at the Moho discontinuity; otherwise the plate has a uniform density. However the observed Bouguer anomaly includes the gravitational attraction of geological features. In this case the gravity Bouguer anomaly may be separated into two parts as (Dorman and Lewis 1970)

$$G_O=G_D+G_G \qquad 5.15$$

where G_O is the observed Bouguer anomaly, G_D is the gravitational attraction due to the displacement on Moho and G_G is the gravitational attraction of geological features. Combining 5.15 and 5.14 gives

$$G_O(k)=R(k)H(k)+G_G(k). \qquad 5.16$$

Estimating the response function from equation 5.16 is discussed in sections 5.6.1 and 5.6.2.

5.4 Topographic Data

Topographic data for the region of southern Britain between the British National Grid coordinates 100 km to 700 km easting, and -50 km to 556 km northing was compiled by using the topographic heights of the gravity stations on the land areas and the water depth over the ship tracks at sea. This information was already available in the gravity data bank. The coverage of the data points is displayed in figure 1.6. These data points were interpolated on to a 2 km grid spacing using Calcomp GPCP computer contouring package (appendix 1). A three dimensional image of the topography is shown in figure 5.2.

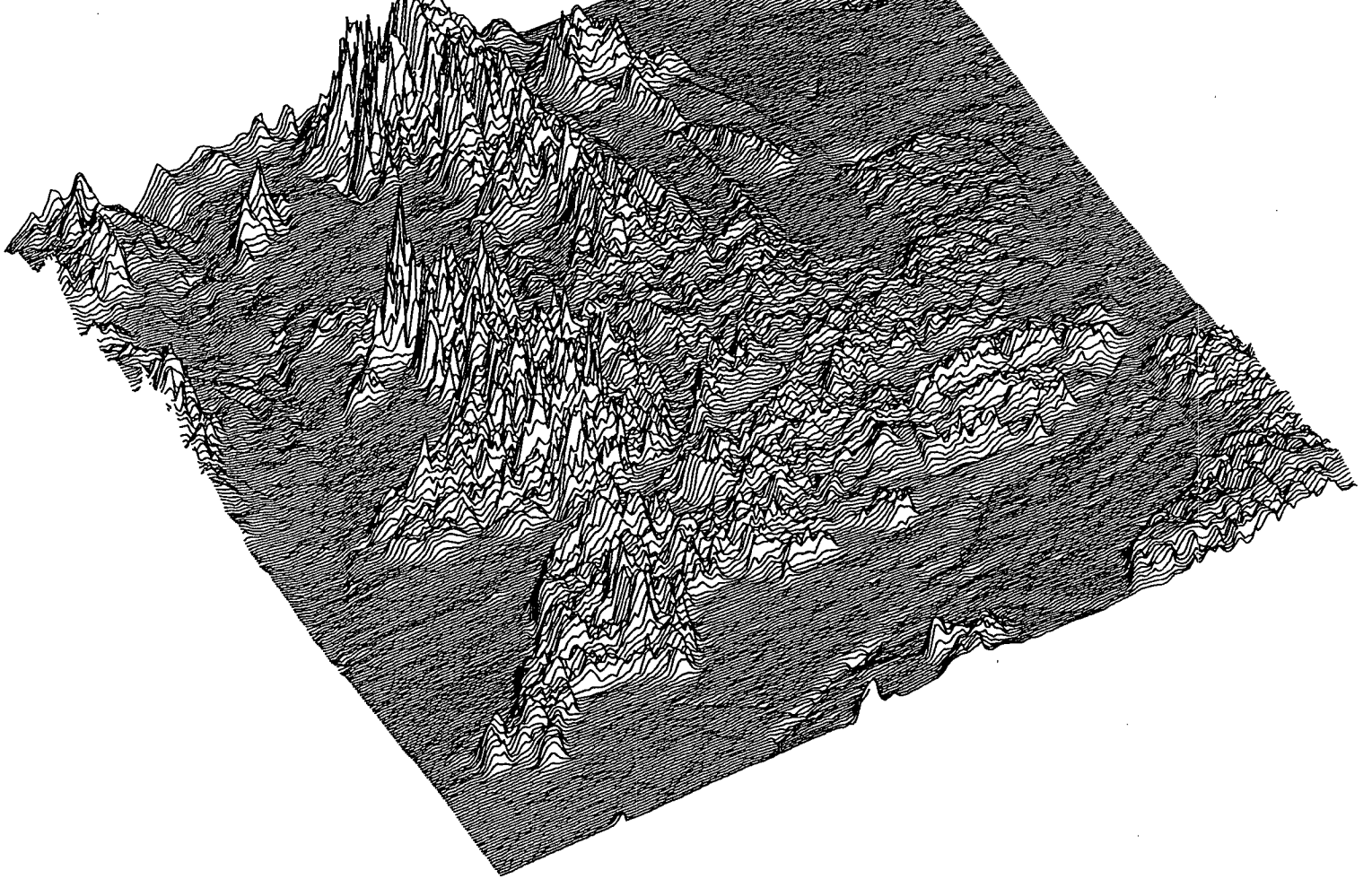

Figure 5.2 A 3-dimensional view of the topography of southern Britain, looking from the south-west.

This gridding progress is necessary not only for producing a contour map of the topography but also for taking the Fourier transform of the topography. Using these sources to determine the topographic representation may well be questioned; but at the time, no better representation of the topography was available. However, over smooth terrain the very high density of the gravity stations should give an adequately representative topographic model. In the mountainous regions where the bias might have been more serious, the gravity data were generally obtained with a combination of ground based survey near roads and helicopter survey accessing hill tops. This should generate a more representative average.

5.5 Load Equivalent Topography

In deriving equations 5.6 and 5.7 in section 5.2, it was assumed that the applied load was due to topography. In general there will be two components to the load: in addition to the topography, defined to have a constant density, ρ_t, there will be the effects of the shallower subsurface density variations. The most important of these is due to low density sediments which reduce the load obtained by considering only the effect of the topography. If sediments have a mean density of ρ_s, and a thickness of h_s, their load is equivalent to extra topography of height $(\rho_s-\rho_t/\rho_t)h_s$. The effect of the total load equivalent topography is then

$$h_e(x,y) = h_t(x,y) + (\rho_s-\rho_t/\rho_t)h_x(x,y). \qquad 5.17$$

Note that the sea-water is converted to the load equivalent topography in the same way. The surface of the load equivalent topography is shown in figure 5.3.

In deriving equations 5.12 and 5.13, the Bouguer anomaly was used rather than free air anomaly. This was because the anomaly was intended to reflect the compensating masses, not those causing the load. Now that the load equivalent

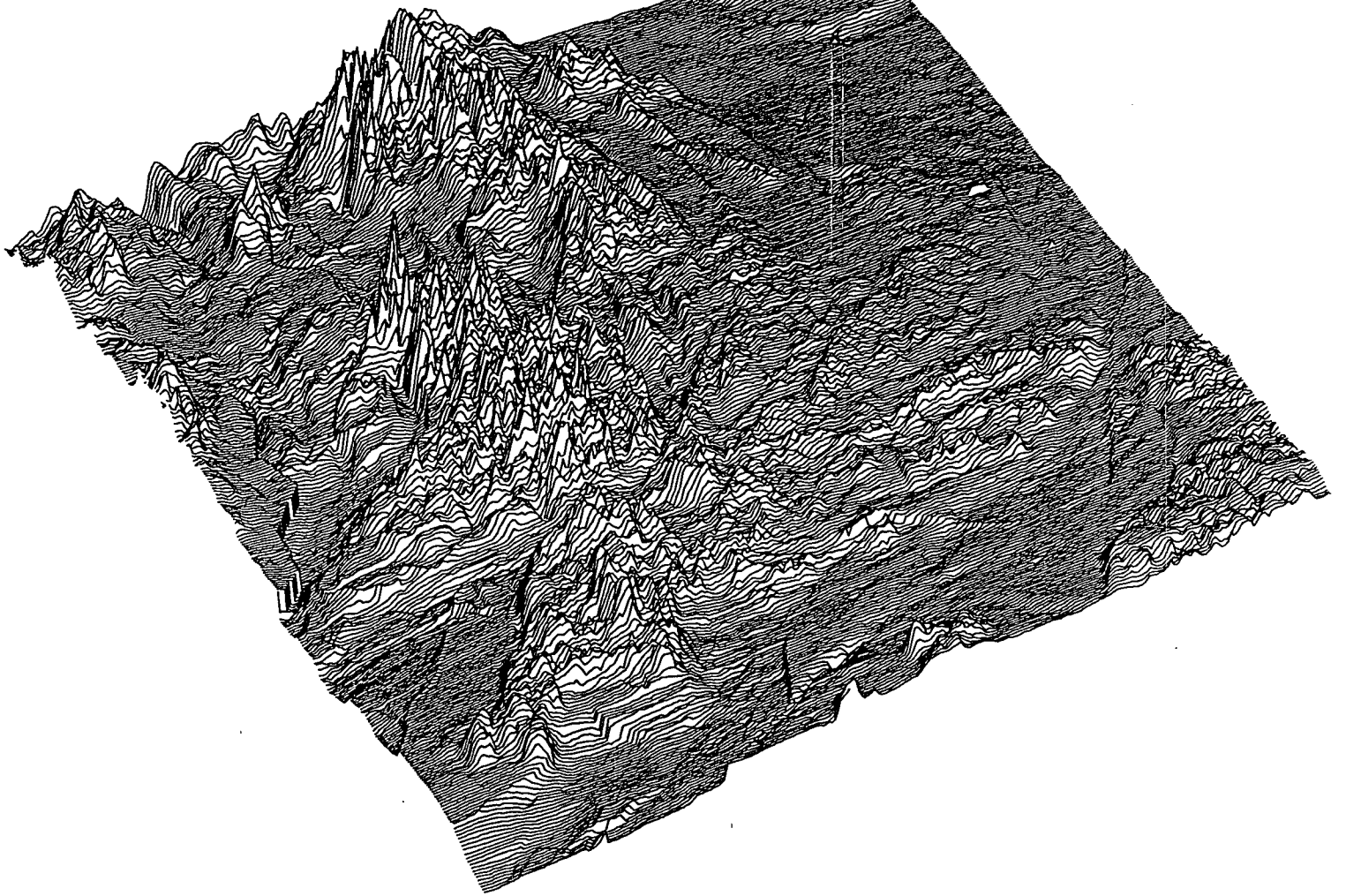

Figure 5.3 A 3-dimensional view of the load-equivalent topography of southern Britain, looking from the south-west.

topography includes the effect of the sediments, the stripped Bouguer anomaly should be used, so that only the anomalies due to compensating masses are included rather than those due to the sediments.

5.6 Estimating the Response Function

5.6.1 Averaging

A solution for R can be obtained by averaging equation 5.15, that is, averaging over all azimuths around an annulus in the wavenumber domain (Dorman and Lewis 1970). If we rewrite the equation as

$$R(k)=G_O(k)/H(k) - G_G(k)/H(k), \qquad 5.18$$

averaging the right hand side will diminish the second term if there is no correlation between topography and the part of the Bouguer anomaly caused by the geological features. For the 600 km by 604 km region defined above, interpolation on to a 2 km grid results in 91200 response function estimates. These were averaged over 1000 equal wavenumber intervals and their logarithm plotted against wavenumber (figure 5.4). If we take the logarithm of the equation 5.13

$$\log R(k)=\log 2\pi\mathcal{G}\rho_t - kz_c \qquad 5.19$$

then plotting log R(k) against k will show a straight line whose gradient is equal to the compensation depth.

Theoretically, averaging gives a response function estimate in every waveband interval. However in practice, the short wavelength end of the spectrum is mainly dominated by noise and any solution obtained using this part of the spectrum may

be unreliable.

The relative size of the signal to the noise is measured by the coherence. The coherence between topography and Bouguer anomaly is given by

$$\gamma^2 = |G(k)H^*(k)|^2 / |G(k)|^2|H(k)|^2 \qquad 5.20$$

where * indicates the complex conjugate. The coherence found by equation 5.20 is positively biased noise. The noise may be reduced by (Munk and Cartwright 1966)

$$\gamma^2_O = N\gamma^2 - 1/N - 1, \qquad 5.21$$

where N is the degrees of freedom. Noise-reduced coherence is shown in figure 5.5.

Linear regression analysis was used to fit the equation 19 to the averaged estimates of the response function. Considering the low coherence of response function estimates at large wavenumber (figure 5.5), and their evident departure from linearity for all but the long wavelengths (figure 5.4), only those estimates corresponding to wavelengths greater than 60 km were included in the analysis (figure 5.6).

With a two parameter regression, the depth of the compensation was 13±5 km and the intercept corresponded to a topographic density of 1.47±0.63 g/cm^3 instead of the chosen value of 2.7 g/cm^3.

5.6.2 Least Squares Fitting

If equation 5.16 holds over a given waveband then we can fit a linear function by least squares over the waveband and estimate constant values R and G_G

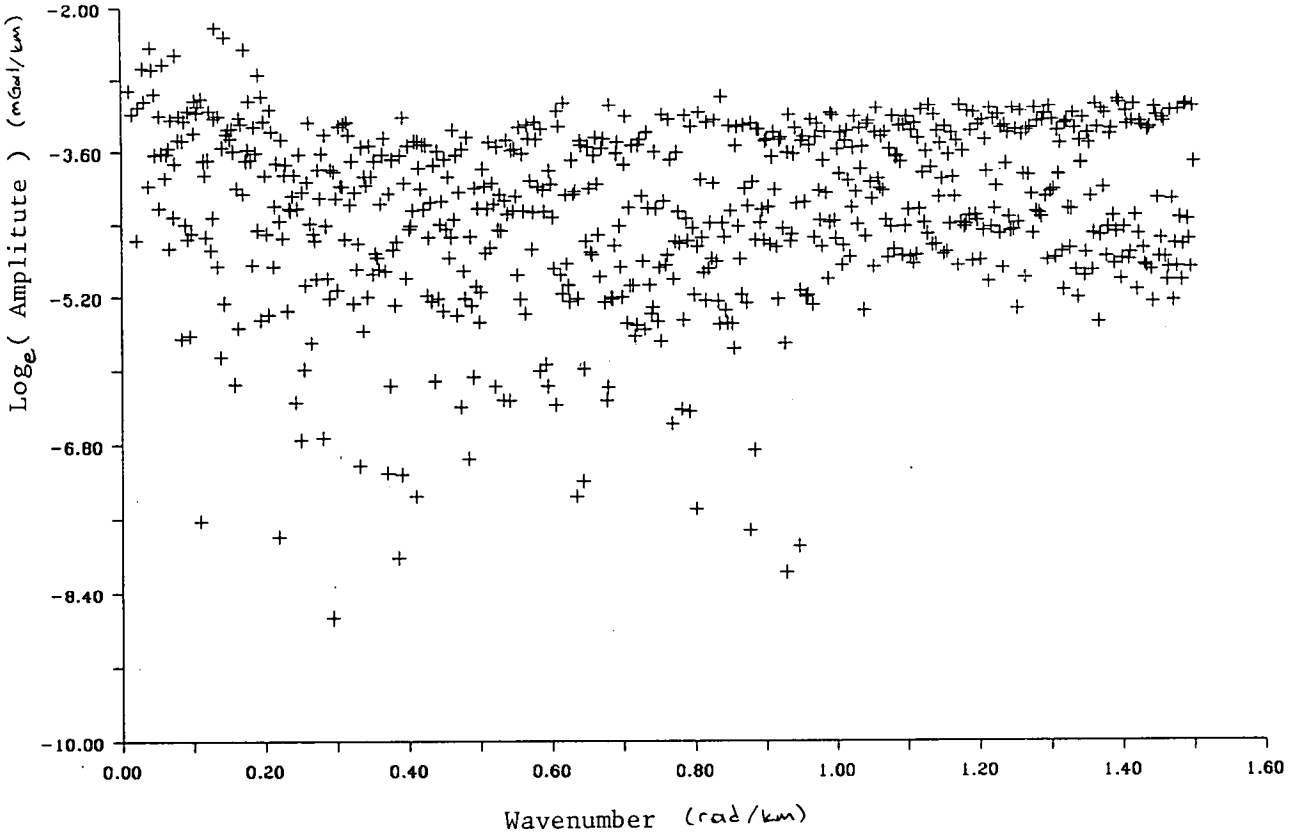

Figure 5.4 Isostatic response function estimated by azimuthal averaging

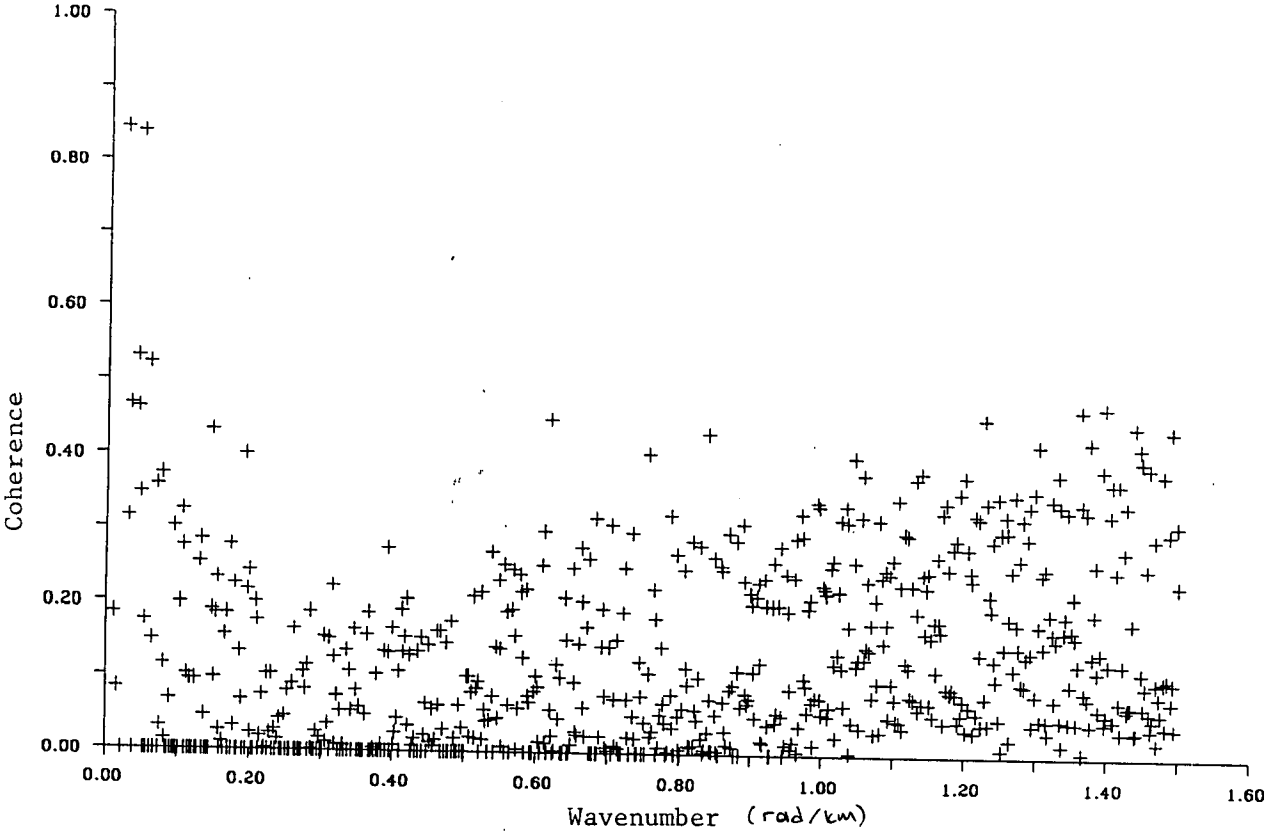

Figure 5.5 Coherence between the stripped Bouguer anomaly and the topography.

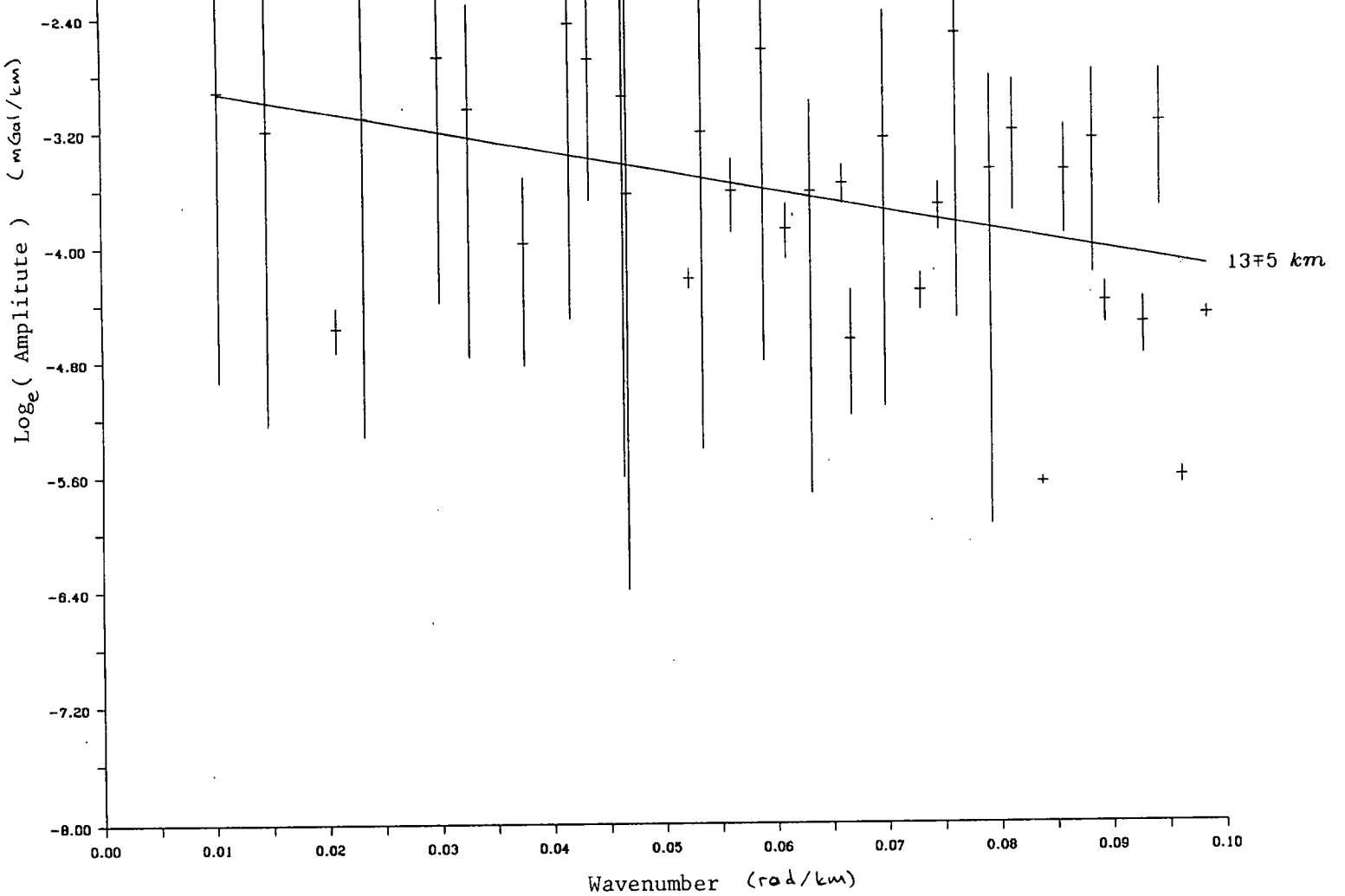

Figure 5.6 Isostatic response function estimated by azimuthal averaging: enlargement at the long wavelength.

appropriate to this waveband. This can be done by minimizing $|E|^2$ where

$$E=G_O(k)-RH(k)-G_G. \qquad 5.22$$

Least square estimates of R and G_G were computed in each of 1000 waveband intervals. Figure 5.7 shows the logarithm of the response function computed in this way R plotted against wavenumber. Fitting a straight line to long wavelength estimates gives a depth of compensation of 11±5 km; however the intercept corresponding to 2.28±0.52 g/cm^3 is now acceptably close to the topographic density.

This method of analysis also estimates G_G, the part of the gravity anomaly which does not correlate with the load. Figure 5.8 shows the logarithm of G_G plotted against wavenumber, so the spectral analysis described in section 3.4 can be repeated for this component of the anomaly. The result is essentially the same, again indicating a source at a depth of about 25±5 km.

The important conclusion is that the data are inherently capable of detecting a source at Moho depths, but that these sources are not correlated with the load, and the isostatic response function is estimated successfully. The density variations causing isostatic compensation lie at a depth of about 11–13 km, that is within the crust and not on the Moho. Moreover, the low signal to noise ratio shows that the compensating masses are only a very minor component of the crustal density distribution.

5.7 Compensation With Elastic Parameters

So far the analysis has assumed an Airy model for isostasy. When a non-zero flexural rigidity is included in the isostatic model, we would expect the Bouguer anomaly caused by loading of the topography to be smaller than with the simple

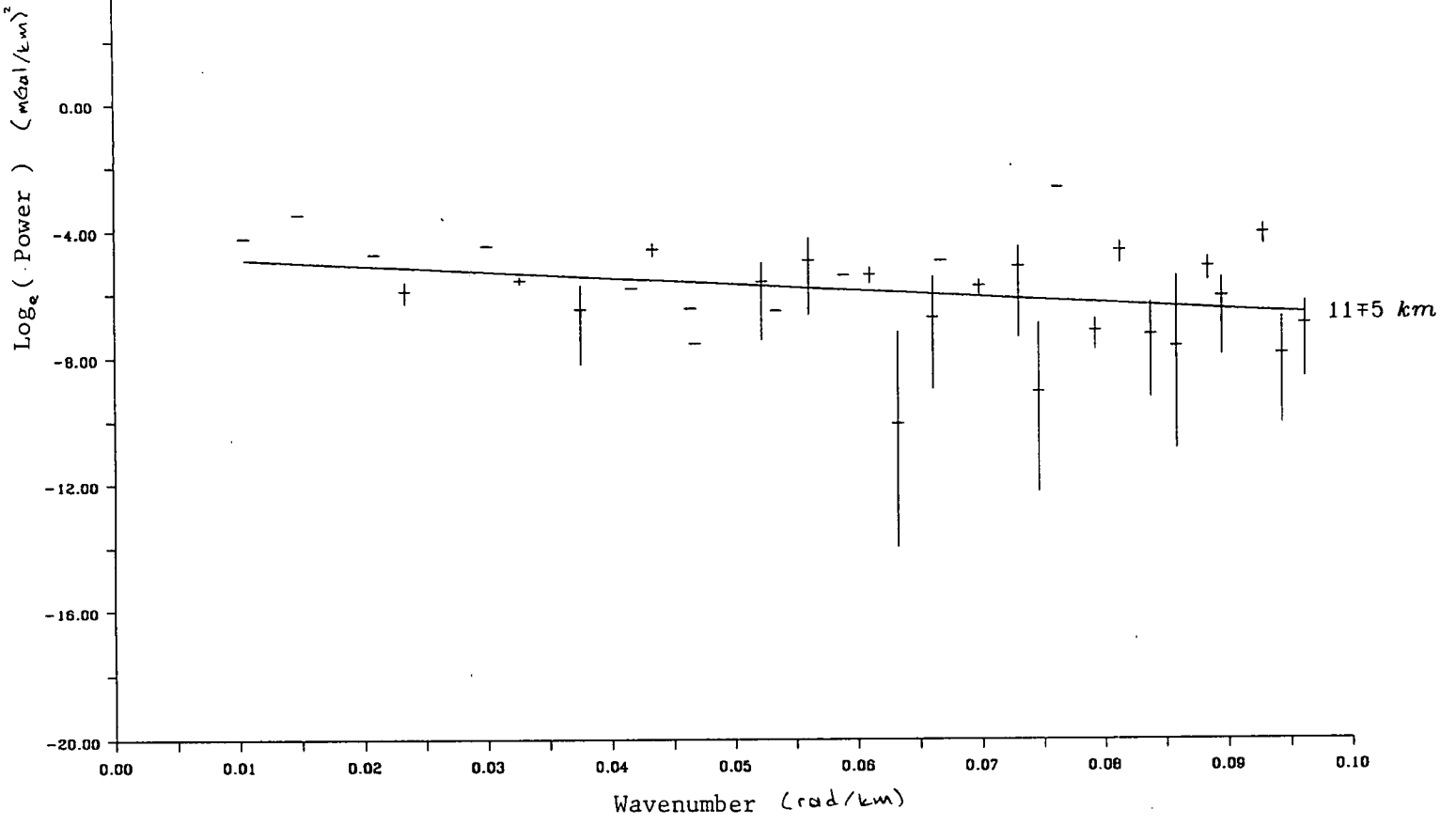

Figure 5.7 Isostatic response function by least squares regression analysis: enlargement at the long wavelength.

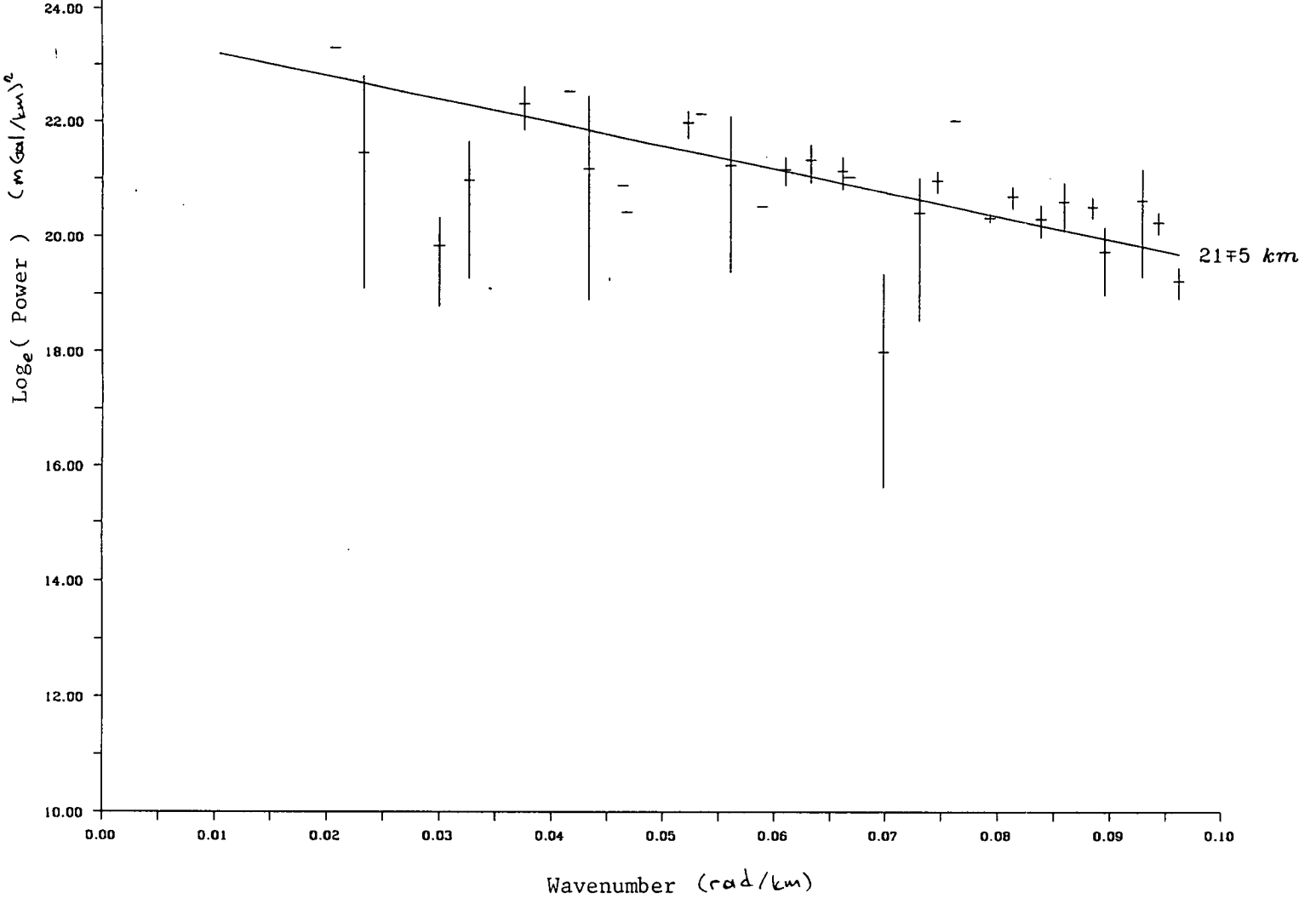

Figure 5.8 Spectrum of the stripped Bouguer anomaly which is not related to the load: enlargement at the long wavelength.

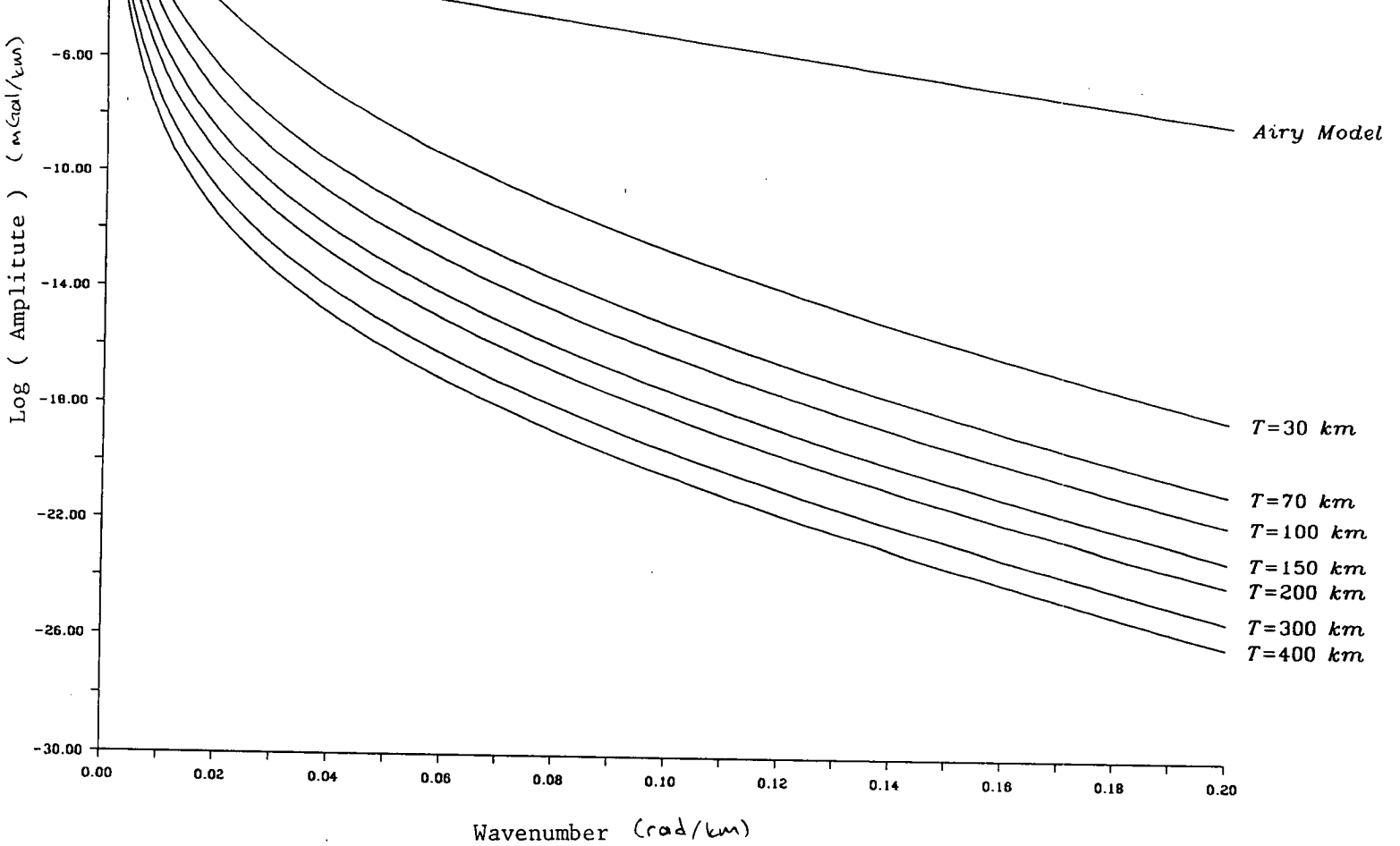

Figure 5.9 Theoretical isostatic response function for different elastic thickness. Compensation is at the Moho at a depth of 30 km.

Airy model. Figure 5.9 shows the theoretical isostatic response functions for the plate thickness of 30 km to 400 km, with the Moho at a depth of 30 km. It shows that every segment of the curves has a slope greater than or equal to the straight line corresponding to the Airy model. Thus, it is clear that, by assuming the Airy model, the depth of compensation may be overestimated, but never underestimated.

5.8 Conclusion

A compensation depth for the load effective topography of 11–13 km depth leads to two conclusions. First, all current models of mountain buildings involve depression of the Moho; such models are supported by seismic refraction of the Alps and the Himalayas, where the Moho depth may exceed 70 km. The observed shallow depth of compensation under a regime which has experienced both Caledonian and Variscan mountain building events leads to the conclusion that these roots have now disappeared, implying ductility in the lower crust. Secondly, the crust is capable of supporting the existing load effective topography.

CHAPTER 6

CONCLUSIONS AND DISCUSSION

6.1 Review

In chapter 3, the gravity anomaly spectrum showed source depths of 25-30 km and 11-12 km. In chapter 4 the magnetic anomaly spectrum showed a source at 14 km. 11-14 km depth may be the depth to the features generating both the gravity and magnetic anomalies. The depth to the lower crust in southern Britain is estimated between 11-22 km (Chadwick 1985a), so 11-14 km depth source may be at the top of the lower crust.

However, the significance of the 25-30 km depth source is less clear. The gravity anomaly is either from the Moho or from density variations in the lower crust. In chapter 5, the isostatic response function of southern Britain showed that no isostatic compensation is generated at Moho depths, leading to the conclusion that the Moho is unaffected by the present load.

6.2 Seismic Refraction Profiles

A seismic refraction profile from Waterford (southern Ireland) to Land's End indicates a flat Moho at a depth of 27-31 km, unaffected by sedimentary basins (Holder and Bott 1971). Preliminary analysis of the Lithospheric Profile of Britain (LISPB), line delta, from the coast of north Wales to the south coast of south-west England shows similar results, the Moho being flat at a depth of around 35 km (Edwards and Blundell 1988). Although it shows a decrease of around 8 km in the depth to the Moho at the southern end, this interpretation includes errors due to low velocity sediments (Edwards, personal communication). LISPB line gamma,

from Carlisle to Buxton, shows Moho depths of 30–35 km (Bamford et al, 1978).

On the filtered stripped Bouguer gravity anomaly map, the Waterford to Land's End profile is over the gravity high on the west of the map. The LISPB profile gamma is over the gravity low on the eastern side of the map. These regional gravity anomalies could be generated by shallower and deeper Moho respectively. The LISPB line delta crosses the gravity anomaly step and on the southern end it is over a gravity high. The preliminary seismic interpretation is again consistent with the shallower Moho to the south. This may be an indication that the 25–30 km anomalies are generated by Moho topography.

6.3 Seismic Reflection Profiles

The Southwest Approaches Traverse (SWAT) seismic reflection lines indicate the reflector patterns are different in the lower crust from the upper crust. Line drawings of SWAT line 3 from the coast of Lundy to the west coast of south Wales show that the upper crust is quiet with the exception of sedimentary basins, while the lower crust has a series of short reflectors (figure 6.1). The upper mantle, like the upper crust, shows a transparent zone.

The different patterns of reflectors in the crust are explained in terms of a change in the mechanical properties from brittle to ductile (Chadwick 1985a). The depth of the transition zone is estimated at 11–22 km. The same approach may be made to explain the pattern changes at Moho depths as being a transition from ductile to less ductile.

Two way travel times to the Moho show a flat reflector along the profiles. Warner (1987) argued that the arrival times from the Moho are generally not separately dependent on the thickness and the velocity structure of the crust, but that high and low velocity regions compensate each other. Under low velocity sedimentary

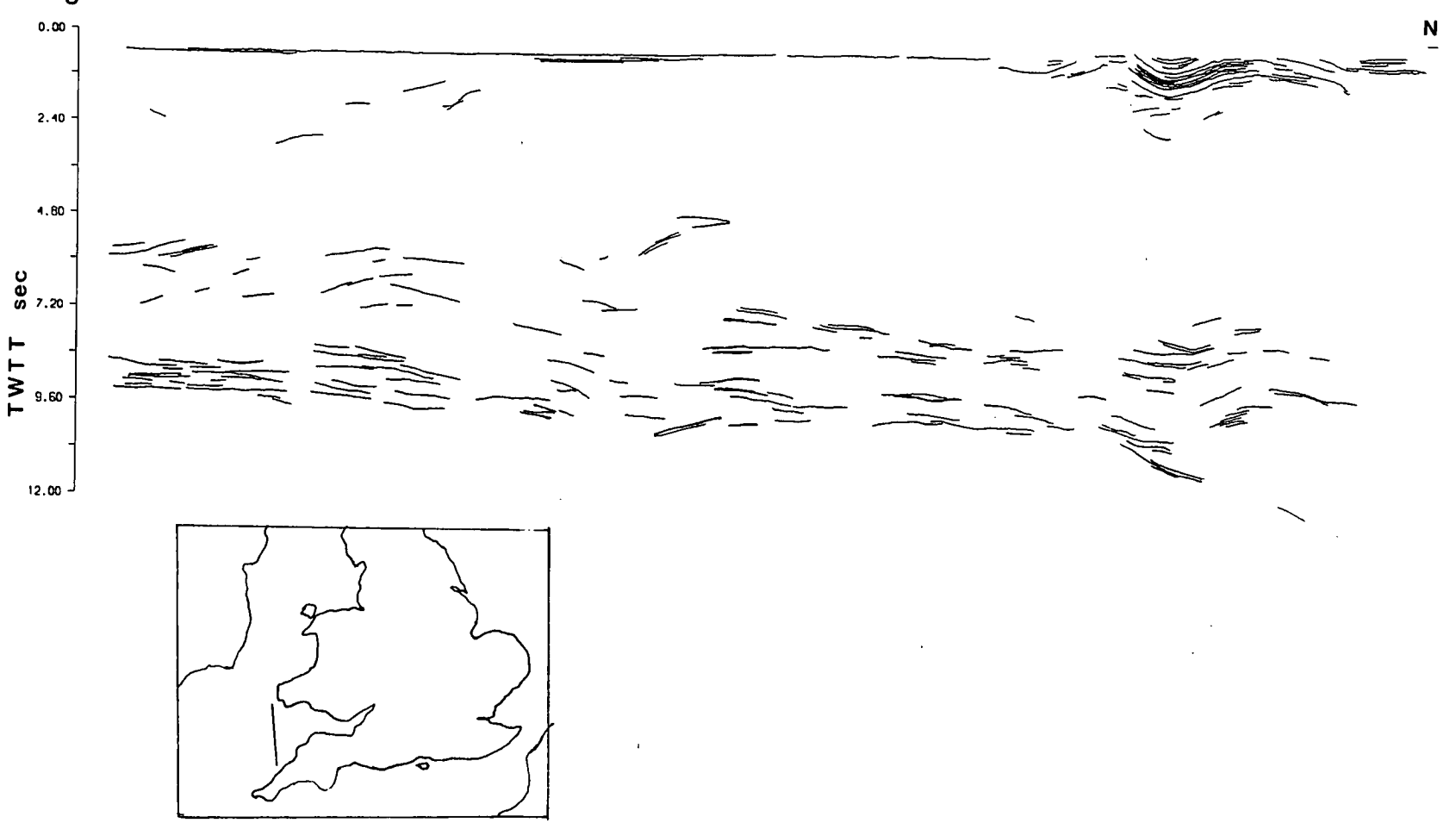

Figure 6.1 Line drawing of SWAT profile 3. Inset is the location profile.

basins, either the Moho is shallow or there is a high velocity layer in the lower crust. Time sections are misleading and must be converted to depth sections.

Determining the depth or the shape of the Moho needs precise estimation of velocities. Velocities can be estimated by refraction and wide-angle reflection experiments or by normal move-out on reflection profiles. These two methods run into problems in estimating the velocity structure of the lower crust. The problems are that there are not enough refraction experiments and they lack resolution and that conventional reflection equipment has too short a spread length to determine the move out of deep reflectors unless more than one ship is used.

The inability of current seismic reflection data to provide adequate control of the shape of the Moho is recognized by Sibuet et al (1988) in their interpretation of the BIRPS SWAT-WAM profile and by Holliger and Klemperer (1988) for BIRPS NSDP lines. Both identifies the upper crust from seismic data, and models the lower crust in response to the gravity data.

6.4 Ductility and Brittleness of the Crust

Studies over new mountain ranges reveal that the depression of the Moho under a load can push it down as deep as 70 km. The same kind of depression of the Moho must have happened during the Caledonian and Variscan orogenies, but since then the mountain roots have disappeared. The disappearance of the mountains roots may depend on temperature changes, as well as time.

For a sudden load, the crust is expected to act as a non-ductile material. This will then generate a depression on the Moho as observed under new mountain ranges. After a given time, buoyancy forces start pushing the Moho up. Depending upon the magnitude of the force, the temperature of the crust and the period of its

application, this may generate plastic flow in the ductile parts of the crust. The brittle part of the crust may be unaffected by this force.

The behaviour of the gravity anomaly then may be explained by having topography on the Moho which reflects the buoyancy or other forces in the Mantle. The load due to topography on the surface is either supported by the strength of the brittle crust or by density anomalies in the brittle crust. The load may cause the brittle crust to sink into the lower crust. The surface load is then transformed into lateral flow in the ductile crust and does not displace the Moho.

If the load is supported only by the strength of the brittle crust, then the isostatic response function will show no compensation. If there is a density contrast between the brittle and ductile crust, then the isostatic response function is expected to show the depth of the transition zone, provided that the load is compensated by brittle crust sinking into ductile crust. In this case the intercept of the response function should correspond to the topographic density. If the density corresponding to the intercept is less than the real value, then some part of the load is supported by the strength of the brittle crust.

The solutions to the isostatic response function indicate that some of the load is supported by the brittle crust, and some is compensated at the boundary of the upper brittle crust and the lower ductile crust.

6.5 Intrusions

The models above assume that the gravity anomaly source at 25–30 km depth is topography on the Moho. Although this source depth is close to the Moho depth estimated from seismic reflection profiles, it is not certain that this is the Moho. Moreover, the model assumes that after the initial load, the only forces acting on the Moho are generated in the Mantle. Under the influence of buoyancy forces,

the Moho will tend to flatten. If the time is long enough, then there can be no topography on the Moho. So the 25-30 km depth may well be in the lower crust.

If the intrusions from the Mantle into the crust take place, then they will generate a gravity anomaly providing that there is a density contrast between these materials and the crust, and that the intrusions are not homogeneous. Because these materials are hot, they will spread over the Moho, and because the lower crust is ductile, the upper crust is unaffected by them. Moreover subhorizontal reflectors may be related to this horizontal layer.

REFERENCES

Anderton, R., Bridges, P. H., Leeder, M. R. and Sellwood, B. W. (1979) A dynamic stratigraphy of the British Isles. George Allen & Unwin, London.

Anderton R. (1982) Dalradian deposition and the late Precambrian-Cambrian history of the N Atlantic region-a review of the early evolution of the Iapetus Ocean. J. Geol. Soc. Lond., **19**, 421-431.

Bacon, M. (1975) A gravity survey of the western English Channel between Lyme Bay and St Brieuc bay. Phil. Trans. R. Soc. Lond., **A279**, 68-78.

Badham, J. P. N. and Halls, C. (1975) Microplate tectonics, oblique collisions, and the evolution of the Hercynian orogenic systems. Geology, **3**, 373-376.

Badham, J. N. P. (1982) Strike-slip orogens - an explanation for the Hercynides J. Geol. Soc. Lond, **139**, 493-504.

Bamford, D., Nunn, K., Prodehl, C. and Jacob, B. (1978) LISPB-IV. Crustal structure of Northern Britain. Geoph. J. R. astr. Soc., **54**, 43-60

Banks, R. J., Parker, R. L. and Huestis, S. P. (1977) Isostatic compensation on a continental scale: local versus regional mechanism. Geoph. J. R. astr. Soc., **51**, 431-452.

Bennett, J. R. P. (1969) Geological surveys at the Alpey Barn borehole. Bull. Geol. Surv. **29**, 93-102.

Bott, M. H. P., Day, A. A., Masson-Smith, D. (1958) A geological interpretation of gravity and magnetic surveys in Devon and Cornwall. Phil. Trans. R. Soc. Lond., **A251**, 161-191

Brown, Sir M. (1985) Map 1: Pre-Permian Geology of the United Kingdom (South), British Geological Survey, Keyworth.

Brown, Sir M. (1985) Map 2: Coutours on the top of the Pre-Permian surface of the United Kingdom (South), British Geological Survey, Keyworth.

Bullerwell, W. (1961) Archerbeck borehole, Appendix D. Bull. Geol. Surv. **18**, 76-78.

Bullerwell, W. (1967) Ashton Park borehole, Appendix B Bull. Geol. Surv. **27**, 136-153.

Burley, A. J. (1971) Geophysical surveys in the Warlingham borehole. Bull. Geol. Surv. **36**, 112-121.

Burne, R. V. (1973) Paleogeography of south west England and Hercynian continental collision. Nature Lond., Phys. Sci., **241**, 129-131.

Burrett, C. F. (1972) Plate tectonics and the Hercynian orogeny. Nature, Lond. **239**, 155-157.

CALCOMP (1973) GPCP A General Purpose Contouring Program. California Computer Products, California.

Chadwick, R. A., Kenolty, N. and Whittaker, A. (1983) Crustal structures beneath southern England from deep seismic reflection profiles. J. Geol. Soc. Lond., **140**, 893-911.

Chadwick, R. A. (1985a) Permian, Mesozoic and Cenozoic structural evolution of England and Wales in relation to the principles of extension and inversion tectonics, in Atlas of onshore sedimentary basins in England and Wales, ed. Whittaker, A., Blackie, Glasgow.

Chadwick, R. A. (1985b) Seismic reflection investigations into the stratigraphy and structural evolution of the Worcester Basin. J. Geol. Soc. Lond., **142**, 187-202.

Chadwick, R. A. and Smith, N. J. P. (1988) Sort Paper: Evidence of negative structural inversion beneath central England from new seismic reflection data. J. Geol. Soc. Lond., **145**, 519-522.

Cocks, L. R. M. and Fortey, R. A. (1982) Faunal evidence for oceanic separations in the Palaeozoic of Britain. J. Geol. Soc. Lond., **139**, 445-478.

Cornwell, J. D. (1977) Geophysical Surveys, in Statigraphy of the Ashton borehole, Oxfordshire, appendix 4. Bull. Geol. Surv. **57**, 43-51.

Cornwell, J. D. (1978) Geophysical surveys at the Withycombe farm borehole. Bull. Geol. Surv. **68**, 33-42.

Day, G. A. (1986) The Hercynian evolution of the south west British continental margin. pp233-241 in Barazangi, M & Brown, L (eds), Reflection Seismology: The Continental Crust, Geodynamics Series, **14**, Amer. Geoph. Un.

Dewey, J. F. and Burke, K. C. A. (1973) Tibetan, Variscan and Precambrian basement reactivation: products of continental collision J. Geol. Chicago, **81**, 683-692.

Dewey, J. F. and Bird, J. M. (1970) Mountain belts and the new global tectonics. J. Geoph. Res. **75**, 2625-2647.

Dorman, L. M. and Lewis, T. R. (1970) Experimental Isostasy I. J. Geoph. Res. **75**, 3357-3365.

Edmonds, E. A., Wright, J. E., Beer, K. E., Williams, M. Freshney, E. C. and Fenning, P. J. (1968) Geology of the country around Okehampton. Institute of Geological Sciences, London.

Edwards, J. W. F. and Blundell, D. J. (1984) Summary of seismic refraction experiments in the English Channel, Celtic Sea and St George's Channel. British Geological Survey, Marine Geophysics report no. 144.

Floyd, P. A. (1972) Geochemical characteristics of spilitic greenstones from south-west England. Nature, Phys. Sci., **239**, 75-76.

Gudmundsson, G. (1967) Spectral analysis of magnetic surveys. Geoph. J. R. astr. Soc., **13**, 325-337.

Henderson, W. J. and Robertson, A. H. G. (1982) The Highland Border rocks and their relations to marginal basin development in the Scotish Caledonides. J. Geol. Soc. Lond., **139**, 433-452.

Hipkin, R. G. and Hussain, A. (1983) Regional gravity anomalies 1 Northern Britain. Inst. Geol. Sci., report 82/10

Hipkin, R. G., Lyness, D., Chacksfield, B. C., Reay, D. Gibbert, A. J. Turnbull, G. and Lumsden, G. I. (1986) Bouguer anomaly map of the British Isles: Southern Sheet. British Geological Survey, Nottingham.

Holder, A. P. and Bott, M. H. P. (1971) Crustal structure in the vicinity of south-west England. Geoph. J. R. astr. Soc., **23**, 465-489.

Holder, M. T. and Leveridge, B. E. (1986) Correlation of the Rhenohercynian Variscides. J. Geol. Soc. Lond., **143**, 141-147

Holliger, K. and Klemperer, S., L. (1988) A comparison of the Moho interpreted from gravity data and from deep seismic reflection data in the northern North Sea. Geoph. J. in press

Huestis, S. P. and Parker, R. L. (1979) Upward and downward continuation as inverse problems. Geoph. J. R. astr. Soc., **57**, 171-188.

Hughes J. G. (1981) The edwin user's guide. University of Edinburgh, Edinburgh.

Jennifer, M. A. (1974) Geophysical Surveys at the Spilmersford borehole east Lothian, Scotland. Bull. Geol. Surv. **45**, 63-72.

Johnson, G. A. L. (1973) Closing of the Carboniferous sea in western Europe, in Implications of Continental Drift to Earth Sciences, vol 2, Tarling, D and Runcorn, S. K. (eds) p:843-850, Academic Press. London & New York.

Karner, G. D. and Watts, A. B. (1983) Gravity anomalies and flexure of the lithosphere at mountain ranges. J. Geoph. Res. **88**, 10449-10447.

Karner, D. G., Weissel, K., Dewey J. F. and Munday, T. J. (1987) Geotectonic imaging of the north-western European continent and shelf. Marine and Petroleum Geology **4**, 94-102

Lee, A. G. (1988) Carboniferous basin configuration of central and northern England modelled using gravity data, in a synorogenic basin compex The upper Carboniferous of northwest Europe, eds Besley, B. M. and Kelling, G. Blackie, Glasgow

Leeder, M. R. (1982) Upper Palaeozic basins of the British Isles - Caledonide inheritance versus Hercynian plate margin processes. J. Geol. Soc. Lond. **139**, 479-491.

Lewis, T. R. and Dorman, L. M. (1970) Experimental isostasy II. J. Geoph. Res. **75**, 3367-3386.

Lewis, B. T. R. (1981) Isostasy, magma chambers and plate driving forces on the east Pacific rise. J. Geoph. Res. **86**, 4868-4880.

Love A. E. H. (1944) A treatise on the mathematical theory of elasticity. Dover Publications, New York.

Lovelock, P. E. R. (1977) Aquifer properties of Permo-Triassic sandstones in the United Kingdom. Bull. Geol. Surv., **56**, 1-49.

Lumsden, G. I., Goodlet, G. A. and Elliot, R. W. (1967) An investigation of a supposed Permian vent at Auchingee, Ayrshire. Bull. Geol. Surv., **26**, 167-191.

Matte, P. (1986) Tectonics and plate tectonics model for the Variscan belt of Europe. Tectonophysics, **126**, 329-374.

McKenzie, D. and Bowin, C. (1976) The relationship between bathymetry and gravity in the Atlantic ocean. J. Geoph. Res. **81**, 1903-1915.

Meissner, R. Matthews, D. and Wever T. (1987) The Moho in and around Great Britain. Annal. Geoph., **4**, 659-664.

Meissner, R. Waver, T. and Fluh, E. R. (1987) The Moho in Europe - Implications for Crustal development. Annal. Geoph., **5**, 357-364.

Munk, W. H., Cartwright, D. E. (1966) Tidal spectroscopy and prediction. Phil. Trans R. Soc. Lond., **A259**, 533-581.

Nicolas, A. (1972) Was the Hercynian orogenic belt of Europe of the Andean type. Nature, Lond., **236**, 221-223.

Pankhurst, R. J. (1974) Rb-Sr whole rock chronology of Caledonian events in NE Scotland. Bull. Geol. Soc. Amer., **85**, 345-350

Paranis, D. S. (1952) A study of rock densities in the English Midlands. Mon. Not. R. astr. Soc., Geoph. Suppl. **6**, 252–271.

Parker, R. L. (1972) Rapid calculation of potential anomalies. Geoph. J. R. astr. Soc., **31**, 447–455.

Phillips, W. E. A., Stillman, C. J. and Murphy, T. A. (1976) Caledonian plate tectonic model. J. Geol. Soc. Lond., **132**, 579–609.

Riding, R. (1974) Model of the Hercynian fold belt. Earth Planet. Sci. Let. **24**, 125–135.

Robinson, A. R. (1981) Least square regression analysis in term of linear algebra. Goose Pond Press, Houston.

Shuey, R. T., Schellinger, D. K., Tripp, A. C. and Alley, L. B. (1977) Curie depth determination from aeromagnetic spectra. Geoph. J. R. astr. Soc., **50**, 75–101.

Sibuet, J. C., Ondreas, H., Duval, M. and Dyment, J. (1988) Constraintes sur la structure crustale de la Manche at de mer Celtique a partir des donnees gravimetriques et des sondages sismiques profonds (SWAT et WAM) preprint to be published in the ECORS volume SWAT-WAM.

Smart, J. G. O., Sabine, P. A. and Bullerwell, W. (1964) The geological survey exploratory borehole at Canvey Island, Essex. Bull. Geol. Surv., **21**, 1–36.

Smith, I. F. and McCann, D. M. (1978) Geophysical investigations in Bryn – Teg borehole, North Wales, appendix 2. Bull. Geol. Surv., **61**, 37–45.

Stoneley, R. (1982) The structural development of Wessex basin. J. Geol. Soc. Lond., **139**, 543–554.

Stubblefield, J. (1965) Aeromagnetic map of Great Britain sheet 2 England & Wales. Ordnance Survey, Surrey.

Talwani, M., Worzel, J. L., Landisman, M. (1959) Rapid gravity computations for two-dimensional bodies with application to the Mendocino sub marine fracture zone. J. Geoph. Res., **64**, 49–59

Talwani, M. and Ewing, M. (1960) Rapid computation of gravitational attraction of three – dimensional bodies of arbitrary shape. Geophysics, **25**, 203–225.

Walcott, R. I. (1970) Flexural rigidity, thickness and viscosity of the Lithosphere. J. Geoph. Res. **75**, 3941–3954.

Warner, M. R. (1987) Seismic reflections from the Moho-the effect of isostasy. Geoph. J. R. astr. Soc., **88**, 425-435

Whittaker, A. (ed) (1985) Atlas of onshore sedimentary basins in England and Wales. Blackie, Glasgow.

Windley, B. F. (1986) The Evolving Continents. John Wiley & Sons, New York.

APPENDIX 1

General Purpose Contouring Program (GPCP)

The GPCP computer program interpolates irregular data points on to a regular grid, and displays them by means of contour map. For drawing purposes, previously interpolated grid values can be given in order to prevent heavy recomputation.

For interpolation, N neighbouring data points are chosen. A tangent plane at a data point is generated in such a way that the plane passes through the function value and the angle between the plane and vectors drawn from the N neighbouring data points are minimized (figure A1). The angles are weighted depending upon the distance.

After the generation of the tangent planes for every data point, N neighbouring data points are chosen around each grid point for the final interpolation. The grid point value is obtained as a weighted average of the values predicted by the N neighbouring tangent planes, weighted according to the distance (figure A2).

The the evaluation of the grid values, each grid is subdivided into smaller grids. The lines are drawn between the subgrids to form a contour display of the data.

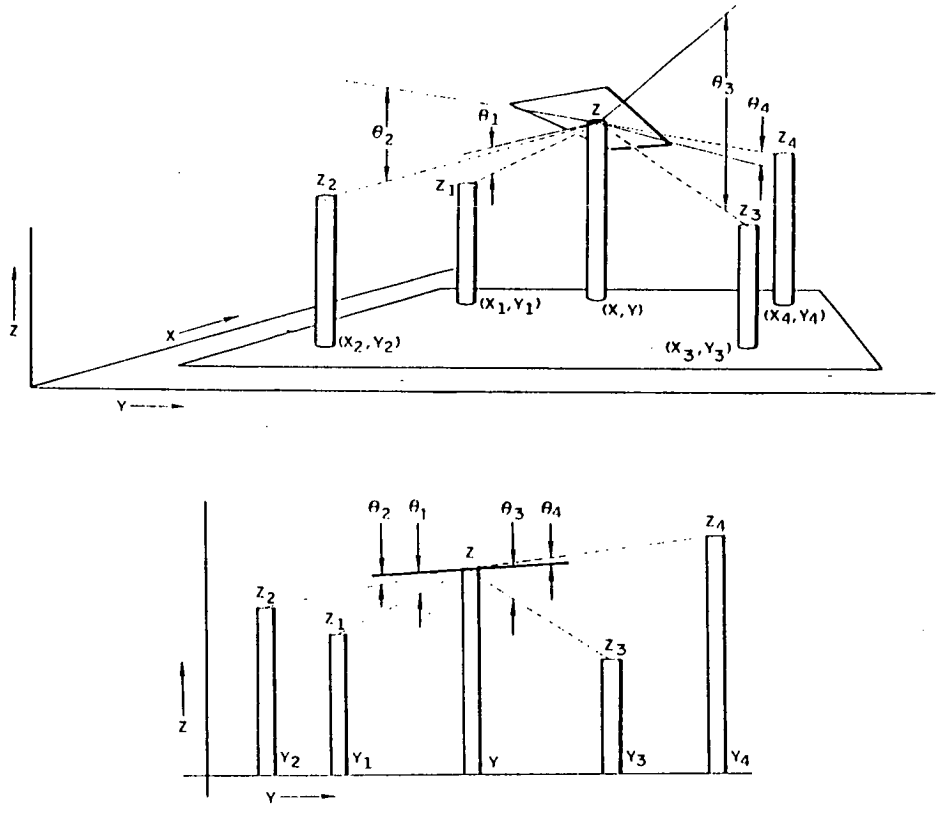

Figure A1 Gradient (Tangent plane) approximation for data point (X,Y).

(from CALCOMP, 1973)

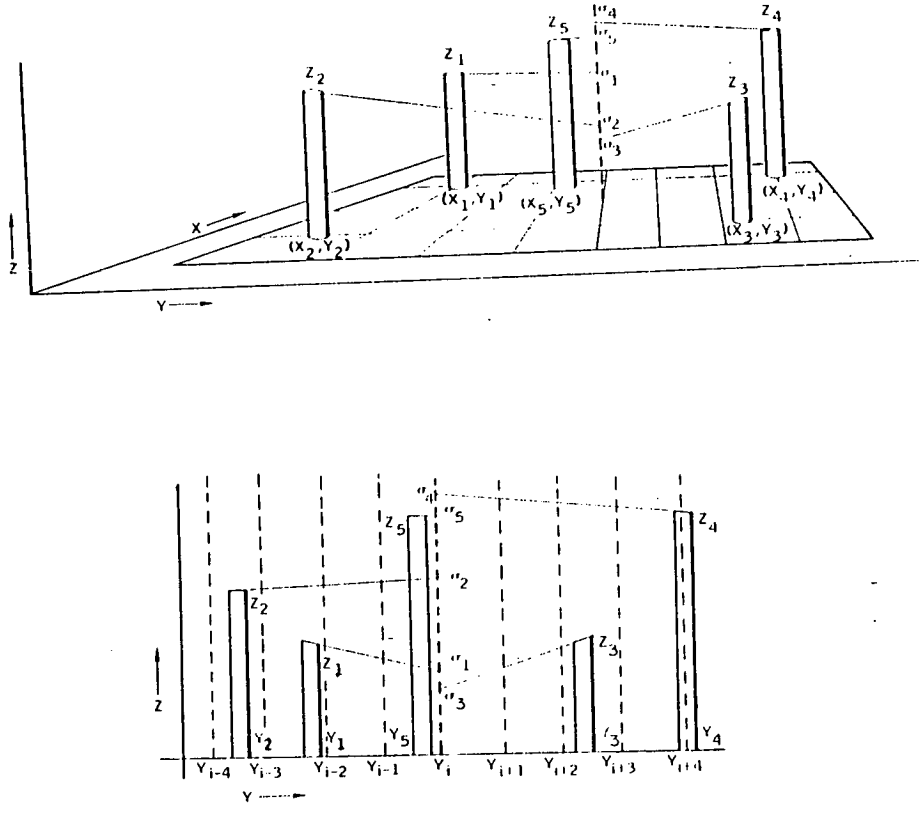

Figure A2 Grid point approximation. (from CALCOMP, 1973)

APPENDIX 2

Table 1

Solutions to regression analysis of the Bouguer anomaly. The first parameter is 10 km square name, the second is the estimated density, the third is the error in estimation, the forth is the number of observations, the fifth is the standard error in fitting the surface to the Bouguer anomaly, and the last is the corresponding age code on the Geological Map of Southern Britain at a scale of 1:625000. The first code is the dominant feature. Brackets are used for very minor constituents. Numbers separated by "-" sign corresponds to a sequence.

NY 2	2.6423	0.0306	58	0.4181	82-83+(68+80+81+84)
NY 3	2.6162	0.0464	47	0.4289	82-83+(89+81+80+68+84)
NY12	2.7940	0.0062	69	0.3591	68
NY19	2.7174	0.0151	38	0.4430	72+(85)
NY29	2.6880	0.0136	37	0.2307	72+(73)
NY39	2.7324	0.0071	34	0.2387	72+73
NY40	2.7658	0.0080	53	0.4027	74+44+48
NY53	2.4168	0.0407	72	0.4891	85+89+(87)
NY61	2.5000	0.0203	59	0.3374	80+85
NY67	2.3802	0.0405	17	0.1785	80
NY68	2.4337	0.0068	21	0.1524	80
NY69	2.4836	0.0120	27	0.3369	80
NY70	2.5878	0.0116	92	0.3992	80+74+(85-89)
NY75	2.5497	0.0129	26	0.2485	81+(80+82-83)
NY76	2.5831	0.0163	55	0.3139	81+80,35
NY77	2.6299	0.0371	21	0.2344	80
NY78	2.5585	0.0390	35	0.2564	80
NY79	2.4681	0.0163	26	0.3538	80
NY80	2.5985	0.0119	88	0.4088	81+80
NY84	2.5199	0.0248	17	0.2618	81+(80)
NY87	2.5746	0.0125	33	0.1764	80,35
NY88	2.5835	0.0193	47	0.3388	80
NY89	2.5208	0.0223	40	0.2774	80
NY91	2.6659	0.0273	10	0.1753	81+(80)
NY93	2.4681	0.0244	22	0.4656	81+80
NY94	2.5989	0.0165	22	0.1986	81+(80+82-83)
NY95	2.6322	0.0336	30	0.4274	81+82-83
NY96	2.6616	0.0186	40	0.3155	81+(82-83+80)
NY97	2.5496	0.0193	37	0.2286	80+(81),35
NY98	2.5914	0.0189	43	0.2010	80,35
NY99	2.5927	0.0176	38	0.2689	80
NZ 0	2.4610	0.0249	24	0.2934	81+80
NZ 1	2.6579	0.0209	19	0.1540	81+80
NZ 2	2.4780	0.0168	19	0.1332	81+82-83
NZ 4	2.5337	0.0160	18	0.2069	81+82-83
NZ 5	2.6899	0.0287	36	0.4568	81+82-83
NZ 6	2.5300	0.0275	31	0.3200	81+82-83
NZ 7	2.5725	0.0239	28	0.1519	81+82-83
NZ 8	2.7173	0.0208	65	0.2168	81+80,35
NZ 9	2.5934	0.0234	19	0.1608	80+81,35

NZ10	2.5501	0.0087	61	0.2228	80+81
NZ11	2.7244	0.0246	14	0.1023	81+86+80
NZ12	2.8593	0.0493	21	0.3640	82-83+81+86
NZ14	2.4630	0.0429	20	0.4614	82-83
NZ15	2.5341	0.0340	22	0.4260	82-83
NZ17	2.1981	0.0446	26	0.2033	81+82-83
NZ18	2.5797	0.0260	64	0.1996	81+82-83
NZ19	2.6144	0.0292	44	0.2821	81+(82-83)
NZ20	2.7018	0.0312	49	0.2557	89+81+80+86+87
NZ22	2.5824	0.0528	14	0.2569	86+(82-83+81)
NZ23	2.6345	0.0340	23	0.2238	82-83+86
NZ24	2.7406	0.0473	22	0.3693	82-83
NZ25	2.4830	0.0394	31	0.4578	82-83
NZ26	2.5713	0.0599	34	0.4566	82-83
NZ28	2.5606	0.0498	65	0.2833	82-83
NZ29	2.5103	0.0443	40	0.2220	82-83
NZ30	2.3759	0.0874	47	0.2776	89+90+(87)
NZ31	2.2516	0.0913	49	0.3293	89+87+(86)
NZ32	2.5036	0.0711	68	0.4052	86+87+81+(89)
NZ33	2.4729	0.0392	103	0.4440	86+82-83
NZ34	2.5236	0.0819	15	0.4099	86+82-83
NZ35	2.5830	0.0590	22	0.2747	86+82-83
NZ37	2.4396	0.0652	16	0.1964	82-83,sea
NZ40	2.3183	0.0354	54	0.2527	90+89+(92-95)
NZ41	2.4677	0.0538	59	0.3543	89+90+(87)
NZ42	1.8699	0.0365	95	0.3315	89+90+87+(86)
NZ44	1.9265	0.0388	14	0.2116	sea+86
NZ50	2.5053	0.0215	58	0.3906	90+91+92-95
NZ51	2.5420	0.0208	59	0.3135	91+90+(92-5)
NZ60	2.4241	0.0116	70	0.3753	92-95
NZ61	2.4838	0.0112	76	0.2828	92-95+(91+96-99)
NZ62	2.6837	0.0146	23	0.0886	sea+91+(92-93)
NZ70	2.4179	0.0105	71	0.3043	94-95+(92-93)
NZ71	2.5241	0.0150	87	0.3305	94-95+97-99+92-93
NZ80	2.4926	0.0099	124	0.3355	94-95+91-93
NZ81	2.4597	0.0151	46	0.2252	sea+95-95+93
NZ90	2.5131	0.0101	125	0.2538	94-95+91-93
SC38	2.6945	0.0265	48	0.8190	64-66
SC39	2.6570	0.0256	40	0.4139	SEA+64-66
SC49	2.6789	0.0161	40	0.4159	SEA+64-66+80

SD38	2.7486	0.0091	72	0.2318	74+(80)
SD39	2.6917	0.0119	75	0.3551	74+(70-73)
SD45	3.0694	0.0632	117	0.4432	sea+81+89
SD48	2.6811	0.0192	73	0.4168	80+74
SD49	2.7058	0.0097	76	0.2129	74+(80)
SD50	2.4990	0.0236	52	0.2442	82+(81+83-87)
SD51	2.5713	0.0611	39	0.2963	82+89+(81+87)
SD55	2.5580	0.0293	60	0.4976	81
SD56	2.5239	0.0148	64	0.3377	81+(80)
SD58	2.6814	0.0101	97	0.2727	74+80
SD59	2.7559	0.0104	68	0.2839	74+(80)
SD60	2.4423	0.0223	55	0.2816	82+(83-87)
SD61	2.5663	0.0190	47	0.2852	81+82
SD62	2.6206	0.0215	30	0.2110	81+82
SD63	2.6896	0.0267	53	0.4564	81+(82)
SD66	2.5483	0.0150	60	0.3720	81
SD69	2.7273	0.0057	60	0.2899	74+(80+70-73)
SD70	2.5919	0.0469	73	0.4248	82+(83-84)
SD71	2.6092	0.0105	80	0.2388	82+81
SD72	2.5908	0.0153	70	0.3301	82+(81)
SD75	2.5459	0.0205	71	0.3497	80+(81)
SD81	2.5689	0.0116	75	0.3496	82+81
SD82	2.6797	0.0198	62	0.4336	82+81
SD83	2.6937	0.0152	74	0.3110	82+(81)
SD85	2.7856	0.0405	71	0.3663	80
SD86	2.5943	0.0097	98	0.4429	80+81+73+74
SD89	2.6442	0.0157	53	0.4814	80+81
SD90	2.5559	0.0230	80	0.4745	82+81+(83-85)
SD91	2.6917	0.0151	50	0.3952	81+82
SD93	2.5274	0.0278	38	0.3569	81+(82)
SD99	2.5860	0.0115	62	0.4682	80+81
SE 1	2.7005	0.0196	68	0.4589	81+(82)
SE 2	2.5268	0.0115	74	0.3659	81+(82)
SE 3	2.5751	0.0078	80	0.2210	81+82
SE 4	2.5730	0.0089	75	0.2605	81
SE 6	2.6019	0.0131	56	0.4286	81+80
SE 7	2.5919	0.0152	54	0.5051	80+(81)
SE 8	2.6043	0.0077	104	0.3720	80+81
SE 9	2.6128	0.0099	76	0.3320	81+80
SE10	2.5351	0.0130	61	0.3115	81+82

SE11	2.5743	0.0197	76	0.4006 82+81
SE12	2.6144	0.0108	75	0.2371 82
SE13	2.5700	0.0090	88	0.2310 82+(81)
SE14	2.5314	0.0082	70	0.2025 81
SE15	2.5911	0.0253	63	0.3472 81
SE16	2.5495	0.0149	70	0.4351 81
SE17	2.5527	0.0092	56	0.2471 81
SE18	2.5093	0.0125	21	0.1015 81+80
SE19	2.5500	0.0139	78	0.2557 81
SE20	2.5272	0.0156	77	0.3705 82
SE21	2.4980	0.0174	71	0.3451 82
SE22	2.5875	0.0128	80	0.1968 82
SE23	2.5510	0.0155	61	0.2181 82+81
SE24	2.4566	0.0202	63	0.3405 81+(82)
SE25	2.5781	0.0268	78	0.4789 81+(80)
SE26	2.6087	0.0247	81	0.4439 81+86
SE27	2.5286	0.0166	103	0.3694 81+86+82
SE28	2.7078	0.0349	91	0.4645 86+81+87+89
SE30	2.4971	0.0163	71	0.2295 82+(83)
SE31	2.4966	0.0227	77	0.2562 82+83
SE32	2.6465	0.0184	72	0.1940 82+(83)
SE33	2.4255	0.0195	74	0.2534 82+(81+86)
SE34	2.4232	0.0315	76	0.3951 81+(86)
SE35	2.6725	0.0428	69	0.4199 81+86+87+89
SE39	2.6403	0.0496	49	0.2595 89+90+(91)
SE40	2.5191	0.0248	69	0.2295 83+(82+86)
SE41	2.4706	0.0298	68	0.2070 83+(86)
SE42	2.5615	0.0383	72	0.2542 83+82+86+(87)
SE43	2.4726	0.0236	73	0.2114 86+(82+87)
SE48	2.4820	0.0193	92	0.2823 90+91+(92-97)
SE49	2.2865	0.0098	66	0.3288 91+94-95+(92+93+97-99)
SE50	2.3856	0.0282	68	0.2382 86+89+(87)
SE57	2.4007	0.0259	81	0.4107 91-99 fault
SE58	2.3807	0.0158	74	0.3638 98+(97+94-95)
SE59	2.4581	0.0183	52	0.3797 94-95+(91-93)
SE67	2.4572	0.0269	75	0.3742 94-99
SE68	2.5759	0.0164	71	0.3226 97+98-99
SE69	2.3971	0.0086	67	0.2505 94-95+(91-93)
SE75	2.2993	0.0353	97	0.2657 90+(89+91)
SE76	2.2511	0.0226	82	0.3348 90-98

SE77	2.4761	0.0405	83	0.3089	98-99
SE78	2.4324	0.0149	80	0.2503	98-99
SE79	2.4765	0.0101	56	0.2236	94-95+(92+93+96+97)
SE81	2.4976	0.0402	71	0.3179	90+(91)
SE84	2.3398	0.0170	103	0.3154	90+106+(91)
SE85	2.2746	0.0159	89	0.3523	106+(90+91)
SE86	2.2930	0.0151	85	0.3246	106+98-99
SE87	2.2249	0.0134	84	0.2135	98-99+(106)
SE88	2.3372	0.0102	76	0.2520	98-99+(97)
SE89	2.3923	0.0322	48	0.3974	94-95+96-98
SE90	2.2744	0.0270	76	0.1708	94+91+97+(92-93+95-97)
SE91	2.3301	0.0268	60	0.1683	94+97+98-99+106+(91-93+95-96)
SE93	2.4918	0.0232	88	0.3294	106+(91-99)
SE94	2.4077	0.0264	95	0.3502	106
SE95	2.5892	0.0390	84	0.5178	106
SE96	2.3386	0.0225	75	0.2491	106
SE97	2.4850	0.0148	100	0.3158	106+98-99+(102-105)
SE98	2.3757	0.0122	85	0.2622	98-99+(96-97)
SE99	2.3619	0.0249	70	0.4134	94-95+(96-98)
SJ 0	2.7244	0.0095	45	0.1759	73-74+72+(71)
SJ 1	2.7941	0.0153	45	0.2391	73-74+72+71
SJ 5	2.7292	0.0132	67	0.4288	73+74
SJ10	2.7453	0.0130	62	0.2719	73-74
SJ11	2.7523	0.0141	59	0.2820	70-74
SJ14	2.7499	0.0108	72	0.3606	73-74
SJ17	2.7763	0.0143	121	0.4149	80+74+81+82
SJ55	1.8554	0.0329	81	0.2671	90+89
SJ68	2.1553	0.0335	99	0.3463	90+89
SJ76	2.5234	0.0533	72	0.2491	91
SJ82	2.4053	0.0407	88	0.2736	90+(89)
SJ83	2.3583	0.0409	86	0.4145	90+89+(84)
SJ84	2.6268	0.0385	92	0.3874	84+(89+82)
SJ91	2.1928	0.0247	90	0.4069	89+90
SJ94	2.6734	0.0244	92	0.3697	82+83+81+(89+90)
SJ95	2.6531	0.0298	78	0.4864	81+82+(89)
SJ99	2.6650	0.0253	72	0.4649	82+81+83+(87)
SK 2	2.3170	0.0449	95	0.3750	90+89
SK 7	2.5589	0.0187	81	0.4579	81+80+82+53
SK 8	2.5313	0.0146	54	0.3384	81+82+80
SK 9	2.4791	0.0131	47	0.3152	81

SK12	2.5308	0.0222	89	0.2123	90
SK17	2.6630	0.0188	73	0.3636	80+81+53+35
SK18	2.5312	0.0205	45	0.4829	81+80
SK19	2.5801	0.0352	14	0.3207	81
SK24	2.3491	0.0326	79	0.4093	89+81+80+90
SK27	2.5780	0.0171	67	0.4705	81+82+80
SK28	2.5231	0.0130	49	0.2924	81+82
SK29	2.5922	0.0198	27	0.3268	81+82
SK34	2.5274	0.0236	93	0.3320	81+82+80
SK36	2.5608	0.0128	74	0.3210	82+81
SK37	2.5306	0.0150	74	0.3470	82
SK38	2.5204	0.0209	72	0.4223	82+81
SK39	2.5626	0.0162	63	0.3050	82
SK43	2.3068	0.0422	90	0.4457	90+82+89
SK45	2.4415	0.0441	55	0.2952	82+80
SK46	2.4053	0.0388	10	0.0775	82+80+83
SK47	2.4694	0.0180	15	0.1074	82+80+83
SK48	2.4556	0.0237	20	0.1694	82+83
SK49	2.5824	0.0334	49	0.3046	83+82
SK54	2.1166	0.0372	100	0.4318	89+90+86+87+82
SK55	2.1309	0.0221	32	0.1646	89+86+87
SK59	2.4986	0.0211	50	0.2343	86+83+89+87
SK60	2.3535	0.0134	89	0.1728	91+90
SK62	2.3992	0.0260	100	0.3000	91+92+90
SK63	2.4186	0.0198	72	0.1456	90+91
SK64	2.4955	0.0249	92	0.3122	90
SK70	2.0246	0.0426	89	0.4100	93+92+91
SK71	2.2347	0.0306	93	0.4409	91+92+93
SK72	2.3437	0.0235	86	0.3083	91+92+93
SK73	2.5231	0.0336	103	0.2806	91+90+92
SK93	2.0918	0.0483	110	0.4843	94+95+92+96+97
SK94	2.2769	0.0221	62	0.1875	94+91+92+93
SK95	2.0834	0.0130	41	0.1129	91+94+92+93
SK96	2.1429	0.0467	74	0.4375	91+94+92+93
SK97	2.1337	0.0302	87	0.2752	91+94+92+93
SK98	2.3271	0.0492	93	0.3551	94+91+95+92+93+96
SK99	2.2717	0.0304	85	0.1816	94+91+92+95+93+97+96
SN 0	2.8314	0.0583	87	0.5612	82+80+81+78+41
SN 1	2.5733	0.0337	75	0.3952	72+82+70-1+81+76
SN 2	2.8060	0.0259	70	0.5992	68+35+46

SN 3	2.7445	0.0210	74	0.8208	68+35+46
SN10	2.6585	0.0321	60	0.3787	82+81+80+SEA
SN11	2.8461	0.0327	80	0.5408	68+76+72+69
SN12	2.8219	0.0228	66	0.4136	68+35+70-1
SN13	2.8839	0.0295	104	0.8892	68+70-1+46+69+35
SN14	2.7503	0.0357	62	0.6630	70-1+SEA
SN20	2.4639	0.0393	16	0.4085	SEA+76+80
SN21	2.6952	0.0178	76	0.3295	68+76+70-1+72
SN22	2.7391	0.0249	65	0.4440	70-1+69+68
SN23	2.7681	0.0217	69	0.4350	70-1
SN24	2.8582	0.0249	68	0.4099	70-1
SN25	2.6844	0.0173	17	0.1689	SEA+70-1
SN30	2.6356	0.0229	15	0.1912	SEA+76+83+82+81+80
SN31	2.6836	0.0252	89	0.4047	68+76+70-1
SN32	2.6775	0.0256	69	0.5313	70-1+72
SN33	2.7692	0.0097	74	0.2673	70-1
SN34	2.7352	0.0163	79	0.3976	70-1+72
SN35	2.7942	0.0144	55	0.2754	72+SEA+70-1
SN40	2.5392	0.0203	71	0.4320	83+82+81+76+80
SN41	2.7283	0.0192	78	0.3380	76+68+82+81+80
SN42	2.7043	0.0237	90	0.6993	70-1+72+68
SN43	2.7074	0.0142	79	0.3376	72+70-1
SN44	2.7870	0.0162	78	0.3656	70-1+72
SN45	2.7754	0.0141	77	0.3664	72
SN46	2.8102	0.0244	22	0.2802	SEA+72
SN50	2.6539	0.0100	64	0.2239	83
SN51	2.7193	0.0227	84	0.4410	82+76+83+80+81
SN52	2.7642	0.0120	71	0.3571	70-1+68
SN53	2.7217	0.0076	69	0.2391	72+70-1
SN54	2.7980	0.0133	82	0.3705	72
SN55	2.8412	0.0180	71	0.3791	72
SN56	2.7385	0.0125	72	0.3338	72+SEA
SN57	2.7180	0.0193	37	0.2531	SEA+72
SN60	2.6446	0.0099	52	0.2670	83
SN61	2.6521	0.0167	77	0.5242	82+76+83+81+80
SN62	2.7473	0.0120	91	0.3485	70-1+69+76
SN63	2.7603	0.0138	69	0.3020	70-1+72
SN64	2.7602	0.0096	65	0.2494	72
SN65	2.7621	0.0104	53	0.3189	72
SN66	2.7324	0.0178	77	0.3207	72

SN67	2.7669	0.0149	80	0.3565 72
SN68	2.7515	0.0145	59	0.3387 72
SN69	2.6510	0.0274	35	0.4032 72+71+SEA
SN70	2.6964	0.0117	67	0.3543 83
SN71	2.5819	0.0114	58	0.5141 82+81+83+80+78
SN72	2.6664	0.0088	74	0.3762 76+73+72+74+70-1
SN73	2.7743	0.0167	76	0.3567 70-1+72+73
SN74	2.7993	0.0139	49	0.4809 72+70-1
SN75	2.7049	0.0191	36	0.3356 72
SN76	2.7483	0.0119	50	0.4060 72
SN77	2.8283	0.0111	51	0.2875 72
SN78	2.7829	0.0186	53	0.3257 72+71
SN79	2.7109	0.0080	40	0.3099 72+71
SN80	2.6809	0.0109	45	0.4680 83+82
SN81	2.7214	0.0088	68	0.3813 82+81+80+75+78
SN82	2.6690	0.0101	60	0.3357 75
SN83	2.6933	0.0091	53	0.2760 75+72+70-1+73+74
SN84	2.7323	0.0098	61	0.3368 70-1+73+72+46
SN85	2.7821	0.0150	45	0.4814 72+70-1
SN86	2.7788	0.0166	49	0.3998 72+71
SN87	2.7945	0.0104	53	0.2935 72
SN88	2.8942	0.0426	26	0.4120 72+71
SN89	2.8629	0.0115	18	0.2420 72+71+73
SN90	2.6266	0.0072	81	0.3093 83+82+81+80
SN91	2.6825	0.0112	73	0.3855 80+75+78+81
SN92	2.7278	0.0064	76	0.2769 75
SN93	2.7096	0.0115	60	0.2486 75+74
SN94	2.6586	0.0093	41	0.2485 75+70-1+74+73
SN95	2.7642	0.0089	57	0.3063 70-1+72+73
SN96	2.7658	0.0150	54	0.4475 72+70-1
SN97	2.8330	0.0173	57	0.4367 72
SN98	2.7973	0.0148	60	0.3463 72+71
SN99	2.7578	0.0111	45	0.3287 72+73-4
SO 0	2.6230	0.0078	85	0.3074 83+82+80+81
SO 1	2.6915	0.0078	58	0.3065 75+80+78
SO 2	2.6814	0.0047	65	0.2960 75
SO 3	2.7444	0.0138	58	0.3000 75+74
SO 4	2.7067	0.0076	53	0.2521 74+75
SO 6	2.7873	0.0216	64	0.4014 70-1+72
SO 7	2.8149	0.0160	43	0.2875 72+73-4+70-1

SO 8	2.7707	0.0069	45	0.2319	73-4+72
SO 9	2.8277	0.0175	61	0.4684	73-4+72
SO10	2.5671	0.0136	71	0.3882	83+82
SO11	2.6923	0.0087	47	0.2959	75+82+81+80
SO12	2.6833	0.0103	64	0.3066	75
SO13	2.6931	0.0105	65	0.2902	75
SO14	2.6823	0.0124	55	0.3729	74+75
SO15	2.7004	0.0135	45	0.2948	74+73-4
SO16	2.8023	0.0124	55	0.3932	73-4+74
SO17	2.7097	0.0168	52	0.3602	74+73-4
SO18	2.7226	0.0106	61	0.2836	74+76+73-3
SO19	2.7360	0.0136	66	0.2393	73-4
SO20	2.5865	0.0102	60	0.3476	83+82+81+80+75
SO21	2.6619	0.0081	54	0.3938	75+82+81+80+78
SO23	2.6815	0.0102	54	0.4153	75
SO24	2.7226	0.0144	53	0.4157	75
SO26	2.7289	0.0117	53	0.3254	74+73+76
SO27	2.7424	0.0129	44	0.2483	74+76
SO28	2.7244	0.0078	57	0.1948	74+76
SO29	2.7413	0.0223	55	0.3623	73-4+70+68
SO30	2.5887	0.0244	63	0.2749	75+73+74
SO31	2.6296	0.0161	66	0.2773	75
SO32	2.6420	0.0221	56	0.3801	75
SO33	2.6425	0.0166	74	0.3824	75
SO39	2.6456	0.0168	68	0.4297	60+73-4+46+35
SO40	2.6295	0.0102	63	0.2173	75
SO41	2.5778	0.0208	67	0.3506	75
SO42	2.5770	0.0141	60	0.3043	75
SO43	2.4072	0.0298	68	0.2687	75
SO44	2.6089	0.0204	70	0.2666	75
SO47	2.7217	0.0131	77	0.2443	74+75+73+66
SO48	2.6781	0.0330	80	0.4856	73+74+70+66+72
SO52	2.5941	0.0138	128	0.1865	75
SO53	2.6189	0.0167	140	0.3384	75+72+73
SO55	2.6105	0.0105	150	0.2828	75
SO56	2.5305	0.0088	154	0.2055	75
SO57	2.5637	0.0097	145	0.3657	75+74+82
SO60	2.7265	0.0453	95	0.8623	83+75+80+90
SO62	2.4612	0.0171	124	0.3039	75+74+73
SO63	2.5678	0.0118	127	0.2605	75+74

SO64	2.5052	0.0229	121	0.3165	75
SO65	2.5989	0.0267	103	0.3675	75
SO69	2.5102	0.0199	126	0.4263	75+84+74+66
SO80	2.2597	0.0151	83	0.4287	95+94+93+92
SO81	2.2424	0.0247	34	0.2085	91+94+93+92
SO90	2.3642	0.0237	89	0.3066	95+94+93
SP 0	2.3367	0.0171	112	0.1922	95
SP 1	2.3170	0.0225	66	0.2736	95+94+93
SP 2	2.3277	0.0182	59	0.2908	94+95+93+91+92
SP 3	2.2460	0.0169	69	0.4022	91+94+93+92
SP 6	2.4340	0.0450	72	0.4554	90
SP10	2.3950	0.0225	105	0.1859	95+96+97
SP11	2.2115	0.0428	88	0.4248	95+94+91+93+92
SP13	2.2384	0.0214	62	0.4466	94+91+93+92
SP15	2.4417	0.0498	121	0.4368	90+91
SP16	2.2857	0.0473	62	0.3434	90
SP20	2.3894	0.0306	105	0.2743	97+95+96
SP21	2.2993	0.0131	117	0.1903	95+91+92+93+94
SP22	2.1932	0.0120	137	0.2129	91+95+94+93+92
SP23	2.1614	0.0224	116	0.3472	91+92+93+94+95
SP24	2.0875	0.0233	106	0.2724	91+90+92
SP26	1.9319	0.0463	95	0.4364	90+84+89
SP31	2.3062	0.0192	114	0.2066	95+97+96+91+92+93+94
SP32	2.3211	0.0127	193	0.2504	95+93+92
SP33	2.1797	0.0178	146	0.2988	95+92+93+94
SP34	2.2456	0.0134	156	0.2875	91+92+93
SP35	2.3875	0.0254	106	0.2069	91+90
SP36	2.1687	0.0438	64	0.2287	90+91+89
SP40	2.0739	0.0265	98	0.2551	97+98+99
SP41	2.2817	0.0286	89	0.2105	97+95+96
SP42	2.2695	0.0178	156	0.2136	95+93+96+92
SP43	2.1980	0.0453	135	0.4088	93+91+92
SP44	2.2839	0.0236	148	0.3000	91+92
SP45	2.4208	0.0393	82	0.3555	91+92
SP50	2.0811	0.0235	89	0.2108	99+97+98+100
SP51	2.2896	0.0324	137	0.3206	97+96+98
SP52	2.1024	0.0283	125	0.2458	95+96+97
SP53	2.3446	0.0458	91	0.3117	95+93+94
SP56	2.2941	0.0312	78	0.3011	91+92+93
SP60	2.1528	0.0356	66	0.1569	105+99+98+97+100+104

SP61	2.1075	0.0158	120	0.2257	97+99+98
SP64	2.3768	0.0475	58	0.2677	95+93+94
SP69	2.2833	0.0326	77	0.2303	91+92
SP70	2.2116	0.0229	80	0.1689	105+106+100+99
SP71	2.1119	0.0304	126	0.2728	99+100+97+98
SP72	2.2187	0.0454	80	0.3125	97+99+98
SP73	2.5152	0.0427	73	0.3112	97+95+96
SP74	2.2660	0.0437	66	0.2574	95+93+94
SP75	2.2771	0.0381	75	0.2978	95+93+94
SP77	2.3203	0.0306	80	0.2772	93+94
SP78	2.1877	0.0391	93	0.3866	93+91+92+94
SP79	2.2879	0.0211	95	0.2988	91+92+93
SP80	2.0299	0.0164	63	0.2560	106+105
SP81	2.0770	0.0204	77	0.2367	105+99+106+100
SP86	2.1172	0.0391	66	0.3323	93+94+95
SP87	2.3881	0.0334	86	0.3204	94+95+93
SP90	2.0606	0.0206	68	0.2308	106
SP91	1.9833	0.0163	97	0.2416	106+105
SP93	2.1459	0.0493	72	0.5144	98-9+97+105
TA 0	2.1606	0.0281	70	0.2052	98-99+106+96
TA 1	2.2854	0.0186	82	0.1523	106+98-99
TA 2	2.3358	0.0308	58	0.1889	106
TA 6	2.3899	0.0170	93	0.2741	106
TA 7	2.4471	0.0147	158	0.2936	106+(98-105)
TA 8	2.2638	0.0234	106	0.2413	98-99+(94-97)
TA10	2.3412	0.0145	97	0.1892	106+(98-99)
TA20	2.3123	0.0396	48	0.2235	106
TF 3	2.3877	0.0410	100	0.3614	97+96+94
TF 4	2.2679	0.0213	89	0.1794	97+94+96+95
TF17	2.2005	0.0301	86	0.1246	98-99
TF18	2.0599	0.0175	84	0.2237	98-99+102-105+106
TF19	2.2509	0.0129	87	0.2116	106
TF26	2.2952	0.0300	89	0.2525	98-99
TF27	2.1517	0.0177	99	0.2249	98-99+102-105
TF28	2.2557	0.0173	97	0.1702	106+102-105
TF29	2.2179	0.0133	87	0.1549	106
TF36	2.1362	0.0159	89	0.2230	98-99+102-105
TF37	2.1575	0.0156	54	0.1576	106+102-105
TF38	2.4399	0.0140	54	0.1278	106+102-105
TF46	2.1901	0.0286	88	0.1752	102-105+98-99+106

TF47	2.3669	0.0146	35	0.1215	106
TF70	2.2392	0.0433	77	0.2075	106
TF71	1.9809	0.0404	75	0.3344	106+102-105+105
TF72	2.0898	0.0231	80	0.2047	106+105
TF73	1.9942	0.0475	82	0.2798	106
TF74	2.0645	0.0279	37	0.1530	106+sea
TF83	2.1641	0.0473	105	0.2942	106
TF84	1.9518	0.0262	41	0.1170	106+sea
TF93	2.1621	0.0309	78	0.1956	106
TF94	2.1506	0.0246	33	0.0759	106+sea
TG 3	2.0451	0.0354	75	0.2201	106
TG13	2.0055	0.0451	71	0.3181	115+106
TG22	1.9143	0.0480	77	0.1453	115+106
TM 5	2.1783	0.0383	75	0.2442	106+115
TM11	2.1739	0.0490	48	0.1041	108+sea
TM14	1.9437	0.0374	73	0.1878	108+115+107+106
TM15	2.0885	0.0397	74	0.2200	106+107+115
TM19	2.1252	0.0449	75	0.1859	106
TM24	1.9997	0.0443	71	0.1404	115+108

Table 2

Hand sampled densities. The first parameter is depth of the layer in meters, the second is saturated density, the third is age, and fourth is the lithology.

Keys

S: Schlumberger F.D.C. Density Log

E.G.U.: Engineering Geology Unit (B.G.S)

WELL SPILMERSFORD [345, 669] Jennifer, 1974

253	2.50		Silt
263	2.55		Shale
281	2.60		Sand
292	2.45		Sand
296	2.32		Sand
328	2.30		Sand
425	2.54		Sand
437	2.59		Tuff
439	2.52		Tuff
440	2.47		Tuff
515	2.45		Anglomera
517	2.48		Tuff
817	2.75		Basalt
1097	2.45		Silt
1208	2.50		Silt
1231	2.75		Basalt

WELL WARLINGHAM [534, 157] Burley, 1971

434	2.56		Sand
463	2.23	Cretaceous	Sand
482	2.24	Cretaceous	Shale
757	2.45	Cretaceous	Silt
887	2.47	Jurassic	Limestone+Clay
922	2.37	Jurassic	Clay
934	2.46	Jurassic	Limestone
964	2.23	Jurassic	Sand
1091	2.32	Jurassic	Clay
1376	2.40	Jurassic	Limestone
1387	2.32	Jurassic	Limestone
1426	2.40	Jurassic	Limestone
1433	2.51	Jurassic	Limestone
1604	2.52	Jurassic	Limestone
1663	2.57	Jurassic	Sand
1735	2.62	Jurassic	Limestone
1769	2.12	Jurassic	Silt+Clay
1771	2.13	Jurassic	Silt+Clay
1900	2.45	Jurassic	Silt+Clay
1901	2.41	Jurassic	Silt+Clay

1919	2.38	Jurassic	Silt+Clay
2063	2.72	Carboniferous	Limestone
2075	2.71	Carboniferous	Limestone
2078	2.72	Carboniferous	Limestone
2030	2.66	Carboniferous	Limestone
2113	2.79	Carboniferous	Limestone
2170	2.72	Carboniferous	Silt
2194	2.44	Carboniferous	Shale+Silt
2215	2.61	Carboniferous	Limestone

WELL STRAT A1 [484, 152] S

668	2.22	Cretaceous	Sand
736	2.15	Cretaceous	Silt+Clay
1218	2.55	Jurassic	Limestone

WELL TRUNCH [629, 334] S

77	1.80	Cretaceous	Limestone
105	1.92	Cretaceous	Limestone
178	2.00	Cretaceous	Limestone
345	2.05	Cretaceous	Limestone
562	2.10	Cretaceous	Limestone
692	2.15	Cretaceous	Chalk
767	2.20	Cretaceous	Limestone

WELL MIDDLENTON-1 [497, 101] S

1281	2.40	Jurassic	Shale+Limestone+Silt
1398	2.35	Jurassic	Shale
1448	2.45	Jurassic	Silt
1499	2.60	Jurassic	Limestone
1588	2.40	Jurassic	Shale
1634	2.50	Jurassic	Limestone+Silt
1713	2.60	Jurassic	Shale
1788	2.25	Jurassic	Sand
1864	2.64	Jurassic	Limestone
1939	2.64	Jurassic	Limestone
2140	2.65	Triassic	Silt+Sand
2653	2.75	Carboniferous	Silt+Sand

WELL PETROCKSTON [252, 110] S

66	2.15	Palaeogene	Clay+Silt

242	2.25	Palaeogene	Clay+Silt
425	2.31	Palaeogene	Clay+Silt
695	2.30	Palaeogene	Clay+Silt
1008	2.64	Carboniferous	Silt+Sand

WELL BLETCHINGLEY3 [532,148] S

314	2.40	Cretaceous	Silt+Clay
447	2.30	Cretaceous	Clay
569	2.35	Cretaceous	Silt
647	2.30	Jurassic	Clay+Silt
745	2.50	Jurassic	Limestone
846	2.50	Jurassic	Sand
1071	2.50	Jurassic	Clay+Limestone
1393	2.65	Jurassic	Limestone
1494	2.55	Jurassic	Clay
1638	2.65	Jurassic	Clay
1715	2.55	Jurassic	Chalk+Limestone

WELL BLETCHINGLEY2 [535,147] S

341	2.35	Cretaceous	Silt+Clay
539	2.25	Jurassic	Clay+Silt
696	2.50	Jurassic	Limestone
809	2.45	Jurassic	Sand
993	2.50	Jurassic	Limestone+Silt+Clay
1276	2.50	Jurassic	Limestone+Silt+Clay
1467	2.63	Jurassic	Clay+Shale
1498	2.35	Jurassic	Silt
1520	2.64	Jurassic	Limestone+Silt+Clay
1563	2.40	Jurassic	Silt

WELL BLETCHINGLEY1 [536,147] S

533	2.10	Jurassic	Silt
609	2.25	Jurassic	Marl
654	2.30	Jurassic	Clay+Shale
717	2.45	Jurassic	Clay+Limestone
767	2.60	Jurassic	Shale
798	2.40	Jurassic	Sand+Shale
824	2.50	Jurassic	Sand
847	2.45	Jurassic	Shale
867	2.55	Jurassic	Sand

885	2.40	Jurassic	Shale
909	2.50	Jurassic	Sand
963	2.45	Jurassic	Shale
1055	2.61	Jurassic	Limestone
1118	2.40	Jurassic	Shale+Limestone
1220	2.40	Jurassic	Silt+Limestone
1310	2.35	Jurassic	Silt
1432	2.20	Jurassic	Silt+Sand
1493	2.55	Jurassic	Sand+Shale
1543	2.55	Jurassic	Limestone+Silt
1593	2.15	Jurassic	Silt+Limestone
1661	2.68	Jurassic	Limestone
1755	2.40	Jurassic	Limestone
1860	2.50	Jurassic	Sand
1892	2.70	Jurassic	Limestone
1949	2.70	Jurassic	Limestone+Shale
2039	2.65	Jurassic	Limestone
2211	2.60	Jurassic	Sand+Silt
2325	2.70	Jurassic	Limestone
2492	2.65	Jurassic	Limestone

WELL MOCHRAS [255,3251 S

55	2.43	Quarternary	Clay
100	2.20	Quarternary	Clay+Silt
175	2.16	Tertiary	Silt+Clay+Sand
250	2.18	Tertiary	Silt+Clay
325	2.18	Tertiary	Clay+Silt
400	2.22	Tertiary	Silt+Clay
475	2.24	Tertiary	Silt+Clay
550	2.27	Tertiary	Clay+Silt+Sand
625	2.31	Tertiary	Silt+Clay
700	2.30	Tertiary	Silt
775	2.32	Tertiary	Silt
850	2.35	Jurassic	Silt
925	2.49	Jurassic	Clay
1334	2.57	Jurassic	Clay
1375	2.57	Jurassic	Clay
1450	2.56	Jurassic	Silt
1525	2.54	Jurassic	Clay+Silt
1600	2.56	Jurassic	Clay+Silt

1675	2.58	Jurassic	Silt
1777	2.63	Jurassic	Clay
1825	2.66	Jurassic	Silt+Clay
1900	2.59	Jurassic	Silt+Clay
1957	2.48	Jurassic	Clay

WELL LULWORTH [382,80] E.G.U. -92

56	2.09	Cretaceous	Chalk
70	2.18	Cretaceous	Chalk
122	2.16	Cretaceous	Chalk
230	2.34	Cretaceous	Chalk
260	2.15	Cretaceous	Chalk

WELL SHERSTON [384,185] E.G.U. -4

4	2.41	Jurassic	Limestone
5	2.59	Jurassic	Limestone
8	2.31	Jurassic	Limestone
13	2.42	Jurassic	Limestone
20	2.45	Jurassic	Limestone
98	2.50	Jurassic	Limestone
100	2.60	Jurassic	Limestone
122	2.33	Jurassic	Limestone
130	2.59	Jurassic	Limestone
139	2.54	Jurassic	Limestone
145	2.32	Jurassic	Limestone
148	2.39	Jurassic	Limestone
151	2.53	Jurassic	Limestone

WELL YATE [370,185] E.G.U. -4

32	2.56	Carboniferous	Gridstone
33	2.33	Carboniferous	Gridstone
35	2.62	Carboniferous	Gridstone
47	2.67	Carboniferous	Gridstone
64	2.60	Carboniferous	Gridstone
71	2.58	Carboniferous	Gridstone
73	2.61	Carboniferous	Gridstone
88	2.62	Carboniferous	Gridstone
90	2.60	Carboniferous	Gridstone
121	2.70	Carboniferous	Gridstone
126	2.60	Carboniferous	Gridstone

132	2.51	Carboniferous	Grit stone
144	2.65	Carboniferous	Grit stone
145	2.63	Carboniferous	Grit stone
151	2.59	Carboniferous	Grit stone
196	2.63	Carboniferous	Grit stone

WELL WITHYCOMBE [443,240] E.G.U. - 69

117	2.32	Jurassic	Clay
481	2.21	Triassic	Sand
556	2.48	Carboniferous	Sand
580	2.46	Carboniferous	Sand
672	2.50	Carboniferous	Clay
715	2.50	Carboniferous	Sand
912	2.51	Carboniferous	Sand
1056	2.36	Carboniferous	Sand
1225	2.50	Carboniferous	Sand

WELL MERTHYR A [308,214] E.G.U. -110

6	2.63	Carboniferous	Clay
18	2.70	Carboniferous	Clay
27	2.55	Carboniferous	Limestone+Sand
30	2.67	Devonian	Sand
48	2.68	Devonian	Sand
61	2.70	Devonian	Silt
76	2.65	Devonian	Sand
94	2.68	Devonian	Silt
105	2.65	Devonian	Sand+Marl
111	2.64	Devonian	Marl
117	2.67	Devonian	Sand

WELL MERTHYR B [298,214] E.G.U. - 110

3	2.70	Carboniferous	Limestone
15	2.71	Carboniferous	Ooilite
31	2.63	Carboniferous	Sand
46	2.67	Devonian	Sand
52	2.68	Devonian	Clay+Conglomerate
61	2.65	Devonian	Silt
76	2.66	Devonian	Sand
97	2.60	Devonian	Sand
108	2.68	Devonian	Clay

120	2.67	Devonian	Clay+Silt
127	2.68	Devonian	Cornstone
129	2.69	Devonian	Clay
133	2.67	Devonian	Sand

WELL MERTHYR C [298,213] E.G.U. - 110

9	2.78	Carboniferous	Limestone
30	2.70	Carboniferous	Clay
43	2.68	Carboniferous	Clay+Limestone
60	2.67	Carboniferous	Ooilite+Sand
72	2.75	Carboniferous	Sand
82	2.68	Devonian	Sand
88	2.68	Devonian	Sand
103	2.67	Devonian	Silt
118	2.64	Devonian	Sand+Clay
129	2.68	Devonian	Sand
138	2.61	Devonian	Sand
156	2.71	Devonian	Clay

WELL EYAM [420,376] E.G.U. - 72

270	2.71	Carboniferous	Limestone
343	2.70	Carboniferous	Limestone
352	2.71	Carboniferous	Limestone
993	2.69	Carboniferous	Limestone
1353	2.70	Carboniferous	Limestone
2469	2.81	Carboniferous	Dolamite
2481	2.72	Carboniferous	Dolamite
2728	2.73	Ordovician	Clay

WELL WREKIN [362,308] E.G.U. - 43

48	2.20	Triassic	Sand
60	2.22	Triassic	Sand
97	2.38	Triassic	Sand
112	2.39	Carboniferous	Sand
129	2.47	Carboniferous	Sand
141	2.48	Carboniferous	Sand
175	2.62	Carboniferous	Silt
198	2.59	Carboniferous	Silt
228	2.54	Pre-Cambrian	Tuff

WELL RAYDALE [390,464] E.G.U. - 45

49	2.68	Carboniferous	Limestone
169	2.69	Carboniferous	Limestone
317	2.72	Carboniferous	Limestone
399	2.70	Carboniferous	Limestone
489	2.82	Carboniferous	Limestone
558	2.73	Carboniferous	Limestone
630	2.71	Carboniferous	Clay+Limestone
723	2.85	Carboniferous	Limestone
802	2.58	Silurian	Granite

WELL KIELDER-TUN. [401,538] E.G.U. - 36

116	2.70	Carboniferous	Limestone
139	2.96	Carboniferous	Limestone
141	2.58	Carboniferous	Sand
168	2.54	Carboniferous	Sand

WELL AYRSHIRE-1 [257,612] Lumsden at al, 1967

4	2.62	Basanite
10	2.85	Basanite
15	2.61	Basanite
28	2.61	Basanite
34	2.50	Agglomerate
39	2.57	Agglomerate
54	2.52	Sand
75	2.59	Sand

WELL AYRSHIRE-2 [257,611] Lumsden at al, 1967

7	2.39	Sand
15	2.37	Sand
34	2.31	Sand
37	2.41	Sand
37	2.21	Sand
39	1.97	Sand
64	2.54	Tuff
129	2.55	Tuff

WELL ASHTON Bullerwell, 1967

205	2.56	Clay+Sand
247	2.59	Sand

306	2.45	Sand
406	2.62	Clay+Silt
522	2.57	Sand
528	2.94	Sand+Clay
565	2.64	Clay
774	2.61	Sand
789	2.64	Clay+Silt
798	2.70	Limestone
822	2.67	Limestone
873	2.69	Limestone
882	2.67	Limestone
891	2.68	Limestone

WELL CANVEY ISLAND [582,183] Smart at al, 1964

622	2.65	Clay
625	2.54	Clay
720	2.59	Silt
729	2.67	Clay
738	2.40	Sand
781	2.66	Clay+Silt

WELL ARCHERBECK [341,578] Bullerwell, 1961

93	2.66	Sand
160	2.65	Sand
163	2.54	Silt+Sand
177	2.71	Sand
261	2.67	Sand
285	2.76	Limestone

WELL APLEY BARN [434,210] Bennett, 1969

544	2.58	Carboniferous
801	2.71	Carboniferous
873	2.62	Carboniferous
927	2.71	Carboniferous
1744	2.70	Carboniferous
1872	2.69	Devonian
1906	2.74	Devonian
2056	2.70	Devonian
2187	2.70	Devonian
2218	2.72	Devonian

Table 3

FDC density logs. The first two parameters are the top and bottom of the unit, the third is average density in the 100 feet range, the fourth is error in estimating the density, the fifth is the age, the sixth is the lithology.

WELL 110/02-01

2900	3000	2.55 0.30	Triassic	Shale+Silt
3000	3100	2.20 0.10	Triassic	Salt+Silt
3100	3200	2.25 0.10	Triassic	Salt+Silt
3100	3200	2.70 0.10	Triassic	Salt+Silt
3200	3300	2.50 0.20	Triassic	Sand
3300	3400	2.45 0.10	Triassic	Sand
3400	3500	2.40 0.10	Triassic	Sand
3500	3600	2.45 0.10	Triassic	Sand
3600	3700	2.50 0.10	Triassic	Sand
3700	3800	2.45 0.10	Triassic	Sand
3800	3900	2.40 0.15	Triassic	Sand
3900	4000	2.45 0.05	Triassic	Sand
4000	4100	2.40 0.05	Triassic	Sand

WELL 106/28-01

9400	9500	2.65 0.05	Jurassic	Shale
9500	9600	2.65 0.05	Jurassic	Shale
9600	9700	2.60 0.20	Jurassic	Shale
9700	9800	2.50 0.20	Jurassic	Shale+Sand
9800	9900	2.50 0.20	Jurassic	Shale+Sand
9900	10000	2.60 0.20	Jurassic	Shale+Sand

WELL 106/24-2B

1700	1800	2.20 0.10	Palaeogene	Clay
1800	1900	2.15 0.10	Palaeogene	Clay
1900	2000	2.22 0.10	Palaeogene	Clay
2000	2100	2.27 0.10	Palaeogene	Clay
2100	2200	2.20 0.15	Palaeogene	Clay
2200	2300	2.25 0.15	Palaeogene	Clay
2300	2400	2.15 0.10	Palaeogene	Clay+Coal
2400	2500	2.25 0.10	Palaeogene	Clay+Sand
2500	2600	2.25 0.05	Palaeogene	Clay+Sand
2600	2700	2.25 0.10	Palaeogene	Clay+Coal+Sand
2700	2800	2.27 0.15	Palaeogene	Sand+Clay
2800	2900	2.32 0.15	Jurassic	Clay+Sand
2900	3000	2.30 0.10	Jurassic	Clay+Sand
3000	3100	2.32 0.10	Jurassic	Sand+Clay
3100	3200	2.30 0.20	Jurassic	Clay+Sand

3200	3300	2.27	0.20	Jurassic	Clay
3300	3400	2.30	0.20	Jurassic	Clay+Sand
3900	4000	2.35	0.10	Jurassic	Clay
4000	4100	2.32	0.20	Jurassic	Clay
4100	4200	2.32	0.20	Jurassic	Clay
4200	4300	2.35	0.10	Jurassic	Clay
4300	4400	2.32	0.15	Jurassic	Clay
4400	4500	2.27	0.20	Jurassic	Clay
4500	4600	2.30	0.20	Jurassic	Clay
4600	4700	2.35	0.10	Jurassic	Clay+Limestone
4700	4800	2.45	0.15	Jurassic	Clay+Limestone
4800	4900	2.50	0.10	Jurassic	Clay
4900	5000	2.52	0.10	Jurassic	Clay+Sand
5000	5100	2.52	0.05	Jurassic	Clay+Sand
5100	5200	2.55	0.05	Jurassic	Clay+Sand
5200	5300	2.57	0.05	Jurassic	Clay+Sand
5300	5400	2.55	0.10	Jurassic	Clay+Sand+Limestone
5300	5400	2.45	0.10	Jurassic	Clay+Sand+Limestone
5400	5500	2.45	0.10	Jurassic	Clay
5700	5800	2.60	0.10	Jurassic	Limestone
5800	5900	2.70	0.10	Jurassic	Limestone+Sand
5800	5900	2.50	0.10	Jurassic	Limestone+Sand
5900	6000	2.70	0.10	Jurassic	Limestone
6300	6400	2.47	0.15	Jurassic	Clay
6400	6500	2.50	0.10	Jurassic	Clay
6500	6600	2.52	0.10	Jurassic	Clay
6600	6700	2.50	0.10	Jurassic	Clay
6700	6800	2.52	0.15	Jurassic	Sand+Clay
6800	6900	2.55	0.10	Jurassic	Sand+Clay
6900	7000	2.60	0.05	Jurassic	Sand+Clay
7000	7100	2.55	0.10	Jurassic	Clay+Sand
7100	7200	2.52	0.15	Jurassic	Clay
7200	7300	2.62	0.10	Jurassic	Clay
7300	7400	2.65	0.05	Jurassic	Clay
7400	7500	2.62	0.10	Jurassic	Clay
7500	7600	2.62	0.15	Jurassic	Clay
7600	7700	2.60	0.20	Jurassic	Clay
7700	7800	2.55	0.15	Jurassic	Clay
7700	7800	2.20	0.10	Triassic	Sand
7800	7900	2.20	0.10	Triassic	Sand

7900	8000	2.20	0.10	Triassic	Sand
8000	8100	2.25	0.10	Triassic	Sand
8100	8200	2.25	0.10	Triassic	Sand
8200	8300	2.25	0.15	Triassic	Sand
8300	8400	2.20	0.10	Triassic	Sand
8400	8500	2.22	0.10	Triassic	Sand
8500	8600	2.22	0.10	Triassic	Sand
8600	8700	2.25	0.10	Triassic	Sand
8700	8800	2.25	0.10	Triassic	Sand
8800	8900	2.20	0.10	Triassic	Sand
8900	9000	2.30	0.25	Triassic	Sand
9000	9100	2.25	0.10	Triassic	Sand

WELL 106/24-01

1800	1900	2.15	0.10	Tertiary	Clay+Sand
1900	2000	2.20	0.05	Tertiary	Clay+Sand
2000	2100	2.30	0.20	Tertiary	Clay+Sand
2100	2200	2.25	0.10	Tertiary	Clay+Sand
2200	2300	2.10	0.05	Tertiary	Clay+Sand
2300	2400	2.20	0.05	Tertiary	Clay+Sand
2400	2500	2.25	0.05	Tertiary	Clay+Sand
2500	2600	2.20	0.05	Tertiary	Clay+Sand+Limestone
2600	2700	2.25	0.10	Tertiary	Clay+Sand+Limestone
2700	2800	2.30	0.10	Tertiary	Clay+Limestone
2800	2900	2.35	0.15	Tertiary	Clay+Sand
2900	3000	2.40	0.10	Tertiary	Clay
3000	3100	2.30	0.15	Tertiary	Clay+Sand
3100	3200	2.35	0.10	Tertiary	Clay+Sand+Limestone
3200	3300	2.35	0.10	Tertiary	Clay+Limestone+Sand
3300	3400	2.40	0.15	Tertiary	Clay+Limestone
3400	3500	2.32	0.15	Jurassic	Clay+Sand
3500	3600	2.35	0.10	Jurassic	Clay+Sand
3600	3700	2.32	0.10	Jurassic	Clay+Sand
3700	3800	2.40	0.15	Jurassic	Clay
3800	3900	2.37	0.15	Jurassic	Clay
3900	4000	2.30	0.20	Jurassic	Clay+Sand
4000	4100	2.35	0.15	Jurassic	Clay+Sand
4100	4200	2.37	0.05	Jurassic	Clay+Sand
4200	4300	2.35	0.15	Jurassic	Clay+Sand
4300	4400	2.30	0.20	Jurassic	Clay

4400 4500	2.40	0.10	Jurassic	Clay
4500 4600	2.37	0.10	Jurassic	Clay+Sand
4600 4700	2.35	0.15	Jurassic	Clay+Sand
4700 4800	2.35	0.15	Jurassic	Clay+Sand
4800 4900	2.40	0.10	Jurassic	Clay+Sand+Limestone
4900 5000	2.40	0.10	Jurassic	Clay+Sand
5000 5100	2.45	0.15	Jurassic	Clay+Sand
5100 5200	2.40	0.10	Jurassic	Clay+Sand
5200 5300	2.47	0.10	Jurassic	Clay
5300 5400	2.40	0.10	Jurassic	Clay+Sand
5400 5500	2.45	0.05	Jurassic	Clay
5500 5600	2.47	0.10	Jurassic	Clay+Limestone
5600 5700	2.45	0.10	Jurassic	Clay+Limestone
5700 5800	2.50	0.10	Jurassic	Clay+Limestone
5800 5900	2.47	0.10	Jurassic	Clay
5900 6000	2.50	0.10	Jurassic	Clay
6000 6100	2.50	0.05	Jurassic	Clay
6100 6200	2.47	0.10	Jurassic	Clay
6200 6300	2.45	0.10	Jurassic	Clay
6300 6400	2.50	0.15	Jurassic	Clay
6400 6500	2.50	0.10	Jurassic	Clay
6500 6600	2.50	0.05	Jurassic	Clay+Sand
6600 6700	2.52	0.10	Jurassic	Clay+Sand
6700 6800	2.55	0.20	Jurassic	Clay+Sand
6800 6900	2.52	0.10	Jurassic	Clay+Sand
6900 7000	2.50	0.10	Jurassic	Clay+Sand
7000 7100	2.50	0.15	Jurassic	Clay+Sand
7100 7200	2.47	0.10	Jurassic	Clay+Sand
7200 7300	2.45	0.20	Jurassic	Clay+Sand
7300 7400	2.50	0.10	Jurassic	Clay+Sand
7400 7500	2.50	0.20	Jurassic	Clay+Oo lite
7500 7600	2.65	0.10	Jurassic	Clay+Oo lite
7600 7700	2.55	0.10	Jurassic	Clay+Oo lite+Limestone
7700 7800	2.60	0.15	Jurassic	Clay+Limestone
7800 7900	2.55	0.10	Jurassic	Clay+Sand
7900 8000	2.25	0.05	Jurassic	Clay+Sand
8000 8100	2.52	0.10	Jurassic	Clay
8100 8200	2.50	0.05	Jurassic	Clay
8200 8300	2.55	0.05	Jurassic	Clay
8300 8400	2.55	0.05	Jurassic	Clay

8400 8500	2.52	0.05	Jurassic	Clay
8500 8600	2.50	0.10	Jurassic	Clay+Sand
8600 8700	2.50	0.05	Jurassic	Clay+Sand
8700 8800	2.50	0.05	Jurassic	Clay+Sand
8800 8900	2.52	0.05	Jurassic	Clay+Sand
8900 9000	2.55	0.05	Jurassic	Clay+Sand

WELL 93/06-01

3600 3700	2.45	0.10	Triassic	Clay
3700 3800	2.42	0.10	Triassic	Clay
3800 3900	2.05	0.10	Triassic	Clay
3900 4000	2.02	0.10	Triassic	Clay
4000 4100	2.07	0.10	Triassic	Salt
4100 4200	2.15	0.10	Triassic	Salt
4200 4300	2.20	0.10	Triassic	Salt
4300 4400	2.15	0.10	Triassic	Salt
4400 4500	2.10	0.10	Triassic	Salt
4500 4600	2.25	0.15	Triassic	Salt
4600 4700	2.25	0.20	Triassic	Salt
4700 4800	2.10	0.10	Triassic	Salt
4800 4900	2.10	0.10	Triassic	Salt
4900 5000	2.05	0.10	Triassic	Salt
5000 5100	2.05	0.10	Triassic	Salt
5100 5200	2.05	0.05	Triassic	Salt
5200 5300	2.05	0.10	Triassic	Salt
5300 5400	2.07	0.10	Triassic	Salt
5400 5500	2.10	0.15	Triassic	Salt+Clay
5500 5600	2.07	0.10	Triassic	Salt
5600 5700	2.25	0.10	Triassic	Salt
5600 5700	2.60	0.10	Triassic	Clay
5700 5800	2.57	0.05	Triassic	Clay
5800 5900	2.60	0.05	Triassic	Clay+Silt
5900 6000	2.60	0.05	Triassic	Silt+Clay
6000 6100	2.60	0.05	Triassic	Silt+Sand
6100 6200	2.57	0.10	Triassic	Sand+Silt
6200 6300	2.55	0.10	Triassic	Sand+Silt
6200 6300	2.40	0.05	Triassic	Sand+Silt+Salt
6300 6400	2.42	0.05	Triassic	Sand+Silt+Salt
6400 6500	2.47	0.05	Triassic	Silt+Salt
6500 6600	2.50	0.20	Triassic	Clay+Silt

6600	6700	2.55	0.20	Triassic	Clay+Silt+Salt
6700	6800	2.60	0.05	Devonian	Silt+Clay
6800	6900	2.62	0.10	Devonian	Silt
6900	7000	2.67	0.05	Devonian	Silt+Clay
7000	7100	2.65	0.05	Devonian	Silt+Clay
7100	7200	2.70	0.10	Devonian	Clay+Silt

WELL 102/29-01

1500	1600	2.25	0.10	Cretaceous	Limestone
1600	1700	2.32	0.10	Cretaceous	Limestone
1700	1800	2.42	0.10	Cretaceous	Clay+Marl
1800	1900	2.40	0.10	Cretaceous	Clay+Sand
1900	2000	2.20	0.10	Cretaceous	Sand
2000	2100	2.25	0.10	Cretaceous	Clay+Sand+Marl
2100	2200	2.30	0.10	Jurassic	Clay
2200	2300	2.40	0.05	Jurassic	Clay
2300	2400	2.42	0.05	Jurassic	Clay
2400	2500	2.42	0.05	Jurassic	Clay
2500	2600	2.40	0.05	Jurassic	Clay+Sand
2600	2700	2.40	0.05	Jurassic	Clay
2700	2800	2.40	0.05	Jurassic	Clay
2800	2900	2.42	0.05	Jurassic	Clay
2900	3000	2.42	0.05	Jurassic	Clay
3000	3100	2.45	0.05	Jurassic	Clay
3100	3200	2.47	0.05	Jurassic	Clay
3200	3300	2.40	0.10	Jurassic	Clay
3400	3500	2.35	0.15	Jurassic	Clay
3500	3600	2.37	0.15	Jurassic	Clay
3600	3700	2.40	0.10	Jurassic	Clay
3700	3800	2.42	0.10	Jurassic	Clay
3800	3900	2.50	0.05	Jurassic	Clay+Sand+Silt
3900	4000	2.47	0.05	Jurassic	Clay+Silt
4000	4100	2.47	0.05	Jurassic	Silt+Clay
4100	4200	2.50	0.05	Jurassic	Clay+Silt
4200	4300	2.50	0.05	Jurassic	Clay+Silt
4300	4400	2.50	0.05	Jurassic	Clay+Silt
4400	4500	2.50	0.05	Jurassic	Silt
4500	4600	2.50	0.05	Jurassic	Silt
4600	4700	2.50	0.05	Jurassic	Silt
4700	4800	2.50	0.05	Jurassic	Silt

4800	4900	2.52	0.05	Jurassic	Silt+Clay
4900	5000	2.52	0.05	Jurassic	Clay+Silt
5000	5100	2.55	0.05	Jurassic	Clay+Silt
5100	5200	2.57	0.05	Jurassic	Clay
5200	5300	2.60	0.05	Jurassic	Clay+Silt
5300	5400	2.55	0.05	Jurassic	Silt+Sand
5400	5500	2.60	0.05	Jurassic	Silt+Sand
5500	5600	2.62	0.05	Jurassic	Silt

WELL 103/21-01

1200	1300	2.40	0.05	Cretaceous	Chalk
1300	1400	2.40	0.05	Cretaceous	Sand+Chalk
1400	1500	2.20	0.10	Cretaceous	Sand
1500	1600	2.25	0.15	Cretaceous	Sand+Silt
1600	1700	2.20	0.20	Jurassic	Silt
1700	1800	2.10	0.10	Jurassic	Silt+Pyrite
1800	1900	2.45	0.10	Jurassic	Marl
1900	2000	2.50	0.05	Jurassic	Marl
2000	2100	2.45	0.15	Jurassic	Marl
2100	2200	2.40	0.20	Jurassic	Marl
2200	2300	2.47	0.10	Jurassic	Marl
2300	2400	2.35	0.10	Jurassic	Marl
2400	2500	2.45	0.10	Jurassic	Marl+Silt
2500	2600	2.24	0.05	Jurassic	Silt+Marl+Sand
2600	2700	2.50	0.05	Jurassic	Sand+Silt+Marl
2700	2800	2.50	0.05	Jurassic	Clay+Silt+Marl
2800	2900	2.50	0.05	Jurassic	Marl+Clay
2900	3000	2.50	0.10	Jurassic	Clay
3000	3100	2.50	0.10	Jurassic	Clay
3300	3400	2.40	0.20	Jurassic	Clay+Silt
3400	3500	2.40	0.20	Jurassic	Clay+Marl+Silt
3500	3600	2.50	0.10	Jurassic	Clay+Silt
3600	3700	2.52	0.10	Jurassic	Silt+Clay
3700	3800	2.50	0.10	Jurassic	Clay+Silt
3800	3900	2.45	0.15	Jurassic	Clay
3900	4000	2.40	0.15	Jurassic	Clay
4000	4100	2.45	0.15	Jurassic	Marl
4100	4200	2.50	0.10	Jurassic	Marl+Clay
4200	4300	2.55	0.15	Jurassic	Limestone+Clay
4300	4400	2.25	0.15	Jurassic	Clay+Limestone

4400	4500	2.60	0.15	Triassic	Clay+Silt
4500	4600	2.60	0.10	Triassic	Clay+Silt
4600	4700	2.65	0.05	Triassic	Clay
4700	4800	2.65	0.05	Triassic	Clay
4800	4900	2.65	0.05	Triassic	Clay
4900	5000	2.65	0.05	Triassic	Clay
5000	5100	2.60	0.10	Triassic	Clay
5100	5200	2.62	0.10	Triassic	Clay
5200	5300	2.67	0.05	Triassic	Clay
5300	5400	2.65	0.10	Triassic	Clay
5300	5400	2.35	0.10	Triassic	Sand
5400	5500	2.35	0.10	Triassic	Clay+Sand
5500	5600	2.25	0.20	Triassic	Clay+Sand
5600	5700	2.40	0.20	Triassic	Clay
5700	5800	2.40	0.20	Triassic	Clay
5800	5900	2.45	0.15	Triassic	Clay
6000	6100	2.65	0.05	Triassic	Silt
6100	6200	2.65	0.05	Triassic	Silt+Sand+Shale
6200	6300	2.60	0.15	Triassic	Shale
6300	6400	2.60	0.15	Devonian	Granite
6400	6500	2.65	0.10	Devonian	Granite

WELL 102/28-01

700	800	1.95	0.10	Cretaceous	Sand
800	900	2.25	0.05	Cretaceous	Sand
900	1000	2.05	0.05	Cretaceous	Chalk
1000	1100	2.07	0.05	Cretaceous	Chalk
1100	1200	2.25	0.05	Cretaceous	Chalk
1300	1400	2.35	0.10	Cretaceous	Chalk+Limestone
1400	1500	2.37	0.15	Cretaceous	Chalk
1500	1600	2.35	0.15	Cretaceous	Chalk+Sand
1600	1700	2.27	0.15	Cretaceous	Sand
1700	1800	2.22	0.20	Cretaceous	Sand+Limestone
1800	1900	2.25	0.15	Jurassic	Limestone+Sand+Coal
1900	2000	2.25	0.15	Jurassic	Sand
2000	2100	2.25	0.15	Jurassic	Sand
2100	2200	2.25	0.15	Jurassic	Sand+Clay
2200	2300	2.27	0.15	Jurassic	Sand
2300	2400	2.32	0.10	Jurassic	Sand+Shale
2400	2500	2.35	0.05	Jurassic	Sand+Shale

2500	2600	2.35	0.10	Jurassic	Shale+Sand
2600	2700	2.32	0.10	Jurassic	Shale+Limestone+Sand
2700	2800	2.50	0.10	Jurassic	Sand+Limestone
2800	2900	2.42	0.10	Jurassic	Sand+Limestone
2900	3000	2.45	0.15	Jurassic	Sand+Clay+Shale
3000	3100	2.50	0.05	Jurassic	Clay
3100	3200	2.42	0.10	Jurassic	Clay
3200	3300	2.45	0.10	Jurassic	Shale+Clay
3300	3400	2.55	0.10	Jurassic	Shale+Clay+Sand
3400	3500	2.50	0.10	Jurassic	Clay+Shale
3500	3600	2.52	0.10	Jurassic	Clay+Shale+Sand
3600	3700	2.55	0.10	Jurassic	Shale+Limestone
3700	3800	2.57	0.10	Jurassic	Limestone+Shale
3800	3900	2.57	0.15	Triassic	Limestone+Shale
3900	4000	2.57	0.15	Triassic	Limestone
4000	4100	2.60	0.20	Triassic	Limestone
4100	4200	2.62	0.15	Triassic	Shale+Limestone
4200	4300	2.62	0.10	Triassic	Shale+Clay
4300	4400	2.62	0.05	Triassic	Shale+Clay
4400	4500	2.62	0.05	Triassic	Shale+Clay
4500	4600	2.62	0.10	Triassic	Shale+Clay
4600	4700	2.60	0.10	Triassic	Shale+Clay
4600	4700	2.12	0.10	Triassic	Salt
4700	4800	2.10	0.05	Triassic	Salt
4800	4900	2.07	0.05	Triassic	Salt
4900	5000	2.07	0.05	Triassic	Salt
5000	5100	2.10	0.10	Triassic	Salt
5100	5200	2.20	0.15	Triassic	Salt+Clay
5200	5300	2.20	0.10	Triassic	Salt+Clay+Shale
5300	5400	2.20	0.15	Triassic	Salt
5400	5500	2.20	0.10	Triassic	Salt
5500	5600	2.22	0.15	Triassic	Salt+Clay
5700	5800	2.10	0.10	Triassic	Salt
5800	5900	2.10	0.10	Triassic	Salt
5900	6000	2.10	0.10	Triassic	Salt
6000	6100	2.07	0.05	Triassic	Salt
6100	6200	2.07	0.05	Triassic	Salt
6200	6300	2.07	0.10	Triassic	Salt
6300	6400	2.05	0.10	Triassic	Salt
6400	6500	2.30	0.15	Triassic	Salt+Shale+Clay

6500	6600	2.32	0.10	Triassic	Salt+Clay+Shale
6600	6700	2.25	0.10	Devonian	Salt+Clay+Shale
6700	6800	2.05	0.05	Devonian	Salt
6800	6900	2.10	0.15	Devonian	Salt+Clay+Shale
7100	7200	2.07	0.10	Devonian	Salt
7200	7300	2.07	0.05	Devonian	Salt
7300	7400	2.55	0.25	Devonian	Shale+Clay+Sand
7400	7500	2.63	0.05	Devonian	Shale+Clay
7500	7600	2.65	0.05	Devonian	Clay+Shale
7600	7700	2.65	0.05	Devonian	Clay
7700	7800	2.67	0.05	Devonian	Clay
7800	7900	2.67	0.05	Devonian	Clay
7900	8000	2.65	0.05	Devonian	Clay
8000	8100	2.67	0.05	Devonian	Clay
8100	8200	2.70	0.05	Devonian	Clay+Sand
8200	8300	2.72	0.05	Devonian	Clay+Sand
8300	8400	2.72	0.05	Devonian	Sand+Clay

WELL 103/02-01

1500	1600	2.42	0.10	Jurassic	Limestone+Sand
1600	1700	2.35	0.20	Jurassic	Sand+Limestone
1700	1800	2.30	0.10	Jurassic	Sand+Limestone+Shale
1800	1900	2.30	0.15	Jurassic	Shale+Clay
1900	2000	2.32	0.10	Jurassic	Shale+Clay
2000	2100	2.30	0.15	Jurassic	Shale+Clay
2100	2200	2.20	0.20	Jurassic	Shale+Clay
2200	2300	2.20	0.15	Jurassic	Shale+Clay
2300	2400	2.25	0.15	Jurassic	Shale+Clay
2400	2500	2.30	0.10	Jurassic	Shale+Clay
3000	3100	2.35	0.10	Jurassic	Shale
3100	3200	2.50	0.05	Jurassic	Shale
3200	3300	2.52	0.05	Triassic	Shale
3800	3900	2.30	0.15	Triassic	Shale+Clay
3900	4000	2.30	0.10	Triassic	Shale+Clay
4000	4100	2.30	0.05	Triassic	Shale+Clay
4100	4200	2.37	0.05	Triassic	Shale
4200	4300	2.35	0.20	Triassic	Shale
4400	4500	2.65	0.10	Triassic	Shale+Clay
4500	4600	2.60	0.15	Triassic	Shale+Clay
4600	4700	2.25	0.15	Triassic	Shale+Clay+Salt

4700	4800	2.25	0.10	Triassic	Clay+Shale+Salt
4800	4900	2.40	0.15	Triassic	Clay+Shale+Salt
4900	5000	2.40	0.20	Triassic	Clay+Shale+Salt
5000	5100	2.20	0.20	Triassic	Clay+Salt+Shale
5100	5200	2.10	0.05	Triassic	Salt
5200	5300	2.10	0.05	Triassic	Salt
5300	5400	2.10	0.05	Triassic	Salt
5400	5500	2.10	0.15	Triassic	Salt
5700	5800	2.10	0.10	Triassic	Salt
5800	5900	2.02	0.05	Triassic	Salt
5900	6000	2.02	0.05	Triassic	Salt
6000	6100	2.02	0.10	Triassic	Salt
6100	6200	2.30	0.20	Triassic	Clay
6200	6300	2.25	0.20	Triassic	Clay+Shale
6300	6400	2.20	0.20	Triassic	Clay+Shale
6400	6500	2.15	0.15	Triassic	Shale
6500	6600	2.15	0.10	Triassic	Shale
6600	6700	2.10	0.10	Triassic	Shale
6700	6800	2.05	0.10	Triassic	Shale
6800	6900	2.05	0.10	Triassic	Shale
6900	7000	2.05	0.05	Triassic	Shale
7000	7100	2.10	0.10	Triassic	Shale
7200	7300	2.20	0.10	Triassic	Clay+Shale
7600	7700	2.60	0.05	Triassic	Shale+Clay
7700	7800	2.60	0.05	Triassic	Shale+Clay
7800	7900	2.60	0.05	Triassic	Shale+Clay
7900	8000	2.55	0.15	Triassic	Shale
8000	8100	2.50	0.20	Triassic	Shale
8100	8200	2.50	0.20	Triassic	Shale
8200	8300	2.60	0.15	Triassic	Shale+Clay
8300	8400	2.65	0.05	Triassic	Clay+Shale
8400	8500	2.65	0.05	Triassic	Clay
8500	8600	2.65	0.05	Triassic	Clay
8600	8700	2.65	0.05	Triassic	Clay
8700	8800	2.65	0.10	Triassic	Clay
8800	8900	2.50	0.10	Triassic	Shale+Clay
8900	9000	2.50	0.10	Triassic	Clay+Shale
9000	9100	2.50	0.10	Triassic	Clay+Shale
9100	9200	2.50	0.10	Triassic	Clay+Shale
9200	9300	2.50	0.10	Triassic	Clay+Sand

9300 9400	2.50	0.10	Triassic	Clay+Sand+Shale
9400 9500	2.55	0.10	Triassic	Sand+Shale
9500 9600	2.55	0.10	Triassic	Shale
9600 9700	2.60	0.05	Triassic	Shale+Clay+Sand
9700 9800	2.60	0.10	Triassic	Shale+Sand+Limestone
9800 9900	2.55	0.15	Triassic	Shale+Sand+Clay
9900 10000	2.60	0.10	Triassic	Shale+Sand+Clay
10000 10100	2.65	0.10	Triassic	Shale+Clay
10100 10200	2.60	0.10	Triassic	Shale+Clay+Sand
10200 10300	2.65	0.05	Triassic	Shale+Clay+Sand
10300 10400	2.65	0.05	Triassic	Shale+Clay

WELL 110/08-01

700 800	2.35	0.05	Triassic	Sand
800 900	2.35	0.05	Triassic	Sand
900 1000	2.35	0.05	Triassic	Sand
1000 1100	2.37	0.05	Triassic	Sand
1100 1200	2.37	0.05	Triassic	Sand
1200 1300	2.37	0.05	Triassic	Sand
1300 1400	2.40	0.05	Triassic	Sand
1400 1500	2.40	0.05	Triassic	Sand
1500 1600	2.40	0.05	Triassic	Sand
1600 1700	2.40	0.05	Triassic	Sand
1700 1800	2.40	0.10	Triassic	Sand
1800 1900	2.40	0.10	Triassic	Sand
1900 2000	2.40	0.10	Triassic	Sand
2000 2100	2.37	0.05	Triassic	Sand
2100 2200	2.37	0.05	Triassic	Sand
2200 2300	2.37	0.05	Triassic	Sand
2300 2400	2.37	0.05	Triassic	Sand
3000 3100	2.45	0.10	Permian	Shale+Sand
3100 3200	2.47	0.05	Permian	Sand+Shale
3200 3300	2.50	0.10	Permian	Sand+Shale
3300 3400	2.55	0.20	Permian	Sand+Shale
3400 3500	2.55	0.20	Permian	Sand+Shale
3500 3600	2.55	0.15	Permian	Sand+Shale
3600 3700	2.52	0.20	Permian	Sand+Shale
3700 3800	2.52	0.10	Permian	Sand+Shale
3800 3900	2.50	0.20	Permian	Shale+Sand

WELL 103/18-01

1200	1300	2.27	0.10	Jurassic	Sand
1400	1500	2.47	0.20	Jurassic	Sand+Coal
1600	1700	2.20	0.20	Jurassic	Sand
2100	2200	2.55	0.10	Jurassic	Sand
2200	2300	2.52	0.05	Jurassic	Sand
2300	2400	2.50	0.05	Jurassic	Sand
2400	2500	2.50	0.05	Jurassic	Sand+Limestone
2500	2600	2.50	0.05	Jurassic	Sand+Limestone
2600	2700	2.45	0.10	Jurassic	Sand+Limestone
2700	2800	2.45	0.10	Jurassic	Sand+Silt
2800	2900	2.50	0.10	Jurassic	Sand
2900	3000	2.47	0.05	Jurassic	Sand
3000	3100	2.57	0.05	Jurassic	Sand
3100	3200	2.50	0.10	Jurassic	Sand+Limestone
3200	3300	2.50	0.10	Jurassic	Sand+Limestone
3300	3400	2.57	0.15	Jurassic	Sand+Limestone
3400	3500	2.45	0.10	Jurassic	Sand+Limestone
3600	3700	2.60	0.10	Jurassic	Sand+Marl
4000	4100	2.60	0.15	Jurassic	Limestone+Sand
4100	4200	2.60	0.15	Triassic	Limestone
4200	4300	2.57	0.10	Triassic	Chalk
4300	4400	2.57	0.05	Triassic	Chalk+Sand
4400	4500	2.60	0.10	Triassic	Sand
4500	4600	2.57	0.10	Triassic	Sand
4600	4700	2.60	0.10	Triassic	Sand
4700	4800	2.62	0.10	Triassic	Sand
4800	4900	2.60	0.10	Triassic	Sand
4800	4900	2.05	0.15	Triassic	Salt
4900	5000	2.05	0.20	Triassic	Salt
5200	5300	2.15	0.20	Triassic	Salt
5300	5400	2.05	0.10	Triassic	Salt
5400	5500	2.15	0.05	Triassic	Salt
5500	5600	2.40	0.10	Triassic	Limestone
5500	5600	2.20	0.10	Triassic	Salt
5600	5700	2.15	0.10	Triassic	Salt
5700	5800	2.15	0.05	Triassic	Salt
5800	5900	2.15	0.05	Triassic	Salt
5800	5900	2.45	0.10	Triassic	Sand
5900	6000	2.45	0.15	Triassic	Sand

6000 6100	2.15	0.10	Triassic	Salt
6100 6200	2.10	0.15	Triassic	Salt
6200 6300	2.15	0.20	Triassic	Salt
6300 6400	2.15	0.20	Triassic	Salt
6400 6500	2.15	0.10	Triassic	Salt
6400 6500	2.65	0.10	Triassic	Sand
6500 6600	2.65	0.05	Triassic	Sand
6600 6700	2.65	0.05	Triassic	Sand
6700 6800	2.65	0.05	Triassic	Sand
6800 6900	2.65	0.05	Triassic	Sand
6900 7000	2.65	0.05	Triassic	Sand
7000 7100	2.70	0.05	Triassic	Sand
7100 7200	2.70	0.05	Triassic	Sand

WELL 112/30-01

1100 1200	2.25	0.15	Carboniferous	Sand+Silt
1200 1300	2.62	0.05	Carboniferous	Sand+Silt+Clay
1300 1400	2.50	0.05	Carboniferous	Silt+Clay
1400 1500	2.50	0.05	Carboniferous	Clay+Silt
1500 1600	2.47	0.10	Carboniferous	Sand+Clay
1600 1700	2.42	0.10	Carboniferous	Sand+Silt
1700 1800	2.40	0.15	Carboniferous	Sand+Silt
1800 1900	2.45	0.10	Carboniferous	Clay+Sand+Silt
1900 2000	2.45	0.10	Carboniferous	Silt
2000 2100	2.47	0.15	Carboniferous	Silt
2100 2200	2.50	0.10	Carboniferous	Silt+Clay
2200 2300	2.50	0.10	Carboniferous	Silt+Clay
2300 2400	2.47	0.10	Carboniferous	Shale+Silt
2400 2500	2.45	0.15	Carboniferous	Silt+Shale
2500 2600	2.40	0.10	Carboniferous	Sand+Shale
2600 2700	2.40	0.10	Carboniferous	Sand+Silt
2700 2800	2.40	0.15	Carboniferous	Silt+Shale
2800 2900	2.40	0.10	Carboniferous	Silt+Shale
2900 3000	2.45	0.10	Carboniferous	Shale+Sand
3000 3100	2.50	0.15	Carboniferous	Shale
3100 3200	2.50	0.10	Carboniferous	Shale+Sand
3200 3300	2.52	0.10	Carboniferous	Shale
3300 3400	2.50	0.15	Carboniferous	Shale
3400 3500	2.50	0.20	Carboniferous	Shale
3500 3600	2.50	0.15	Carboniferous	Shale

3600	3700	2.52	0.10	Carboniferous	Shale
3700	3800	2.60	0.15	Carboniferous	Shale
3800	3900	2.57	0.15	Carboniferous	Shale+Sand
3900	4000	2.62	0.10	Carboniferous	Shale
4000	4100	2.62	0.10	Carboniferous	Shale
4100	4200	2.62	0.10	Carboniferous	Shale
4200	4300	2.65	0.10	Carboniferous	Shale
4300	4400	2.62	0.10	Carboniferous	Shale+Silt+Sand

WELL 110/07-02

1200	1300	2.05	0.10	Triassic	Salt
1300	1400	2.15	0.20	Triassic	Salt
1400	1500	2.25	0.20	Triassic	Salt+Clay
1500	1600	2.25	0.20	Triassic	Clay+Salt
1700	1800	2.02	0.05	Triassic	Salt
1800	1900	1.95	0.05	Triassic	Salt
1900	2000	1.97	0.05	Triassic	Salt
2000	2100	1.97	0.05	Triassic	Salt
2100	2200	1.97	0.10	Triassic	Salt
2200	2300	2.05	0.10	Triassic	Salt
2300	2400	2.05	0.10	Triassic	Salt
2500	2600	2.40	0.20	Triassic	Clay+Limestone
2600	2700	2.42	0.20	Triassic	Sand+Silt+Clay
2700	2800	2.40	0.15	Triassic	Sand
2800	2900	2.42	0.10	Triassic	Sand
2900	3000	2.42	0.10	Triassic	Sand
3000	3100	2.45	0.10	Triassic	Sand
3100	3200	2.45	0.10	Triassic	Sand
3200	3300	2.45	0.15	Triassic	Sand
3300	3400	2.45	0.05	Triassic	Sand
3400	3500	2.50	0.10	Triassic	Sand
3500	3600	2.50	0.15	Permian	Sand+Silt+Clay
3600	3700	2.45	0.15	Permian	Clay+Silt
3700	3800	2.50	0.20	Permian	Clay+Limestone
3900	4000	2.42	0.15	Permian	Sand
4000	4100	2.40	0.20	Permian	Sand+Clay
4100	4200	2.60	0.10	Permian	Clay+Sand
4500	4600	2.63	0.15	Carboniferous	Clay+Silt+Sand
4600	4700	2.60	0.15	Carboniferous	Silt+Clay
4700	4800	2.60	0.10	Carboniferous	Silt

WELL 110/07-01

2700	2800	2.15	0.15	Triassic	Salt
2800	2900	2.10	0.10	Triassic	Salt
2900	3000	2.47	0.10	Triassic	Shale
3000	3100	2.50	0.10	Triassic	Shale+Silt
3100	3200	2.55	0.10	Triassic	Shale+Silt
3200	3300	2.52	0.10	Triassic	Silt+Sand
3300	3400	2.57	0.05	Triassic	Silt
3300	3400	2.15	0.10	Triassic	Salt
3400	3500	2.15	0.10	Triassic	Salt
3600	3700	2.50	0.15	Triassic	Shale
3700	3800	2.45	0.15	Triassic	Sand+Shale
3800	3900	2.45	0.15	Triassic	Sand+Shale
3900	4000	2.45	0.10	Triassic	Sand+Shale
4000	4100	2.50	0.15	Triassic	Sand+Shale
4100	4200	2.47	0.15	Triassic	Sand
4200	4300	2.50	0.15	Triassic	Sand+Shale
4300	4400	2.45	0.10	Triassic	Sand+Shale
4400	4500	2.47	0.10	Triassic	Sand+Shale
4500	4600	2.50	0.10	Triassic	Sand+Shale
4600	4700	2.47	0.10	Triassic	Sand+Shale

WELL 98/22-02

1200	1300	2.47	0.05	Jurassic	Clay
1300	1400	2.52	0.05	Jurassic	Clay
1400	1500	2.55	0.05	Jurassic	Limestone+Clay
1500	1600	2.57	0.10	Jurassic	Silt
1600	1700	2.57	0.05	Jurassic	Silt+Clay
1700	1800	2.57	0.10	Jurassic	Limestone+Clay
1800	1900	2.55	0.10	Jurassic	Clay+Limestone
1900	2000	2.52	0.20	Jurassic	Clay+Limestone
2000	2100	2.52	0.15	Jurassic	Clay
2100	2200	2.50	0.15	Jurassic	Clay
2200	2300	2.55	0.15	Jurassic	Clay+Limestone
2300	2400	2.57	0.15	Jurassic	Limestone
2400	2500	2.55	0.10	Triassic	Clay+Limestone
2500	2600	2.57	0.05	Triassic	Clay
2700	2800	2.62	0.05	Triassic	Clay+Sand
2800	2900	2.62	0.05	Triassic	Clay
2900	3000	2.62	0.05	Triassic	Clay

3000	3100	2.65	0.10	Triassic	Clay
3100	3200	2.60	0.20	Triassic	Clay+Sand
3200	3300	2.52	0.10	Triassic	Conglomera
3300	3400	2.55	0.15	Triassic	Conglomera+Breccia
3400	3500	2.60	0.15	Triassic	Breccia
3500	3600	2.60	0.10	Triassic	Breccia
3600	3700	2.57	0.05	Triassic	Breccia
3700	3800	2.57	0.05	Triassic	Breccia
3800	3900	2.55	0.10	Triassic	Breccia
3900	4000	2.60	0.10	Triassic	Breccia
4000	4100	2.60	0.20	Triassic	Breccia
4100	4200	2.75	0.20	Permian	Methamorfic
4200	4300	2.75	0.10	Permian	Methamorfic
4300	4400	2.75	0.10	Permian	Methamorfic

WELL 110/09-01

1100	1200	1.97	0.05	Triassic	Salt
1200	1300	1.97	0.05	Triassic	Salt
1300	1400	2.25	0.20	Triassic	Salt+Silt
1400	1500	2.45	0.20	Triassic	Silt+Salt
1500	1600	2.50	0.15	Triassic	Silt+Clay
1600	1700	2.45	0.15	Triassic	Silt+Clay
1700	1800	2.45	0.15	Triassic	Silt+Clay
1800	1900	2.40	0.15	Triassic	Clay+Silt+Salt
2000	2100	2.40	0.15	Triassic	Silt+Clay
2100	2200	2.45	0.10	Triassic	Clay
2200	2300	2.52	0.10	Triassic	Clay
2300	2400	2.45	0.10	Triassic	Clay
2300	2400	2.10	0.10	Triassic	Salt
2400	2500	2.10	0.10	Triassic	Salt
2400	2500	2.45	0.10	Triassic	Clay
2500	2600	2.45	0.15	Triassic	Silt+Clay
2700	2800	2.42	0.10	Triassic	Sand
2800	2900	2.45	0.10	Triassic	Sand
2900	3000	2.42	0.10	Triassic	Sand
3000	3100	2.40	0.10	Triassic	Sand
3100	3200	2.45	0.10	Triassic	Sand
3200	3300	2.47	0.05	Triassic	Sand
3300	3400	2.45	0.05	Triassic	Sand
3400	3500	2.45	0.10	Triassic	Sand

3500	3600	2.40	0.10	Triassic	Sand
3600	3700	2.42	0.05	Triassic	Sand
3700	3800	2.42	0.05	Triassic	Sand
3800	3900	2.42	0.05	Triassic	Sand
3900	4000	2.42	0.05	Triassic	Sand
4000	4100	2.45	0.05	Triassic	Sand
4100	4200	2.50	0.05	Triassic	Sand
4200	4300	2.50	0.05	Triassic	Sand
4300	4400	2.50	0.10	Triassic	Sand
4400	4500	2.50	0.10	Triassic	Sand
4500	4600	2.45	0.05	Triassic	Sand
4600	4700	2.40	0.10	Triassic	Sand
4700	4800	2.52	0.15	Triassic	Sand
4800	4900	2.60	0.10	Triassic	Sand
4900	5000	2.60	0.05	Triassic	Sand
5000	5100	2.60	0.05	Triassic	Sand
5100	5200	2.60	0.05	Triassic	Sand
5200	5300	2.55	0.10	Triassic	Sand
5300	5400	2.55	0.10	Triassic	Sand
5400	5500	2.62	0.05	Triassic	Sand
5500	5600	2.60	0.10	Triassic	Sand
5600	5700	2.60	0.10	Triassic	Sand
5700	5800	2.60	0.05	Triassic	Sand
5800	5900	2.57	0.05	Triassic	Sand
5900	6000	2.56	0.05	Triassic	Sand
6000	6100	2.58	0.05	Triassic	Sand
6100	6200	2.57	0.10	Triassic	Sand
6200	6300	2.60	0.05	Triassic	Sand
6300	6400	2.60	0.10	Triassic	Sand
6400	6500	2.58	0.10	Triassic	Sand
6500	6600	2.58	0.10	Triassic	Sand
6600	6700	2.57	0.10	Triassic	Sand
6700	6800	2.56	0.10	Triassic	Sand
6800	6900	2.56	0.10	Triassic	Sand
6900	7000	2.58	0.05	Triassic	Sand
7000	7100	2.65	0.05	Permian	Sand
7100	7200	2.70	0.03	Permian	Sand
7800	7900	2.50	0.15	Permian	Sand
7900	8000	2.50	0.10	Permian	Sand
8000	8100	2.50	0.15	Permian	Sand

8100 8200	2.55	0.15	Permian	Sand
8200 8300	2.60	0.10	Permian	Sand
8300 8400	2.65	0.05	Permian	Sand
8400 8500	2.62	0.10	Carboniferous	Clay+Sand

WELL 110/08-2X

500 600	2.20	0.20	Triassic	Clay+Sand
600 700	2.25	0.20	Triassic	Clay+Sand+Salt
700 800	2.35	0.20	Triassic	Clay+Sand+Salt
800 900	2.35	0.20	Triassic	Clay+Sand
900 1000	2.40	0.10	Triassic	Clay
1000 1100	2.10	0.10	Triassic	Salt
1100 1200	2.20	0.15	Triassic	Salt+Clay
1200 1300	2.20	0.15	Triassic	Salt+Clay
1300 1400	2.25	0.10	Triassic	Clay+Sand
1400 1500	2.20	0.25	Triassic	Clay+Salt+Sand
1500 1600	2.10	0.15	Triassic	Salt+Clay
1600 1700	2.10	0.10	Triassic	Salt
1700 1800	2.07	0.10	Triassic	Salt
1800 1900	2.10	0.10	Triassic	Salt
1900 2000	2.17	0.15	Triassic	Salt
2000 2100	2.35	0.10	Triassic	Clay+Salt
2100 2200	2.40	0.10	Triassic	Clay
2200 2300	2.40	0.10	Triassic	Clay
2300 2400	2.42	0.10	Triassic	Clay
2400 2500	2.45	0.10	Triassic	Clay
2500 2600	2.15	0.10	Triassic	Salt
2600 2700	2.10	0.10	Triassic	Salt
2600 2700	2.50	0.10	Triassic	Clay
2700 2800	2.50	0.15	Triassic	Clay
2800 2900	2.50	0.15	Triassic	Clay
2900 3000	2.50	0.15	Triassic	Clay
3000 3100	2.20	0.15	Triassic	Salt
3100 3200	2.20	0.20	Triassic	Salt
3200 3300	2.20	0.20	Triassic	Salt
3200 3300	2.40	0.20	Triassic	Sand
3300 3400	2.50	0.10	Triassic	Sand+Clay
3400 3500	2.35	0.20	Triassic	Sand+Clay
3500 3600	2.37	0.25	Triassic	Sand
3600 3700	2.37	0.25	Triassic	Sand

3700	3800	2.35	0.20	Triassic	Sand
3800	3900	2.35	0.15	Triassic	Sand
3900	4000	2.35	0.10	Triassic	Sand
4000	4100	2.35	0.10	Triassic	Sand
4100	4200	2.35	0.10	Triassic	Sand
4200	4300	2.50	0.05	Triassic	Sand+Clay
4300	4400	2.50	0.10	Triassic	Sand+Clay
4400	4500	2.50	0.15	Triassic	Sand+Clay
4500	4600	2.50	0.15	Triassic	Sand+Clay
4600	4700	2.45	0.15	Triassic	Sand+Clay
4700	4800	2.42	0.10	Triassic	Sand+Clay
4800	4900	2.37	0.10	Triassic	Sand+Clay
4900	5000	2.42	0.10	Triassic	Sand+Clay
5000	5100	2.45	0.10	Triassic	Sand+Clay
5100	5200	2.45	0.05	Triassic	Sand+Clay
5200	5300	2.50	0.05	Triassic	Sand+Clay
5300	5400	2.50	0.05	Triassic	Sand+Clay
5400	5500	2.50	0.10	Triassic	Sand+Clay
5500	5600	2.50	0.10	Triassic	Sand+Clay
5600	5700	2.50	0.05	Triassic	Sand+Clay
5700	5800	2.50	0.05	Triassic	Sand+Clay
5800	5900	2.50	0.05	Triassic	Sand+Clay
5900	6000	2.47	0.10	Triassic	Sand+Clay
6000	6100	2.47	0.10	Triassic	Sand+Clay
6100	6200	2.47	0.10	Triassic	Sand+Clay
6200	6300	2.50	0.15	Triassic	Sand+Clay
6300	6400	2.50	0.10	Triassic	Sand+Clay
6400	6500	2.55	0.05	Triassic	Sand+Clay
6500	6600	2.55	0.05	Triassic	Sand+Clay
6600	6700	2.57	0.05	Triassic	Sand+Clay
6700	6800	2.57	0.05	Triassic	Sand+Clay
6900	7000	2.60	0.05	Triassic	Sand+Clay
7000	7100	2.60	0.05	Triassic	Sand+Clay
7100	7200	2.57	0.05	Triassic	Sand+Clay
7200	7300	2.60	0.05	Triassic	Sand+Clay
7300	7400	2.60	0.05	Triassic	Sand+Clay
7400	7500	2.60	0.05	Triassic	Sand+Clay
7500	7600	2.60	0.05	Triassic	Sand+Clay
7600	7700	2.57	0.05	Triassic	Sand+Clay
7700	7800	2.57	0.05	Triassic	Sand+Clay

7800	7900	2.57	0.05	Triassic	Sand+Clay
7900	8000	2.60	0.05	Triassic	Sand+Clay
8000	8100	2.60	0.05	Triassic	Sand+Clay
8100	8200	2.10	0.20	Permian	Salt
8200	8300	2.10	0.20	Permian	Salt
8300	8400	2.07	0.05	Permian	Salt
8400	8500	2.07	0.05	Permian	Salt
8500	8600	2.07	0.05	Permian	Salt
8600	8700	2.07	0.05	Permian	Salt
8700	8800	2.07	0.05	Permian	Salt
8800	8900	2.05	0.05	Permian	Salt
8900	9000	2.05	0.05	Permian	Salt
9000	9100	2.60	0.05	Permian	Sand+Clay
9100	9200	2.65	0.05	Permian	Sand+Clay
9200	9300	2.65	0.05	Permian	Sand+Clay
9800	9900	2.70	0.05	Permian	Clay
9900	10000	2.72	0.05	Carboniferous	Clay
10000	10100	2.72	0.05	Carboniferous	Clay
10100	10200	2.72	0.05	Carboniferous	Sand+Clay

WELL 110/02-03

1100	1200	2.05	0.10	Triassic	Salt
1200	1300	2.05	0.10	Triassic	Salt
1300	1400	2.10	0.15	Triassic	Salt
1400	1500	2.07	0.10	Triassic	Salt
1500	1600	2.05	0.10	Triassic	Salt
1600	1700	2.05	0.10	Triassic	Salt
1600	1700	2.45	0.10	Triassic	Silt
1700	1800	2.05	0.10	Triassic	Salt
1700	1800	2.45	0.10	Triassic	Silt
1800	1900	1.95	0.10	Triassic	Salt
1800	1900	2.30	0.10	Triassic	Clay
1900	2000	2.10	0.15	Triassic	Salt
2000	2100	2.10	0.10	Triassic	Salt
2100	2200	2.00	0.10	Triassic	Salt
2200	2300	2.00	0.10	Triassic	Salt
2200	2300	2.40	0.10	Triassic	Clay
2300	2400	1.90	0.10	Triassic	Salt
2300	2400	2.30	0.10	Triassic	Clay
2400	2500	1.90	0.10	Triassic	Salt

2400	2500	2.30	0.10	Triassic	Clay
2500	2600	2.10	0.10	Triassic	Salt
2600	2700	2.00	0.10	Triassic	Salt
2600	2700	2.30	0.10	Triassic	Clay
2700	2800	2.20	0.10	Triassic	Salt
2700	2800	2.50	0.10	Triassic	Clay
2800	2900	2.20	0.10	Triassic	Salt
2900	3000	2.00	0.10	Triassic	Salt
3000	3100	1.95	0.10	Triassic	Salt
3100	3200	2.50	0.25	Triassic	Sand+Clay
3200	3300	2.45	0.20	Triassic	Sand+Clay
3300	3400	2.45	0.10	Triassic	Sand
3400	3500	2.40	0.10	Triassic	Sand
3500	3600	2.40	0.10	Triassic	Sand
3600	3700	2.50	0.10	Triassic	Sand
3700	3800	2.40	0.10	Triassic	Sand
3800	3900	2.45	0.10	Triassic	Sand
3900	4000	2.50	0.10	Triassic	Sand
4000	4100	2.50	0.10	Triassic	Sand+Clay
4100	4200	2.45	0.15	Triassic	Sand+Clay
4200	4300	2.40	0.20	Triassic	Sand+Clay
4300	4400	2.37	0.10	Triassic	Sand
4400	4500	2.40	0.10	Triassic	Sand
4500	4600	2.40	0.10	Triassic	Sand

WELL 110/03-01

1200	1300	2.05	0.05	Triassic	Salt
1300	1400	2.07	0.05	Triassic	Salt
1400	1500	2.07	0.05	Triassic	Salt
1400	1500	2.35	0.20	Triassic	Silt
1500	1600	2.40	0.20	Triassic	Silt
1600	1700	2.55	0.20	Triassic	Silt
1600	1700	2.05	0.10	Triassic	Salt
1700	1800	2.10	0.10	Triassic	Salt
1700	1800	2.55	0.10	Triassic	Clay
1800	1900	2.10	0.10	Triassic	Salt
1800	1900	2.45	0.10	Triassic	Clay
1900	2000	2.00	0.10	Triassic	Salt
1900	2000	2.40	0.10	Triassic	Clay
2000	2100	2.10	0.10	Triassic	Salt

2100	2200	2.05	0.10	Triassic	Salt
2200	2300	2.05	0.15	Triassic	Salt
2300	2400	2.10	0.15	Triassic	Salt
2400	2500	2.20	0.15	Triassic	Salt+Clay
2500	2600	2.20	0.10	Triassic	Salt+Clay
2600	2700	2.15	0.15	Triassic	Salt
2700	2800	2.20	0.15	Triassic	Salt+Silt+Clay
3000	3100	1.95	0.10	Triassic	Salt
3000	3100	2.40	0.10	Triassic	Clay
3100	3200	2.15	0.10	Triassic	Salt
3100	3200	2.45	0.10	Triassic	Clay
3200	3300	1.90	0.10	Triassic	Salt
3200	3300	2.40	0.10	Triassic	Clay
3300	3400	1.95	0.15	Triassic	Salt
3400	3500	1.90	0.15	Triassic	Salt
3500	3600	1.90	0.15	Triassic	Salt
3600	3700	2.20	0.15	Triassic	Salt
3600	3700	2.70	0.10	Triassic	Anhydrite
3700	3800	2.35	0.10	Triassic	Sand+Clay
3800	3900	2.35	0.20	Triassic	Sand+Clay
3900	4000	2.40	0.10	Triassic	Sand
4000	4100	2.45	0.10	Triassic	Sand
4100	4200	2.42	0.10	Triassic	Sand
4200	4300	2.40	0.10	Triassic	Sand
4300	4400	2.37	0.10	Triassic	Sand
4400	4500	2.50	0.10	Triassic	Sand+Silt+Clay
4500	4600	2.60	0.10	Triassic	Sand+Silt+Clay

WELL 110/03-02

1200	1300	2.05	0.05	Triassic	Salt
1300	1400	2.05	0.05	Triassic	Salt
1400	1500	2.05	0.05	Triassic	Salt
1500	1600	2.05	0.05	Triassic	Salt
1600	1700	2.05	0.05	Triassic	Salt
1700	1800	2.05	0.05	Triassic	Salt
1800	1900	2.05	0.05	Triassic	Salt
1900	2000	2.05	0.05	Triassic	Salt
2000	2100	2.05	0.05	Triassic	Salt
2100	2200	2.07	0.05	Triassic	Salt
2200	2300	2.05	0.05	Triassic	Salt

2300	2400	2.05	0.05	Triassic	Salt
2400	2500	2.02	0.05	Triassic	Salt
2500	2600	2.05	0.10	Triassic	Salt
2600	2700	2.07	0.10	Triassic	Salt
2700	2800	2.05	0.05	Triassic	Salt
2800	2900	2.05	0.05	Triassic	Salt
2900	3000	2.05	0.05	Triassic	Salt
3000	3100	2.10	0.10	Triassic	Salt
3200	3300	2.05	0.10	Triassic	Salt
3200	3300	2.45	0.10	Triassic	Clay
3300	3400	2.50	0.10	Triassic	Clay+Silt
3400	3500	2.52	0.10	Triassic	Clay
3500	3600	2.55	0.15	Triassic	Clay
3600	3700	2.50	0.20	Triassic	Clay+Silt
3700	3800	2.52	0.20	Triassic	Clay+Silt
3800	3900	2.55	0.20	Triassic	Clay+Silt
3900	4000	2.57	0.15	Triassic	Clay+Silt
4000	4100	2.60	0.15	Triassic	Clay
4000	4100	2.05	0.10	Triassic	Salt
4100	4200	2.05	0.10	Triassic	Salt
4100	4200	2.50	0.10	Triassic	Clay
4200	4300	2.05	0.10	Triassic	Salt
4200	4300	2.50	0.10	Triassic	Clay
4300	4400	2.52	0.10	Triassic	Clay+Silt
4400	4500	2.50	0.15	Triassic	Clay+Silt
4500	4600	2.05	0.15	Triassic	Salt
4500	4600	2.50	0.15	Triassic	Clay
4600	4700	2.50	0.15	Triassic	Clay
4700	4800	2.10	0.15	Triassic	Salt
4700	4800	2.55	0.15	Triassic	Clay
4800	4900	2.10	0.15	Triassic	Salt
4800	4900	2.55	0.15	Triassic	Clay
4900	5000	2.05	0.15	Triassic	Salt
4900	5000	2.50	0.15	Triassic	Clay
5000	5100	2.05	0.05	Triassic	Salt
5100	5200	2.05	0.10	Triassic	Salt
5100	5200	2.45	0.10	Triassic	Clay
5200	5300	2.05	0.10	Triassic	Salt
5200	5300	2.50	0.15	Triassic	Clay
5300	5400	2.05	0.10	Triassic	Salt

5400	5500	2.07	0.10	Triassic	Salt
5500	5600	2.60	0.10	Triassic	Clay+Silt
5600	5700	2.60	0.10	Triassic	Silt+Clay
5700	5800	2.65	0.05	Triassic	Clay+Silt
5800	5900	2.65	0.05	Triassic	Silt+Clay
5900	6000	2.65	0.05	Triassic	Silt+Clay
6000	6100	2.62	0.05	Triassic	Clay+Silt
6100	6200	2.65	0.05	Triassic	Silt+Clay
6200	6300	2.62	0.05	Triassic	Silt+Clay
6300	6400	2.62	0.05	Triassic	Silt+Clay
6300	6400	2.05	0.10	Triassic	Salt
6400	6500	2.10	0.10	Triassic	Salt
6500	6600	2.10	0.15	Triassic	Salt
6600	6700	2.05	0.05	Triassic	Salt
6700	6800	2.55	0.15	Triassic	Silt+Clay
6800	6900	2.55	0.25	Triassic	Silt+Clay
6900	7000	2.55	0.15	Triassic	Sand
7000	7100	2.45	0.10	Triassic	Sand
7100	7200	2.42	0.15	Triassic	Sand
7200	7300	2.42	0.15	Triassic	Sand
7300	7400	2.45	0.10	Triassic	Sand
7400	7500	2.47	0.10	Triassic	Sand
7500	7600	2.55	0.05	Triassic	Sand

APPENDIX 3

Computer Programs Program for subdividing the depth contours into 100 km squares. The blocks are organized for computation of their attraction by contour integration method.

```
c
c      Computer program for seperating contour lines into
c      100 km squares. The outputs are written in files whose
c      names starts with the corresponding latters.
c
      DIMENSION X(1000),Y(1000),NT(12,12),X0(12,12,400)
     1,Y0(12,12,400),IDT(12,12),IDN(12,12)
     1 ,IOVER(12,12),XCROS(12,12),YCROS(12,12),NCRO(12,12)
     1 ,POTY(12,12,20),POTX(12,12,20),POTXZ(20),POTYZ(20),IRI(12,12)
      CHARACTER*5 FILENAME(12,12),NAME,CD
      INTEGER PX,PY
      DATA FILENAME/144*'A'/
c
c     Read 3 charcters to be added at the end of the files names
c        if CD is given as XXX, the output files appears as SQXXX, XDXXX...
c
      WRITE(6,3000)
      READ(5,3001) CD
 3001 FORMAT(A4)
 3000 FORMAT(' Give the identification of the output files')
      NUR=6
c   Read the contour lines from a file. DEP is depth, NTR is
c   number of data points in presentation of the countour, and ITYPE
c   is the identifier for digitizing direction. If ITYPE=1, the
c   direction is changed.
c
    4 READ(3,1,END=500) DEP,NTR,ITYPE
      READ(3,2) (X(I),Y(I),I=1,NTR)
c
c      Find the soulution on X direction
c
      DO 121 I=1,12
      DO 122 J=1,12
      IOVER(I,J)=0
      NT(I,J)=0
      IDN(I,J)=0
      IRI(I,J)=0
      NCRO(I,J)=0
  122 CONTINUE
  121 CONTINUE
      KKTEST=(X(1)+30000)/10000
      NNTEST=(Y(1)+30000)/10000
      XCROS(KKTEST,NNTEST)=X(1)
      YCROS(KKTEST,NNTEST)=Y(1)
      DO 5 I=1,NTR
      KK=(X(I)+30000)/10000
      NN=(Y(I)+30000)/10000
c
c      Test if the data point crosses a boundary of 100 km square.
c
      IF (KK.NE.KKTEST.OR.NN.NE.NNTEST) THEN
c
c     Fing the crossing point
c
        CALL BAUND(X(I-1),Y(I-1),X(I),Y(I),FX,FY)
        NT(KKTEST,NNTEST)=NT(KKTEST,NNTEST)+1
        X0(KKTEST,NNTEST,NT(KKTEST,NNTEST))=FX
        Y0(KKTEST,NNTEST,NT(KKTEST,NNTEST))=FY
      IF (IRI(KKTEST,NNTEST).EQ.0) THEN
      NCRO(KKTEST,NNTEST)=NCRO(KKTEST,NNTEST)+1
```

```
      END IF
      IRI(KKTEST,NNTEST)=1
      IRI(KK,NN)=1
      NCRO(KKTEST,NNTEST)=NCRO(KKTEST,NNTEST)+1
      POTX(KKTEST,NNTEST,NCRO(KKTEST,NNTEST))=FX
      POTY(KKTEST,NNTEST,NCRO(KKTEST,NNTEST))=FY
      IDN(KKTEST,NNTEST)=IDN(KKTEST,NNTEST)+1
      IF (IDN(KK,NN).NE.0) THEN
      PX=(KK*10000)-30000
      PY=(NN*10000)-30000
C
C     Find how to close the countour line within the square.
C
      CALL JOINER(CR1X,CR2X,CR3X,CR4X,CR1Y,CR2Y,CR3Y,CR4Y,NCOR
     *,X0(KK,NN,NT(KK,NN)),Y0(KK,NN,NT(KK,NN)),FX,FY,PX,PY,IREM)
      GO TO(151,152,153,154,155) NCOR
  152 NT(KK,NN)=NT(KK,NN)+1
      NCRO(KK,NN)=NCRO(KK,NN)+1
      X0(KK,NN,NT(KK,NN))=CR1X
      Y0(KK,NN,NT(KK,NN))=CR1Y
      POTX(KK,NN,NCRO(KK,NN))=CR1X
      POTY(KK,NN,NCRO(KK,NN))=CR1X
      GO TO 151
  153 NT(KK,NN)=NT(KK,NN)+2
      X0(KK,NN,NT(KK,NN)-1)=CR1X
      Y0(KK,NN,NT(KK,NN)-1)=CR1Y
      X0(KK,NN,NT(KK,NN))=CR2X
      Y0(KK,NN,NT(KK,NN))=CR2Y
      NCRO(KK,NN)=NCRO(KK,NN)+2
      POTX(KK,NN,NCRO(KK,NN)-1)=CR1X
      POTX(KK,NN,NCRO(KK,NN))=CR2X
      POTY(KK,NN,NCRO(KK,NN)-1)=CR1Y
      POTY(KK,NN,NCRO(KK,NN))=CR2Y
      GO TO 151
  154 NT(KK,NN)=NT(KK,NN)+3
      X0(KK,NN,NT(KK,NN)-2)=CR1X
      Y0(KK,NN,NT(KK,NN)-2)=CR1Y
      X0(KK,NN,NT(KK,NN)-1)=CR2X
      Y0(KK,NN,NT(KK,NN)-1)=CR2Y
      X0(KK,NN,NT(KK,NN))=CR3X
      Y0(KK,NN,NT(KK,NN))=CR3Y
      NCRO(KK,NN)=NCRO(KK,NN)+3
      POTX(KK,NN,NCRO(KK,NN)-2)=CR1X
      POTX(KK,NN,NCRO(KK,NN)-1)=CR2X
      POTX(KK,NN,NCRO(KK,NN))=CR3X
      POTY(KK,NN,NCRO(KK,NN)-2)=CR1Y
      POTY(KK,NN,NCRO(KK,NN)-1)=CR2Y
      POTY(KK,NN,NCRO(KK,NN))=CR3Y
      GO TO 151
  155 NT(KK,NN)=NT(KK,NN)+4
      X0(KK,NN,NT(KK,NN)-3)=CR1X
      Y0(KK,NN,NT(KK,NN)-3)=CR1Y
      X0(KK,NN,NT(KK,NN)-2)=CR2X
      Y0(KK,NN,NT(KK,NN)-2)=CR2Y
      X0(KK,NN,NT(KK,NN)-1)=CR3X
      Y0(KK,NN,NT(KK,NN)-1)=CR3Y
      X0(KK,NN,NT(KK,NN))=CR4X
      Y0(KK,NN,NT(KK,NN))=CR4Y
      NCRO(KK,NN)=NCRO(KK,NN)+4
      POTX(KK,NN,NCRO(KK,NN)-3)=CR1X
```

```
      POTX(KK,NN,NCRO(KK,NN)-2)=CR2X
      POTX(KK,NN,NCRO(KK,NN)-1)=CR3X
      POTX(KK,NN,NCRO(KK,NN))=CR4X
      POTY(KK,NN,NCRO(KK,NN)-3)=CR1Y
      POTY(KK,NN,NCRO(KK,NN)-2)=CR2Y
      POTY(KK,NN,NCRO(KK,NN)-1)=CR3Y
      POTY(KK,NN,NCRO(KK,NN))=CR4Y
  151 CONTINUE
      END IF
        NT(KK,NN)=NT(KK,NN)+1
        X0(KK,NN,NT(KK,NN))=FX
        Y0(KK,NN,NT(KK,NN))=FY
        NT(KK,NN)=NT(KK,NN)+1
        X0(KK,NN,NT(KK,NN))=X(I)
        Y0(KK,NN,NT(KK,NN))=Y(I)
      NCRO(KK,NN)=NCRO(KK,NN)+1
      POTX(KK,NN,NCRO(KK,NN))=FX
      POTY(KK,NN,NCRO(KK,NN))=FY
      XCROS(KK,NN)=FX
      YCROS(KK,NN)=FY
        KKTEST=KK
        NNTEST=NN
      ELSE
        NT(KK,NN)=NT(KK,NN)+1
        X0(KK,NN,NT(KK,NN))=X(I)
        Y0(KK,NN,NT(KK,NN))=Y(I)
      END IF
    5 CONTINUE
C
C     Repeat the same process for Y direction
C
      DO 30 I=1,12
      DO 31 J=1,12
      IF (NT(I,J).EQ.0) GO TO 31
      PX=(I*10000)-30000
      PY=(J*10000)-30000
      IF (X0(I,J,NT(I,J)).EQ.X0(I,J,1).AND.Y0(I,J,NT(I,J)).EQ
     1.Y0(I,J,1)) GO TO 1001
      IDN(I,J)=IDN(I,J)+1
      CALL JOINER(CR1X,CR2X,CR3X,CR4X,CR1Y,CR2Y,CR3Y,CR4Y,NCOR,
     1X0(I,J,NT(I,J)),Y0(I,J,NT(I,J)),X0(I,J,1),Y0(I,J,1),PX,PY,IREM)
      GO TO (1002,1003,1004,1005,1006) NCOR
 1003 NT(I,J)=NT(I,J)+1
      X0(I,J,NT(I,J))=CR1X
      Y0(I,J,NT(I,J))=CR1Y
      NCRO(I,J)=NCRO(I,J)
      POTX(I,J,NCRO(I,J))=CR1X
      POTY(I,J,NCRO(I,J))=CR1Y
      GO TO 1002
 1004 NT(I,J)=NT(I,J)+2
      X0(I,J,NT(I,J)-1)=CR1X
      Y0(I,J,NT(I,J)-1)=CR1Y
      X0(I,J,NT(I,J))=CR2X
      Y0(I,J,NT(I,J))=CR2Y
      NCRO(I,J)=NCRO(I,J)+2
      POTX(I,J,NCRO(I,J)-1)=CR1X
      POTX(I,J,NCRO(I,J))=CR2X
      POTY(I,J,NCRO(I,J)-1)=CR1Y
      POTY(I,J,NCRO(I,J))=CR2Y
      GO TO 1002
```

```
 1005 NT(I,J)=NT(I,J)+3
      X0(I,J,NT(I,J)-2)=CR1X
      Y0(I,J,NT(I,J)-2)=CR1Y
      X0(I,J,NT(I,J)-1)=CR2X
      Y0(I,J,NT(I,J)-1)=CR2Y
      X0(I,J,NT(I,J))=CR3X
      Y0(I,J,NT(I,J))=CR3Y
      NCRO(I,J)=NCRO(I,J)+3
      POTX(I,J,NCRO(I,J)-2)=CR1X
      POTX(I,J,NCRO(I,J)-1)=CR2X
      POTX(I,J,NCRO(I,J))=CR3X
      POTY(I,J,NCRO(I,J)-2)=CR1Y
      POTY(I,J,NCRO(I,J)-1)=CR2Y
      POTY(I,J,NCRO(I,J))=CR3Y
      GO TO 1002
 1006 NT(I,J)=NT(I,J)+4
      X0(I,J,NT(I,J)-3)=CR1X
      Y0(I,J,NT(I,J)-3)=CR1Y
      X0(I,J,NT(I,J)-2)=CR2X
      Y0(I,J,NT(I,J)-2)=CR2Y
      X0(I,J,NT(I,J)-1)=CR3X
      Y0(I,J,NT(I,J)-1)=CR3Y
      X0(I,J,NT(I,J))=CR4X
      Y0(I,J,NT(I,J))=CR4Y
      NCRO(I,J)=NCRO(I,J)+4
      POTX(I,J,NCRO(I,J)-3)=CR1X
      POTX(I,J,NCRO(I,J)-2)=CR2X
      POTX(I,J,NCRO(I,J)-1)=CR3X
      POTX(I,J,NCRO(I,J))=CR4X
      POTY(I,J,NCRO(I,J)-3)=CR1Y
      POTY(I,J,NCRO(I,J)-2)=CR2Y
      POTY(I,J,NCRO(I,J)-1)=CR3Y
      POTY(I,J,NCRO(I,J))=CR4Y
 1002 CONTINUE
      NT(I,J)=NT(I,J)+1
      X0(I,J,NT(I,J))=X0(I,J,1)
      Y0(I,J,NT(I,J))=Y0(I,J,1)
      GO TO 1553
 1001 IF(NCRO(I,J).EQ.0) GO TO 1553
      POTY(I,J,1)=POTY(I,J,NCRO(I,J))
      POTX(I,J,1)=POTX(I,J,NCRO(I,J))
 1553 IF (NCRO(I,J).GT.2) THEN
      ISUN=NCRO(I,J)
      DO 1891 NIT=1,NCRO(I,J)
      POTXZ(NIT)=POTX(I,J,NIT)
      POTYZ(NIT)=POTY(I,J,NIT)
 1891 CONTINUE
C
C     Check if thare are more correction in joining the contours
C
      CALL OVERRUN(POTXZ,POTYZ,NCRO(I,J)
     1,PX,PY,IOVER(I,J))
      END IF
      IF(IOVER(I,J).GT.0) THEN
      DO 1351 II=1,IOVER(I,J)
      NT(I,J)=NT(I,J)+4
      X0(I,J,NT(I,J)-3)=(I*10000)-30000
      X0(I,J,NT(I,J)-2)=(I*10000)-30000
      X0(I,J,NT(I,J)-1)=(I*10000)-20000
      X0(I,J,NT(I,J))=(I*10000)-20000
```

```
      YO(I,J,NT(I,J)-3)=(J*10000)-30000
      YO(I,J,NT(I,J)-2)=(J*10000)-20000
      YO(I,J,NT(I,J)-1)=(J*10000)-20000
      YO(I,J,NT(I,J))=(J*10000)-30000
 1351 CONTINUE
      NT(I,J)=NT(I,J)+1
      XO(I,J,NT(I,J))=(I*10000)-30000
      YO(I,J,NT(I,J))=(J*10000)-30000
      NT(I,J)=NT(I,J)+1
      XO(I,J,NT(I,J))=XO(I,J,1)
      YO(I,J,NT(I,J))=YO(I,J,1)
      END IF
      IF(FILENAME(I,J).EQ.'A') THEN
      XPUT=(I*10000)-30000
      YPUT=(J*10000)-30000
c
c      Fing the corresponding file name, up to 2 latters
c
        CALL FILENAM(XPUT,YPUT,NAME,CD)
        FILENAME(I,J)=NAME
        NUR=NUR+1
        IDT(I,J)=NUR
        NA=NUR
        OPEN(NUR,FILE=NAME,FILETYPE='C')
      ELSE
        NA=IDT(I,J)
      END IF
      WRITE(NA,34) NT(I,J),DEP,ITYPE
      WRITE(NA,33) (XO(I,J,L),YO(I,J,L),L=1,NT(I,J))
   31 CONTINUE
   30 CONTINUE
      GO TO 4
  500 CONTINUE
      WRITE(6,114)
      DO 112 I=1,12
c
c      Write the output files to the user terminal
c
      DO 113 J=1,12
      IF(FILENAME(I,J).EQ.'A') GO TO 113
      WRITE(1,1150) FILENAME(I,J)
      WRITE(6,115) FILENAME(I,J)
  113 CONTINUE
  112 CONTINUE
 1150 FORMAT(A5)
   33 FORMAT(5X,2F10.0)
    1 FORMAT(16X,F8.2,6X,I4,7X,I2)
    2 FORMAT(5X,2F10.0)
   34 FORMAT(' There are ',I4,' points Depth=',F10.0,I1)
  101 FORMAT(11X,I4,14X,F10.0)
  102 FORMAT(5X,2F10.0)
  115 FORMAT(1X,A5)
  114 FORMAT(' There are the output files')
      STOP
      END
c
c    Subroutine Bound finds the corssing points on the border of
c    the squares.
c
      SUBROUTINE BAUND(REMX,REMY,AX,AY,FX,FY)
```

```
      DOUBLE PRECISION GRAD,CONST
      IX1=(REMX+30000)/10000
      IX2=(AX+30000)/10000
      IY1=(REMY+30000)/10000
      IY2=(AY+30000)/10000
      IF((AX-REMX).EQ.0) GO TO 33
      GRAD=(AY-REMY)/(AX-REMX)
      CONST=REMY-(REMX*GRAD)
      IF(IX1.EQ.IX2) THEN
        IF(IY1.GT.IY2) THEN
          FY=(IY1*10000)-30000
        ELSE
          FY=(IY2*10000)-30000
        END IF
        FX=(FY-CONST)/GRAD
      ELSE
        IF(IX1.GT.IX2) THEN
          FX=(IX1*10000)-30000
        ELSE
          FX=(IX2*10000)-30000
        END IF
        FY=(FX*GRAD)+CONST
      END IF
      RETURN
   33 IF(IY1.GT.IY2) THEN
      FY=(IY1*10000)-30000
      ELSE
      FY=(IY2*10000)-30000
      END IF
      FX=REMX
      RETURN
      END
C
C   Subroutine Filenam finds the two latters of the square name
C
      SUBROUTINE FILENAM(X,Y,NAME,CD)
      CHARACTER T(5,5)
      CHARACTER*5 NAME,CD
      DATA T/'V','Q','L','F','A','W','R','M','G'
     1 ,'B','X','S','N','H','C','Y','T','O','J'
     1 ,'D','Z','U','P','K','E'/
      I=(X+150000)/50000
      J=(Y+100000)/50000
      X=X+150000
      Y=Y+100000
      KX=ABS(X-(I*50000))
      KX=(KX+10000)/10000
      KY=ABS(Y-(J*50000))
      KY=(KY+10000)/10000
      NAME=T(J,I)//T(KY,KX)//CD
      RETURN
      END
C
C   Subroutine Joiner finds which way the contour closes. The
C   corners of the square is returned.
C
      SUBROUTINE JOINER(CR1X,CR2X,CR3X,CR4X,CR1Y,CR2Y,CR3Y
     1,CR4Y,NCOR,X2,Y2,X1,Y1,PX,PY,NTYPE)
      INTEGER PX,PY
      IF(X2.EQ.PX) NTYPE=1
```

```
    IF(Y2.EQ.PY+10000) NTYPE=2
    IF(X2.EQ.PX+10000) NTYPE=3
    IF(Y2.EQ.PY) NTYPE=4
    GO TO (15,20,25,30) NTYPE
15  IF(X1.EQ.X2) THEN
    IF(Y1.GT.Y2) THEN
    NCOR=5
    CR1X=PX
    CR2X=PX+10000
    CR3X=PX+10000
    CR4X=PX
    CR1Y=PY
    CR2Y=PY
    CR3Y=PY+10000
    CR4Y=PY+10000
    ELSE
    NCOR=1
    END IF
    RETURN
    END IF
    CR1X=PX
    CR1Y=PY
    IF(Y1.EQ.PY) THEN
    NCOR=2
    RETURN
    END IF
    CR2X=PX+10000
    CR2Y=PY
    IF(X1.EQ.PX+10000) THEN
    NCOR=3
    RETURN
    END IF
    CR3X=PX+10000
    CR3Y=PY+10000
    NCOR=4
    RETURN
20  IF(Y1.EQ.Y2) THEN
    IF(X1.GT.X2) THEN
    NCOR=5
    CR1X=PX
    CR2X=PX
    CR3X=PX+10000
    CR4X=PX+10000
    CR1Y=PY+10000
    CR2Y=PY
    CR3Y=PY
    CR4Y=PY+10000
    ELSE
    NCOR=1
    END IF
    RETURN
    END IF
    CR1X=PX
    CR1Y=PY+10000
    IF(X1.EQ.PX) THEN
    NCOR=2
    RETURN
    END IF
    CR2X=PX
    CR2Y=PY
```

```
    IF(Y1.EQ.PY) THEN
    NCOR=3
    RETURN
    END IF
    CR3X=PX+10000
    CR3Y=PY
    NCOR=4
    RETURN
25  IF(X1.EQ.X2) THEN
    IF(Y2.GT.Y1) THEN
    NCOR=5
    CR1X=PX+10000
    CR2X=PX
    CR3X=PX
    CR4X=PX+10000
    CR1Y=PY+10000
    CR2Y=PY+10000
    CR3Y=PY
    CR4Y=PY
    ELSE
    NCOR=1
    END IF
    RETURN
    END IF
    CR1X=PX+10000
    CR1Y=PY+10000
    IF(Y1.EQ.PY+10000) THEN
    NCOR=2
    RETURN
    END IF
    CR2X=PX
    CR2Y=PY+10000
    IF(X1.EQ.PX) THEN
    NCOR=3
    RETURN
    END IF
    CR3X=PX
    CR3Y=PY
    NCOR=4
    RETURN
30  IF(Y1.EQ.Y2) THEN
    IF(X1.LT.X2) THEN
    NCOR=5
    CR1X=PX+10000
    CR2X=PX+10000
    CR3X=PX
    CR4X=PX
    CR1Y=PY
    CR2Y=PY+10000
    CR3Y=PY+10000
    CR4Y=PY
    ELSE
    NCOR=1
    END IF
    RETURN
    END IF
    CR1X=PX+10000
    CR1Y=PY
    IF(X1.EQ.PX+10000) THEN
    NCOR=2
```

```
      RETURN
      END IF
      CR2X=PX+10000
      CR2Y=PY+10000
      IF(Y1.EQ.PY+10000) THEN
      NCOR=3
      RETURN
      END IF
      CR3X=PX
      CR3Y=PY+10000
      NCOR=4
      RETURN
      END
C
C     Subroutine Overrun finds if the there are too many
C     data points return from subroutine joiner. If so
C     return IOVER value for corections.
C
      SUBROUTINE OVERRUN(X,Y,N,PX,PY,IOVER)
      DIMENSION X(N),Y(N)
      INTEGER PX,PY
      IF(Y(1).EQ.PY) ITYPE=1
      IF (X(1).EQ.PX+10000) ITYPE=2
      IF (Y(1).EQ.PY+10000) ITYPE=3
      IF (X(1).EQ.PX) ITYPE=4
      IF (N.LT.3) RETURN
      GO TO (10,11,12,13) ITYPE
   10 DO 100 I=3,N-1
      IF(Y(I).EQ.Y(1).AND.Y(I-1).EQ.Y(1)
     1.AND.X(I).GT.X(1).AND.X(1).GT.X(I-1)) THEN
      IOVER=IOVER+1
      END IF
  100 CONTINUE
      RETURN
   11 DO 101 I=3,N-1
      IF(X(I).EQ.X(1).AND.X(I-1).EQ.X(1).
     1AND.Y(I).GT.Y(1).AND.Y(1).GT.Y(I-1)) THEN
      IOVER=IOVER+1
      END IF
  101 CONTINUE
      RETURN
   12 DO 102 I=3,N-1
      IF(Y(I).EQ.Y(1).AND.Y(I-1).EQ.Y(1).
     1AND.X(1).GT.X(I).AND.X(I-1).GT.X(1)) THEN
      IOVER=IOVER+1
      END IF
  102 CONTINUE
      RETURN
   13 DO 103 I=3,N-1
      IF(X(I).EQ.X(1).AND.X(I-1).EQ.X(1).
     1AND.Y(1).GT.Y(I).AND.Y(I-1).GT.Y(1)) THEN
      IOVER=IOVER+1
      END IF
  103 CONTINUE
      RETURN
      END
```

Program for interpolating the depth contours on a regular grid by linear approximation. The outer contour line is assumed to be zero. For different purposes, the modification may be essential.

```
C_____________________________________________________________________
C
C          PROGRAM LININT
C
C
C       This program interpolates the dititized contour maps into
C  regular grid. Only the values inside the countours are interlopalted.
C  The interpolation is done by linear analysis of the cross points of
C  countours on the grid lines.

      DIMENSION X(2000),Y(2000),LNWE0(1150),LNNS0(1150)
     1 ,NUMWE(330),NUMNS(330),XWE(330,330),YWE(330),SAMQ(330)
     1 ,XNS(330),YNS(330,330),CWE(330,330),CNS(330,330)
     1 ,YNEW(330,330),XNEW(330,330),CNWE(330,330),CNNS(330,330)
     1 ,XGIR(50),DGIR(50),SL(330),SLP(330)
      CHARACTER*1 IWE(1150),INS(1150)
      DATA IWE/1150*'*'/
      DATA INS/1150*'*'/
c
c       Funcl interpolates the grid value by quadratic function.
c   This function is called when only two cross points have the
c   same depth value.
c
      FUNCl(X,X0,Xl,X2,F0,Fl,F2)=
     1 ((((X-Xl)*(X-X2))/((X0-Xl)*(X0-X2)))*F0)+
     1 ((((X-X0)*(X-X2))/((Xl-X0)*(Xl-X2)))*Fl)+
     1 ((((X-X0)*(X-Xl))/((X2-X0)*(X2-Xl)))*F2)
c
c     Func0 interpolates the grid point by a linear function
c
      FUNC0(X,X0,Xl,F0,Fl)=
     1 (((X-Xl)/(X0-Xl))*F0)+(((X-X0)/(Xl-X0))*Fl)
c
c       Read the user controled data points
c        Shiftings on x and y directions for the control
c   of the dimension of the array.
c
      WRITE(6,'('' Give the grid specing'')')
      READ(5,*) GRSP
      WRITE(6,'('' Give the shifting on X direction'')')
      READ(5,*) DENl
      WRITE(6,'('' Give the shifting on Y direction'')')
      READ(5,*) DEN2
      WRITE(6,'('' Give the coordinates of area'',/,
     1 '' X min ?'')')
      READ(5,*) XNMIN
      WRITE(6,'('' X max ?'')')
      READ(5,*) XNMAX
      WRITE(6,'('' Y min ?'')')
      READ(5,*) YNMIN
      WRITE(6,'('' Y max ?'')')
      READ(5,*) YNMAX
      WRITE(6,'('' Give the error distance'')')
      READ(5,*) HICTEN
      WRITE(6,'('' Give contour interval'')')
      READ(5,*) ARA
      SAFE=4*GRSP
      LNWE=0
      LNNS=0
c
```

```
c     Read the digitized contours on channel 3
c
    4 READ(3,1,END=500) DEP,NUMBER
    1 FORMAT(16X,F8.2,6X,I4)
    2 FORMAT(5X,2F10.0)
      READ(3,2) (X(I),Y(I),I=1,NUMBER)
      KKT=(Y(1)+30000+DEN2)/GRSP
      NNT=(X(1)+30000+DEN1)/GRSP
      DO 120 I=2,NUMBER
      KK=(Y(I)+30000+DEN2)/GRSP
      NN=(X(I)+30000+DEN1)/GRSP
      IF(KK.NE.KKT) THEN
c
c      The contour line crosses the grid line on x direction
c
      ADUM=KKT-KK
      IF(ABS(ADUM).NE.1) THEN
c
c       Error ! The digitizing space is greater than grid space
c
      WRITE(6,'('' Error 0'')')
      STOP
      END IF
c
c    Find the crossing point
c
      CALL BAUND(X(I-1),Y(I-1),X(I),Y(I),FX,FY,1,GRSP,DEN1,DEN2)
c
c      Check if the digitizing error occured
c
      IF(FX.LT.XNMIN-SAFE.OR.FX.GT.XNMAX+SAFE.OR.
     1 FY.LT.YNMIN-SAFE.OR.FY.GT.YNMAX+SAFE) THEN
      KKT=KK
      GO TO 1543
      END IF
      NNX=(FY+30000+DEN2)/GRSP
      IF (IWE(NNX).EQ.'*') THEN
c
c  new grid line
c
      LNWE=LNWE+1
      LNWE0(NNX)=LNWE
      NUMWE(LNWE)=1
      XWE(LNWE,1)=FX
      YWE(LNWE)=FY
      CWE(LNWE,1)=DEP
      IWE(NNX)=''
      ELSE
      NUMWE(LNWE0(NNX))=NUMWE(LNWE0(NNX))+1
      XWE(LNWE0(NNX),NUMWE(LNWE0(NNX)))=FX
      CWE(LNWE0(NNX),NUMWE(LNWE0(NNX)))=DEP
      END IF
      KKT=KK
      END IF
 1543 CONTINUE
      IF(NNT.NE.NN) THEN
c
c     Contour line crosses the grid line
c
      ADUM=NN-NNT
```

```
      IF(ABS(ADUM).NE.1) THEN
c
c   Eroor ! Digitized spacing is greater than grid spacing
c
      WRITE(6,'('' Error 1'')')
      STOP
      END IF
      CALL BAUND(X(I-1),Y(I-1),X(I),Y(I),FX,FY,2,GRSP,DEN1,DEN2)
      IF(FX.LT.XNMIN-SAFE.OR.FX.GT.XNMAX+SAFE.OR.
     1 FY.LT.YNMIN-SAFE.OR.FY.GT.YNMAX+SAFE) THEN
      NNT=NN
      GO TO 120
      END IF
      NNX=(FX+30000+DEN1)/GRSP
      IF (INS(NNX).EQ.'*') THEN
c
c    new grid line
c
      LNNS=LNNS+1
      LNNS0(NNX)=LNNS
      NUMNS(LNNS)=1
      XNS(LNNS)=FX
      YNS(LNNS,1)=FY
      CNS(LNNS,1)=DEP
      INS(NNX)=''
      ELSE
      NUMNS(LNNS0(NNX))=NUMNS(LNNS0(NNX))+1
      YNS(LNNS0(NNX),NUMNS(LNNS0(NNX)))=FY
      CNS(LNNS0(NNX),NUMNS(LNNS0(NNX)))=DEP
      END IF
      NNT=NN
      END IF
  120 CONTINUE
      GO TO 4
  500 CONTINUE
c    End of the input file. Now the crossing points
c  of contours and grid lines recorded in the arrays
c  XEW and YNS with the contour values if CNEW, CNNS
c   Next stage is to organise the corossing points
c
      DO 121 I=1,LNWE
      NUR=0
   15 CONTINUE
      TEST=XWE(I,1)
      NTRUST=1
      DO 122 J=2,NUMWE(I)
      IF(TEST.GT.XWE(I,J)) THEN
      TEST=XWE(I,J)
      NTRUST=J
      END IF
  122 CONTINUE
      NUR=NUR+1
      IF (NUR.GT.NUMWE(I)) GO TO 121
      XNEW(I,NUR)=TEST
      XWE(I,NTRUST)=99999999.
      CNWE(I,NUR)=CWE(I,NTRUST)
      GO TO 15
  121 CONTINUE
      DO 123 I=1,LNNS
      NUR=0
```

```
   25 CONTINUE
      TEST=YNS(I,1)
      NTRUST=1
      DO 124 J=1,NUMNS(I)
      IF (TEST.GT.YNS(I,J)) THEN
      TEST=YNS(I,J)
      NTRUST=J
      END IF
  124 CONTINUE
      NUR=NUR+1
      IF(NUR.GT.NUMNS(I)) GO TO 123
      YNEW(I,NUR)=TEST
      YNS(I,NTRUST)=99999999.
      CNNS(I,NUR)=CNS(I,NTRUST)
      GO TO 25
  123 CONTINUE
C
C    The data is rearranged, in the arrays XNEW YNEW C? and C?
C    Now look for the fault lines
C
      DO 1099 I=1,LNWE
      IDT=0
      XWE(I,1)=XNEW(I,1)
      CWE(I,1)=CNWE(I,1)
      NUMA=1
      DO 1013 J=1,NUMWE(I)-1
      DIST=XNEW(I,J)-XNEW(I,J+1)
      IF(ABS(DIST).GT.HICTEN) THEN
      IF(IDT.NE.0) THEN
C
C     There is a Fault in the structure
C
      CALL FAULT(IDT,XGIR,DGIR,X1,D1,X2,D2)
      IF(X1.GT.X2) THEN
      ADD=X1
      ELSE
      ADD=X2
      END IF
      IF(NUMA.EQ.1) THEN
      NUB=NUMA
      ELSE
      NUB=NUMA-1
      END IF
      AR=D1-CWE(I,NUB)
      BR=D2-CWE(I,NUB)
      IF(ABS(AR).LT.ABS(BR)) THEN
      NUMA=NUMA+1
      XWE(I,NUMA-1)=ADD
      XWE(I,NUMA)=ADD
      CWE(I,NUMA-1)=D1
      CWE(I,NUMA)=D2
      ELSE
      NUMA=NUMA+1
      XWE(I,NUMA-1)=ADD
      XWE(I,NUMA)=ADD
      CWE(I,NUMA-1)=D2
      CWE(I,NUMA)=D1
      END IF
      IDT=0
      END IF
```

```
      NUMA=NUMA+1
      XWE(I,NUMA)=XNEW(I,J+1)
      CWE(I,NUMA)=CNWE(I,J+1)
      ELSE
      IF (IDT.EQ.0) THEN
      IDT=1
      XGIR(1)=XNEW(I,J)
      DGIR(1)=CNWE(I,J)
      END IF
      IDT=IDT+1
      XGIR(IDT)=XNEW(I,J+1)
      DGIR(IDT)=CNWE(I,J+1)
      IF(J+1.EQ.NUMWE(I)) THEN
      IF(NUMA.LT.2) GO TO 7382
C
C   There is fault
C
      CALL FAULT(IDT,XGIR,DGIR,X1,D1,X2,D2)
      IF(X1.GT.X2) THEN
      ADD=X1
      ELSE
      ADD=X2
      END IF
      AR=D1-CWE(I,NUMA-1)
      BR=D2-CWE(I,NUMA-1)
      IF(ABS(AR).LT.ABS(BR)) THEN
      NUMA=NUMA+1
      XWE(I,NUMA-1)=ADD
      XWE(I,NUMA)=ADD
      CWE(I,NUMA-1)=D1
      CWE(I,NUMA)=D2
      ELSE
      NUMA=NUMA+1
      XWE(I,NUMA-1)=ADD
      XWE(I,NUMA)=ADD
      CWE(I,NUMA-1)=D2
      CWE(I,NUMA)=D1
      END IF
      END IF
 7382 CONTINUE
      END IF
 1013 CONTINUE
      NUMWE(I)=NUMA
 1099 CONTINUE
      DO 1014 I=1,LNNS
      IDT=0
      YNS(I,1)=YNEW(I,1)
      CNS(I,1)=CNNS(I,1)
      NUMA=1
      DO 1091 J=1,NUMNS(I)-1
      DIST=YNEW(I,J)-YNEW(I,J+1)
      IF(ABS(DIST).GT.HICTEN) THEN
      IF(IDT.NE.0) THEN
C
C    There is fault
C
      CALL FAULT(IDT,XGIR,DGIR,X1,D1,X2,D2)
      IF(X1.GT.X2) THEN
      ADD=X1
      ELSE
```

```
      ADD=X2
       END IF
      IF(NUMA.EQ.1) THEN
      NUB=NUMA
      ELSE
      NUB=NUMA-1
      END IF
      AR=D1-CNS(I,NUB)
      BR=D2-CNS(I,NUB)
      IF(ABS(AR).LT.ABS(BR)) THEN
      NUMA=NUMA+1
      YNS(I,NUMA-1)=ADD
      YNS(I,NUMA)=ADD
      CNS(I,NUMA-1)=D1
      CNS(I,NUMA)=D2
      ELSE
      NUMA=NUMA+1
      YNS(I,NUMA-1)=ADD
      YNS(I,NUMA)=ADD
      CNS(I,NUMA-1)=D2
      CNS(I,NUMA)=D1
      END IF
      IDT=0
      END IF
      NUMA=NUMA+1
      YNS(I,NUMA)=YNEW(I,J+1)
      CNS(I,NUMA)=CNNS(I,J+1)
      ELSE
      IF(IDT.EQ.0) THEN
      IDT=1
      XGIR(1)=YNEW(I,J)
      DGIR(1)=CNNS(I,J)
      END IF
      IDT=IDT+1
      XGIR(IDT)=YNEW(I,J+1)
      DGIR(IDT)=CNNS(I,J+1)
      IF(J+1.EQ.NUMNS(I)) THEN
      IF(NUMA.LT.2) GO TO 7287
C
C     There is fault
C
      CALL FAULT(IDT,XGIR,DGIR,X1,D1,X2,D2)
      IF(X1.GT.X2) THEN
      ADD=X1
      ELSE
      ADD=X2
      END IF
      AR=D1-CNS(I,NUMA-1)
      BR=D2-CNS(I,NUMA-1)
      IF(ABS(AR).LT.ABS(BR)) THEN
      NUMA=NUMA+1
      YNS(I,NUMA-1)=ADD
      YNS(I,NUMA)=ADD
      CNS(I,NUMA-1)=D1
      CNS(I,NUMA)=D2
      ELSE
      NUMA=NUMA+1
      YNS(I,NUMA-1)=ADD
      YNS(I,NUMA)=ADD
      CNS(I,NUMA-1)=D2
```

```
      CNS(I,NUMA)=D1
      END IF
      END IF
 7287 CONTINUE
      END IF
 1091 CONTINUE
      NUMNS(I)=NUMA
 1014 CONTINUE
c
c     Ready to interpolate into regular grid
c  First on WE direction
c
      DO 126 I=1,LNWE
      IF(XWE(I,1).EQ.XWE(I,2).AND.CWE(I,1).EQ.CWE(I,2)) THEN
      DO 1291 J=1,NUMWE(I)-1
      XWE(I,J)=XWE(I,J+1)
      CWE(I,J)=CWE(I,J+1)
 1291 CONTINUE
      NUMWE(I)=NUMWE(I)-1
      END IF
  126 CONTINUE
      DO 127 I=1,LNNS
      IF(YNS(I,1).EQ.YNS(I,2).AND.CNS(I,1).EQ.CNS(I,2)) THEN
      DO 1292 J=1,NUMNS(I)-1
      YNS(I,J)=YNS(I,J+1)
      CNS(I,J)=CNS(I,J+1)
 1292 CONTINUE
      NUMNS(I)=NUMNS(I)-1
      END IF
  127 CONTINUE
      DO 1300 I=1,LNWE
      DO 3002 KL=1,NUMWE(I)
      SAMQ(KL)=XWE(I,KL)
 3002 CONTINUE
c
c   Find if the contours are inceasing or decreasing.
c
      CALL SLOPE(NUMWE(I),SAMQ,SLP)
      ISTART=(XWE(I,1)+30000+DEN1)/GRSP
      START=(ISTART+1)*GRSP-DEN1-30000
      DO 1200 J=1,NUMWE(I)-1
 1111 CONTINUE
      IF(START.GE.XWE(I,J).AND.START.LE.XWE(I,J+1)) THEN
      IF(CWE(I,J).EQ.CWE(I,J+1)) THEN
      C1=CWE(I,J)
      C2=CWE(I,J)+(ARA*SLP(J))
      C3=CWE(I,J+1)
      X1=XWE(I,J)
      X2=(XWE(I,J)+XWE(I,J+1))/2.
      X3=XWE(I,J+1)
      CON=FUNC1(START,X1,X2,X3,C1,C2,C3)
      XP=START
      YP=YWE(I)
      ELSE
      C1=CWE(I,J)
      C2=CWE(I,J+1)
      X1=XWE(I,J)
      X2=XWE(I,J+1)
      IF(X1.EQ.X2) THEN
      IF(J+1.EQ.NUMWE(I)) THEN
```

```
      CON=C1
      ELSE
      CON=C2
      END IF
      GO TO 9516
      END IF
      CON=FUNC0(START,X1,X2,C1,C2)
 9516 CONTINUE
      XP=START
      YP=YWE(I)
      END IF
c
c     Find the solutions on NS direction
c
      DO 1500 II=1,LNNS
      IF(XP.NE.XNS(II)) GO TO 1500
      DO 3001 KL=1,NUMNS(II)
      SAMQ(KL)=YNS(II,KL)
 3001 CONTINUE
      CALL SLOPE(NUMNS(II),SAMQ,SL)
      DO 1501 JJ=1,NUMNS(II)-1
      IF(YNS(II,JJ).LE.YP.AND.YNS(II,JJ+1).GE.YP) THEN
      IF(CNS(II,JJ).EQ.CNS(II,JJ+1)) THEN
      C1=CNS(II,JJ)
      C2=CNS(II,JJ)+(ARA*SL(JJ))
      C3=CNS(II,JJ+1)
      X1=YNS(II,JJ)
      X2=(YNS(II,JJ)+YNS(II,JJ+1))/2.
      X3=YNS(II,JJ+1)
      C=FUNC1(YP,X1,X2,X3,C1,C2,C3)
      CON=(CON+C)/2.
      ELSE
      C1=CNS(II,JJ)
      C2=CNS(II,JJ+1)
      X1=YNS(II,JJ)
      X2=YNS(II,JJ+1)
      IF(X1.EQ.X2) THEN
      IF(JJ+1.EQ.NUMNS(II)) THEN
      C=C1
      ELSE
      C=C2
      END IF
      GO TO 1873
      END IF
      C=FUNC0(YP,X1,X2,C1,C2)
 1873 CONTINUE
c
c    Average the result found on x and y directions.
c
      CON=(CON+C)/2.
      END IF
      GO TO 1520
      END IF
 1501 CONTINUE
 1500 CONTINUE
 1520 CONTINUE
      START=START+GRSP
      WRITE(7,'(2F10.0,F10.4)') XP,YP,CON
      GO TO 1111
      END IF
```

```
 1200 CONTINUE
 1300 CONTINUE
      STOP
      END


C      Souroutine Baund finds the crossing of points on the grid lines
C

      SUBROUTINE BAUND(REMX,REMY,AX,AY,FX,FY,N,GRSP,DEN1,DEN2)
      DOUBLE PRECISION GRAD,CONST
      IX1=(REMX+30000+DEN1)/GRSP
      IX2=(AX+30000+DEN1)/GRSP
      IY1=(REMY+30000+DEN2)/GRSP
      IY2=(AY+30000+DEN2)/GRSP
c
c     check if the equation is y=x+c or x=c
c
      GO TO(50,60) N
   50 IF((AX-REMX).EQ.0) GO TO 33
      GRAD=(AY-REMY)/(AX-REMX)
      CONST=REMY-(REMX*GRAD)
      IF(IY1.GT.IY2) THEN
      FY=(IY1*GRSP)-30000-DEN2
      ELSE
      FY=(IY2*GRSP)-30000-DEN2
      END IF
      FX=(FY-CONST)/GRAD
      RETURN
   60 GRAD=(AY-REMY)/(AX-REMX)
      CONST=REMY-(REMX*GRAD)
      IF(IX1.GT.IX2) THEN
      FX=(IX1*GRSP)-30000-DEN1
      ELSE
      FX=(IX2*GRSP)-30000-DEN1
      END IF
      FY=(FX*GRAD)+CONST
      RETURN
   33 IF(IY1.GT.IY2) THEN
      FY=(IY1*GRSP)-30000-DEN2
      ELSE
      FY=(IY2*GRSP)-30000-DEN2
      END IF
      FX=REMX
      RETURN
      END

C
C     Subroutine fault indentifies the fault lines.
C

      SUBROUTINE FAULT(N,X,D,X1,D1,X2,D2)
      DIMENSION X(N),D(N)
      D1=D(1)
      D2=D1
      X1=X(1)
      X2=X1
      DO 1 I=2,N
      IF(D1.GT.D(I)) THEN
      D1=D(I)
```

```
      X1=X(I)
      END IF
      IF(D2.LT.D(I)) THEN
      D2=D(I)
      X2=X(I)
      END IF
    1 CONTINUE
      RETURN
      END

C
C     Subroutine slope finds the if there is an increase or
C  dicrease along the grid line
C

      SUBROUTINE SLOPE(N,D,S)
      DIMENSION D(N),S(N)
      S(1)=1
      IT=1
      DO 1 I=2,N-1
      IF(D(I).EQ.D(I+1)) THEN
      S(I)=IT
      IT=IT*(-1)
      ELSE
      A=D(I+1)-D(I)
      S(I)=ABS(A)/A
      IT=S(I)
      END IF
    1 CONTINUE
      S(N)=0
      RETURN
      END
```

APPENDIX 4

DOCUMENTATION ON THE IGM (Interactive Gravity Modelling) PROGRAM GMODEL

This program allows the user to change the structure of the Earth model without stopping the program by using the graphical control keys. The main aim is to reduce the computing time as well as the real time which the user spends on modelling a gravity profile. The algorithm for computing the gravitational attraction of the model is the two dimensional contour integration method described by Talwani et all (1959). Graphics routines are part of the E.R.C.C. (Edinburgh Regional Computing Centre) EDWIN package. The routines are stored in the ERCLIB directory GRAPHICS, and may be accessed.

The commands to access the drawing routines and the gravity modelling program are as follows;

Command:SEARCHDIR ERCLIB:GRAPHICS

Command:SEARCHDIR EGPV17:EDWINDIR.

This order of the commands is necessary, because routines in EGPV17:EDWINDIR has the same entry points as some routines in ERCLIB:GRAPHICS. The commands need be given only once.

The user now has access to the gravity modelling program. The run can be executed by giving the command GMODEL. The program checks the user terminal and informs the user what type of terminal is being used. If the terminal type is the same one as reported by the program, user should not have any difficulty. The success of the test should result in clearing the screen. If there is any doubt

about the success, reply to the question asked by the computer "no". This takes the user to the available terminal types supported by the E.R.C.C.

There are 3 phases in the program.

Phase 1

This phase is to inform the program about the parameters on the modelling. The program needs input of the observed gravity values. This information should be stored in a file before running the program. The reading format is free and any error in the file will result in ignoring that particular line and carrying on to read next line. In the case of error in the data, the user will be informed on which line the error occurred. The data should have first the gravity (in mgal) and then distance along a profile (in km), and one pair of data per line. The next step is to give the Z axes of the model. The maximum and minimum depth of the model has to be given by the user (in km). The last step in this phase is to tell the program if a hardcopy of the picture is wanted at the end. If the answer is "yes" then the final picture on the screen will stored in a RCO plot file. Note that this process slows down the real time of computing. The user is advised to reply to the question "no" if the modelling is not a final version. After obtaining the final model, the program can be rerun to produce a hardcopy of the model.

Phase 2

After giving the computer with the necessary information for phase 1 the observed gravity anomaly will be plotted on the top part of the screen. The command prompt ">" appears after plotting the anomaly. Now the program is ready to execute the modelling commands received from the user. The valid optional commands are given alphabetically. The user should start with commands "S" or "F"

Command A

This command is to alter the position of the node points, displayed on the screen. The cursor will appear on the screen if the terminal supports such an action. Move the cursor to the node points which to be altered, and press any key (except non-printing characters such as return, escape, line feed). The node point will be highlighted if the terminal supports highlighting. Move the cursor to the new position of the node point, and press any key. The screen should be cleared and the new picture should be displayed on the screen.

Command C

This command is to compute the gravitational attraction of the given structure, and plot the results. The regional anomaly is added to the calculated anomaly. Note that the regional anomaly is taken as a constant such that the mean residual is zero. Producing a different regional anomaly is left to the user.

Command D

This command is to change the density contrast of the given layer. To identify the layer, move the cursor to any node point which represents the structure, and press any key. After this the new density value of the structure can be given.

Command F

This command allows the user insert a structure which is prepared before running the program. The input file should contain this following information.

First line : Density, Number, Identifier

Following Lines : X coordinate, Z coordinate

Follow the same process until end of the data.

The parameters are as follows:

Density : Density Contrast of the Structure (in g/cm^3)

Number : Number of Node Points (corners) in the Layer

Identity: 0 if the layer is closed inside the visible area,

1 if the structure closed outside the visible area.

X and Z coordinate : X and Z coordinates of the node points which represents the layer (in km)

Reading format is free and in the event of an error occurring in the data file, the program restores the original data, and no data will be added from the file. The user will be informed.

Command H

This command is to give brief information about the commands.

Command I

This command is to investigate the density contrast of the structure. If the user give the layer number to the prompt; the density contrast will be given on the screen.

Command N

Same as command D, but the layer number is given rather than using the cursor to identify the layer. This method is suggested if the same node point is representing two different layer.

Command Q

This command is to quit from phase 2 to phase 3.

Command S

This command allows the user input a layer using the cursor. The first step is to give the density contrast of the layer. Then the cursor appears on the user

terminal. There are only two keys user is allowed to use. They are R (record) and F (finish). The cursor should be moved to a node point, and R should be pressed to record the data point. If the layer is to be extended outside the visible area, the recording should start and finish on the edges of the visible area. The program extends the layer outside the visible area on each side, twice the length of the visible area. If the layer is to be closed inside the visible area, the first and last points should be as close as possible. If they are too far apart the program terminates and all the information submitted will be lost. After completing the layer, the key F should be pressed to return to command level. Note that this key does not record the point.

Command T

This is to put a text on the screen. Move the cursor where the text is wanted. Press any key, and give the text. Note that no text is stored in the program, but if the text is on the screen when quitting the program, then the text will appear on the hardcopy.

Command Z

This command is to zoom and dezoom the structure. It may be necessary to have a high resolution of the shallow features. This command allows the user to blow up the structure and resolution of the structure by rescaling the depth axes. The new scale is to be given by the user.

Phase 3

After giving the command Q in phase 2, program goes to the phase 3. In this part the output is written in files if desired. If the hardcopy of the picture is wanted, then the x axis and y axis length of the graph is supplied by the user. (The dimensions are in cm.)

PLATE 1

BOUGUER GRAVITY ANOMALY MAP

Contour Interval 5 mgal

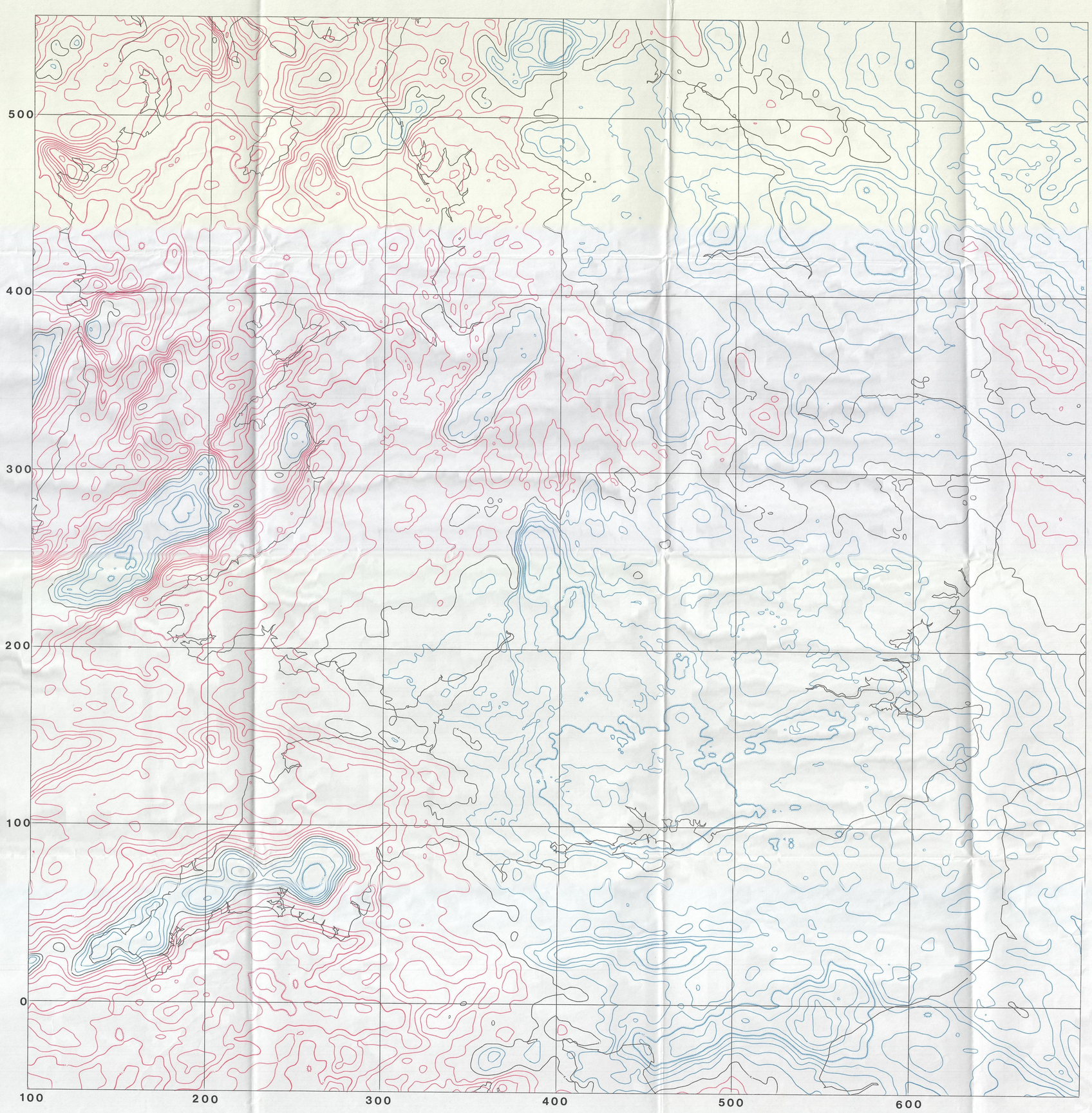

PLATE 2

STRIPPED BOUGUER GRAVITY ANOMALY MAP

Contour Interval 5 mgal

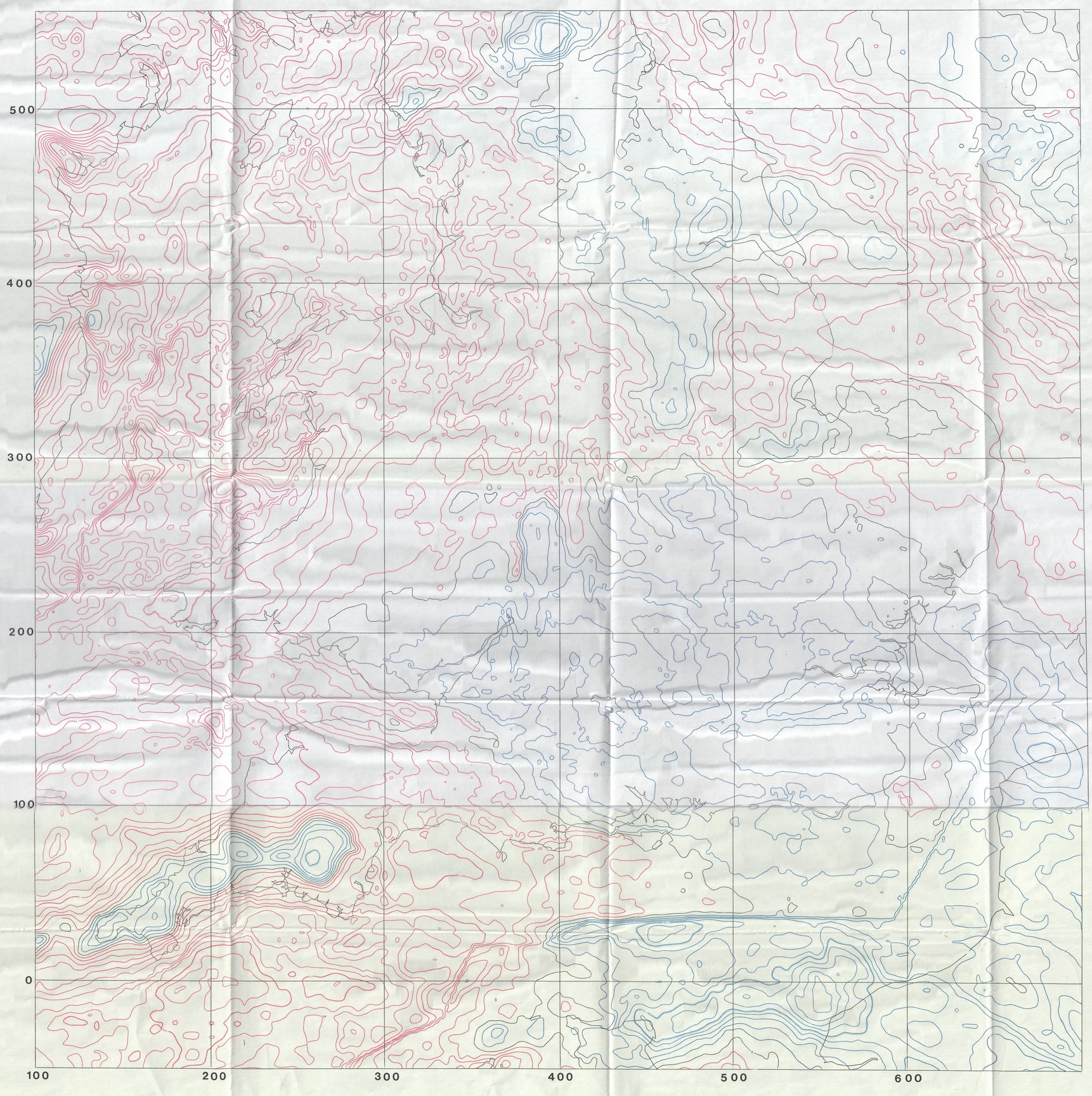

PLATE 3

COMPOSITE MAGNETIC ANOMALY MAP

Contour Interval 20 nT